A STUDY ON FLOW FORMATION OF CONDUCTING FLUID IN MACRO AND MICRO-CHANNELS

By

SANI ISA

DEPARTMENT OF MATHEMATICS

AHMADU BELLO UNIVERSITY, ZARIA NIGERIA

AUGUST, 2015

A STUDY ON FLOW FORMATION OF CONDUCTING FLUID IN MACRO AND MICRO-CHANNELS

By

Sani ISA

B.Sc. (UNIMAID)1996, MSc. (UNIMAID) 2005

Ph.D/SCIE/00223/2008-2009

A THESIS SUBMITTED TO THE SCHOOL OF POSTGRADUATE STUDIES, AHMADU BELLO UNIVERSITY, ZARIA

IN PARTIAL FULFILMENT OF THE REQUIREMENTS FOR THE AWARD OF DOCTOR OF PHILOSOPHY DEGREE IN MATHEMATICS

DEPARTMENT OF MATHEMATICS

FACULTY OF SCIENCE

AHMADU BELLO UNIVERSITY, ZARIA

NIGERIA

AUGUST, 2015

CERTIFICATION

This thesis titled "A STUDY OF FLOW FORMATION OF CONDUCTING FLUID IN MICRO-CHANNELS AND MACRO-CHANNELS" by Sani, ISA meets the regulations governing the award of the degree of Doctor of Philosophy of the Ahmadu Bello University, Zaria and is approved for its contribution to knowledge and literary presentation.

Prof. Basant K. Jha _____ Signature _____ Date

Chairman, Supervisory Committee

_____ _____

Dr. A. O. Ajibade Date

Member, Supervisory Committee

_____ _____

Prof. D. Singh Date

Member, Supervisory Committee

_____ _____

Prof. B. Sani Date

Head of Department

_____ _____

Prof. AA. A. BB Date

External Examiner

_____ _____

Prof. Z. A. Hassan Date

Dean Postgraduate School

ACKNOWLEDGEMENTS

Alhamd-Lillah. Indeed it is a pleasure to extend my sincere gratitude to my supervisor Prof. Basant K. Jha for his painstaking guide, dedication and encouragement. I am lacking words to express my feelings to a person who have done much despite his tight schedule in ensuring the successful completion of this work. To him, I say a big thank you. I would also like to express my gratitude to other members of the supervisory committee, Dr. A. O. Ajibade and Prof. D. Singh for their invaluable contributions, correction and guide towards making this work meeting the required standard.

My thanks goes to the Head, Department of Mathematics, Prof. B. Sani and all other members in the department for their friendly disposition and support throughout the period of my studies. Also, I would like to thank Prof. S. B. Junaidu, Prof. G. U. Garba, Prof. J. Singh, Prof. A. A. Tijjani. I owe special thanks to Dr. H. M. Jibril, Dr. H. G. Dikko, Dr. A. Yahaya, Dr. A. A. Obiniyi, Dr. A. AbdulRaheem, Mal. A. I. Fulatan, Mal. Y. M. Baraya, Mal. A. Alkali, A.T.Imam, Mal. G. Jamil and many others that are not mentioned. You were all wonderful to me and have made my stay a lot more easier in ABU Zaria. My special thanks goes to Dr. A. M. Ibrahim for his guide, advice and consolation during the period of uncertainties.

My gratitude goes to Alhaji Abubakar A. Makinta, Mohammad Kalli, Dr.Shuaibu Hassan,Usman Bida, Dr. Maimuna Waziri, Dr. Samaila K. Kamba, and Dr. Clement. A. Apere, for their advice and encouragement. Let me also use this medium to acknowledge and thank all my friends and fellows, too numerous to mention each one of them by name, whom we shared pleasantries and time during the turbulence period.

Special thanks goes to Yobe State University; my colleagues and all members of the department of mathematics.

Finally, my gratitude goes to my loving wives Fatsuma Yusuf Ibrahim, Sa'adatu Suleiman and the entire members of my family for their patience, unflinching support, encouragement, perseverance and endurance through out the period of my studies. Once again thank you all.

DEDICATION

To my late parents

DECLARATION

I declare that the work in this **thesis** entitled "A STUDY ON FLOW FORMATION OF CONDUCTING FLUID IN MACRO AND MICRO-CHANNELS" has been performed by me in the Department of Mathematics.The information derived from the literature has been duly acknowledged in the text and a list of references provided. No any part of this thesis was previously presented for another degree or diploma at this or any other Institution.

_____ _____

Sani ISA Date

ABSTRACT

Motion of an electrically conducting fluid in two types of geometries **was** studied; the macro-channels formed by two vertical parallel plates and annular micro-channels formed by two vertical concentric cylinders. The flow **was** assumed to be unsteady, fully developed laminar or steady laminar flow of viscous, incompressible and electrically conducting fluid with magnetic field applied perpendicular to the flow direction. The governing equations describing the different flow situations have been formulated and solved semi-analytically using a combination of Laplace transform technique and the Riemann-sum approximation, a method of taking the inverse of Laplace transform technique. However, the corresponding steady state solution and numerical solution by implicit finite difference method have also been obtained in the case of time dependent problems as a means of validating the obtained results. An excellent agreement at large values of time have been recorded. **MATLAB programmes are** written to compute and generate line graphs for the velocities, induced magnetic field, current density, volume flow rate and the skin frictions. A parametric study depicting the effect of the various dimensionless parameters on the velocity and skin friction **was** conducted. These parameters include the Prandtl number (Pr), the time (t), the suction/injection parameter (S), the Hartmann number (M), radius ratio (η), rarefaction parameter ($\beta_\nu Kn$), and the fluid - wall interaction parameter (F). The effects of changing the parameters mentioned above **were** observed either to increase, to decrease or to have no effect on the velocity profiles and the skin friction indicating the existence of a Lorentz force generated by the interaction of the magnetic field and the electric field. To understand the fluid flow and the heat transfer characteristics of buoyancy-induced micropump and microheat exchanger in microfluidic and thermal systems, fully developed. MHD natural convection flow in a vertical annular microchannel with asymmetric wall temperature distributions **was studied semi-analytically**. Both of the velocity slip and

the temperature jump conditions were considered because they have counter effects both on the volume flow rate and the heat transfer rate. Results revealed that in most of the natural convection situations, the volume flow rate at microscale is higher than that at macroscale, while the heat transfer rate is lower. It is, therefore, concluded that the temperature jump condition induced by the effects of rarefaction and fluid-wall interaction plays an important role in slip-flow natural convection.

TABLE OF CONTENTS

Cover Page i

Fly leaf i

Title Page ii

Approval Page iii

Acknowledgement iv

Dedication vi

Declaration vii

Abstract viii

Table of Contents viii

List of Figures xiii

List of Tables xxi

Dimensionless Quantities xxiv

Symbols and Notations xxvii

CHAPTER ONE

GENERAL INTRODUCTION 1

1.1 Introduction 1

1.1.1 Governing Equations of MHD 3

1.1.2 Continuity Equation 3

1.1.3 Navier-Stokes Equation 4

1.1.4 MHD Induction Equation 5

1.1.5 Energy Equation 5

1.1.6 Maxwell′s Equations 5

1.2 Statement of the Problem 6

1.3 Research Objectives 7

1.3.1 General Objective 7
1.3.2 Specific Objectives 8
1.4 Significance of the Study 9
1.5 Research Questions 9
1.6 Research Methodology 10
1.6.1 Laplace Transform 11
1.6.2 Riemann Sum Approximation 12
1.6.3 Implicit Finite Difference Method 13
1.6.4 Exact Solution 15
1.7 Some Basic Definitions 15
1.7.1 Pressure 16
1.7.2 Density 16
1.7.3 Viscosity 16
1.7.4 Mass and Volumetric Flow Rate 17
1.7.5 Compressible fluid/Incompressible fluid 17
1.7.6 Validation 18
1.7.7 Boundary Layer Concept in Fluid Dynamics 18
1.7.8 Skin-friction 19
1.7.9 Suction/Injection 19
1.7.10 Couette Flow 19
1.7.11 Current Density 20
1.8 Dissertation Layout 20

CHAPTER TWO

LITERATURE REVIEW 22

2.1 Introduction 22
2.2 Macro-channel Configurations: MHD Free Convective Flow in Vertical Parallel Plate Channel 22
2.3 Suction-Injection Combination (SIC) on MHD Transient Free Convective Flow in a Vertical Channel 27

2.4 MHD Couette Flow in a Vertical Channel 29
2.5 Micro-channel Configurations: MHD Free-Convective Flow in Annular Micro-channel 32

CHAPTER THREE

MHD FREE CONVECTION FLOW IN VERTICAL CHANNEL 36

3.1 Role of Induced Magnetic Field on Transient Natural Convection flow in a vertical channel: The Riemann-sum Approximation Approach 36
3.1.1 Introduction 36
3.1.2 Mathematical Analysis 37
3.1.3 Skin Friction and Current density 40
3.1.4 Validation of the Method: 41
3.1.5 Results and Discussion 43
3.2 46
3.3 Computational treatment of MHD transient natural convection flow in a vertical channel due to symmetric heating in presence of induced magnetic field 58
3.3.1 Mathematical Analysis 58
3.3.2 Skin Friction and Current Density 61
3.3.3 Steady State Solution 62
3.3.4 Implicit Finite Difference Method 62
3.3.5 Results and Discussion 64

CHAPTER FOUR

TIME DEPENDENT MHD FREE CONVECTIVE FLOW IN VERTICAL CHANNEL 77

4.1 Effects of suction-injection combination (SIC) on MHD transient free-convective flow in a vertical channel in presence of induced magnetic field 77

4.1.1 Mathematical Analysis 78

4.1.2 Skin-friction and Current density 81

4.1.3 Validation 82

4.1.4 Steady State Solution 82

4.1.5 Implicit Finite Difference Method (IFDM) 82

4.1.6 Results and Discussion 83

4.2 Unsteady MHD free-convective Couette flow in presence of Induced Magnetic Field: Impulsive motion 98

4.2.1 Mathematical Analysis 98

4.2.2 Skin-friction 102

4.2.3 Validation 103

4.2.4 Results and Discussion 104

4.2.5 Concluding Remarks 107

CHAPTER FIVE

MHD FREE CONVECTION FLOW IN VERTICAL MICRO-CHANNEL 120

5.1 MHD NATURAL CONVECTION FLOW IN VERTICAL MICRO-CONCENTRIC ANNULI IN PRESENCE OF RADIAL MAGNETIC FIELD: AN EXACT SOLUTION 120

5.1.1 Mathematical Analysis 121

5.1.2 Results and Discussion 124

5.1.3 Concluding Remark 127

5.2 FULLY DEVELOPED MHD NATURAL CONVECTION FLOW IN A VERTICAL ANNULAR MICRO-CHANNEL: AN EXACT SOLUTION 134
5.2.1 Mathematical Analysis 134
5.2.2 Results and Discussion 138
5.2.3 Concluding Remark 141

CHAPTER SIX

MHD FREE CONVECTIVE FLOW IN ANNULAR MICRO-CHANNEL 146

6.1 TRANSIENT MHD FREE CONVECTIVE FLOW IN VERTICAL MICRO-CONCENTRIC ANNULI 147
6.1.1 Mathematical Analysis 147
6.1.2 Transient Volume Flow Rate 151
6.1.3 Skin-Friction and Rate of Heat Transfer 151
6.1.4 Validation of the Method 152
6.1.5 Results and Discussion 153

CHAPTER SEVEN

CONCLUSIONS AND RECOMMENDATIONS 166

7.1 Summary 166
7.2 Conclusion 167
7.3 Recommendations 167

REFERENCES 169

Appendices 184

LIST OF FIGURES

3.2.1 Temperature distribution(θ) for $Pr = 0.71(a)$ and $Pr = 7.0(b)$ at different values of time t. 47

3.2.2 Temperature profiles at different values of Pr for $t = 0.2$. . . . 47

3.2.3 Velocity profiles at different values of time (t) for $M = 0.5$, $Pr = 0.71(a)$ and $7.0(b)$. 48

3.2.4 Velocity profiles at different values of M for $t = 0.2$, $Pr = 0.71(a)$ and $7.0(b)$. 48

3.2.5 Velocity profiles at different values of Pr for $t = 0.2$, $M = 0.5$. 49

3.2.6 Induced Magnetic Field profiles at different values of time (t) for $M = 0.5$, $Pr = 0.71(a)$ and $7.0(b)$. 49

3.2.7 Induced Magnetic Field profiles at different values of M for $t = 0.2$, $Pr = 0.71(a)$ and $7.0(b)$. 50

3.2.8 Induced Magnetic Field profiles at different values of Pr for $t = 0.2$, $M = 0.5$. 50

3.2.9 Current Density profiles at different values of time (t) for $M = 0.5$, $Pr = 0.71(a)$ and $7.0(b)$. 51

3.2.10 Current Density profiles at different values of M for $t = 0.2$, $Pr = 0.71(a)$ and $7.0(b)$. 51

3.2.11 Current Density profiles at different values of Pr for $t = 0.2$, $M = 0.5$ 52

3.2.12 Skin-friction (τ_0) against M at different values of time (t) for $Pr = 0.71(a)$ and $7.0(b)$. 52

3.2.13 Skin-friction (τ_0) against M at different values of Pr for $t = 0.2$. 53

3.2.14 Skin-friction (τ_0) against Pr at different values of t for $M = 0.5$. 53

3.2.15 Skin-friction (τ_1) against M at different values of time (t) for $Pr = 0.71(a)$ and $7.0(b)$. 54

3.2.16 Skin-friction (τ_1) against M at different values of Pr for $t = 0.2$. 54

3.2.17 Skin-friction (τ_1) against Pr at different values of t for $M = 0.5$. 55

3.3.1 Temperature distribution(θ) for $Pr = 0.71(a)$ and $Pr = 7.0(b)$ at different values of time t. 70
3.3.2 Temperature distribution(θ) for $t = 0.2$ at different values of Pr. 70
3.3.3 Velocity profile for $M = 2.0, Pr = 0.71(a)$ and $Pr = 7.0(b)$at different values of t 71
3.3.4 Velocity profile for $t = 0.2$, $Pr = 0.71(a)$ and $Pr = 7.0(b)$ at different values of M 71
3.3.5 Velocity profile for $M = 2.0$ and $t = 0.2$, at different values of Pr 72
3.3.6 Induced Magnetic Field for $M = 2.0, Pr = 0.71(a)$ and $Pr = 7.0(b)$ at different values of t 72
3.3.7 Induced Magnetic Field for $t = 0.2$, $Pr = 0.71(a)$ and $Pr = 7.0(b)$ at different values of M 73
3.3.8 Induced Magnetic Field for $M = 2.0$ and $t = 0.2$, at different values of Pr 73
3.3.9 Current density distribution for $M = 2.0, Pr = 0.71(a)$ and $Pr = 7.0(b)$ at different values of t 74
3.3.10 Current density distribution for $t = 0.2$, $Pr = 0.71(a)$ and $Pr = 7.0(b)$ at different values of M 74
3.3.11 Current density distribution for $M = 2.0$ and $t = 0.2$, at different values of Pr 75
3.3.12 Skin-friction profile at $y = 1$ for $Pr = 0.71(a)$ and $Pr = 7.0(b)$ at different values of M and t. 75
3.3.13 Skin-friction profile at $y = 1$ for $t = 0.2$ at different values of M and Pr. 76
3.3.14 Skin-friction profile at $y = 1$ for $M = 2.0$ at different values of Pr and t. 76

4.1.1 Temperature (θ) against y for different values of dimensionless time (t) at $S = -0.5$, $Pr = 0.71(a), Pr = 7.0(b)$. 89
4.1.2 Temperature (θ) against y for different values of suction/injection (S), at $t = 0.2$, $Pr = 0.71(a), Pr = 7.0(b)$. 89
4.1.3 Velocity (u) profiles against y for different values of dimensionless time (t) at $M = 2.0$, $S = -0.5$, $Pr = 0.71(a), Pr = 7.0(b)$. 90
4.1.4 Velocity (u) profiles against y for different values of magnetic parameter (M) at $t = 0.2$, $S = -0.5$, $Pr = 0.71(a), Pr = 7.0(b)$. 90
4.1.5 Velocity (u) profiles against y for different values of suction/injection (S) at $M = 2.0$, $t = 0.2$, $Pr = 0.71(a), Pr = 7.0(b)$. 91
4.1.6 Velocity (u) profiles versus S for different values of Pr at $M = 2.0$, $t = 0.2$ and $y = 0.5$. 91
4.1.7 Induced magnetic field (h) against y for different values of dimensionless time (t) at $S = -0.5$, $M = 2.0$, $Pr = 0.71(a), Pr = 7.0(b)$. 92
4.1.8 Induced magnetic field (h) against y for different values of magnetic parameter (M) at $S = -0.5$, $t = 0.2$, $Pr = 0.71(a), Pr = 7.0(b)$. 92
4.1.9 Induced magnetic field (h) against y for different values suction/injection (S) at $M = 2.0$, $t = 0.2$, $Pr = 0.71(a), Pr = 7.0(b)$. 93
4.1.10 Induced magnetic field (h) versus S for different values of Pr at $M = 2.0$, $t = 0.2$ and $y = 0.5$. 93
4.1.11 Current density (J) against y for different values of dimensionless time (t), at $S = -0.5$, $M = 2.0$, $Pr = 0.71(a), Pr = 7.0(b)$. 94
4.1.12 Current density (J) against y for different values of magnetic parameter (M), at $S = -0.5$, $t = 0.2$, $Pr = 0.71(a), Pr = 7.0(b)$. 94

4.1.13 Current density (J) against y for different values of suction/injection S, at $t = 0.2$, $M = 2.0$, $Pr = 0.71(a), Pr = 7.0(b)$. 95
4.1.14 Skin-friction (τ_0) versus S for different values of dimensionless time (t) for $M = 2.0$, $Pr = 0.71(a), Pr = 7.0(b)$. 95
4.1.15 Skin-friction (τ_1) versus S for different values of dimensionless time (t) at $M = 2.0$, $Pr = 0.71(a), Pr = 7.0(b)$. 96
4.1.16 Skin-friction (τ_0) versus M for different values of Pr at $S = -0.5$, $t = 0.2$. 96
4.1.17 Skin-friction (τ_1) versus M for different values of Pr at $S = -0.5$, $t = 0.2$. 97
4.2.1 Velocity (u) distribution at different values of time t for $Gr = 10$, $M = 0.5$, $Pr = 0.71(a)$ and $7.0(b)$. 108
4.2.2 Velocity (u) distribution at different values of Gr for $t = 0.2$, $M = 0.5$, $Pr = 0.71(a)$ and $7.0(b)$. 111
4.2.3 Velocity (u) distribution at different values of M for $Gr = 10$, $t = 0.2$, $Pr = 0.71(a)$ and $7.0(b)$. 112
4.2.4 Velocity (u) distribution at different values of Pr for $Gr = 10$, $M = 0.5$, $t = 0.2$. 112
4.2.5 Induced Magnetic Field (h) at different values of time t for $Gr = 10$, $M = 0.5$, $Pr = 0.71(a)$ and $7.0(b)$. 113
4.2.6 Induced Magnetic Field (h) at different values of Gr for $t = 0.2$, $M = 0.5$, $Pr = 0.71(a)$ and $7.0(b)$. 113
4.2.7 Induced Magnetic Field (h) at different values of M for $Gr = 10$, $t = 0.2$, $Pr = 0.71(a)$ and $7.0(b)$. 114
4.2.8 Induced Magnetic Field (h) at different values of Pr for $Gr = 10$, $M = 0.5$, $t = 0.2$. 114
4.2.9 Current density (J) at different values of time t for $Gr = 10$, $M = 0.5$, $Pr = 0.71(a)$ and $7.0(b)$. 115

4.2.10 Current density (J) at different values of Gr for $t = 0.2$, $M = 0.5$, $Pr = 0.71(a)$ and $7.0(b)$. 115
4.2.11 Current density (J) at different values of M for $Gr = 10$, $t = 0.2$, $Pr = 0.71(a)$ and $7.0(b)$. 116
4.2.12 Current density (J) at different values of Pr for $Gr = 10$, $M = 0.5$, $t = 0.2$. 116
4.2.13 Skin-friction (τ_0) against M at different values of time t for $Gr = 10$, $M = 0.5$, $Pr = 0.71(a)$ and $7.0(b)$. 117
4.2.14 Skin-friction (τ_0) against M at different values of Gr for $t = 0.2$, $M = 0.5$, $Pr = 0.71(a)$ and $7.0(b)$. 117
4.2.15 Skin-friction (τ_0) against M at different values of Pr for $Gr = 10$, $t = 0.2$. 118
4.2.16 Skin-friction (τ_1) against M at different values of time t for $Gr = 10$, $M = 0.5$, $Pr = 0.71(a)$ and $7.0(b)$. 118
4.2.17 Skin-friction (τ_1) against M at different values of Gr for $t = 0.2$, $M = 0.5$, $Pr = 0.71(a)$ and $7.0(b)$. 119
4.2.18 Skin-friction (τ_1) against M at different values of Pr for $Gr = 10$, $t = 0.2$. 119

5.1.1 Flow configuration and coordinate system. 122
5.1.2 Velocity distribution for different values of $\beta_\nu Kn$ with $F = 1.64$ and $M = 2.0$ 129
5.1.3 Velocity distribution for different values of F with $\beta_\nu Kn = 0.05$ and $M = 2.0$ 129
5.1.4 Velocity distribution for different values of M with $\beta_\nu Kn = 0.05$ and $F = 1.64$ 130
5.1.5 Volume flow rate versus $\beta_\nu Kn$ for different values of F with $M = 2.0$ 130
5.1.6 Volume flow rate versus $\beta_\nu Kn$ for different values of M with $F = 1.64$ 131

5.1.7 Variation of skin friction for different values of F at $R = 0$ . . 131
5.1.8 Variation of skin friction for different values of F at $R = 1$ . . 132
5.1.9 Variation of skin friction for different values of M at $R = 0$. 132
5.1.10 Variation of skin friction for different values of M at $R = 1$ . . 133
5.2.1 Flow configuration and coordinate system. 135
5.2.2 Velocity distribution for different values of $\beta_\nu Kn$ with $F =$ 1.64 and $M = 2.0$ 142
5.2.3 Velocity distribution for different values of F with $\beta_\nu Kn =$ 0.05 and $M = 2.0$ 142
5.2.4 Velocity distribution for different values of M with $\beta_\nu Kn =$ 0.05 and $F = 1.64$ 143
5.2.5 Volume flow rate versus $\beta_\nu Kn$ for different values of F with $M = 2.0$ 143
5.2.6 Volume flow rate versus $\beta_\nu Kn$ for different values of M with $F = 1.64$ 144
5.2.7 Variation of skin friction for different values of F at $R = 0$ . . 144
5.2.8 Variation of skin friction for different values of F at $R = 1$ . . 145
5.2.9 Variation of skin friction for different values of M at $R = 0$. 145
5.2.10 Variation of skin friction for different values of M at $R = 1$ . . 145

6.1.1 Flow configuration and coordinate system. 148
6.1.2 Temperature distribution for different values of time (t) with $F = 1.64$, $Pr = 0.71$, $\beta_\nu Kn = 0.05$. 158
6.1.3 Temperature distribution for different values of Pr with $t =$ 0.2,$\beta_\nu Kn = 0.05$, $F = 1.64$ 158
6.1.4 Temperature distribution for different values of $\beta_\nu Kn$ with $t = 0.2$, Pr, $F = 1.64$ 158
6.1.5 Temperature distribution for different values of F with $t =$ 0.2, $Pr = 0.71$, $\beta_\nu Kn = 0.05$. 159

6.1.6 Velocity distribution for different values of time (t) with $M = 2$, $F = 1.64$, $Pr = 0.71$, $\beta_\nu Kn = 0.05$. 159
6.1.7 Velocity distribution for different values of Pr with $M = 2.0$, $t = 0.2$, $\beta_\nu Kn = 0.05$, $F = 1.64$ 159
6.1.8 Velocity distribution for different values of $\beta_\nu Kn$ with $t = 0.2$, $Pr = 0.71$, $F = 1.64$ 160
6.1.9 Velocity distribution for different values of F with $M = 2$, $t = 0.2$, $Pr = 0.71$, $\beta_\nu Kn = 0.05$. 160
6.1.10 Velocity distribution for different values of M, with $t = 0.2$, Pr, $F = 1.64$, $\beta_\nu Kn$ 160
6.1.11 Volume flow rate versus $\beta_\nu Kn$ for different values of time (t) with $F = 1.64$, $M = 2.0$, $Pr = 0.71$. 161
6.1.12 Volume flow rate versus $\beta_\nu Kn$ for different values of F with $M = 2$, $t = 0.2$, $Pr = 0.71$. 161
6.1.13 Volume flow rate versus $\beta_\nu Kn$ for different values of M with $t = 0.2$, $Pr = 0.71$, $F = 1.64$ 161
6.1.14 Rate of heat transfer versus $\beta_\nu Kn$ for different values of time (t) with $F = 1.64$, $Pr = 0.71$ at $r = 0$. 162
6.1.15 Rate of heat transfer versus $\beta_\nu Kn$ for different values of time (t) with $F = 1.64$, $Pr = 0.71$ at $r = 1$. 162
6.1.16 Rate of heat transfer versus $\beta_\nu Kn$ for different values of Pr with $t = 0.2$, $F = 1.64$ at $r = 0$. 162
6.1.17 Rate of heat transfer versus $\beta_\nu Kn$ for different values of Pr with $t = 0.2$, $F = 1.64$ at $r = 1$. 163
6.1.18 Rate of heat transfer versus $\beta_\nu Kn$ for different values of F with $t = 0.2$, $Pr = 0.71$ at $r = 0$. 163
6.1.19 Rate of heat transfer versus $\beta_\nu Kn$ for different values of F with $t = 0.2$, $Pr = 0.71$ at $r = 1$. 163

6.1.20 Skin friction versus $\beta_\nu Kn$ for different values of time (t) with $F = 1.64$, $M = 2.0$, $Pr = 0.71$ at $r = 0$. 164
6.1.21 Skin friction versus $\beta_\nu Kn$ for different values of time (t) with $F = 1.64$, $M = 2.0$, $Pr = 0.71$ at $r = 1$. 164
6.1.22 Skin friction versus $\beta_\nu Kn$ for different values of F with $M = 2.0$, $t = 0.2$, $Pr = 0.71$ at $r = 0$. 164
6.1.23 Skin friction versus $\beta_\nu Kn$ for different values of F with $M = 2.0$, $t = 0.2$, $Pr = 0.71$ at $r = 1$. 165
6.1.24 Skin friction versus $\beta_\nu Kn$ for different values of M with $F = 1.64$, $t = 0.2$, $Pr = 0.71$ at $r = 0$. 165
6.1.25 Skin friction versus $\beta_\nu Kn$ for different values of M with $F = 1.64$, $t = 0.2$, $Pr = 0.71$ at $r = 1$. 165

LIST OF TABLES

3.2.1 Numerical values of the flow velocity u obtained using the Riemann-Sum approximation method (RSM) compared to those obtained by the finite difference method FDM) and the Steady State (SS) for $Pr = 0.71, Pm = 1.0$ and $M = 0.5$ at different value of t. 56

3.2.2 Numerical values of the induced magnetic field h obtained using the Riemann-Sum approximation method (RSM) compared to those obtained by the finite difference method (FDM) and the Steady State (SS) for $Pr = 0.71$, $Pm = 1.0$ and $M = 0.5$ at different value of t. 56

3.2.3 Numerical values for velocity u and that of the Induced Magnetic field h obtained by the finite difference for $Pr = 0.71$, $M = 0.5$, $t = 0.2$, at different value of Pm. 57

3.3.1 Numerical values of the velocity u obtained using the Riemann-Sum approximation method (RSM) compared to those obtained by the finite difference method (FDM) and the steady state (SS) for $Pr = 0.71, Pm = 1.0$ and $M = 2.0$ at varying values of t. 68

3.3.2 Numerical values of the induced magnetic field h obtained using the Riemann-Sum approximation method (RSM) compared to those obtained by the finite difference method (FDM) and the steady state (SS) for $Pr = 0.71$, $Pm = 1.0$ and $M = 2.0$ at varying values of t. 68

3.3.3 Numerical values for velocity u and that of the induced magnetic field h obtained by the finite difference method for $Pr = 0.71$, $Pm = 1.0$, $t = 4.0$ at varying values of M 69

3.3.4 Numerical values for velocity u and that of the Induced Magnetic field h obtained by the finite difference for $Pr = 0.71$, $M = 2.0$, $t = 4.0$, at varying values of Pm 69

4.1.1 Numerical values of the velocity (u) obtained using the Riemann-Sum approximation method (RSM) compared to those obtained by the finite difference method (FDM) and the steady state (SS) for $Pr = 0.71$, $Pm = 1.0$, $S = -0.5$ and $M = 2.0$ at varying values of t. 87

4.1.2 Numerical values of the induced magnetic field (h) obtained using the Riemann-Sum approximation method (RSM) compared to those obtained by the finite difference method (FDM) and the steady state (SS) for $Pr = 0.71$, $Pm = 1.0$,$S = -0.5$ and $M = 2.0$ at varying values of t. 88

4.1.3 Numerical values for velocity (u) and that of the Induced Magnetic field h obtained by the finite difference (FDM) for $Pr = 0.71$, $M = 2.0$, $t = 0.2$, $S = -0.5$ for various values of Pm 88

4.2.1 Numerical values of the velocity u obtained using the Riemann-Sum approximation method (RSM) compared to those obtained by the finite difference method (FDM) and the steady state (SS) for $Gr = -10.0$ $Pr = 0.71, Pm = 1.0$ and $M = 0.5$ with varying values of t. 108

4.2.2 Numerical values of the induced magnetic field h obtained using the Riemann-Sum approximation method (RSM) compared to those obtained by the finite difference method (FDM) and the steady state (SS) for $Gr = -10.0$ $Pr = 0.71$, $Pm = 1.0$ and $M = 0.5$ with varying values of t. 109

4.2.3 Numerical values for velocity u and that of the induced magnetic field h obtained by the finite difference method (FDM) for $Gr = -10.0$, $Pr = 0.71$, $Pm = 1.0$, $t = 0.2$ at varying values of M. 109

4.2.4 Numerical values of the velocity u obtained using the Riemann-Sum approximation method (RSM) compared to those obtained by the finite difference method (FDM) and the steady state (SS) for $Gr = -10.0$ $Pr = 0.71, Pm = 1.0$ and $M = 0.5$ with varying values of t. 110

4.2.5 Numerical values of the induced magnetic field h obtained using the Riemann-Sum approximation method (RSM) compared to those obtained by the finite difference method (FDM) and the steady state (SS) for $Gr = -10.0$ $Pr = 0.71$, $Pm = 1.0$ and $M = 0.5$ with varying values of t. 110

4.2.6 Numerical values for velocity u and that of the induced magnetic field h obtained by the finite difference method (FDM) for $Gr = -10.0$, $Pr = 0.71$, $M = 0.5$, $t = 0.2$ at varying values of Pm. 111

5.1.1 Comparison of the values of velocity obtained in the present work with those obtained by Weng and Chen (2009) 127

6.1.1 Comparison of the numerical value of the transient state velocity obtained using Riemann-sum approximation method and the steady state obtained analytically when $M = 2.0$, $F = 1.64$, $Pr = 0.71$, $\beta_\nu Kn = 0.05$ and $\eta = 0.5$. 157

DIMENSIONLESS QUANTITIES

The problems formulated in this thesis results to partial differential equations, which can be solved using advanced mathematical techniques. In the process of obtaining the solution however, involves decoupling of the coupled equations, which is very tedious. Moreover, the solution involves too many parameters that make graphical presentation of results impossible. Therefore, the need to reduce the number of parameters by nondimensionalizing the problem in question by defining suitable dimensionless quantities. The dimensionless quantities that are frequently used in this thesis are;

Reynolds number

This is a dimensionless quantity that can be defined for several different situations where a fluid is in relative motion to a surface. These definitions generally include the fluid properties of density and viscosity, plus a velocity and a characteristic length or characteristic dimension. The concept was introduced by Stokes (1851), but the Reynolds number is named after Osborne Reynolds (1842–1912), who popularized its use in 1883. It is defined as the ratio of inertial forces to viscous forces and consequently quantifies the relative importance of these two types of forces for given flow conditions. It is expressed as

$$Re = \frac{Inertia\ forces}{Viscous\ forces} = \frac{U_0 L}{\nu}.$$

Magnetic Reynolds number

This is one the dimensionless quantity appearing in MHD which is indicative of the relative strengths of advection and diffusion in the induction equation

(1.1.9)

$$Rm = \frac{Convection\ of\ B}{Diffusion\ of\ B} = \frac{Induced\ field}{Applied\ field} = \frac{U_0 L}{\nu} = \mu_e \sigma U_0 L.$$

Prandtl number

The relative thickness of the velocity and the thermal boundary layers is best described by the dimensionless parameter called Prandtl number (Pr) which is defined as

$$\begin{aligned} Pr &= \frac{Molecular\ diffusivity\ of\ momentum}{Molecular\ diffusivity\ of\ heat} \\ &= \frac{\nu}{\alpha} = \frac{\mu C_p}{k}. \end{aligned}$$

Magnetic Prandtl number

This is a dimensionless quantity occurring in magnetohydrodynamics which approximates the ratio of momentum diffusivity (viscosity) and magnetic diffusivity. It is defined as

$$\mathrm{Pm} = \frac{\mathrm{Rm}}{\mathrm{Re}} = \frac{\nu}{\mu_e} = \frac{\text{viscous diffusion rate}}{\text{magnetic diffusion rate}}.$$

Grashof number

This is a dimensionless number which approximates the ratio of the buoyancy to viscous force acting on a fluid. It is named after the German engineer Franz Grashof and frequently arises in the study of situations involving natural convection. Mathematically, it is presented as;

$$\mathrm{Gr} = \frac{g\beta(T_s - T_\infty)L^3}{\nu^2}.$$

Hartmann number

This represents the ratio of the Lorentz force (Electromagnetic forces) to viscous forces and are expressed as;

$$\mathrm{M} = \left[\frac{Electromagnetic\ forces}{Viscous\ forces}\right]^{\frac{1}{2}} = BL\sqrt{\frac{\sigma}{\nu\rho}}$$

Knudsen number

This is another dimensionless number defined as the ratio of the molecular mean free path length to a representative physical length scale. This length scale could be, for example, the radius of the body in a fluid. It is named after Danish physicist Martin Knudsen (1871–1949). The number is express as

$$\mathrm{Kn} = \frac{\lambda}{\mathrm{L}}$$

SYMBOLS AND NOTATIONS

B - magnetic field intensity

Gr - Grashof number

g - acceleration due to gravity (gs^{-2})

F - fluid-wall interaction parameter

H_0' - Uniform external magnetic field

L - characteristic length (L)

M - Hrtmann number

I_0 - zeroth-order modified Bessel function of the first kind

I_1 - first-order modified Bessel function of the first kind

K_0 - zeroth-order modified Bessel function of the second kind

K_1 - first-order modified Bessel function of the second kind

k - thermal conductivity

k_1 - dimensionless radius of inner cylinder

k_2 - dimensionless radius of outer cylinder

Kn - Knudsen number

u - dimensionless velocity

h - dimensionless induced magnetic field

T_s - surface temperature (K)

T_∞ - bulk temperature (K)

t - dimensionless time

y - dimensionless coordinate normal to the channel plates

Pm - magnetic Prandtl number

Pr - Prandtl number

Q - dimensionless volume flow rate

q - volume flow rate

R - dimensionless radial coordinate

r - dimensional radial coordinate

$\hat{R}$ - specific gas constant

Re - Reynolds number

$\Re e$ - real part of a complex number

u' - velocity of the fluid

h' - induced magnetic field

t' - time

T' - dimensional temperature of the fluid

T - temperature of the fluid

U_0 - reference velocity

Greek Letters

α - thermal diffusivity of the fluid

β - coefficient of thermal expansion

β_ν, β_t - dimensionless parameters

$\beta_\nu Kn$ - rarefaction parameter

η - radius ratio

λ - molecular mean free path

σ - electrical conductivity of fluid

σ_t, σ_ν - thermal and tangential momentum accommodation coefficient respectively

τ - skin-friction

ν - kinematic viscosity

μ - dynamic viscosity

μ_e - magnetic permeability

μ_0 - shear viscosity

ρ_0 - density (ML^{-3})

θ' - the dimensionless temperature

CHAPTER ONE

GENERAL INTRODUCTION

1.1 Introduction

Magnetohydrodynamics (MHD) can be regarded as a combination of fluid mechanics and electromagnetism, that is, the behaviour of electrically conducting fluids in the presence of magnetic and electric fields (Sutton and Sherman, 1965). MHD phenomenon basically, result from mutual interaction effect of magnetic field and electrically conducting fluid flowing across the channel and these interactions generate a force called the Lorentz force. Examples of such fluids include plasmas (hot ionized gases), liquid metals, and salt water or electrolytes. The word Magnetohydrodynamics (MHD) is derived from *magneto-* meaning magnetic field, *hydro-* meaning liquid (fluids), and *dynamics*-meaning movement (forces and laws of motion (Alfvén, 1942)). In 1832, Faraday had tried vainly to measure the voltage induced across the river Thames by the motion of the water in the earth's magnetic field (electromagnetic induction). The principle behind this unsuccessful experiment laid the foundations of modern MHD flow meters (Faraday, 1832). The first appearance of a proposal for applying electromagnetic induction phenomenon in technical devices with electrically-conducting liquids and gases was seen in the beginning of the 20th century. The description of MHD flows involves the Navier-Stokes equations of fluid dynamics and the Maxwell's equations (equations of electrodynamics); which are mutually coupled through the Lorentz force and Ohm's law for moving electrical conductors. Systematic studies of magnetohydrodynamic (MHD) flows began in the 30s, through the pioneering works of Hartmann (1937) [1], Hartmann and Lazarus (1937) who studied both theoretically and experimen-

[1] Hartmann,(1881 - 1951), was a leading Professor at the Technical University of Denmark, in Copenhagen, where he founded the Laboratoriet for teknisk fysik, now Department of Applied Physics.

tally, the flow of an electrically conducting fluid between two parallel plates. However, these studies on the flow of an electrically conducting incompressible fluid between two parallel horizontal plates lead to the well-known Hartmann flow and had since then, laid the foundation for MHD investigations. In 1942, Celebrated Nobel laureate, Swedish electrical engineer and plasma physicist Hannes Olof Góasta Alfvén [2], had combined classical electromagnetism with fluid mechanics and developed the theory of magnetohydrodynamics and was the first to introduce the term Magnetohydrodynamics (MHD).

The interests of many researches have been acknowledged in the study of behaviours of unsteady laminar free convection flow for some decade ago. However, this area continue to draw much attention due to its vast scientific and technological applications, such as in the early stage of melting and in transient heating of insulating air gap by heat input at the start-up of furnace, solar heating, ventilating passive systems and electric equipment in construction of vertical circuit boards which can be modelled by parallel heated plates with upward flow in the intervening space as reported by Jha et al (2011). Also, unsteady laminar free convection is used in energy storage system, combustion in underground reservoir for enhancement of oil recovery, storage of grain, food and vegetables, industrial and agricultural water distribution as identified by Singh et al (2011). It is generally accepted that prior to this decade, heat transfer characterised by laminar free-convection were studied with deep-seated scientific and engineering curiosity. Hence the literature continues to grow. This is evident when one realizes that the Industrial Revolution has been largely based on man's increasing ability to convert heat to useful work, and this inevitably involved the ability to design systems to transfer a predictable amount of heat per unit of time. The interest in this area stems largely to its important applications, for instance, the requirement of obtaining high rates of heat extraction from reactors with irreversible temperature drop as little as

[2]Winner of the 1970 Nobel Prize in Physics.

possible in nuclear engineering, the need for effective blade-cooling systems in gas turbines. However, combined heat and mass transfer problems are important in many processes and have therefore received a considerable amount of attention. In many mass transfer processes, heat transfer considerations arise due to the very nature of the process. In processes such as drying, evaporation at the surface of a water body, energy transfer in a wet cooling tower and the flow in a desert cooler, heat and mass transfer occur simultaneously.

1.1.1 Governing Equations of MHD

The set of equations describing MHD are set of equations comprising the Navier-Stokes equations of fluid dynamics and the Maxwell's equations of electromagnetism. The solutions of these differential equations are obtain simultaneously, either analytically or numerically.

1.1.2 Continuity Equation

Continuity Equation or Conservation of mass is a basic tool in the study of fluid flow. It expresses the fact that, in a fluid particle, per unit volume, V , the total sum of all masses, m, flowing in and out per unit time t, must be equal to the change in mass due to change in density, ρ, per unit time (Dalton, 2009). For unsteady flows of a general fluid, this yields,

$$\frac{\partial \rho}{\partial t} + \nabla \cdot (\rho V) = 0 \tag{1.1.1}$$

which is the mass continuity equation. However, the term $\nabla \cdot (\rho V)$ in (eq.1.1.1) is called the divergence of (ρV) and it is written in the case of 3D-fluid flow as;

$$\nabla \cdot (\rho V) = \frac{\partial}{\partial x}(\rho u) + \frac{\partial}{\partial y}(\rho v) + \frac{\partial}{\partial z}(\rho w) \tag{1.1.2}$$

For a constant ρ in the case of incompressible fluid flow, which is our concern in this study. The mass continuity equation reduces ($\frac{\partial \rho}{\partial t} = 0$) to;

$$\nabla \cdot V = 0 \tag{1.1.3}$$

and for $V = (u, v, w)$ is the velocity vector having components u in the x-direction, v in the y-direction and w in the z-direction, therefore, the continuity equation is given as

$$\frac{\partial u}{\partial x} + \frac{\partial v}{\partial y} + \frac{\partial w}{\partial z} = 0 \tag{1.1.4}$$

In the dissertation, we have considered one dimensional flow so that the continuity equation is

$$\frac{\partial u}{\partial x} = 0 \tag{1.1.5}$$

1.1.3 Navier-Stokes Equation

Navier-Stokes equations described the motion of fluid substances. They arise from applying Newton′s second law to fluid motion, assuming that the fluid stress is the sum of a diffusing viscous term (proportional to the gradient of velocity) and a pressure term. They are named after Claude-Louis Navier and George Gabriel Stokes. Their Solution is called a velocity field or flow field, which is a description of the velocity of the fluid at a given point in space and time is given by.

$$\rho \frac{\partial V}{\partial t} + \rho(V \cdot \nabla)V + \nabla p = \mu \nabla^2 V + \rho g + J \times B \tag{1.1.6}$$

In the absence of gravity and considering incompressibility (i.e $g = 0$ and $\nabla \cdot V = 0$, the Navier- Stokes Equation is

$$\rho \frac{\partial V}{\partial t} + \rho(V \cdot \nabla)V + \nabla p = \mu \nabla^2 V \tag{1.1.7}$$

which is the normal Navier-Stokes equation for incompressible fluid.

1.1.4 MHD Induction Equation

The MHD induction equation is given as (Davidson, 2001)

$$\frac{\partial \mathbf{B}}{\partial t} = \nabla \times (V \times \mathbf{B}) - \frac{1}{\mu_e}\nabla \times \frac{\nabla \times \mathbf{B}}{\sigma} - \nabla \times \left[\frac{\mathbf{B}}{\mu_e}(\nabla \times \mathbf{B}) \times \mathbf{B}\right] \tag{1.1.8}$$

or

$$\frac{\partial \mathbf{B}}{\partial t} = \nabla \times (V \times \mathbf{B}) + \alpha \nabla^2 \mathbf{B} \tag{1.1.9}$$

where α is the magnetic diffusivity which is given as $\frac{1}{\mu_e \sigma}$

1.1.5 Energy Equation

The energy equation is written as (Davidson, 2001)

$$\rho c_p \left[\frac{\partial T}{\partial t} + (q\nabla)T\right] = \kappa \nabla^2 T + \phi + \frac{J^2}{\sigma} \tag{1.1.10}$$

1.1.6 Maxwell's Equations

Maxwell′s equations are a set of partial differential equations that, together with the Lorentz force law, form the foundation of classical electrodynamics, classical optics, and electric circuits. These fields in turn underlie modern electrical and communications technologies. These equations describe the behaviour of electric E and magnetic B fields and are named after a Scottish mathematical physicist, James Clerk Maxwell (Fleisch, 2008). Therefore, the simplified form of these equations are;

$$Faraday's\ Law \qquad \nabla \times E = -\frac{\partial \mathbf{B}}{\partial t} \tag{1.1.11}$$

$$Ampere's\ CircuitalLaw \qquad \nabla \times \mathbf{B} = \mu_e J \tag{1.1.12}$$

$$Solenoidal\ Constrant \qquad \nabla \cdot \mathbf{B} = 0 \tag{1.1.13}$$

$$Charge\ Conservation \qquad \nabla \cdot J = 0 \tag{1.1.14}$$

$$Ohm's\ Law \qquad J = \sigma[E + V \times \mathbf{B}] \tag{1.1.15}$$

$$Lorentz\ force \qquad F = J \times \mathbf{B} \tag{1.1.16}$$

Note that total magnetic field $\mathbf{B}$ is related to the magnetic field intensity (or magnetic field strength, H) as $\mathbf{B} = \mu_0\mathbf{H}$ if the magnetization is proportional to the magnetic field. Also, it is assumed accurate for liquid metals and gases in most MHD problems, although it is not true in general for all types of flows. When $E \neq 0$, the polarization effects are non-negligible and the magnetic Reynold's number is large, thereby considering the induced magnetic field. These are some of the assumptions used to reduce the Maxwell's equations to an MHD approximation form.

1.2 Statement of the Problem

In recent years studies on macro and micro channels have been on the increase due to their wider application in many technological and engineering processes. Also, the flow analysis of MHD natural convection in both macro- and micro-channels has been an important area of investigation due to its practical application in industry. This configuration exists in several practical systems such as electronic equipment, furnace and heat exchangers (Jha, 1998). Considering this enormous increase in practical applications as enunciated in Singh et al. (2010) and Weng and Chen (2009), it is imperative that this present study is undertaken. Therefore, the need in this study, to investigate the flow behaviour of an electrically conducting fluid in macro and micro-channel under different geometries and the following problems are formulated;

1. Role of induced magnetic field on transient natural convection flow in a vertical channel: The Riemann-sum Approximation Approach[3]

[3] ***Int. J. of Applied Mechanics and Engineering, vol. 20, No.1, (2015), pp.65-85(DOI: 10.1515/ijame-2015-0005)*** Poland

2. Computational treatment of MHD transient natural convection flow in a vertical channel due to symmetric heating in presence of induced magnetic field[4]

3. Effects of suction-injection combination (SIC) on MHD transient free-convective flow in a vertical channel in presence of induced magnetic field

4. Unsteady MHD free-convective Couette flow in presence of Induced Magnetic Field: Impulsive motion

5. MHD natural convection flow in vertical micro-concentric annuli in presence of radial magnetic field: An exact solution[5]

6. Fully Developed MHD Natural Convection flow in a Vertical annular Microchannel: An exact solution[6]

7. Transient MHD Free Convective Flow in Vertical Micro-concentric Annuli [7]

1.3 Research Objectives

1.3.1 General Objective

The general objective of this dissertation is to study the flow behaviour of an electrically conducting, viscous and incompressible fluid flowing in a macro-channel formed by two vertical parallel plates and also in vertical annular micro-channel formed by two concentric cylinders with a magnetic field applied

[4] ***Journal of the Physical Society of Japan(JPSJ) 82 (2013)*** *084401* ($IF = 2.087$)
[5] **Ain Shams Engineering Journal (2015) Accepted** (Elsevier)
[6] ***Journal of King Saud University - Science vol. 27, (2015), 253 - 259*** ($IF = 0.787$)
[7] ***J. Nanoengineering and Nanosystems 1 - 12 IMechE 2015 DOI: 10.1177/1740349915578956*** (SAGE)UK

perpendicular to the flow direction, subjected to different boundary conditions and fluid properties. In addition, the influence of different parameters that govern the flows shall be discussed.

1.3.2 Specific Objectives

The targeted specific objectives are to;

1. investigate the role of Induced Magnetic Field on Transient Natural Convection Flow in a Vertical Channel:The Riemann Sum Approximation Approach

2. present a computational treatment of MHD transient natural convection flow in a vertical channel due to symmetric heating in presence of induced magnetic field

3. investigate the effects of suction-injection combination (SIC) on MHD transient free-convective flow in a vertical channel in presence of induced magnetic field

4. present a semi-analytical solution to unsteady MHD free-convective Couette flow in presence of Induced Magnetic Field: Impulsive motion

5. discuss transient MHD free convective flow in vertical micro-concentric annuli

6. present a solution of fully developed MHD natural convection flow in a vertical annular micro-channel: An Exact Solution

7. investigate the influence of wall surface curvature on steady fully developed MHD natural convection flow of viscous, incompressible, electrically conducting fluid in micro-concentric annuli in presence of radial magnetic field

1.4 Significance of the Study

Natural convection in real fluids has been extensively studied due to its widespread applications in industry and geophysics. Most of the studies on natural convective heat and mass transfer phenomena under different physical geometries in the presence of a magnetic field have been limited to the case when the induced magnetic field is not taken into consideration, despite its vital role in many physical situations (Singh et al., 2010). Moreover, the progress in science and technology in recent years have promoted a rapid development of different microfluidic devices in physical, chemical, biological, medical, engineering, and energy-related fields. Due to the difficulty in making precise measurements, microscale gas flow and heat transfer modeling was emphasized in modern microfluidic applications, such as microelectrochemical cell transport, microheat exchanging, and microchip cooling, etc. (Weng and Chen, 2013). Therefore, the results obtained in the present investigations will no doubt find its application in these and similar areas. Most importantly, this study will form the basis for further mathematical investigations in macro and micro- channel flows.

1.5 Research Questions

The stated objectives above will be achieved by answering the following questions:

1. which mathematical model(s) and the necessary boundary conditions can be formulated for Macro- and Micro-channel problems considered for the present study?

2. what shall be the role of Induced Magnetic Field on MHD transient natural convection flow in a vertical channel due to asymmetric and

symmetric heating of the channel walls?

3. what are the effects of suction/injection combination (SIC) on MHD transient free-convective flow in a vertical channel in presence of induced magnetic field?

4. is the exact solution of fully developed MHD natural convection flow in a vertical annular micro-channel possible?

5. what are the effects of wall surface curvature on MHD natural convective flow in micro-concentric annuli in presence of radial magnetic field ?

1.6 Research Methodology

The methodology to be employ in this investigation involves;

1. formulation and modification of existing mathematical models and boundary conditions (Singh et al. (2010), Jha and Apere (2010) and Weng and Chen (2009)).

2. obtain analytical solutions through Laplace transform technique where possible, otherwise we use Riemann sum approximation method.

3. validate the obtained results using finite difference method

4. generate line graphs for the numerical values using MATLAB

5. interpret, discuss and draw conclusions.

The mathematical methods used in obtaining several solutions in mathematics, mathematical physics and engineering problems as part of the methodology found worthy for the present study are as follows;

1.6.1 Laplace Transform

This is an integral transform introduced by Laplace[8] during his studies of probability. The English mathematician and engineer Oliver Heaviside had extensively used the methods of Laplace transforms in the name of operational calculus in solving linear differential equations arising from electrical networks. The Laplace transform, in its common form, applies to functions that are causal. This limitation, compared to the Fourier transform, is more than compensated by the fact that the Laplace transform can be applied to exponentially growing functions. These two features make the Laplace transform ideal for time-dependent functions, which are zero for $t < 0$ and bounded by an exponentially growing function. The main idea behind the Laplace Transform is that, it is a technique that stood the test of time that convert system of differential equations to a purely algebraic equations. These equations are solved and their solutions are inverted back to the function solving the initial value problem. This makes the problem much easier to solve.

Exponential Order

A function $f(t)$ is said to be of exponential order as $t \to \infty$ if there exists a real number ϱ and positive constants M and T such that

$$|f(t)| < Me^{\varrho t} \quad \forall t \in T \tag{1.6.1}$$

Definition

Let $f(t)$ be continuous and single valued function of the real variable t for all $0 < t < \infty$, and is of exponential order. Then the Laplace transform of $f(t)$ is

[8]French mathematician Pierre Simon de Laplace (1749 - 1827)

defined as a function $\bar{f}(s)$ denoted by the integral

$$L|f(t)| = \bar{f}(s) = \int_0^\infty f(t)e^{-st}dt, s > 0 \tag{1.6.2}$$

over that range of values of s for which the integral exist. Here s is a parameter which may be real or complex. Obviously, $L(f(t))$ is a function of s. Thus,

$$L|(f(t))| = \bar{f}(s) \tag{1.6.3}$$

$$f(t) = L^{-1}[\bar{f}(s)] = \frac{1}{2\pi}\int_{\lambda_1-i\infty}^{\lambda_1+i\infty} \bar{f}(s)e^{st}ds \tag{1.6.4}$$

where L is the operator which transforms $f(t)$ into $\bar{f}(s)$, called the Laplace transform operator, and L^{-1} is the inverse Laplace transform operator.

Theorem

If the causal function $f(t)$ is piecewise-continuous on $[0, \infty]$ and is of exponential order, with abscissa of convergence ϱ_c,then the Laplace transform $F(s)$ of $f(t)$ exists, with region of convergence $\Re e(s) > \varrho_c$ in the s domain; that is

$$L\{f(t)\} = F(s) = \int_0^\infty e^{-st}f(t)dt, \tag{1.6.5}$$

for $\mathrm{Re}(s) > \varrho_c$.

1.6.2 Riemann Sum Approximation

Although, numerical inverse Laplace transform is generally an ill posed problem, it become necessary when Laplace transform cannot be inverted analytically by manipulating tabled formulas of special cases. There is no universal method which works well for all problems (Quanrong and Hongbin, 2015). In this study, we have chosen Riemann-sum approximation method which is found suitable. Simplified Fourier-series by the Poisson summation formula is applied by replacing the integral with a series which corresponds to the

trapezoidal rule with a specified discretization error. The Fourier integral thus obtained can be approximated by its Riemann-sum. The Fourier-series method for the numerical inversion of Laplace transforms might be first proposed by (Dubner and Abate, 1968) and to speed up the convergence, Simon et al Simon et al. (1972) firstly introduced the Euler summation and proposed a model as follows

$$f(y,t) = \frac{\exp \epsilon t}{t}[\frac{1}{2}\bar{f}(y,\epsilon) + \Re e \sum_{k=1}^{N} \bar{f}(y, \epsilon + \frac{ik\pi}{t})(-1)^k] \tag{1.6.6}$$

Where $\Re e$ refers to the real part of the complex number, $i = \sqrt{-1}$ is imaginary number, N is the number of terms used in the Riemann-sum approximation and ϵ is the real part of the Bromwich contour that is used in inverting Laplace transforms. The Riemann-sum approximation for the Laplace inversion involves a single summation for the numerical process. Its accuracy depends on the value of ϵ and the truncation error dictated by N. According to Tzou (1997), the value of ϵ must be selected so that the Bromwich contour encloses all the branch point. For faster convergence the quantity $\epsilon t = 4.7$ gives the most satisfactory results.

1.6.3 Implicit Finite Difference Method

Implicit Finite difference method (IFDM) works by replacing the region over which the independent variables in the PDE are defined by a finite grid of points at which the dependent variable is approximated. The partial derivatives in the PDE at each grid point are approximated based on Taylor's theorem. Basically, three steps are involve in obtaining finite difference solution;

a. Divide the solution into grids of nodes

b. Approximate the given differential equation by finite difference equivalence that relates the solutions to grid points

c. Solve the difference equations subject to the prescribed initial and boundary conditions

Derivatives in the partial differential equation are approximated by linear combinations of function values at the grid points. By Taylor's series expansion

$$\frac{\partial u}{\partial t}(y_i, t_j) \approx \frac{u(y_i, t_j) - u(y_i, t_{j-1})}{\Delta t} + O\left((\Delta t)^2\right) \tag{1.6.7}$$

$$\frac{\partial h}{\partial t}(y_i, t_j) \approx \frac{h(y_i, t_j) - h(y_i, t_{j-1})}{\Delta t} + O\left((\Delta t)^2\right) \tag{1.6.8}$$

$$\frac{\partial \theta}{\partial t}(y_i, t_j) \approx \frac{\theta(y_i, t_j) - \theta(y_i, t_{j-1})}{\Delta t} + O\left((\Delta t)^2\right) \tag{1.6.9}$$

while the first and second order space derivatives to be approximated by the central difference formula.

$$\frac{\partial u}{\partial y}(y_i, t_j) \approx \frac{u(y_{i+1}, t_j) - u(y_{i-1}, t_j)}{2(\Delta y)} + O\left((\Delta y)^2\right) \tag{1.6.10}$$

$$\frac{\partial h}{\partial y}(y_i, t_j) \approx \frac{h(y_{i+1}, t_j) - h(y_{i-1}, t_j)}{2(\Delta y)} + O\left((\Delta y)^2\right) \tag{1.6.11}$$

$$\frac{\partial \theta}{\partial y}(y_i, t_j) \approx \frac{\theta(y_{i+1}, t_j) - \theta(y_{i-1}, t_j)}{2(\Delta y)} + O\left((\Delta y)^2\right) \tag{1.6.12}$$

$$\frac{\partial^2 u}{\partial y^2}(y_i, t_j) \approx \frac{u(y_{i+1}, t_j) - 2u(y_i, t_j) + u(y_{i-1}, t_j)}{(\Delta y)^2} + O\left((\Delta y)^2\right) \tag{1.6.13}$$

$$\frac{\partial^2 h}{\partial y^2}(y_i, t_j) \approx \frac{h(y_{i+1}, t_j) - 2h(y_i, t_j) + h(y_{i-1}, t_j)}{(\Delta y)^2} + O\left((\Delta y)^2\right) \tag{1.6.14}$$

$$\frac{\partial^2 \theta}{\partial y^2}(y_i, t_j) \approx \frac{\theta(y_{i+1}, t_j) - 2\theta(y_i, t_j) + \theta(y_{i-1}, t_j)}{(\Delta y)^2} + O\left((\Delta y)^2\right) \tag{1.6.15}$$

Thus, the transport equations at the grid points will be constructed such that the iterative system will not restrict the time steps, which is reach, and less expensive compared to some implicit schemes. Customised codes will be implemented using Fortran and MATLAB software packages to obtain the numerical

values, which will be presented in figures (line graphs) and tables to illustrate physical situations of the problems under study and draw valid conclusions.

1.6.4 Exact Solution

This is a mathematical model that have solution which does not involve any approximation. The analytical solution of a given problem is referred to as the exact solution if it satisfies the differential equation and the boundary conditions. This can be verified by substituting the solution function into the differential equation and the boundary conditions. Distinction should be made between an actual real-world problem and the mathematical model that is an idealized representation of it. The solutions we get are the solutions of mathematical models, and the degree of applicability of these solutions to the actual physical problems depends on the accuracy of the model. An 'approximate' solution of a realistic model of a physical problem is usually more accurate than the 'exact' solution of a crude mathematical model (Cengel, 2003). Since, the derived equations in this thesis do not necessarily vanish identically, the solution of these equations proves challenging and therefore, only solution of two cases are obtained.

1.7 Some Basic Definitions

The macro-channels referred in this dissertation are those channels that function in the continuum domain, with no velocity slip and temperature jump, whose flow and heat transfer behaviour can be predicted from the continuum theory, while micro-channels are those for which this approach failed. Since, MHD free convection flow of viscous incompressible fluids between vertical infinite parallel plates and annular macro-channel and micro-channel is the

theme of this dissertation, the flow is subjected to different physical situations, different boundary conditions and different fluid properties. We give here a brief overviews/definitions of some of the different flow situations on which the dissertation is based

1.7.1 Pressure

This is one of the basic properties of all fluids. Pressure is the force exerted on or by the fluid on a unit of surface area. Mathematically expressed;

$$pressure = \frac{Force}{surface\ \ area} \tag{1.7.1}$$

The basic unit of pressure is Pascal (Pa). When a fluid exerts a force of $1N$ over an area of $1m^2$, the pressure equals one Pascal, i.e., $1Pa = 1N/m2$.

1.7.2 Density

This is another basic fluid property. Symbolically represented by ρ and is defined as mass (m) of a unit of volume (V). Its basic unit is kg/m^3. Mathematically it is expressed as;

$$\rho = \frac{m}{V} \tag{1.7.2}$$

1.7.3 Viscosity

This is a measure of the fluid's resistance to flow due to its internal friction. Viscosity is measured in two ways: dynamic (absolute) and kinematic. These two parameters are related since the kinematic viscosity may be obtained by dividing the dynamic viscosity by density. Symbolically $\nu = \frac{\mu}{\rho}$. Dynamic (absolute) viscosity (μ) is the measure of the tangential force needed to shear one parallel plane of fluid over another parallel plane of fluid. The thicker

or more viscous the fluid, the larger the area of contact, and the larger the velocity change between the layers of the fluid, the larger the tangential force. The basic unit is the pascal second (Pas). In a nutshell one can think of terms like "thickness" or "internal friction" in the case of water which is thin compared with a honey which is thick.

1.7.4 Mass and Volumetric Flow Rate

These are two types of flow rate, since fluid quantity can be expressed as volume or mass. Volumetric flow rate (V) is the volume of the fluid passing through a given cross section in a unit of time. The basic unit is m^3/s. It is a function of the fluid velocity (u) and the cross section of the channel through which the fluid is flowing. While the Mass flow rate (m) is the mass of fluid passing through a given cross section in a unit of time. Its basic unit is kg/s.

1.7.5 Compressible fluid/Incompressible fluid

This is the fluid flow where the volume of the fluid particle changes with position. This implies that density, ρ, will vary throughout the flow. Furthermore, compressible flows are classified according to the value of the dimensionless Mach number, M, which is given by

$$M = \frac{u}{c} \tag{1.7.3}$$

where, u, is the velocity of the fluid and, c, is the speed of sound. Whereas the fluid flow where the volume of the given fluid particle does not change with position. This implies that the density, ρ, of the fluid is constant everywhere and this is essentially valid for all liquids (McDonough, 2009).

1.7.6 Validation

This is to check on whether the mathematical model is a good representation for the real life problem being studied. It is also a means of comparing numerical results with established results from similar physical problem. Physically results may emerge either from real life or small-scale laboratory experiments. In either way errors are bound to occur, therefore the failure of the model is likely to occur or may not capture all the underlying physics. In this situation the numerical and the physical results may not agree and the user is at liberty to decide what is 'close enough'.

1.7.7 Boundary Layer Concept in Fluid Dynamics

In a lecture delivered titled 'On fluid flow with very little friction' by Ludwig Prandtl in 1904 at the International Mathematical Congress in Heidelberg, Germany, explained that the viscosity of a fluid plays a role in a thin layer adjacent to the surface, which he called 'boundary layer' or 'shear layer'. In this lecture, the understanding of fluid flow was significantly increased. As a result of this, the d'Alembert's Paradox, which states that a body placed in a potential flow does not experience a force which is clearly in conflict with every - day experience was resolved (Experimentally, it is proved that drag force exists when a body is immersed in a fluid which is an apparent contradiction between theory and experiment). He first proposed the interactively coupled, two layer solution which properly models many flow problems. As an object moves through a fluid, or as a fluid moves past an object, the molecules of the fluid near the object are disturbed and move around the object. Subsequently, it could be explained further, why birds, air planes can fly (Veldman, 2011).

1.7.8 Skin-friction

Skin friction is a component of drag, the force resisting the motion of solid body through a fluid. It arises from the friction of the fluid against the skin of the object that is moving through it. Skin friction arises from the interaction between the fluid and the skin of the body, and is directly related to the area of the surface of the body that is in contact with the fluid. Skin friction follows the drag equation and rises with the square of the velocity (Jibril, 2012).

1.7.9 Suction/Injection

The simplest active flow control system is surface suction/injection as they significantly affect the flow field. Controlling fluid flow within vertical channel with suction and injection is an interesting exercise as both activities are carried out simultaneously on opposite channel plates. The influence of suction on rate of heat transfer and skin friction is opposite to the influence of injection (Ajibade, 2009).

1.7.10 Couette Flow

This is a flow between two parallel plates where one plate is moving while the other is stationary. It is of two type, the plane Couette flow and the generalized Couette flow. In the case of plane Couette flow, the pressure gradient is constant (zero) and the only force on the fluid is the force due to the moving plate. While in the later case the pressure gradient is imposed in the direction parallel to the plates (for detail see Schlichting (1960)).

1.7.11 Current Density

In this dissertation, the flow of electrically conducting fluid is considered, in either vertical parallel plates channel or between two concentric cylinders. The charges are in continuous random motion with a velocity distribution. Therefore, from the Amphere's law (1.1.12), we have

$$J = \frac{\nabla \times \mathbf{B}}{\mu_e} \tag{1.7.4}$$

where J is the total current density in a medium, while for a moving charges, the current density is given by the sum of products of the charge on each particle and its velocity eq.(1.1.15). Charged particles executing helical or cylindrical motion motion, their velocity can be decomposed in a circular motion plus the motion of the centre of curvature called the guiding-centre velocity (drift velocity) (Sutton and Sherman, 1965).

1.8 Dissertation Layout

This dissertation is divided into eight chapters. Chapter One deals with the general introduction and provides the background information on the basic equations describing the MHD flow behaviour. Chapter Two provides the available related literature consulted in this study and all acknowledged. In Chapter Three, we begin the study by looking at the computational treatments of time-dependent MHD transient natural convection flow in vertical channel due to asymmetric and symmetric heating of the channel walls in presence of induced magnetic field viz; Role of induced magnetic field on transient natural convection flow in a vertical channel: The Riemann Sum Approximation Approach and Computational treatment of MHD transient natural convection flow in a vertical channel due to symmetric heating in presence of induced magnetic field are examined. The Effects of suction-injection combination

(SIC) on MHD transient free-convective flow in a vertical channel in presence of induced magnetic field and the time dependent MHD Couette flow of an incompressible, viscous and electrically conducting fluid between two vertical parallel plates were presented in Chapter Four. Chapters Five and Six, discussed the steady/unsteady fully developed MHD free-convective flow in an annular micro-channel. The problems considered here includes; Fully developed MHD natural convection flow in a vertical annular micro-channel: An exact solution. MHD Natural Convection flow in a vertical Micro-concentric Annuli in presence of Radial Magnetic Field: An exact solution and Transient MHD free convective flo in vertical micro-concentric annuli. Finally, conclusions and recommendations are given in Chapter Seven.

CHAPTER TWO

LITERATURE REVIEW

2.1 Introduction

In this chapter, we have focused our attention only on the review of materials related to the present study. The chapter is divided into two sections macro-channel configurations and micro-channel configurations. We have also identified the shortcomings that motivated the study and are addressed in the subsequent chapters. Highlight to the knowledge gap also provided.

2.2 Macro-channel Configurations: MHD Free Convective Flow in Vertical Parallel Plate Channel

MHD plays an important roles in many natural phenomena such as astrophysics, geophysics, example is the generation of the magnetic field of planets and stars, the interaction of Earth's magnetic field with the solar wind as well as lightening. The Coriolis force has a considerable influence on the Hydromagnetic flow in the Earth liquid core and large number of astronomical bodies i.e Sun, Earth, Jupiter, magnetic stars and pulsars possesses fluid interiors and magnetic field. Beyond these areas, MHD is actually more frequently encountered in the industrial application than one can imagine. MHD application can also be found in many engineering processes such as plasma confinement, liquid metal cooling of nuclear reactors, electromagnetic casting, rotating hydromagneic generators, MHD power generators, fission, fusion, agriculture, Metallurgic, and Medicine, (magnetic drug targeting and micro fluidics). As

a matter of fact, the influence of magnetic field on the flow behaviours of an electrically conducting viscous fluid has shown its importance in many applications such as in the manufacture of rayon and nylon in textile industry, the production of pulp in the paper industry, and the purification of crude oil in the petroleum industry. For instance, the cooling of threads or sheets of some polymer materials in the production line can be controlled more critically and more accurately with the presence of an electrically conducting fluid when subjected to an externally applied magnetic field. If an external magnetic field is applied in the transverse direction, the magnitude of the flow velocity decreases with the strength of the external magnetic field because the external magnetic field generates the Lorentz force, which is electromagnetic force acting on the conducting fluid. Not only so, the flow pattern also depends heavily on the wall conductivity. The velocity gradients on perfectly insulated walls are always the same irrespective of the value of Ha (Molokov et al., 2007).

Natural convection flows in vertical channels have been studied extensively because of its importance in many engineering applications, such as in accelerators, aerodynamic heating, electrostatic precipitation, polymer technology, petroleum industry, purification of crude oil and fluid droplet sprays to mention but few. The work of Ostrach (1952) and Aung (1972) are among the early major contributions to the study of convective flow and heat transfer in vertical channel. Realizing the importance of transient convection in designing cooling systems using parallel plates, Joshi (1988) studied the transient effects in natural convection cooling of vertical parallel plates while Jha et al. (2003), Paul et al. (1996) and, Singh and Paul (2006) also carried out extensive study on the free convective flow. Literature survey also revealed that natural convection in an electrically conducting viscous fluid subject to an externally applied magnetic field has also received significant attention. Hartmann (1937) analyzed the effect of transverse uniform magnetic field on the flow of a viscous incompressible electrically conducting fluid exiting through

parallel stationary plates that are insulated. Romig (1964), studied the influence of electric and magnetic field on heat transfer to electrical conducting fluids. Soundalgekar (1965) discussed the hydromagnetic flow near an accelerated plate in the presence of magnetic field. Mishra and Mohapatra (1975), also studied the unsteady free convective flow from a vertical plate in the presence of a uniform transverse and induced magnetic field. Attia (1998) and Attia (2004) also studied the influence of the magnetic field on the velocity and temperature fields of an unsteady Hartmann flow of a conducting Newtonian fluid between two infinite non-conducting horizontal parallel fixed and porous plates. Other works under different physical situations on the free convective flow in the presence of magnetic field includes that of Poots (1961), Osterle and Young (1961), Raptis et al. (2003), Ram et al. (2010), Oreper and Szekely (1983) amongst others. Jha and Apere (2011) considered the unsteady magnetohydrodynamic free convective Couette flow of a viscous incompressible electrically-conducting fluid between two parallel vertical porous plates. Recently, Jha and Apere (2012) have carried out a theoretical analysis of an unsteady magnetohydrodynamic free-convective flow of a viscous incompressible and electrically conducting fluid between two concentric vertical cylinders considering thermal boundary condition of the second kind at the outer surface of the inner cylinder.

In addition to the earlier mentioned areas of application of natural convection flows in vertical channel includes many diverse field such as nuclear reactors, chemical processing equipment, geothermal energy extraction, cooling appliances in electronic instruments and in different engineering fields. Studies related to transient natural convection flows in vertical channels due to symmetric heating of the channel walls are; Jha et al. (2003), Bianco et al. (2006), Langellotto et al. (2007), Andreozzi et al. (2009) and Jha and Ajibade (2010). Narahari et al. (2002) studied the transient free convection flow between two infinite vertical parallel plates with constant heat flux at one boundary. In

another work Narahari (2008), analyzed the transient free convection flow of a viscous incompressible fluid between two infinite vertical parallel plates in the presence of constant temperature and mass diffusion. Paul et al. (1996) studied the transient free convective flow in a vertical channel having a constant temperature and constant heat flux on the channel walls. Singh et al. (1996) discussed the transient free convection flow between two infinite vertical parallel plates heated asymmetrically. In an another article Singh and Paul (2006) obtained the closed form solution of the transient free convective flow of a viscous and incompressible fluid between two vertical walls as a result of symmetric heating or cooling of walls.

Moreover, role of induced magnetic field are encountered in many important problems in geophysics, astrophysics, cosmical and geophysical fluid dynamics as well as in many engineering processes. Takhar et al. (1999) considered induced magnetic field effects in transient laminar hydromagnetic boundary layer convection along an impulsively started semi-infinite at plate with an aligned magnetic field, indicating that a reduction in magnetic Prandtl number will enhance the surface shear stress, surface component of the induced magnetic field and also the surface heat transfer. Ghosh and Bhattacharjee (2000) investigated steady Hartmann flow of a viscous incompressible electrically conducting fluid in a rotating channel in the presence of an inclined magnetic field taking into account induced magnetic field. Koshiba et al. (2002) presented a detailed study of the large-scale pulsed MHD generator system flow including induced magnetic field effects. Gupta et al. (2005) analyzed the hydromagnetic steady shear flow along an electrically insulating porous at plate. They concluded that the velocity at a given point increases with increase in either the magnetic field or suction velocity and the induced magnetic field at a given location is reduced with increasing magnetic field. Alom et al. (2008) investigated the steady MHD heat and mass transfer by mixed convection flow from a moving vertical plate with induced magnetic, thermal diffusion, constant

heat and mass fluxes. The non-linear coupled equations governing the flow are solved by shooting technique. Nonsimilar, laminar, steady, electrically-conducting forced convection liquid metal boundary layer flow with induced magnetic field effects have been presented by Anwar et al. (2009). Krishna (2009) studied the analytical solution to the problem of free convective flow of an electrically conducting fluid between two heated parallel plates in the presence of an induced magnetic field. Analytical solution to the problem of MHD free convective flow of an electrically conducting fluid between two heated parallel plates in the presence of an induced magnetic field is analysed by Singha (2009). Ghosh et al. (2010) presented an exact solution for hydro-magnetic natural convection boundary layer flow past an infinite vertical flat plate with induced magnetic field effects. Nadeem and Akbar (2010) studied the influence of heat transfer and induced magnetic field on peristaltic flow of a Johnson-Segalman fluid in a vertical channel. Singh et al. (2010), discussed free convection in an electrically conducting fluid in a vertical channel under the action of an applied magnetic field noting the induced magnetic field in the flow analysis. Singh and Singh (2012) considered the steady fully developed laminar natural convective flow in open ended vertical concentric annuli in the presence of radial magnetic field by taking into account the induced magnetic field produced by the motion of an electrically conducting fluid. Studies on the steady and unsteady mixed convective MHD flow of an incompressible viscous electrically-conducting fluid taking into account the induced magnetic field has been carried out by Ahmed (2012) and Ahmed et al. (2012). Źivojin et al. (2012b) studied the MHD flow of two immiscible, electrically conducting fluids between isothermal and insulated moving plates in the presence of an applied electric and inclined magnetic field with the effects of induced magnetic field.Kumar and Singh (2013) have discussed effect of the induced magnetic field on free convection when the concentric cylinders heated/cooled asymmetrically. Fully developed laminar free convective flow in open ended vertical

concentric annuli in presence of a radial magnetic field has been considered by Sarveshanand and Singh (2014). It is observed in their conclusion that the effect of the induced magnetic field is to increase the velocity profiles. In another article by Singh et al. (2014) studied the steady mixed convective flow of a viscous incompressible and electrically conducting fluid between two vertical walls when there is a uniform axial temperature variation along the walls.

2.3 Suction-Injection Combination (SIC) on MHD Transient Free Convective Flow in a Vertical Channel

Studies on free-convection processes in porous channels are well-developed field of investigation due to its importance in a variety of situations. Typical examples are, thermal insulations, geothermal system, surface catalysis of chemical reactions, solid matrix heat exchanger, microelectronic heat transfer equipment, porous flat collectors, coal and grain storage, petroleum industries, dispersion of chemical contaminants in various processes, nuclear waste material, and catalytic beds. Some of the examples mentioned above involve two or more fluids, multidimensional and unsteady flows (Mahmud and Andrew, 2005). The problem of unsteady flow in porous tubes received much attention in recent years because of its various applications in biomedical engineering, for example in the dialysis of blood in artificial kidney, in the flow of blood in the capillaries, in the flow in blood oxygenators, as well as in many other engineering areas such as the transpiration cooling (Tsangaris et al., 2007). The first attempt to study the problem of laminar flow between two parallel porous plane walls driven by uniform injection and suction is attributed to Berman (1953). Nanousis et al. (1980) studied the effect of a uniform transverse magnetic field on the free-convection flow of a viscous, incompress-

ible and electrically-conducting fluid past an infinite non-conducting vertical porous plate when the fluid is subjected to a suction of uniform velocity. Terrill (1982, 1983) gave an exact series solution for the laminar flow in a pipe of circular cross section with porous wall driven by a spatially variable although time independent suction and/or injection. Very recently, Jha and Apere Jha and Apere (2013) presented a unified solution for the MHD transient Couette flow in a porous annulus formed by two concentric porous cylinders of infinite length when the magnetic field is fixed with fluid or moving cylinder, where they found out that suction accelerate the flow whereas injection retards the flow. Jha et al. (2011) analyzed both analytically and numerically, the transient free-convection flow of viscous reactive fluid in a vertical channel. They concluded in their findings that both velocity and temperature increase with the increase in the value of reactant consumption parameter and non-dimensional time until they reach steady-state value. Recently same authors Jha et al. (2012), extended this problem to the case of Couette flow bounded by two porous plates. In a recent article,Jha et al. (2014a) examined the role of suction/injection on steady free-convective flow in a micro-channel.

Considerable achievements have been recorded on the effect of magnetic field on conducting fluid flow in presence of convection current by many investigators. Gupta et al. (1974) considered the effect of radiation on the combined free and forced convection flow of an electrically conducting fluid inside an open-ended vertical channel and permeated by uniform transverse magnetic field. Garandet et al. (1992) investigated the buoyancy driven convection in a rectangular enclosure with a transverse magnetic field. Unsteady viscous incompressible free convection flow of an electrically conducting fluid between two heated vertical parallel plates is considered in the presence of uniform magnetic field applied transverse to the flow by Singha and Deka (2006). Terrill and Shrestha (1966) studied the laminar flow between parallel plates in the presence of a magnetic field. Megakhed (1974) considered the non stationary

hydromagnetic flow from a flat porous plate with induced magnetic field and heat transfer, presenting an exact expression for the flow rate and the induced magnetic field for constant suction and magnetic Prandtl number equal to unity. He showed that such a solution is very easy to work with only when the Alfven speed is less than the suction rate. Gupta et al. (2005) have analysed the hydromagnetic steady shear flow along an electrically insulating porous flat plate, showing that the velocity at a given point increases with increase in either the magnetic field or suction velocity and the induced magnetic field at a given location is reduced with increasing magnetic field.

2.4 MHD Couette Flow in a Vertical Channel

The problem of flow formation in Couette motion as predicted by the classical fluid mechanics have been presented by Schlichting (1960). The problem provides the exact solution of the non-linear Navier-Stokes equation and exposed the relationship between the velocity and the time, and also how the boundary layer spread throughout the flow regime. The study of MHD Couette flow has been an active area of research due to its geophysical and astrophysical applications (Jha and Apere, 2011). Couette flow is used as a fundamental method for measuring viscosity and a means of estimating the drag force in many wall driven applications (Muzychka and Yovanovich, 2006). Keeping in view of the importance of unsteady MHD Couette flow in many engineering processes,Katagiri (1962) and Muhuri (1963) have studied the unsteady hydromagnetic Couette flow of a viscous, incompressible and electrically conducting fluid between two infinite plates in the presence of a uniform transverse magnetic field when the fluid flow within the channel is induced due to impulsive movement of one of the plates of the channel. Soundalgekar (1967) analyzed this problem in a parallel plate porous channel when the fluid flow within the channel is induced due to uniformly accelerated movement of one of the plates

of the channel. Jana and Datta (1977) and Mishra and Muduli (1980) considered this problem when the velocity of moving plate varies as t^m , t and m being time variable and any positive integer respectively. Singh and Kumar (1983) discussed the effect of a uniform transverse magnetic field on the Couette flow of an electrically conducting fluid between two parallel plates for impulsive and uniformly accelerated motion of one the plates. Singh (1988) studied the effect of free convection in unsteady Couette motion between two vertical parallel plates. MHD free convection Couette flow between two vertical parallel plates has been studied by by Jha (2001). *et al.*Barletta et al. (2008) investigated analytically the Steady fully-developed combined forced and free convection Couette flow with viscous dissipation in a vertical channel,where the moving wall is thermally insulated and the wall at rest is kept at a uniform temperature.Seth et al. (2011) have studied unsteady MHD Couette flow of a viscous incompressible electrically conducting fluid, in the presence of a transverse magnetic field, between two parallel porous plates. Deka and Bhattacharya Deka and Bhattacharya (2011) obtained an exact solution of unsteady free convective Couette flow of a viscous incompressible heat generating/ absorbing fluid confined between two vertical plates in a porous medium.

In all the above investigations on MHD Couette flow stated earlier, the induced magnetic field produced as a result of fluid motion is negligible in comparison to the applied magnetic field. This assumption is valid for small magnetic Reynolds number fluids such as metallic liquids and partially ionized fluids (Cramer and Pai, 1973). Moreover, problems of geophysics, astrophysics and in so many MHD devices such as MHD power generators, MHD pumps, plasma flow in accelerators etc magnetic Reynolds number is not very small, therefore, the induced magnetic field cannot be neglected. In view of this, Jana et al. (1977) studied MHD Couette flow of class-I of a viscous, incompressible and electrically conducting fluid in a rotating system in the presence of a uniform transverse magnetic field taking induced magnetic field into account when the

stationary plate of the channel is perfectly conducting and the moving plate of the channel is electrically non-conducting. Seth and Maiti (1982) considered this problem when both plates of the channel are electrically non-conducting.

The effects of the induced magnetic and electric field play an implicit role in partially ionized fluid media which derive its application in industrial and astrophysical MHD flows. Ghosh et al. (2010) presented an exact solution for hydromagnetic natural convection boundary layer flow past an infinite vertical flat plate with induced magnetic field effects. Chauhan and Agrawal (2012), studied the effects of Hall current on steady MHD Couette flow of class-I in a rotating system in the presence of a uniform inclined magnetic field taking induced magnetic field into account. Singh et al. (2010) considered unsteady free convection between two insulated infinitely long vertical walls under the action of a uniform transverse magnetic field. Recently, Singh and Singh (2012) discussed the steady fully developed laminar natural convective flow in open ended vertical concentric annuli in the presence of radial magnetic field by taking into account the induced magnetic field produced by the motion of an electrically conducting fluid. Ahmed et al. (2012) presented an exact solution for the unsteady mixed convective MHD flow of an incompressible viscous electrically conducting fluid over an infinite vertical isothermal plate impulsively held fixed in a uniform stream taking into account the induced magnetic field. Źivojin et al. (2012a) studied the MHD flow of two immiscible, electrically conducting fluids between isothermal and insulated moving plates in the presence of an applied electric and inclined magnetic field with the effects of induced magnetic field.

2.5 Micro-channel Configurations: MHD Free-Convective Flow in Annular Micro-channel

One of the major themes in science and technology during the past half century has been miniaturization down to the micro and nano scale. The area of micro and nanofluidics is fundamentally important due to the necessity of understanding the nature of fluid flow at this scale (Gad-el Hak, 1999). The annular geometry is widely employed in the field of heat exchangers. Its typical application is the gas cooled nuclear reactors in which the cylindrical fissionable fuel elements are placed axially in vertical coolants channel within the graphite moderators and the cooling gas is flowing along the channel parallel to the fuel elements (Singh et al., 1997). The practical application of flow in annular space can also be found for example in drilling operation of oil and gas wells. The MHD flow problem in an annulus was first discussed by Globe (1959) who considered fully developed laminar MHD flow in an annular channel. Jain and Mehta (1962) extended the problem by imposing suction/injection on the walls. An exact solution of electrically conducting viscous incompressible flow in an annulus with porous wall under an external radial magnetic field was obtained by Nandi (1973). Antimirov and Kolyshkin (1984) studied the unsteady magneto hydrodynamic flow in an annular channel with radial magnetic field while Takhar et al. (1989) examined the stability of MHD Couette flow in a narrow gap annulus.Avci and Aydin (2006) analyzed analytically the forced convection heat transfer in fully developed flows of viscous dissipating fluids in concentric annular ducts. While Avci and Aydin (2008) analyzed analytically, the hydrodynamically and thermal fully developed flows of viscous dissipating gases in annular micro-duct between two concentric cylinders. In another work, El-Shaarawi and Al-Nimr (1990) considered the fully developed natural convection in open-ended vertical concentric annuli. Analytical solutions for transient fully developed natural convection in open-ended vertical con-

centric annuli are presented by Al-Nimr (1993). Also, Al-Nimr (1995) carried out analytical solutions for fully developed MHD natural-convection flow in open-ended vertical concentric porous annuli. Al-Nimr and Darabseh (1995) presented the closed forms on transient fully developed free convection solutions, corresponding to four fundamental thermal boundary conditions in vertical concentric annuli.

Recently, a growing interest in micro-channel fluid mechanics and heat transfer has emerged because of possible cooling applications in space systems, manufacturing and material processing operations, and in high-power-density chips in supercomputers and other electronics Al-Nimr and Khadrawi (2004). As this area continue to grow, it becomes increasingly important to understand the mechanisms and fundamental differences involved with fluid mechanics and heat transfer mechanisms in macro-channel and micro-channel. A series of investigations have been conducted recently in the field of micro geometry flow. However, to cite a few works in this direction, Chen and Weng (2005) analytically studied the fully developed natural convection in open-ended vertical parallel plate micro-channel with asymmetric wall temperature distribution in which the effect of rarefaction and fluid wall interaction were shown to increase the volume flow rate and decrease the heat transfer. This result is further extended by taking into account suction/injection on the micro-channel walls by Jha et al. (2014a). They concluded that skin frictions as well as the rate of heat transfer are strongly dependent on suction/injection parameter. In another work, Weng and Chen (2009) studied the impact of wall surface curvature on steady fully developed natural convection flow in an open-ended vertical micro-annulus with an asymmetric heating of annulus surface. Recently, Jha et al. (2014b) further extended the work of Weng and Chen (2009) by taking into account suction/injection on vertical annular micro-channel. They discovered that skin-friction decrease at the outer surface of inner porous cylinder with increase of fluid- wall interaction parameter in case of injection at outer

surface of the inner porous cylinder and simultaneous suction at inner surface of the outer porous cylinder while the result is just reverse at the inner surface of outer porous cylinder.

On the other hand, the MHD phenomenon has received considerable attention during the last two decades due to its importance from the energy generation point of view, and one may envisage MHD generators for power generation. MHD pumps are already in use in chemical energy technology for pumping electrically conducting fluids at some of the atomic energy centre. Besides these applications, when the fluid is electrically conducting, the free convection flow is appreciably influenced by an imposed magnetic field. Therefore, to refer to few works in this direction, Sheikholeslamia et al. (2014b) investigated the magnetic field effect on nanofluid flow and heat transfer in a semi-annulus enclosure via control volume based finite element method. Khan and Ellahi (2008) observed the effects of magnetic field and porous medium on some unidirectional flows of a second grade fluid. Farhad et al. (2012b) examines the slip effect on hydromagnetic rotating flow of viscous fluid through a porous space. In another work, Farhad et al. (2012a) investigated the effects of slip condition on the unsteady magnetohydrodynamics (MHD) flow of incompressible visscoelasstic fluids in a porous channel under the influence of transverse magnetic field and Hall current with heat and mass transfer. An analysis to investigate the combined effects of heat and mass transfer on free convection unsteady magnetohydrodynamics (MHD) flow of viscous fluid embedded in a porous medium is presented by Farhad et al. (2013b).

Some recent works related to the present investigation are found in literature [Farhad et al. (2013a), Sheikholeslamia et al. (2014a), Farhad et al. (2014), Ashorynejad et al. (2013),Sheikholeslami et al. (2014) and Sheikholeslami et al. (2012)]. Farhad et al. (2013a) presented an exact analysis of combined effects of radiation and chemical reaction on the magnetohydrodynamics (MHD) free

convection flow of an electrically conducting incompressible viscous fluid over an inclined plate embedded in a porous medium. Farhad et al. (2014) studied the unsteady free convection flow of a second grade fluid past an isothermal vertical plate oscillating in its plane with constant viscosity. Also, Sheikholeslamia et al. (2014a) studied magnetohydrodynamic effect on natural convection heat transfer of Cu-water nanofluid in an enclosure with hot elliptic cylinder. While Sheikholeslami et al. (2014) numerically examined the natural convection of nanofluids in a concentric annulus between a cold outer square cylinder and a heated inner circular. Flow and heat transfer of a nanofluid over a stretching cylinder in the presence of magnetic field has been investigated by Ashorynejad et al. (2013). Recently, Sheikholeslami et al. (2012) presented the numerical solution for natural convection of nanofluids in a cold outer circular enclosure containing a hot inner sinusoidal cylinder. Sheikholeslamia et al. (2013) carried out a numerical investigation on natural convection nanofluid flow in a half annulus enclosure with one wall under constant heat flux in presence of magnetic field.

Having in mind, the chain of work so far done on different configurations by many researchers, and the enormous increase in applications of both macro- and micro-channel findings, it is very pertinent to undertake the present study so as to enrich the existing literature.

CHAPTER THREE

MHD FREE CONVECTION FLOW IN VERTICAL CHANNEL

Natural convection is a mechanism, or type of heat transport in which the fluid motion is not generated by any external source (like a pump, fan, suction device, etc.) but only by density differences in the fluid occurring due to temperature gradients, concentration gradient or both. In natural convection, fluid surrounding a heat source receives heat, becomes less dense and rises. The surrounding, cooler fluid then moves to replace it. This cooler fluid is then heated and the process continues, forming a convection current; this process transfers heat energy from the bottom of the convection cell to top. The driving force for natural convection is buoyancy, as a result of differences in fluid density. Free convection flow is encountered in cooling of nuclear reactors or in the study of the structure of stars and planets.

3.1 Role of Induced Magnetic Field on Transient Natural Convection flow in a vertical channel: The Riemann-sum Approximation Approach

3.1.1 Introduction

In this section we have investigated the role of induced magnetic field on transient natural convection flow of an electrically conducting, incompressible and viscous fluid in a vertical channel formed by two infinite vertical parallel plates. The transient flow formation inside the channel is due to sudden asymmetric heating of channel plates. The time dependent momentum, magnetic induction

and energy equations are solved semi-analytically using the Laplace transform technique along with the Riemann-sum approximation method. The solutions obtained are validated by assenting comparison with the closed form solutions obtained for the steady states which has been derived separately and also by the implicit finite difference method. Graphical results for temperature, velocity, induced magnetic field, current density, and skin-friction based on the semi-analytical solutions are presented and discussed.

3.1.2 Mathematical Analysis

We consider transient natural convection flow of an incompressible viscous fluid in a vertical channel. At time $t' \leq 0$, both the fluid and the channel walls are assumed to be at the same temperature T_0. At time $t' > 0$, the temperature of the wall at $y' = 0$ is raised to T_1 while that at the wall $y' = d$ is maintained at T_0. The x'- axis is taken along the channel walls in the direction of the flow and y'-axis taken normal to it. A uniform magnetic field of strength H_0' is applied perpendicular to the flow direction. However, the velocity, the induced magnetic field and the temperature are given by $(u', 0, 0)$, $(h', H_0, 0)$ and T' respectively. Using the Boussinesq's approximation, the mathematical model representing the present physical situation by taking into consideration of induced magnetic field are;

$$\frac{\partial T'}{\partial t'} = \alpha \frac{\partial^2 T'}{\partial y'^2}, \tag{3.1.1}$$

$$\frac{\partial u'}{\partial t'} = \nu \frac{\partial^2 u'}{\partial y'^2} + \frac{\mu_e H_0, \partial h'}{\rho \partial y'} + g\beta(T' - T_0), \tag{3.1.2}$$

$$\frac{\partial h'}{\partial t'} = \frac{1}{\sigma \mu_e} \frac{\partial^2 h'}{\partial y'^2} + H_0 \frac{\partial u'}{\partial y'}. \tag{3.1.3}$$

Together with

$$\begin{aligned} &u' = 0, \quad T' = T_0, \quad h' = 0, \ for\ 0 \le y' \le d \ \ at\ t' \le 0, \\ &u' = 0, \quad T' = T_1, \quad h' = 0, \ for\ y' = 0 \ at\ t' > 0, \\ &u' = 0, \quad T' = T_0, \quad h' = 0, \ for\ y' = 1 \ at\ t' > 0, \end{aligned} \tag{3.1.4}$$

where u' is the velocity of the fluid, h' is the induced magnetic field, H_0 is the applied magnetic field, T' is the temperature of the fluid, ν is the kinematic viscosity, g is the acceleration due to gravity, β is the coefficient of thermal expansion, μ_e is the magnetic permeability, ρ the density, α is thermal diffusivity of fluid. By introducing the following dimensionless quantities:

$$\begin{aligned} y &= \frac{y'}{d}, t = \frac{t'\nu}{d^2}, \ \theta = \frac{(T' - T_0)}{(T_1 - T_0)}, \quad u = \frac{u'\nu}{g\beta(T_1 - T_0)d^2}, \\ M &= \frac{dH_0}{\nu}\sqrt{\frac{\mu_e}{\rho}}, \quad Pr = \frac{\nu}{\alpha}, \quad Pm = \sigma\mu_e\nu, \\ h &= \frac{h'(\frac{\mu_e}{\rho})^{\frac{1}{2}}\nu}{g\beta d^2(T_1 - T_0)}, \end{aligned} \tag{3.1.5}$$

where u is the dimensionless velocity, h is the dimensionless induced magnetic field, t the dimensionless time, y is the dimensionless coordinate normal to the channel walls, θ the dimensionless temperature, M the magnetic parameter and Pm is the magnetic Prandtl number. The dimensionless governing equations are

$$\frac{\partial\theta}{\partial t} = \frac{1}{Pr}\frac{\partial^2\theta}{\partial y^2}, \tag{3.1.6}$$

$$\frac{\partial u}{\partial t} = \frac{\partial^2 u}{\partial y^2} + M\frac{\partial h}{\partial y} + \theta, \tag{3.1.7}$$

$$\frac{\partial h}{\partial t} = \frac{1}{Pm}\frac{\partial^2 h}{\partial y^2} + M\frac{\partial u}{\partial y}. \tag{3.1.8}$$

The corresponding initial and boundary conditions for the velocity, temperature and the induced magnetic field in dimensionless form are;

$$\begin{aligned} &u = 0, \quad \theta = 0, \quad h = 0, \ for\ 0 \leq y \leq 1 \ \ at\ t \leq 0, \\ &u = 0, \quad \theta = 1, \quad h = 0, \ for\ y = 0\ at\ t > 0, \\ &u = 0, \quad \theta = 0, \quad h = 0, \ for\ y = 1\ at\ t > 0. \end{aligned} \tag{3.1.9}$$

The solution of (3.1.6) - (3.1.8) using initial conditions (3.1.9) for $Pm = 1$ can be obtained using the Laplace transform technique, equation (1.6.2), we obtain the following ordinary differential equations;

$$\frac{d^2\bar{\theta}}{dy^2} - sPr\theta = 0, \tag{3.1.10}$$

$$\frac{d^2\bar{u}}{dy^2} + M\frac{d\bar{h}}{dy} - s\bar{u} = -\bar{\theta}, \tag{3.1.11}$$

$$\frac{d^2\bar{h}}{dy^2} + M\frac{d\bar{u}}{dy} - s\bar{h} = 0. \tag{3.1.12}$$

The boundary conditions now become

$$\begin{aligned} &\bar{u} = 0, \quad \bar{\theta} = \frac{1}{s}, \ \bar{h} = 0 \ for\ y = 0 \\ &\bar{u} = 0 \quad \bar{\theta} = 0 \ \ \bar{h} = 0 \ for\ y = 1. \end{aligned} \tag{3.1.13}$$

Therefore, the solution of (3.1.10) - (3.1.12) considering equation (3.1.13) are respectively;

$$\bar{\theta}(y,s) = \frac{\sinh(\sqrt{sPr}(1-y))}{s\sinh(\sqrt{sPr})}, \tag{3.1.14}$$

$$\begin{aligned} \bar{u}(y,s) &= \frac{1}{2}[[a_1\cosh(\lambda y) + a_2\sinh(\lambda y)]e^{\frac{-M}{2}y} + [a_3\cosh(\lambda y) + a_4 sinh(\lambda y)]e^{\frac{M}{2}y}] \\ &+ \frac{\sinh(\sqrt{sPr}(1-y)(sPr-s))}{s\sinh(\sqrt{sPr})[(sPr-s)^2 - M^2 sPr]}, \end{aligned} \tag{3.1.15}$$

$$\begin{aligned} \bar{h}(y,s) &= \frac{1}{2}[[a_1\cosh(\lambda y) + a_2\sinh(\lambda y)]e^{\frac{-M}{2}y} - [a_3\cosh(\lambda y) + a_4\sinh(\lambda y)]e^{\frac{M}{2}y}] \\ &+ \frac{M\sqrt{sPr}\cosh(\sqrt{sPr}(1-y))}{s\cosh(\sqrt{sPr})[(sPr-s)^2 - M^2 sPr]}. \end{aligned} \tag{3.1.16}$$

Equations (3.1.14) - (3.1.16) are to be inverted in order to determine the temperature, the velocity and the induced magnetic field in the time domain. Since the inverse closed form of this equation is difficult, we resort to numerical procedure used in Khadrawi and Al-Nimr (2007) and Jha and Apere (2010), which is based on the Riemann-sum approximation defined in eq.(1.6.6)

3.1.3 Skin Friction and Current density

The skin-friction and the current density are obtained by differentiating equation (1.6.6) with respect to y. Therefore, the following;

$$\tau(y,t) = \frac{\partial u}{\partial y} = \frac{\exp(\epsilon t)}{t}[\frac{1}{2}\bar{u_1}(y,\epsilon) + \Re e\sum_{k=1}^{N}\bar{u_1}(y,\epsilon + \frac{ik\phi}{t})(-1)^k], \qquad (3.1.17)$$

where

$$\begin{aligned}\bar{u_1} &= \frac{\lambda}{2}\left[(a_1\sinh(\lambda y) + a_2\cosh(\lambda y))e^{-\frac{M}{2}y} + (a_3\cosh(\lambda y) + a_4\sinh(\lambda y))e^{\frac{M}{2}y}\right] \\ &+ \frac{M}{4}\left[(a_1\sinh(\lambda y) + a_2\cosh(\lambda y))e^{-\frac{M}{2}y} - (a_3\cosh(\lambda y) + a_4\sinh(\lambda y))e^{\frac{M}{2}y}\right] \\ &- \frac{\sqrt{sPr}\cosh(\sqrt{sPr}(1-y))(M^2\sqrt{sPr} + (sPr - s))}{s\sinh(\sqrt{sPr})[(sPr - s) - M^2 sPr]}. \qquad (3.1.18)\end{aligned}$$

Therefore, the skin friction at $y = 0$ and $y = 1$ is given as

$$\tau|_{y=0} = \frac{\lambda}{2}[a_2 + a_4] + \frac{M}{4}[a_1 - a_3] - \frac{\sqrt{sPr}\cosh(\sqrt{sPr})[M^2\sqrt{sPr} + (sPr - s)]}{s\sinh(\sqrt{sPr})[(sPr - s) - M^2 sPr]}, \qquad (3.1.19)$$

$$\begin{aligned}\tau|_{y=1} &= \frac{\lambda}{2}\left[(a_1\sinh(\lambda) + a_2\cosh(\lambda))e^{-\frac{M}{2}} + (a_3\cosh(\lambda) + a_4\sinh(\lambda))e^{\frac{M}{2}}\right] \\ &+ \frac{M}{4}\left[(a_1\sinh(\lambda) + a_2\cosh(\lambda))e^{-\frac{M}{2}} - (a_3\cosh(\lambda) + a_4\sinh(\lambda))e^{\frac{M}{2}}\right], \qquad (3.1.20)\end{aligned}$$

$$J = -\frac{\partial h}{\partial y} = \frac{\exp\epsilon t}{\eta}\left[\frac{1}{2}\bar{h_1}(y,\epsilon) + \Re e\sum_{k=1}^{N}\bar{h_1}(y,\epsilon + \frac{ik\pi}{\eta})(-1)^k\right], \qquad (3.1.21)$$

where

$$\begin{aligned}\bar{h_1} &= \left\{\lambda[a_1\sinh(\lambda y)+a_2\cosh(\lambda y)]-\frac{M}{2}[a_1\cosh(\lambda y)+a_2\sinh(\lambda y)\right\}e^{-\frac{M}{2}y}\\ &+ \left\{\lambda[a_3\sinh(\lambda y)+a_4\cosh(\lambda y)]-\frac{M}{2}[a_3\cosh(\lambda y)+a_4\sinh(\lambda y)\right\}e^{\frac{M}{2}y}\\ &- \frac{2MPr\cosh(\sqrt{sPr}(1-y))}{sinh(\sqrt{sPr})[(sPr-s)^2-M^2sPr]}. \qquad (3.1.22)\end{aligned}$$

3.1.4 Validation of the Method:

In order to validate the accuracy of the Riemann-sum approximation method, we set out in this section to find the solution of the steady state and the implicit finite difference method, which should coincide with the transient solution at large time.

Steady-State Solution

The steady state equations are obtained by setting $\frac{\partial}{\partial t}()$ to zero in equations (3.1.6)- (3.1.8), as;

$$\theta_s = 1-y, \qquad (3.1.23)$$

$$u_s = \frac{1}{2M}(a_5-a_7)+\frac{1}{M^2}-\frac{y}{M^2}+\frac{1}{2}(a_8e^{My}+a_6e^{-My})), \qquad (3.1.24)$$

$$h_s = \frac{1}{2M}(a_5+a_7)+\frac{1}{M^3}-\frac{y}{M}+\frac{y^2}{2M}+\frac{1}{2}(a_6e^{-My}-a_8e^{My}), \qquad (3.1.25)$$

$$\tau_s = \frac{M}{2}(a_8e^{My}-a_6e^{-My})-\frac{1}{M^2}, \qquad (3.1.26)$$

$$J_s = \frac{y}{M}-\frac{M}{2}[a_8e^{My}+a_6e^{-My}]-\frac{1}{M}, \qquad (3.1.27)$$

where all constants are defined in appendix A.

Implicit Finite Difference Method

Here, implicit finite difference method is used to ascertain the correctness of the Riemann-sum approximation method. The procedure adopted involves approximation of differential equations by the finite difference equations and then solving the difference equations subject to the prescribed initial and boundary conditions. As defined in section 1.6.3, eqns.(3.1.6) - (3.1.8) become

$$\frac{u(i,j)-u(i,j-1)}{\Delta t} = \frac{1}{(\Delta y)^2}\left[u(i+1,j)-2u(i,j)+u(i-1,j)\right] + \frac{M}{2\Delta y}\left[h(i+1,j)-h(i-1,j)\right]+\theta(i,j), \tag{3.1.28}$$

$$\frac{h(i,j)-h(i,j-1)}{\Delta t} = \frac{1}{Pm}\frac{1}{(\Delta y)^2}[h(i+1,j)-2h(i,j)+h(i-1,j)] + \frac{M}{2\Delta y}[u(i+1,j)-u(i-1,j)], \tag{3.1.29}$$

$$\frac{\theta(i,j)-\theta(i,j-1)}{\Delta t} = \frac{1}{Pr}\frac{1}{(\Delta y)^2}[\theta(i+1,j)-2\theta(i,j)+\theta(i-1,j)]. \tag{3.1.30}$$

The index i refers to y and j refers to t. The time derivative is replaced by the backward difference formula, while the spatial derivatives are replaced by central difference formula. The above equations are solved by Thomas algorithm by manipulating into a system of linear algebraic equations in the tridiagonal form. At each time step, the process of numerical integration for every dependent variable starts from the first neighbouring grid point of the right vertical plate at $y = 1$ and proceeds towards the axis of symmetry at $y = 0$. The process of computation is advanced until a steady state is approached by satisfying the following convergence criterion:

$$\frac{\sum |A_{i,j+1}-A_j|}{M^*|A|_{max}} \leq 10^{-6}, \tag{3.1.31}$$

with respect to the fluid velocity field, the induced magnetic field and temperature. Here $A_{(i,j)}$ stand for the fluid velocity field, induced magnetic field or the temperature field. M^* is the number of interior grid points and $|A|_{max}$is

the maximum absolute value of $A_{(i,j)}$. In the numerical computation special attention is needed to specify Δt to get steady state solution as rapid as possible, yet small enough to avoid instabilities. It is set, which is suitable for the present computation, as

$$\Delta t = Stabr \times (\Delta y)^2. \tag{3.1.32}$$

The parameter $Stabr$ is determined by numerical experimentation in order to achieve convergence and stability of the solution procedure. Numerical experiments show that the value 2 is suitable for the present numerical computation. The obtained numerical values using implicit finite difference method are in excellent agreement with numerical values obtained semi-analytically for the transient state using Riemann-sum for velocity field, induced magnetic field, current density and the skin friction for $Pm = 1$.

3.1.5 Results and Discussion

In order to get a physical insight into the problem, a MATLAB programme is written to compute and generate the graphs for the temperature, velocity, induced magnetic field, current density, and the skin-friction for various values of the parameter embedded in the problem. The results are presented graphically in Figures 3.2.1 to 3.2.17. The values of $Pr = 0.71$ and $Pr = 7.0$ are considered in the computation which correspond to air and water as working fluid respectively. Figures 3.2.1 - 3.2.1 show the temperature profiles for varying values of time (t) and Prandtl number (Pr) respectively. It is observed from Figures 3.2.1(a) and 3.2.1(b), that the temperature increases as time increases and ultimately attained steady state in both cases of air and water. During the numerical computation, it is observed that the time required to reach steady state is directly proportional to Prandtl number. Also it is observed that the temperature is higher near the left plate at $y = 0$ than at the right plate at

$y = 1$. This is as a result of rise in the temperature at the left plate. Decease in the temperature as the Prandtl number Pr increases is observed in Figure 3.2.2. The temperature decreases as Pr increases which is an expected phenomena, since increase in Pr decrease thermal diffusivity of the fluid and this causes low heat penetration and a reduce thermal boundary layer. Figures 3.2.3 - 3.2.8 display the velocity and induced magnetic field in the channel for different values of dimensionless time (t), the magnetic parameter (M), and the Prandtl number (Pr). From Figures 3.2.3(a) and 3.2.3(b) it is observed that the velocity increases as time (t) increases and attains its steady state. These Figures show that time required to reach steady state is higher in case of water ($Pr = 7.0$) than air ($Pr = 0.71$). The velocity at varying values of magnetic parameter (M) is illustrated in Figure 3.2.4. From Figures 3.2.4(a) and 3.2.4(b) it is clear that as M increases, velocity decreases in the central region and a reverse trend observed near the channel wall ($y = 1$). This phenomenon is more visible in case of water than air.This phenomenon is more visible in case of water than air. This finding is very different from the general perception deduced from the Hartman flow which states that external magnetic field produces the Lorentz force that brakes the fluid. This result suggest that it is inappropriate to imagine Lorentz force purely as a braking force, instead it would be more precise to think of the Lorentz force as a force that actually resists a change in motion due to external factors. It suggests that in presence of induced magnetic field, magnetic parameter play a role to accelerate the fluid motion. It is remarkable to point out that for all magnetic parameters considered here, there exists a location inside the flow domain where the velocity field is independent of magnetic parameter. The velocity variation with Pr is shown in Figure 3.2.5. It reveals that velocity decreases with increase of Pr. This is attributed to the fact that as Prandtl number (Pr) increases, thermal conductivity of the fluid decreases, causing weak convection current. Figures 3.2.6 - 3.2.8 exhibit the behaviour of induced magnetic field at dif-

ferent values of dimensionless time (t), the magnetic parameter (M) and the Prandtl number. Induced magnetic field is of parabolic type in upward and downward direction in all cases assuming both positive and negative values. Figure 3.2.6(a) reveal that as time increases induced magnetic field increases in the range $0 < y < 0.4$ while it decreases in the range $0.4 < y < 1$. Similar behaviour is observed in Figure 3.2.6(b) with a shift in the location of inflection point ($approximatelyy = 0.25$). This indicates an existence of a location where induced magnetic field is independent of time. Also, this particular location is strongly dependent on the nature of working fluid. Furthermore, it is seen from Figure 3.2.7(a) that the strength of the induced magnetic field is directly proportional to the strength of magnetic parameter in the region $0 < y < 0.3$ while it is inversely proportional in the region $0.3 < y < 1$. Also in Figure 3.2.7(b), a similar behaviour is noticed with a shift in location of inflection point ($approximately\ y = 0.15$). Hence, we conclude that there exists a point in the flow domain where induced magnetic field is independent of applied magnetic field. Also, the point of inflexion where induced magnetic field changes it character is strongly dependent on the nature of working fluid. Variation of induced magnetic field with Prandtl number is shown in Figure 3.2.8. From this Figure, it is evident that induced magnetic field increases as well as decreases with increase of Pr. Figures 3.2.9 - 3.2.11 depicts the current density distribution. From Figures 3.2.9(a) and 3.2.9(b) it is seen that increase in the dimensionless time (t) increases the current density in the range $0.2 < y < 0.8$ and $0.15 < y < 0.7$ in case of air and water respectively while it decreases with increase of time near the walls $y = 0$ and $y = 1$. In Figures 3.2.10(a) and 3.2.10(b), similar trend as in Figure 3.2.9 for the effect of magnetic parameter (M) on the current density is observed with a little shift in point of inflection. The current density decreases with increase in Pr in the central region of the channel while it increases near the channel walls as shown in Figure 3.2.11. It is interesting to note that current density changes its behaviour at

two different location inside the flow domain for all considered values of Pr. Skin-friction at both plates $y = 0$ and $y = 1$ are plotted against M in Figures 3.2.12, 3.2.13, 3.2.15 and 3.2.16. Figures 3.2.12(a) and 3.2.12(b) show the skin-friction behaviour corresponding to air and water respectively. It is observed that the skin-friction at $y = 0$ increases with time, while it decreases as M increases. An opposite behaviour to this is notice at wall $y = 1$ (Figure 3.2.15). Figure 3.2.13 shows that the skin-friction at $y = 0$ decreases with increase of M and Pr for fixed time ($t = 0.2$) while a reverse trend is observed in the case of skin-friction at $y = 1$ (Figure 3.2.16). In Figure 3.2.14, skin-friction is plotted against Pr at different values of time (t) for fixed magnetic parameter ($M = 0.5$). From this Figure, it is observed that the skin-friction increases as time increases while it decreases as Pr increases. A similar behaviour is observed in the case of as seen in Figure 3.2.17. Tables 3.2.1 and 3.2.2 show the comparison of transient state and steady state numerical values of velocity and the induced magnetic field obtained by using Riemann-sum approximation method (RSM), finite difference method (FDM) and exact solution for steady state (SS) at varying values of time (t) for $Pr = 0.71$, $Pm = 1.0$ and $M = 0.5$. This shows an excellent agreement between the three methods at large value of time. Table 3.2.3 shows the numerical values of the velocity and the induced magnetic field obtained by implicit finite difference method at varying values of magnetic Prandtl number Pm and fixed values of $Pr = 0.71$, $M = 0.5$, and $t = 0.2$. It is found that as Pm increases the velocity increases while induced magnetic field decreases.

3.2

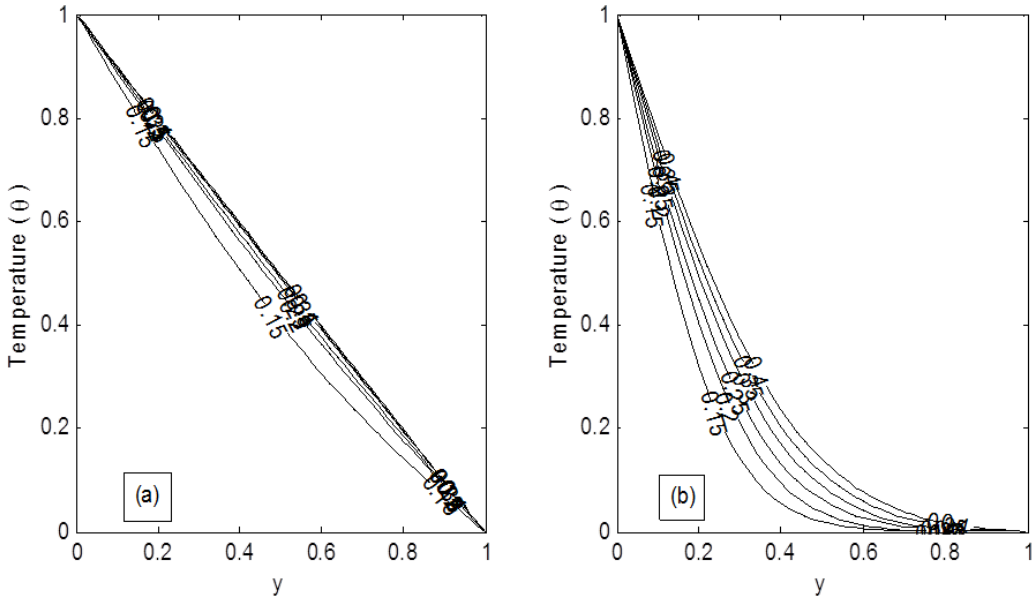


Figure 3.2.1: Temperature distribution(θ) for $Pr = 0.71(a)$ and $Pr = 7.0(b)$ at different values of time t.

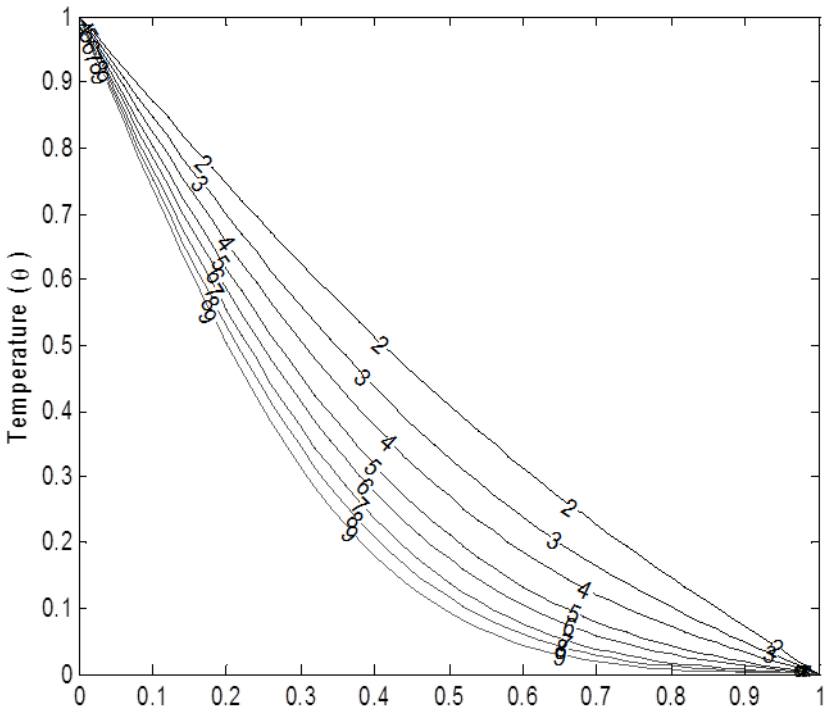


Figure 3.2.2: Temperature profiles at different values of Pr for $t = 0.2$.

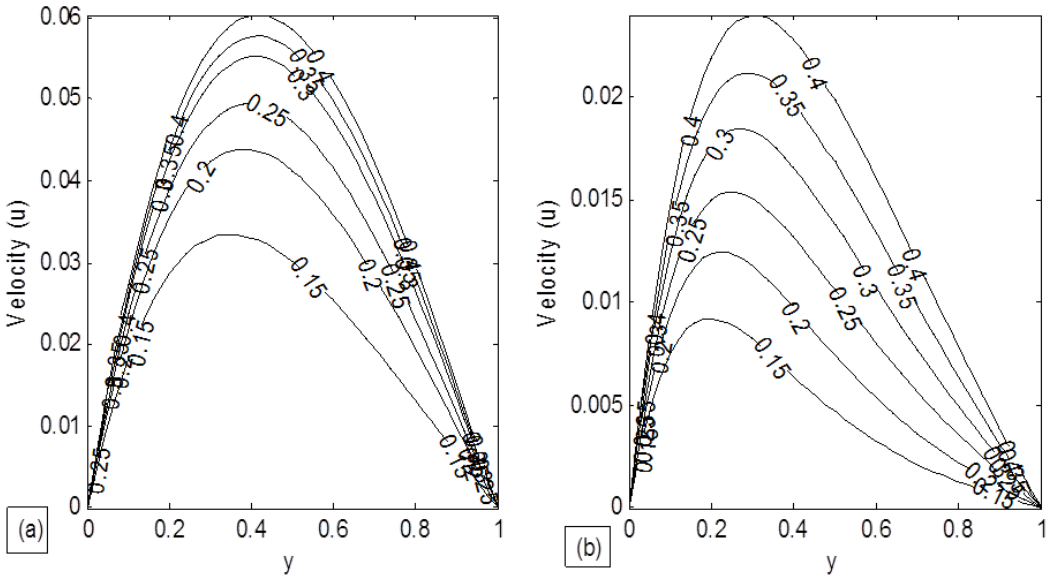


Figure 3.2.3: Velocity profiles at different values of time (t) for $M = 0.5$, $Pr = 0.71(a)$ and $7.0(b)$.

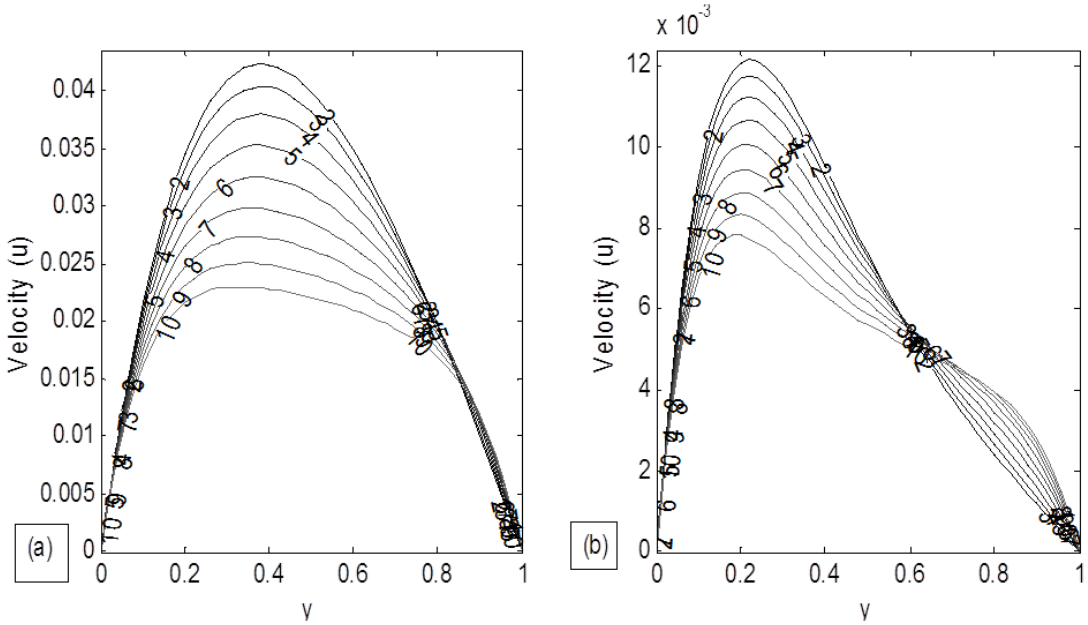


Figure 3.2.4: Velocity profiles at different values of M for $t = 0.2$, $Pr = 0.71(a)$ and $7.0(b)$.

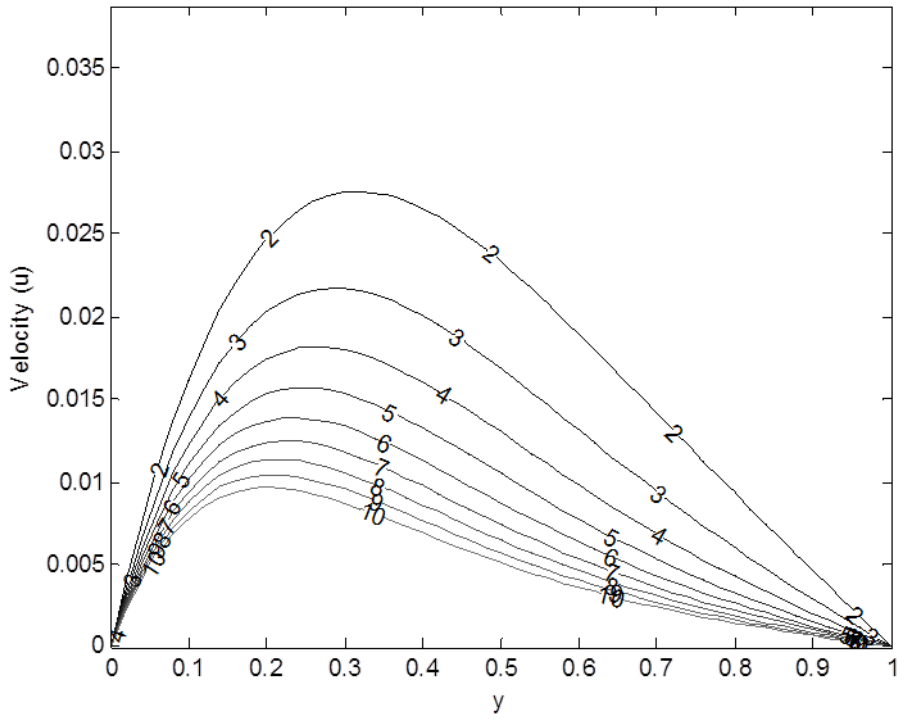


Figure 3.2.5: Velocity profiles at different values of Pr for $t = 0.2$, $M = 0.5$.

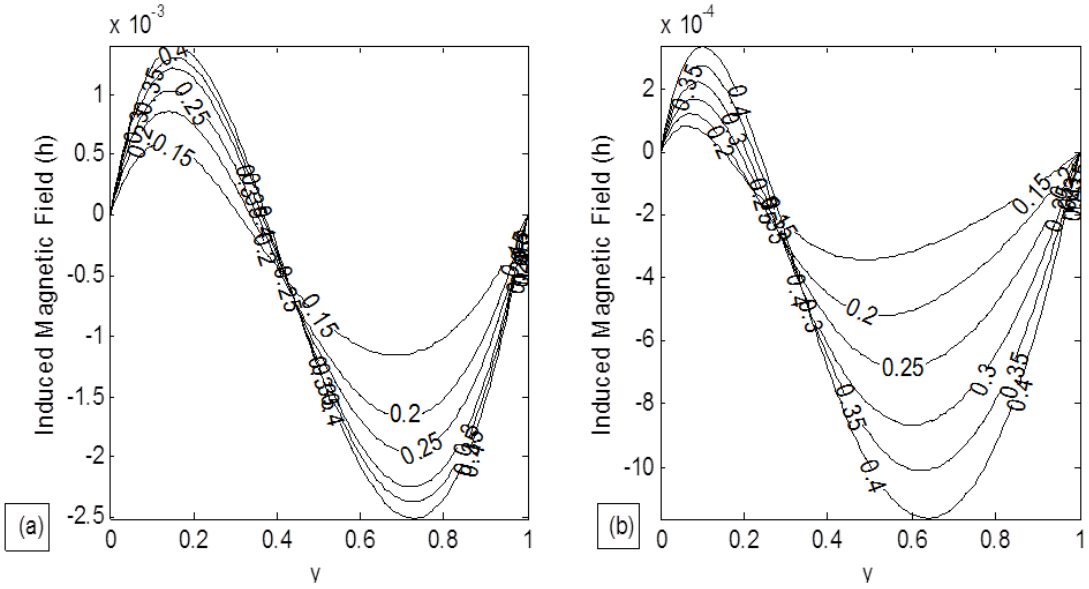


Figure 3.2.6: Induced Magnetic Field profiles at different values of time (t) for $M = 0.5$, $Pr = 0.71(a)$ and $7.0(b)$.

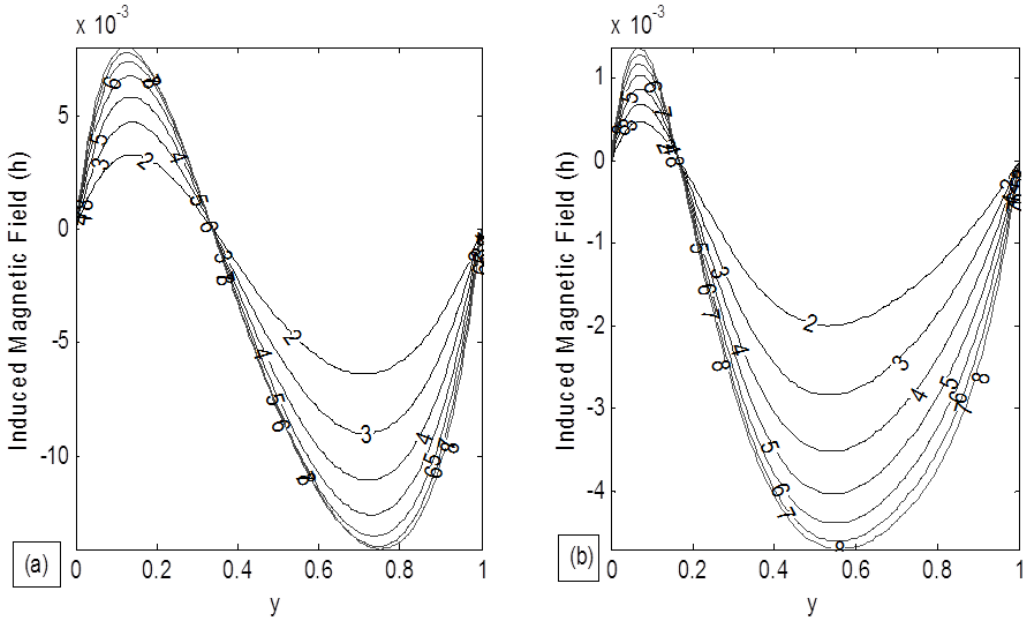


Figure 3.2.7: Induced Magnetic Field profiles at different values of M for $t = 0.2$, $Pr = 0.71(a)$ and $7.0(b)$.

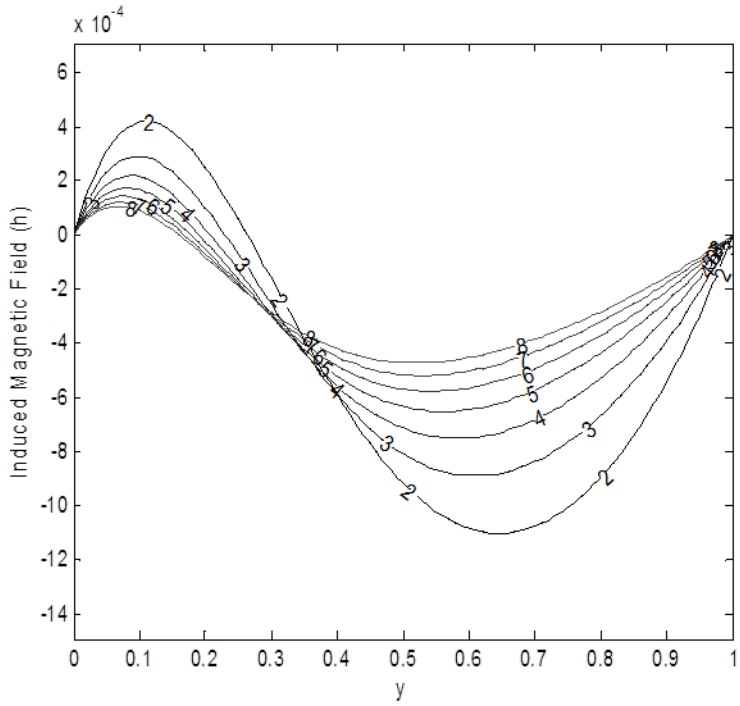


Figure 3.2.8: Induced Magnetic Field profiles at different values of Pr for $t = 0.2$, $M = 0.5$.

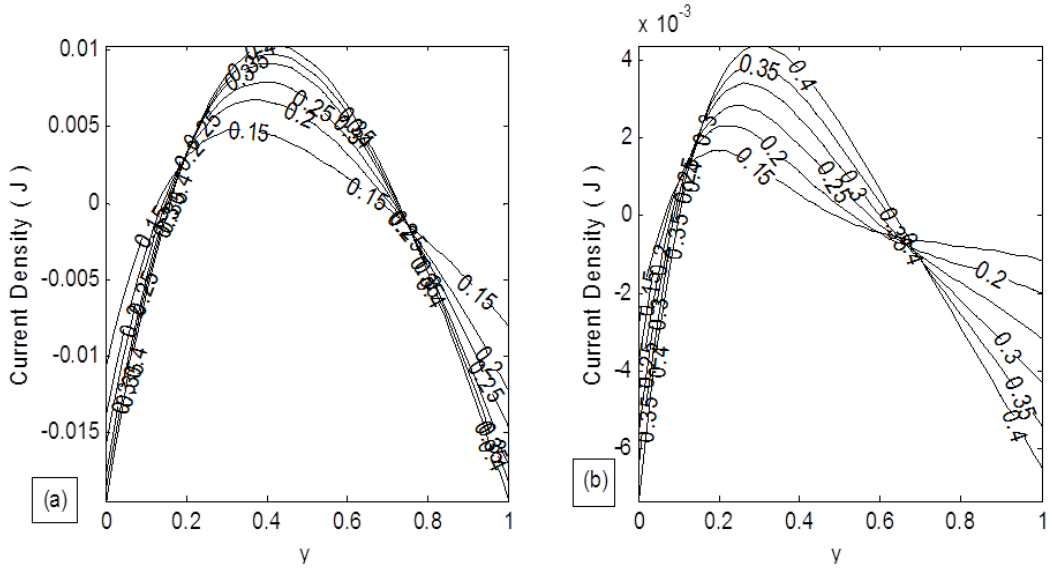


Figure 3.2.9: Current Density profiles at different values of time (t) for $M = 0.5$, $Pr = 0.71(a)$ and $7.0(b)$.

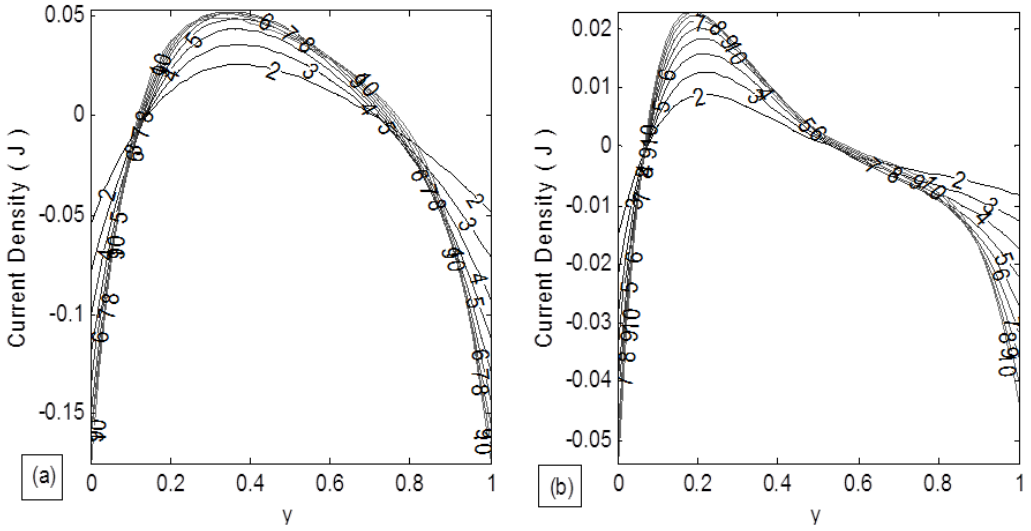


Figure 3.2.10: Current Density profiles at different values of M for $t = 0.2$, $Pr = 0.71(a)$ and $7.0(b)$.

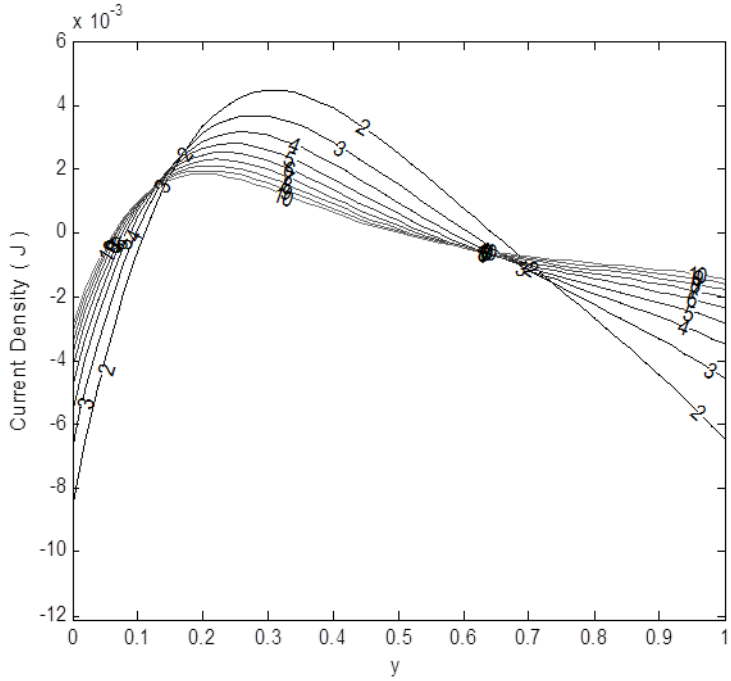


Figure 3.2.11: Current Density profiles at different values of Pr for $t = 0.2$, $M = 0.5$

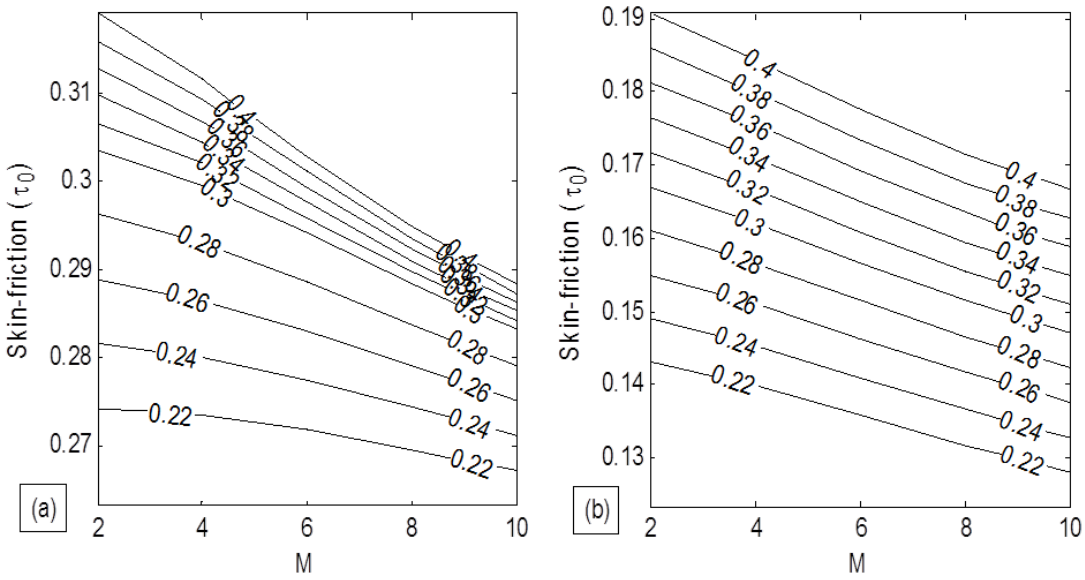


Figure 3.2.12: Skin-friction (τ_0) against M at different values of time (t) for $Pr = 0.71(a)$ and $7.0(b)$.

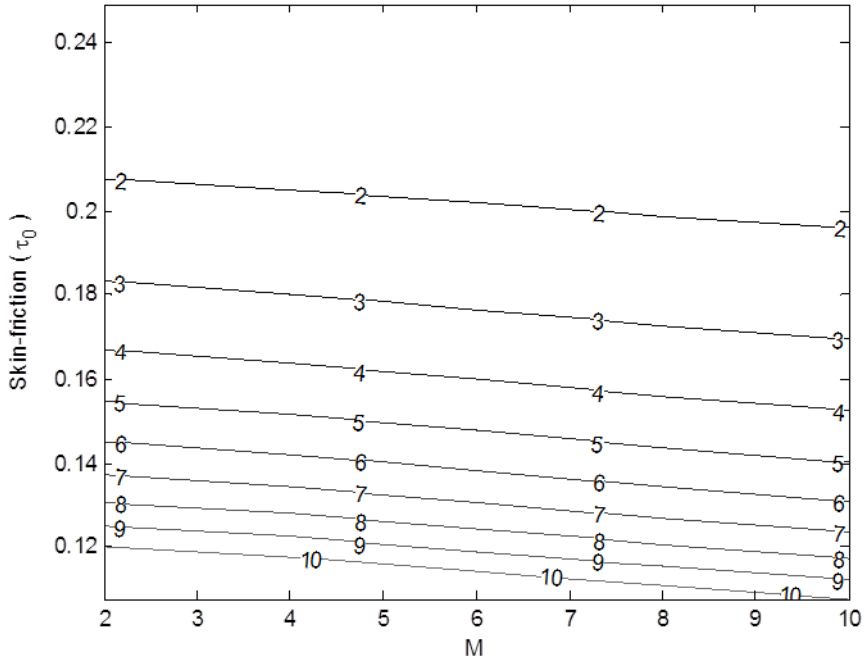


Figure 3.2.13: Skin-friction (τ_0) against M at different values of Pr for $t = 0.2$.

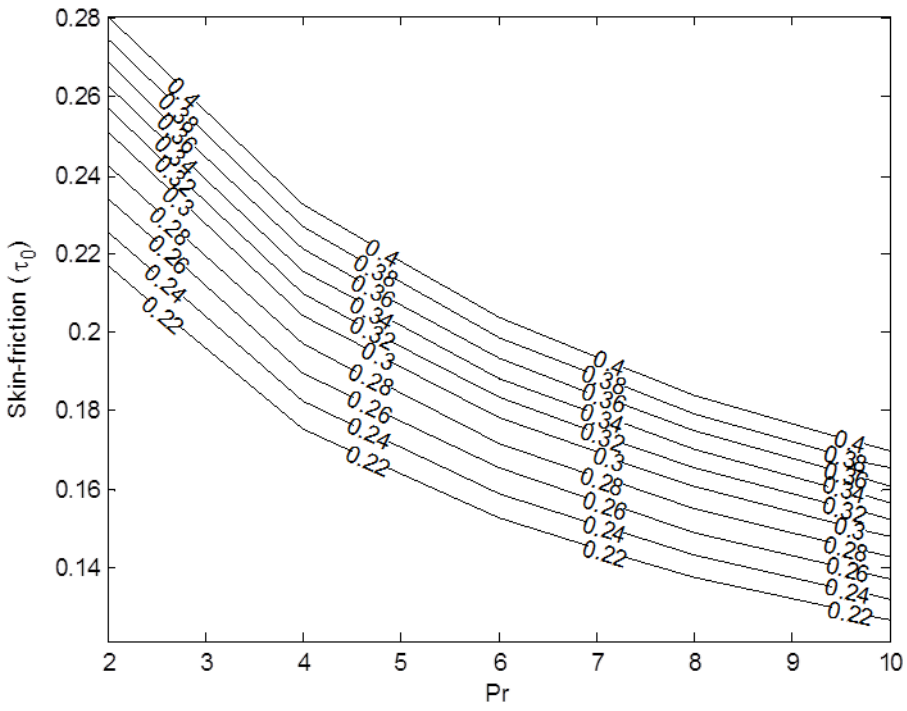


Figure 3.2.14: Skin-friction (τ_0) against Pr at different values of t for $M = 0.5$.

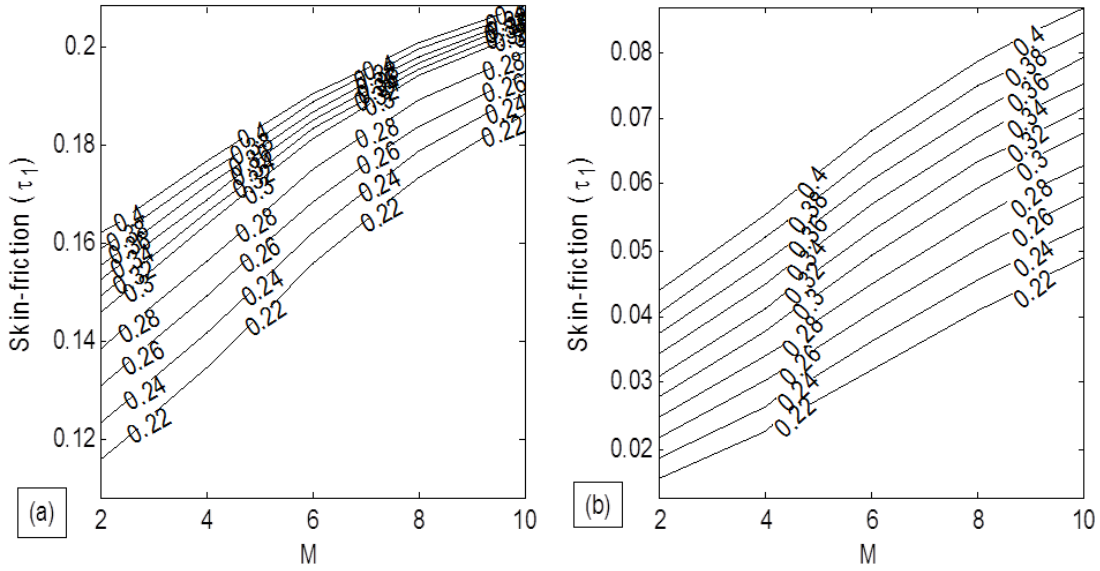


Figure 3.2.15: Skin-friction (τ_1) against M at different values of time (t) for $Pr = 0.71(a)$ and $7.0(b)$.

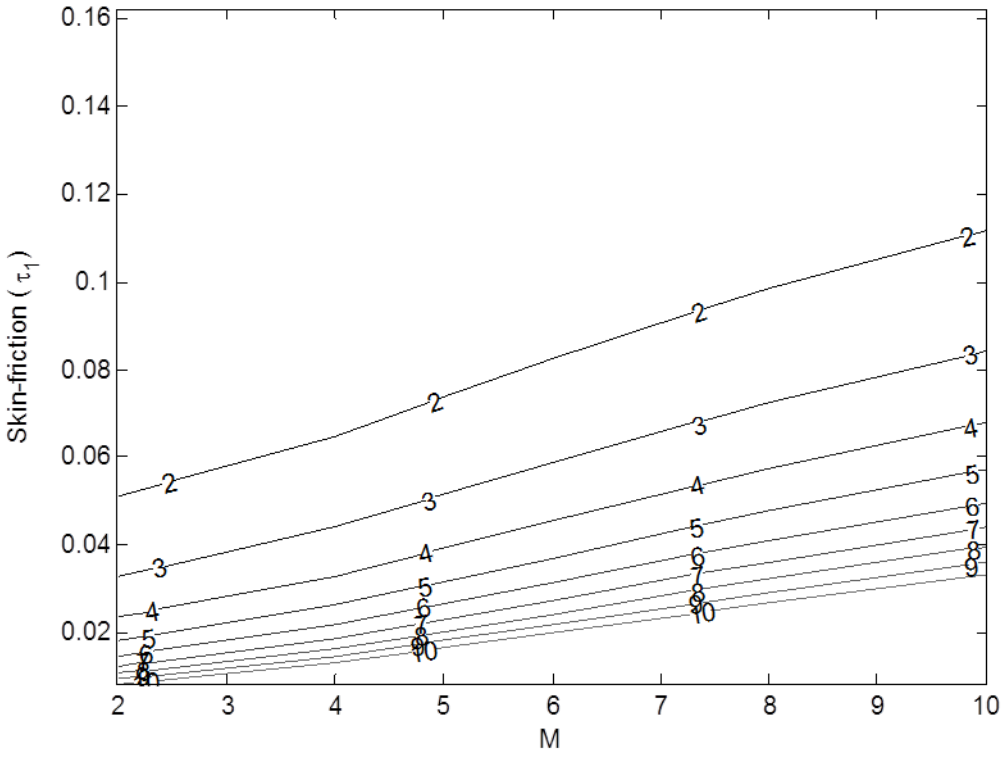


Figure 3.2.16: Skin-friction (τ_1) against M at different values of Pr for $t = 0.2$.

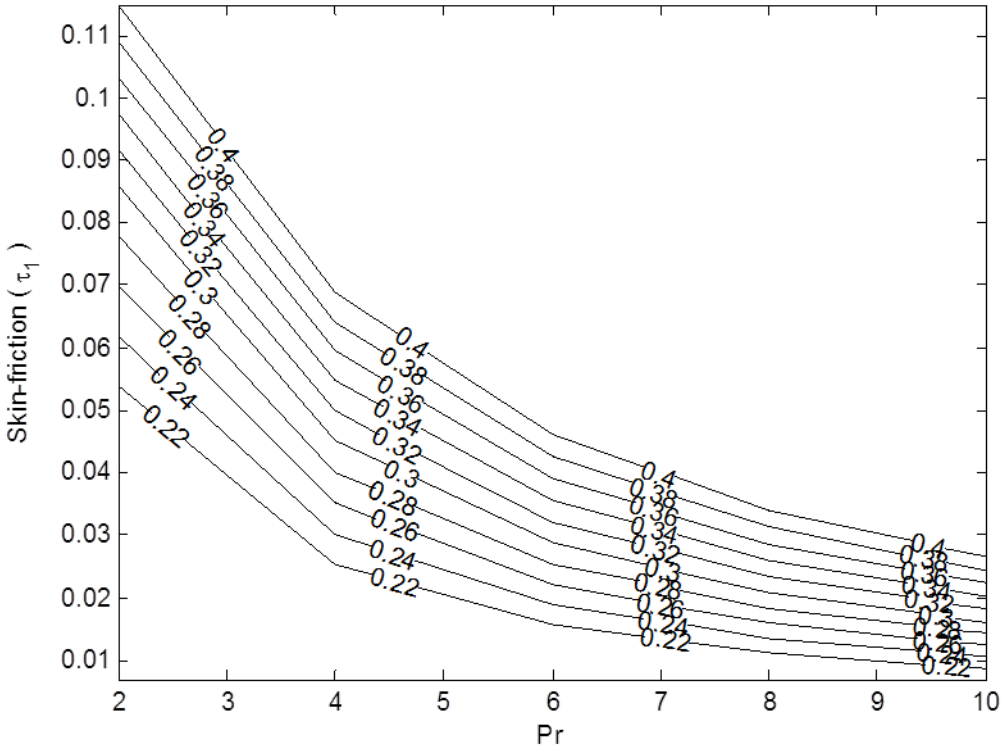


Figure 3.2.17: Skin-friction (τ_1) against Pr at different values of t for $M = 0.5$.

Table 3.2.1: Numerical values of the flow velocity u obtained using the Riemann-Sum approximation method (RSM) compared to those obtained by the finite difference method FDM) and the Steady State (SS) for $Pr = 0.71, Pm = 1.0$ and $M = 0.5$ at different value of t.

	t = 0.2		t = 0.4		t = 0.6		
y	FDM	RSM	FDM	RSM	FDM	RSM	SS
0.0	0.0000	0.0000	0.0000	0.0000	0.0000	0.0000	0.0000
0.1	0.0219	0.0219	0.0273	0.0273	0.0283	0.0283	0.0284
0.2	0.0355	0.0355	0.0457	0.0457	0.0475	0.0475	0.0478
0.3	0.0422	0.0423	0.0563	0.0563	0.0588	0.0588	0.0592
0.4	0.0437	0.0438	0.0602	0.0602	0.0631	0.0632	0.0637
0.5	0.0412	0.0413	0.0585	0.0586	0.0616	0.0616	0.0622
0.6	0.0358	0.0359	0.0523	0.0523	0.0552	0.0552	0.0557
0.7	0.0283	0.0284	0.0424	0.0424	0.0449	0.0449	0.0453
0.8	0.0195	0.0196	0.0298	0.0298	0.0316	0.0316	0.0319
0.9	0.0997	0.0100	0.0154	0.0154	0.0163	0.0163	0.0165
1.0	0.0000	0.0000	0.0000	0.0000	0.0000	0.0000	0.0000

Table 3.2.2: Numerical values of the induced magnetic field h obtained using the Riemann-Sum approximation method (RSM) compared to those obtained by the finite difference method (FDM) and the Steady State (SS) for $Pr = 0.71$, $Pm = 1.0$ and $M = 0.5$ at different value of t.

	t = 0.2		t = 0.4		t = 0.6		
y	FDM	RSM	FDM	RSM	FDM	RSM	SS
0.0	0.0000	0.0000	0.0000	0.0000	0.0000	0.0000	0.0000
0.1	0.0008	0.0008	0.0012	0.0012	0.0013	0.0013	0.0013
0.2	0.0008	0.0008	0.0013	0.0013	0.0015	0.0014	0.0015
0.3	0.0002	0.0002	0.0007	0.0007	0.0008	0.0008	0.0008
0.4	-0.0004	-0.0004	-0.0003	-0.0002	-0.0002	-0.0002	-0.0002
0.5	-0.0010	-0.0010	-0.0013	-0.0012	-0.0012	-0.0012	-0.0013
0.6	-0.0015	-0.0015	-0.0020	-0.0020	-0.0022	-0.0022	-0.0022
0.7	-0.0017	-0.0017	-0.0025	-0.0025	-0.0026	-0.0026	-0.0027
0.8	-0.0015	-0.0015	-0.0023	-0.0023	-0.0025	-0.0025	-0.0025
0.9	-0.0010	-0.0010	-0.0015	-0.0015	-0.0017	-0.0016	-0.0017
1.0	0.0000	0.0000	0.0000	0.0000	0.0000	0.0000	0.0000

Table 3.2.3: Numerical values for velocity u and that of the Induced Magnetic field h obtained by the finite difference for $Pr = 0.71$, $M = 0.5$, $t = 0.2$, at different value of Pm.

	Pm = 0.5		Pm = 1.0		Pm = 1.5	
y	u	h	u	h	u	h
0.0	0.0000	0.0000	0.0000	0.0000	0.0000	0.0000
0.1	0.0219	0.0004	0.0219	0.0008	0.0219	0.0012
0.2	0.0355	0.0004	0.0355	0.0008	0.0354	0.0011
0.3	0.0423	0.0001	0.0422	0.0003	0.0422	0.0004
0.4	0.0438	-0.0003	0.0437	-0.0004	0.0437	-0.0005
0.5	0.0412	-0.0006	0.0412	-0.0010	0.0412	-0.0013
0.6	0.0358	-0.0009	0.0358	-0.0015	0.0357	-0.0019
0.7	0.0283	-0.0010	0.0283	-0.0017	0.0283	-0.0022
0.8	0.0195	-0.0009	0.0195	-0.0015	0.0195	-0.0199
0.9	0.0996	-0.0005	0.0997	-0.0010	0.0998	-0.1300
1.0	0.0000	0.0000	0.0000	0.0000	0.0000	0.0000

3.3 Computational treatment of MHD transient natural convection flow in a vertical channel due to symmetric heating in presence of induced magnetic field

In this section we have studied the effect of induced magnetic field on transient hydromagnetic natural convection flow of an incompressible viscous electrically conducting fluid in the presence of transverse magnetic field in a vertical channel formed by electrically non-conducting infinite vertical parallel plates due to symmetric heating of vertical parallel plates. The problem is solved using Laplace transform technique and the inversion of the Laplace domain to the time domain is obtained by Riemann-sum approximation method. In order to verify the accuracy of Riemann-Sum approximation method, analytical solution for steady state mathematical model is obtained in closed form. The governing equations are also solved using an implicit finite difference method to confirm the method used in the present problem. During the course of numerical computation an excellent agreement was found between steady state solution obtained exactly and transient solution obtained by implicit finite difference method or Riemann sum approximation method at large values of time.

3.3.1 Mathematical Analysis

A transient free-convective flow of conducting fluid through vertical channel formed by two infinite electrically non-conducting plates is considered.The x'-axis is taken along the flow direction and y'-axis is perpendicular to it. A uniform magnetic field of strength H_0' is applied perpendicular to the flow direction. At time $t' \leq 0$, the fluid and non-conducting plates are at same

temperature T_0. At time $t' > 0$, the temperature of the plates at $y' = -d$ and $y' = d$ are instantaneously raised or lower to T_1 which is their after maintained constant. Since the objective of the present work is to analyze the impact of induced magnetic field on transient free-convective flow in a vertical channel, the induced magnetic field h' is taken into account in the present mathematical model. As the plates are of infinite extent, the variables describing the mathematical model are functions of y' and t' only. In addition, it is assumed that all the fluid properties are constant except that the density variation with temperature is considered in the body force term. Using the Boussinesq's approximation, the mathematical model representing the present physical situation are

$$\frac{\partial u'}{\partial t'} = \nu \frac{\partial^2 u'}{\partial y'^2} + \frac{\mu_e H_0}{\rho} \frac{\partial h'}{\partial y'} + g\beta(T' - T_0), \tag{3.3.1}$$

$$\frac{\partial h'}{\partial t'} = \frac{1}{\sigma \mu_e} \frac{\partial^2 h'}{\partial y'^2} + H_0 \frac{\partial u'}{\partial y'}, \tag{3.3.2}$$

$$\frac{\partial T'}{\partial t'} = \alpha \frac{\partial^2 T'}{\partial y'^2}, \tag{3.3.3}$$

The initial and boundary conditions for the present problem are

$$\begin{aligned} &u' = 0, \quad T' = T_0, \quad h' = 0, \quad for \quad -d \leq y' \leq +d \ \ at \ \ t' \leq 0, \\ &u' = 0, \quad T' = T_1, \quad h' = 0, \quad at \ \ y' = -d \ \ for \ t' > 0, \\ &u' = 0, \quad T' = T_1, \quad h' = 0, \quad at \ \ y' = +d \ \ for \ t' > 0. \end{aligned} \tag{3.3.4}$$

where u' is the velocity of the fluid, h' is the induced magnetic field, t' is the time, T' is the temperature of the fluid, ν is the kinematic viscosity, g is the acceleration due to gravity, β is the coefficient of thermal expansion, μ_e is the magnetic permeability, ρ the density and α is thermal diffusivity of the fluid. By introducing the following non-dimensional quantities;

$$\begin{aligned} &u = \tfrac{u'\nu}{g\beta(T_1 - T_0)d^2}, \ h = \tfrac{h'(\frac{\mu_e}{\rho})^{\frac{1}{2}}\nu}{g\beta d^2(T_1 - T_0)}, \quad \theta = \tfrac{(T' - T_0)}{(T_1 - T_0)}, \\ &y = \tfrac{y'}{d} \quad t = \tfrac{t'\nu}{d^2}, \quad M = \tfrac{dH_0}{\nu}(\tfrac{\mu_e}{\rho})^{\frac{1}{2}}, \quad Pm = \sigma\mu_e\nu, \quad Pr = \tfrac{\nu}{\alpha}, \end{aligned} \tag{3.3.5}$$

Where u is the dimensionless velocity, h is the dimensionless induced magnetic field, t the dimensionless time, y is the dimensionless coordinate normal to the channel plates, θ the dimensionless temperature, others are magnetic parameter M, magnetic Prandtl number Pm and the Prandtl number Pr. The governing dimensionless equations are;

$$\frac{\partial u}{\partial t} = \frac{\partial^2 u}{\partial y^2} + M\frac{\partial h}{\partial y} + \theta, \tag{3.3.6}$$

$$\frac{\partial h}{\partial t} = \frac{1}{Pm}\frac{\partial^2 h}{\partial y^2} + M\frac{\partial u}{\partial y}, \tag{3.3.7}$$

$$\frac{\partial \theta}{\partial t} = \frac{1}{Pr}\frac{\partial^2 \theta}{\partial y^2}. \tag{3.3.8}$$

Also, due to symmetric nature of the physical situation the corresponding initial and boundary conditions for the velocity, temperature and the induced magnetic field in dimensionless form are;

$$\begin{aligned} &u = 0, \quad \theta = 0, \quad h = 0, \quad at \;\; 0 \le y \le 1 \;\; for \;\; t \le 0, \\ &\tfrac{\partial u}{\partial y} = 0, \quad \frac{\partial \theta}{\partial y} = 0, \quad \frac{\partial h}{\partial y} = 0, \quad at \;\; y = 0 \;\; for \;\; t > 0, \\ &u = 0, \quad \theta = 1, \quad h = 0, \quad at \;\; y = 1 \;\; for \;\; t > 0. \end{aligned} \tag{3.3.9}$$

The solutions of Eqns. (3.3.6) - (3.3.8) under the initial conditions Eq.(3.3.9)for $Pm = 1$, can be obtained using the Laplace transform technique as defined in section 1.6.1;

$$\frac{d^2\bar{u}}{dy^2} - s\bar{u} + M\frac{d\bar{h}}{dy} + \bar{\theta} = 0, \tag{3.3.10}$$

$$\frac{d^2\bar{h}}{dy^2} - s\bar{h} + M\frac{d\bar{u}}{dy} = 0, \tag{3.3.11}$$

$$\frac{d^2\bar{\theta}}{dy^2} - s\bar{\theta}Pr = 0. \tag{3.3.12}$$

The boundary conditions now become

$$\begin{aligned} &\tfrac{d\bar{u}}{\partial y} = 0, \quad \frac{d\bar{\theta}}{dy} = 0, \quad \frac{d\bar{h}}{dy} = 0, \quad at \;\; y = 0, \\ &\bar{u} = 0, \quad \bar{\theta} = s^{-1}, \quad \bar{h} = 0, \quad at \;\; y = 1. \end{aligned} \tag{3.3.13}$$

Therefore, the solutions of Eqs.(3.3.10) - (3.3.12) are respectively

$$\begin{aligned}\bar{u}(y,s) &= \tfrac{1}{2}[[a_9\cosh(\lambda y)+a_{10}\sinh(\lambda y)]e^{\frac{-M}{2}y} \\ &\quad +[a_{11}\cosh(\lambda y)+a_{12}\sinh(\lambda y)]e^{\frac{M}{2}y}] \\ &\quad -\tfrac{2\cosh(by)(sPr-s)}{s\cosh(b)[(sPr-s)^2-M^2sPr]},\end{aligned} \tag{3.3.14}$$

$$\begin{aligned}\bar{h}(y,s) &= \tfrac{1}{2}[[a_9\cosh(\lambda y)+a_{10}\sinh(\lambda y)]e^{\frac{-M}{2}y} \\ &\quad -[a_{11}\cosh(\lambda y)+a_{12}\sinh(\lambda y)]e^{\frac{M}{2}y}] \\ &\quad +\tfrac{2Mb\sinh(by)}{s\cosh(b)[(sPr-s)^2-M^2sPr]},\end{aligned} \tag{3.3.15}$$

$$\bar{\theta}(y,s) = \frac{\cosh(by)}{s\cosh(b)}. \tag{3.3.16}$$

where all the constants are defined in appendix A.

Similarly, Eqs.(3.3.14) - (3.3.16) are to be inverted in order to obtain the velocity, the induced magnetic field and the temperature in the time domain using equation (1.6.6).

3.3.2 Skin Friction and Current Density

The skin friction (τ) and the current density (J) are similarly obtained by differentiating Equation.(1.6.6) with respect to y as obtained in equations (3.1.17 and 3.1.21);

where

$$\begin{aligned}\bar{u_1} &= \tfrac{\lambda}{2}\left[(a_9\sinh(\lambda y)+a_{10}\cosh(\lambda y))e^{-\frac{M}{2}y}+(a_{11}\cosh(\lambda y)+a_{12}\sinh(\lambda y))e^{\frac{M}{2}y}\right] \\ &\quad +\tfrac{M}{4}\left[(a_9\sinh(\lambda y)+a_{10}\cosh(\lambda y))e^{-\frac{M}{2}y}+(a_{11}\cosh(\lambda y)+a_{12}\sinh(\lambda y))e^{\frac{M}{2}y}\right] \\ &\quad -\tfrac{2b\sinh(b)(sPr-s)+M\cosh(b)}{s\cosh(b)[(sPr-s)-M^2sPr]},\end{aligned} \tag{3.3.17}$$

and

$$\begin{aligned}\bar{h_1} &= -\tfrac{\lambda}{2}\left\{\left[a_9\sinh(\lambda y)+a_{10}\cosh(\lambda y)\right]e^{-\frac{M}{2}y}-\left[a_{11}\sinh(\lambda y)+a_{12}\cosh(\lambda y)\right]e^{\frac{M}{2}y}\right\}\\ &+\tfrac{M}{4}\left\{\left[a_9\cosh(\lambda y)+a_{10}\sinh(\lambda y)\right]e^{-\frac{M}{2}y}-\left[a_{11}\cosh(\lambda y)+a_{12}\sinh(\lambda y)\right]e^{\frac{M}{2}y}\right\}\\ &-\tfrac{2MsPr\cosh(by)}{s\cosh(b)[(sPr-s)^2-M^2sPr]}. \qquad (3.3.18)\end{aligned}$$

3.3.3 Steady State Solution

The steady state solutions are obtain by setting $\frac{\partial}{\partial t}$ to zero in Eqs.(3.3.6) - (3.3.8) as

$$u_s = -\frac{1}{M^2}\left[\cosh(M)-\cosh(My)\right], \qquad (3.3.19)$$

$$h_s = 2+\frac{1}{M}[\frac{\sinh(My)}{M}-\frac{\sinh(M)}{M}-y]. \qquad (3.3.20)$$

The steady-state skin-friction is;

$$\tau_s = \frac{\sinh(My)}{M}, \qquad (3.3.21)$$

and the steady-state current density is;

$$J_s = \frac{\cosh(My)}{M}-\frac{1}{M}. \qquad (3.3.22)$$

3.3.4 Implicit Finite Difference Method

With reference to section 1.6.3, equations.(3.3.6) - (3.3.8) reduces to

$$\begin{aligned}\frac{u(i,j)-u(i,j-1)}{\Delta t} &= \tfrac{1}{(\Delta y)^2}[u(i+1,j)-2u(i,j)+u(i-1,j)]\\ &+\tfrac{M}{2\Delta y}[h(i+1,j)-h(i-1,j)]+\theta(i,j), \qquad (3.3.23)\end{aligned}$$

$$\begin{aligned}\frac{h(i,j)-h(i,j-1)}{\Delta t} &= \tfrac{1}{Pm}\tfrac{1}{(\Delta y)^2}[h(i+1,j)-2h(i,j)+h(i-1,j)]\\ &+\tfrac{M}{2\Delta y}[u(i+1,j)-u(i-1,j)], \qquad (3.3.24)\end{aligned}$$

$$\frac{\theta(i,j)-\theta(i,j-1)}{\Delta t} = \frac{1}{Pr}\frac{1}{(\Delta y)^2}[\theta(i+1,j)-2\theta(i,j)+\theta(i-1,j)]. \qquad (3.3.25)$$

The index i refers to y and j refers to t. The time derivative is replaced by the backward difference formula, while the spatial derivatives are replaced by central difference formula. The above equations are solved by Thomas algorithm by manipulating into a system of linear algebraic equations in the tridiagonal form. At each time step, the process of numerical integration for every dependent variable starts from the first neighbouring grid point of the right vertical plate at $y = 1$ and proceeds towards the axis of symmetry at $y = 0$. The process of computation is advanced until a steady state is approached by satisfying the following convergence criterion:

$$\frac{\sum |A_{i,j+1} - A_j|}{M^* |A|_{max}} \leq 10^{-6}, \tag{3.3.26}$$

with respect to the fluid velocity field, the induced magnetic field and temperature. Here $A_{(i,j)}$ stand for the fluid velocity field, induced magnetic field or the temperature field. M^* is the number of interior grid points and $|A|_{max}$is the maximum absolute value of $A_{(i,j)}$. In the numerical computation special attention is needed to specify Δt to get steady state solution as rapid as possible, yet small enough to avoid instabilities. It is set, which is suitable for the present computation, as

$$\Delta t = Stabr \times (\Delta y)^2 \tag{3.3.27}$$

The parameter $Stabr$ is determined by numerical experimentation in order to achieve convergence and stability of the solution procedure. Numerical experiments show that the value 2 is suitable for the present numerical computation. The obtained numerical values using implicit finite difference method are in excellent agreement with numerical values obtained semi-analytically for the transient state using Riemann-sum for velocity field, induced magnetic field, current density and the skin friction for $Pm = 1$. Furthermore, results are in close agreement at large value of time with exact solution derived for steady state solution as shown in Tables 3.3.1 and 3.3.2.

3.3.5 Results and Discussion

In order to get a physical insight into the problem, temperature, velocity, induced magnetic field, current density, and skin-friction are presented graphically for different values of time t, magnetic parameter (M) and Prandtl number (Pr). The effect of dimensionless time (t) on the temperature for air ($Pr = 0.71$) and water ($Pr = 7.0$) is shown in Figures 3.3.1(a) and 3.3.1(b) respectively. It is observed that an increase in dimensionless time parameter (t) causes an increase in the temperature profile in case of both air and water, and this is more prominent in air than water. It is clear from Figure 3.3.2, that temperature decreases with increase in (Pr). This behaviour is obvious, since fluids with high Pr have small thermal conductivity and high viscosity which causes low heat penetration and reduce thermal boundary layer.

Comparison between Figures 3.3.3(a) and 3.3.3(b) reveal that increase in dimensionless time (t) led to increase in velocity which is symmetrical about the axis of the channel ($y = 0$). Furthermore, we noticed that velocity is higher in case of air in comparison to water. This is true since convection current is weak for water than air. From Figures 3.3.4(a) and 3.3.4(b) it is clear that as M increases, velocity decreases in the central region and a reverse trend observed near the channel wall. This phenomena is more visible in case of water than air. This finding is very different from the general perception deduced from the Hartman flow which states that external magnetic field produces the Lorentz force that inhibit the fluid motion. This result suggest that it is inappropriate to imagine Lorentz force purely as a braking force, instead it would be more precise to think of the Lorentz force as a force that actually resists a change in motion due to external factors. It suggest that in presence of induced magnetic field, magnetic parameter play a role to accelerate the fluid motion. It is remarkable to point out that for all magnetic parameters considered here, there exists a location inside the flow domain where the velocity field is in-

dependent of magnetic parameter. The variation of velocity with respect to Prandtl number (Pr) is depicted in Figure 3.3.5. From this Figure, it is clear that velocity decreases with increase of Pr.

Figures 3.3.6 - 3.3.8 describe the behaviour of induced magnetic field at different values of dimensionless time (t), the magnetic parameter M and the Prandtl number Pr. Induced magnetic field is of parabolic type in downward direction in all cases and symmetrical about the axis of the channel ($y = 0$). Figures 3.3.6(a) and 3.3.6(b) reveals that as time increases induced magnetic field increases in the range $0 \leq y \leq 0.45$ while it decreases in the range $0.45 \leq 1.0$ in case of air (Figure 3.3.6(a)). Similar behaviour is observed in Figure 3.3.6(b) with a shift in the location of inflection point. It implies that there exists a location where induced magnetic field is independent of time. Also, this particular location is strongly dependent on the nature of working fluid. It is clear from Figures 3.3.7(a) and 3.3.7(b) that the strength of the induced magnetic field is directly proportional to the strength of magnetic parameter in the region $0 \leq y \leq 0.55$ while it is inversely proportional in the region $0.55 \leq y \leq 1.0$ (Figure 3.3.7(a)). Also in Figure 3.3.7(b), a similar behaviour is noticed with a shift in location of inflection point. It is also observed that there exists a point in the flow domain where induced magnetic field is independent of magnetic parameter. From Figures 3.3.7(a) and 3.3.7(b) we conclude that the point of inflection is a function of Prandtl number. Variation of induced magnetic field with Prandtl number is shown in Figure 3.3.8. From the Figure, it is clear that induced magnetic field decreases with Pr near the axis ($y = 0$) and increases near the channel plate ($y = 1$). Figures 3.3.9 - 3.3.11 depict the current density distribution. Increase in the dimensionless time (t) increases the current density in the range $0 \leq y \leq 0.8$ and then decreases with increase of time in the range $0.8 \leq y \leq 1$ for air (Figure 3.3.9(a)). It is interesting to note that current density changes its behaviour with time at two different location inside the flow domain in case of water (Figure 3.3.9(b)).

Furthermore, the effect of magnetic parameter M is to increase the the current density in $0 \leq y \leq 0.85$ and decrease in $0.85 \leq y \leq 1.0$, in the case of air (Figure 3.3.10(a)). In Figure 3.3.10(b), the current density decreases as M increases in $0 \leq y \leq 0.45$ while it increases in $0.45 \leq y \leq 0.9$ and then decreases in $0.9 \leq y \leq 1.0$. Existence of a location where the current density is independent of time and the magnetic parameter are respectively observed in Figures 3.3.9 and 3.3.10. It is also observed that in the case of $Pr = 0.71$ there is a single point of inflection while for $Pr = 7.0$ there are two points of inflection. The current density decreases with increase in Pr around the central region of the channel as noted in Figure 3.3.11. Skin-friction (τ) is plotted against M in Figures 3.3.12 - 3.3.13. Figures 3.3.12(a) and 3.3.12(b) shows the skin-friction behaviour corresponding to air and water. From these Figures, it is seen that the skin-friction decreases as the dimensionless time (t) increases in the case of both air and water while the impact of magnetic parameter on skin-friction is just opposite in case of air and water. Figure 3.3.13 show the effect of skin friction against (M), with different values of (Pr). It is observed that as Pr increases the skin-friction increases, this is true since higher Pr fluids posses higher viscosities and lower thermal conductivities. It is seen from Figure 3.3.14 that the skin-friction (τ) increases as Pr increases while it decreases with increase of dimensionless time (t).

Tables 3.3.1 and 3.3.2 show the comparison of transient state and steady state numerical values of velocity and the induced magnetic field obtained using Riemann-sum approximation method (RSM), finite difference method (FDM) and exact solution for steady state (SS) at varying values of time t for $Pr = 0.71$, $Pm = 1.0$ and $M = 2.0$. This reveals an excellent agreement between the three methods at large value of time. Table 3.3.3 depict the numerical solution of the velocity and the induced magnetic field obtained by finite difference method for varying values of magnetic parameter M for fixed values of $Pr = 0.71$, $Pm = 1.0$ and $t = 4.0$. It is observed that as M increases the velocity

decreases. This is true since application of transverse magnetic field normal to the flow direction has a tendency to create a drag-like Lorentz force which has a decreasing effect on the flow velocity. Table 3.3.4 show the numerical solution of the velocity and the induced magnetic field obtained by finite difference method at varying values of magnetic Prandtl number Pm for fixed values of $Pr = 0.71$, $M = 2.0$, $M = 2.0$ and $t = 4.0$. It is found that as Pm increases the velocity increases while induced magnetic field decreases.

Table 3.3.1: Numerical values of the velocity u obtained using the Riemann-Sum approximation method (RSM) compared to those obtained by the finite difference method (FDM) and the steady state (SS) for $Pr = 0.71, Pm = 1.0$ and $M = 2.0$ at varying values of t.

	$t = 4.0$		$t = 6.0$		$t = 8.0$		
y	RSM	FDM	RSM	FDM	RSM	FDM	SS
0.0	0.6761	0.6709	0.6886	0.6879	0.6903	0.6906	0.6905
0.1	0.6711	0.6661	0.6836	0.6829	0.6853	0.6856	0.6855
0.2	0.6562	0.6512	0.6684	0.6677	0.6701	0.6703	0.6703
0.3	0.6305	0.6258	0.6424	0.6417	0.6440	0.6442	0.6442
0.4	0.5932	0.5888	0.6045	0.6038	0.6060	0.6062	0.6062
0.5	0.5429	0.5388	0.5532	0.5526	0.5546	0.5548	0.5548
0.6	0.4773	0.4737	0.4865	0.4860	0.4877	0.4879	0.4879
0.7	0.3941	0.3911	0.4017	0.4012	0.4027	0.4029	0.4028
0.8	0.2897	0.2876	0.2953	0.2950	0.2961	0.2962	0.2962
0.9	0.1601	0.1589	0.1632	0.1630	0.1636	0.1637	0.1637
1.0	0.0000	0.0000	-0.0000	0.0000	0.0000	0.0000	0.0000

Table 3.3.2: Numerical values of the induced magnetic field h obtained using the Riemann-Sum approximation method (RSM) compared to those obtained by the finite difference method (FDM) and the steady state (SS) for $Pr = 0.71$, $Pm = 1.0$ and $M = 2.0$ at varying values of t.

	$t = 4.0$		$t = 6.0$		$t = 8.0$		
y	RSM	FDM	RSM	FDM	RSM	FDM	SS
0.0	-0.3922	-0.3872	-0.4048	-0.4042	-0.4066	-0.4069	-0.4067
0.1	-0.3920	-0.3870	-0.4045	-0.4038	-0.4063	-0.4065	-0.4064
0.2	-0.3899	-0.3850	-0.4022	-0.4015	-0.4039	-0.4041	-0.4040
0.3	-0.3839	-0.3792	-0.3958	-0.3951	-0.3974	-0.3976	-0.3976
0.4	-0.3718	-0.3673	-0.3830	-0.3824	-0.3845	-0.3848	-0.3847
0.5	-0.3510	-0.3469	-0.3613	-0.3608	-0.3626	-0.3630	-0.3629
0.6	-0.3188	-0.3152	-0.3279	-0.3275	-0.3290	-0.3294	-0.3293
0.7	-0.2718	-0.2689	-0.2794	-0.2791	-0.2804	-0.2807	-0.2806
0.8	-0.2063	-0.2042	-0.2119	-0.2117	-0.2127	-0.2129	-0.2128
0.9	-0.1176	-0.1164	-0.1207	-0.1205	-0.1212	-0.1212	-0.1212
1.0	-0.0000	0.0000	0.0000	-0.0000	-0.0000	0.0000	0.0000

Table 3.3.3: Numerical values for velocity u and that of the induced magnetic field h obtained by the finite difference method for $Pr = 0.71$, $Pm = 1.0$, $t = 4.0$ at varying values of M

	M = 2.0		M = 4.0		M = 6.0	
y	u	h	u	h	u	h
0.0	0.6709	-0.3872	0.1115	-0.9264	0.1429	-0.1290
0.1	0.6661	-0.3870	0.1111	-0.9271	0.1427	-0.1292
0.2	0.6512	-0.3850	0.1099	-0.9263	0.1420	-0.1295
0.3	0.6258	-0.3792	0.1078	-0.9205	0.1407	-0.1295
0.4	0.5888	-0.3673	0.1044	-0.9052	0.1386	-0.1289
0.5	0.5388	-0.3469	0.9920	-0.8744	0.1351	-0.1269
0.6	0.4737	-0.3152	0.9150	-0.8196	0.1289	-0.1223
0.7	0.3911	-0.2689	0.8006	-0.7283	0.1181	-0.1131
0.8	0.2876	-0.2042	0.6305	-0.5820	0.9871	-0.9540
0.9	0.1589	-0.1164	0.3774	-0.3530	0.6368	-0.6202
1.0	0.0000	0.0000	0.0000	0.0000	0.0000	0.0000

Table 3.3.4: Numerical values for velocity u and that of the Induced Magnetic field h obtained by the finite difference for $Pr = 0.71$, $M = 2.0$, $t = 4.0$, at varying values of Pm

.

	Pm = 1.0		Pm = 2.0		Pm = 3.0	
y	u	h	u	h	u	h
0.0	0.6709	-0.3872	0.7641	-0.7241	0.7695	-0.9023
0.1	0.6661	-0.3870	0.7597	-0.7248	0.7654	-0.9048
0.2	0.6512	-0.3850	0.7461	-0.7241	0.7532	-0.9082
0.3	0.6258	-0.3792	0.7225	-0.7181	0.7322	-0.9073
0.4	0.5888	-0.3673	0.6876	-0.7025	0.7012	-0.8965
0.5	0.5388	-0.3469	0.6387	-0.6722	0.6574	-0.8688
0.6	0.4737	-0.3152	0.5725	-0.6209	0.5966	-0.8149
0.7	0.3911	-0.2689	0.4837	-0.5403	0.5122	-0.7225
0.8	0.2876	-0.2042	0.3655	-0.4200	0.3948	-0.5739
0.9	0.1589	-0.1164	0.2085	-0.2460	0.2306	-0.3448
1.0	0.0000	0.0000	0.0000	0.0000	0.0000	0.0000

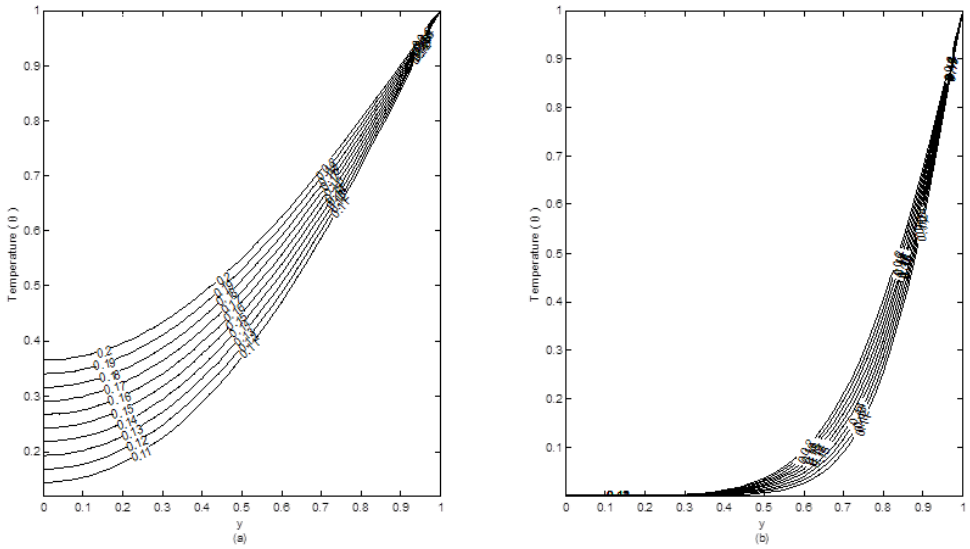


Figure 3.3.1: Temperature distribution(θ) for $Pr = 0.71(a)$ and $Pr = 7.0(b)$ at different values of time t.

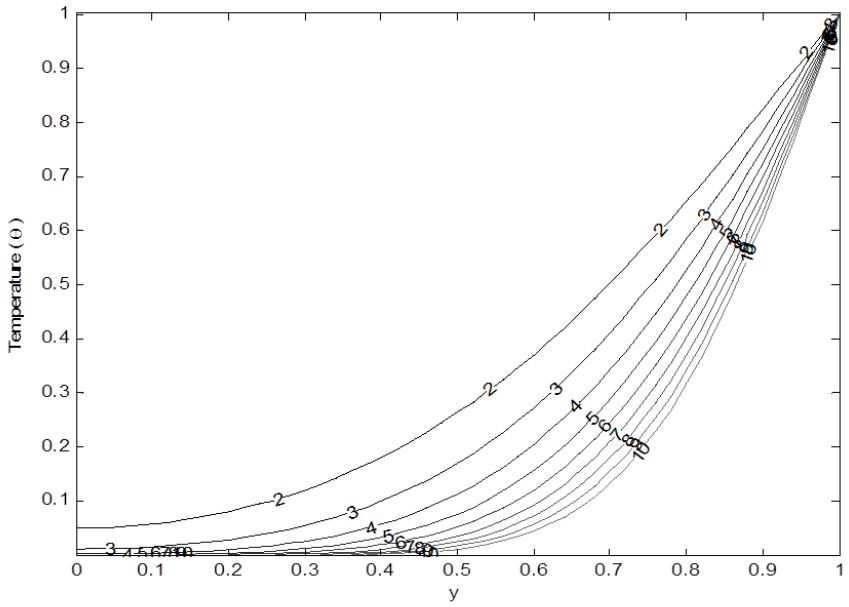


Figure 3.3.2: Temperature distribution(θ) for $t = 0.2$ at different values of Pr.

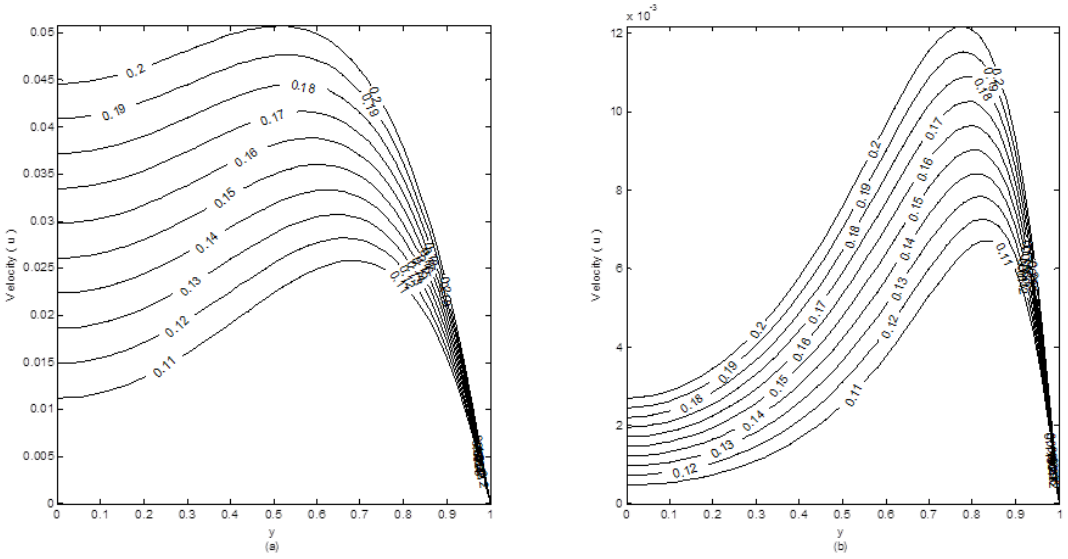


Figure 3.3.3: Velocity profile for $M = 2.0, Pr = 0.71(a)$ and $Pr = 7.0(b)$at different values of t

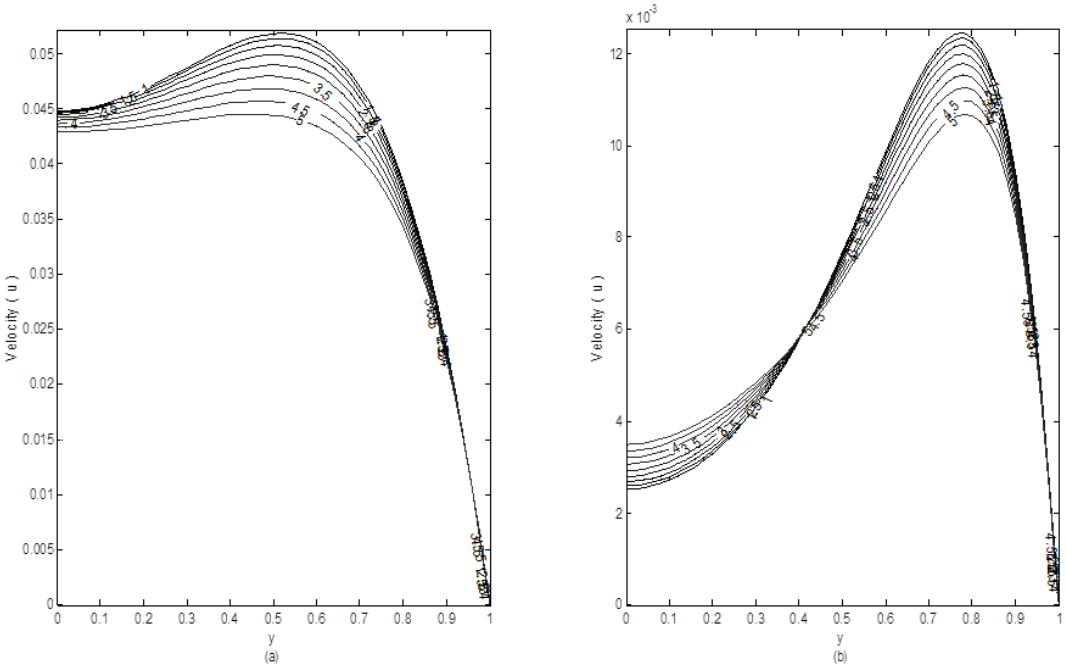


Figure 3.3.4: Velocity profile for $t = 0.2$, $Pr = 0.71(a)$ and $Pr = 7.0(b)$ at different values of M

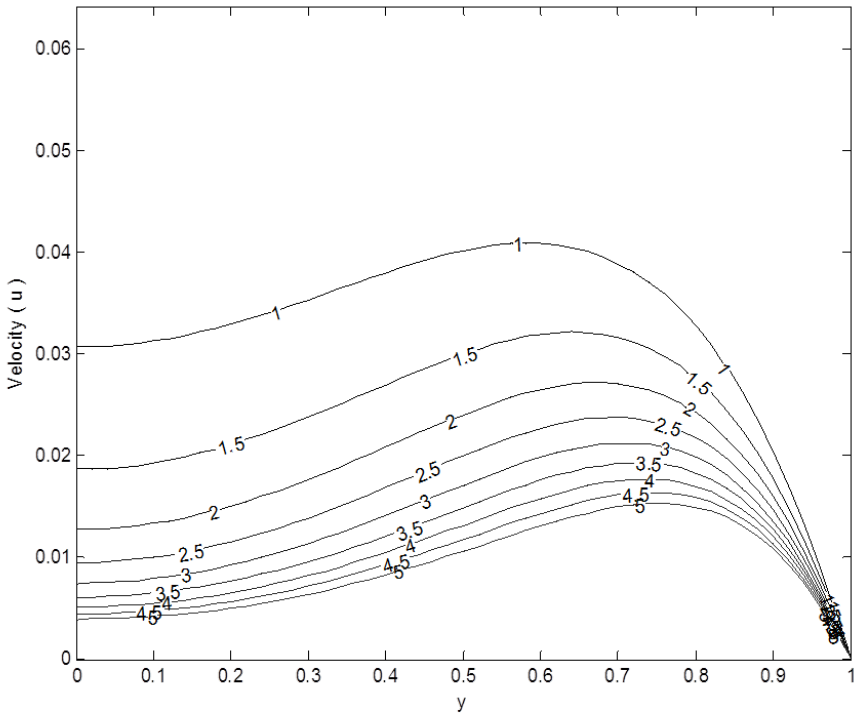


Figure 3.3.5: Velocity profile for $M = 2.0$ and $t = 0.2$, at different values of Pr

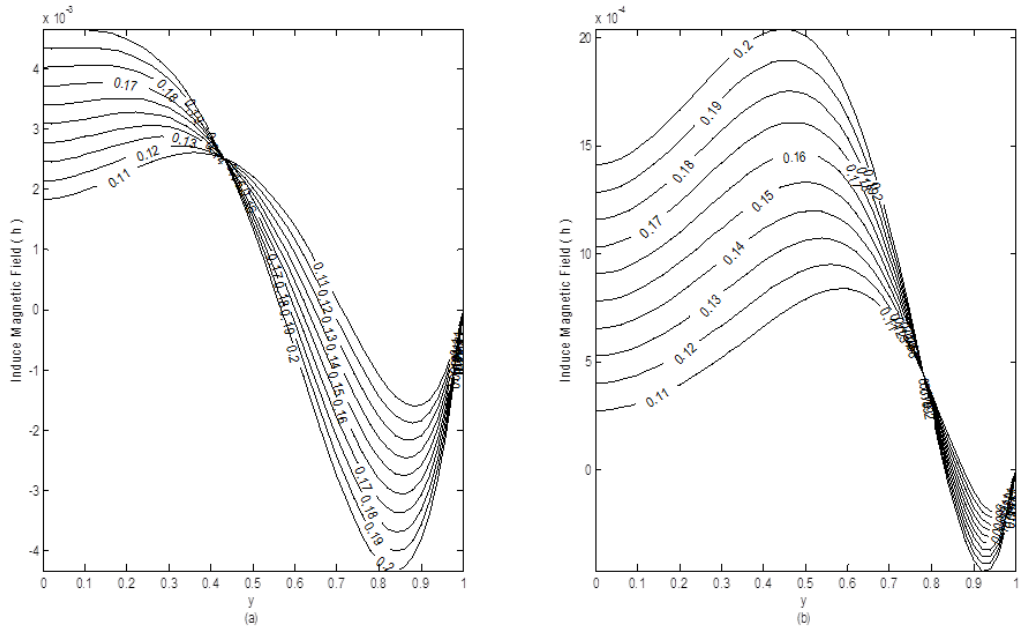


Figure 3.3.6: Induced Magnetic Field for $M = 2.0, Pr = 0.71(a)$ and $Pr = 7.0(b)$ at different values of t

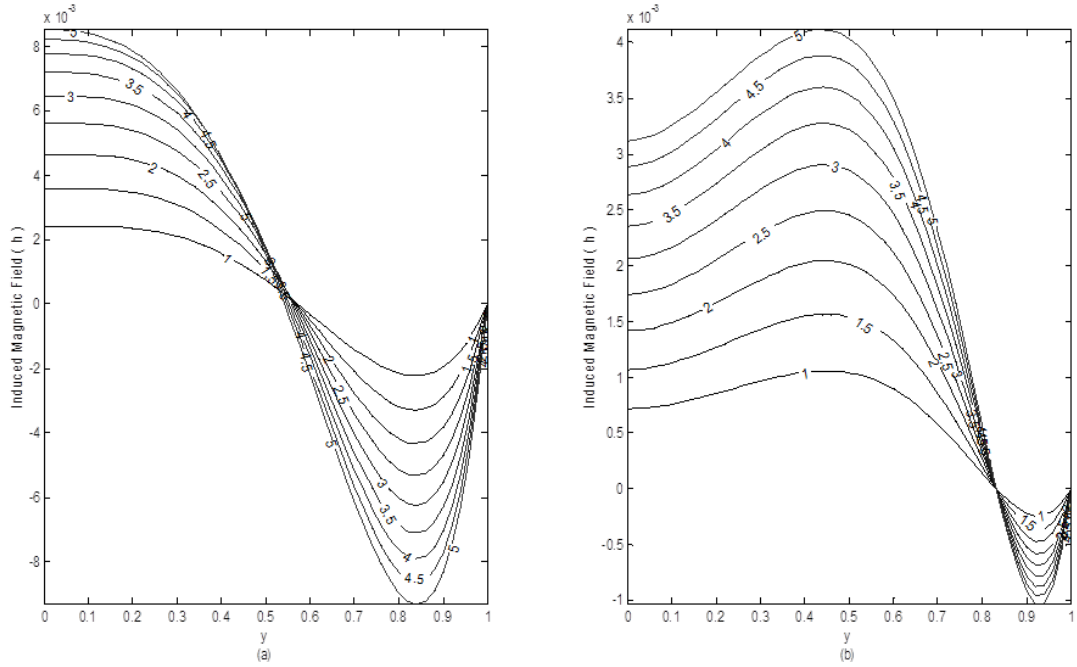


Figure 3.3.7: Induced Magnetic Field for $t = 0.2$, $Pr = 0.71(a)$ and $Pr = 7.0(b)$ at different values of M

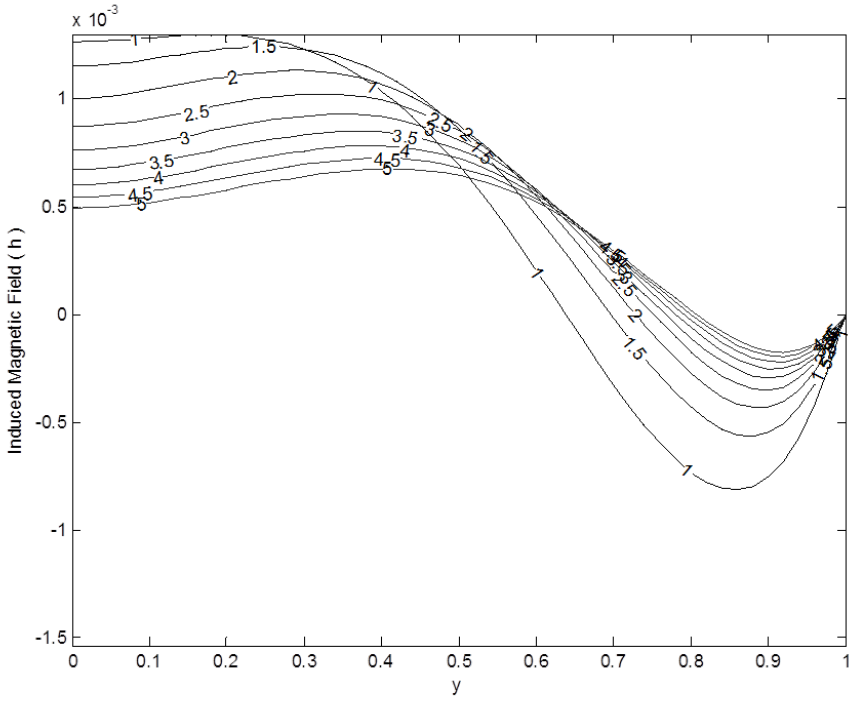


Figure 3.3.8: Induced Magnetic Field for $M = 2.0$ and $t = 0.2$, at different values of Pr

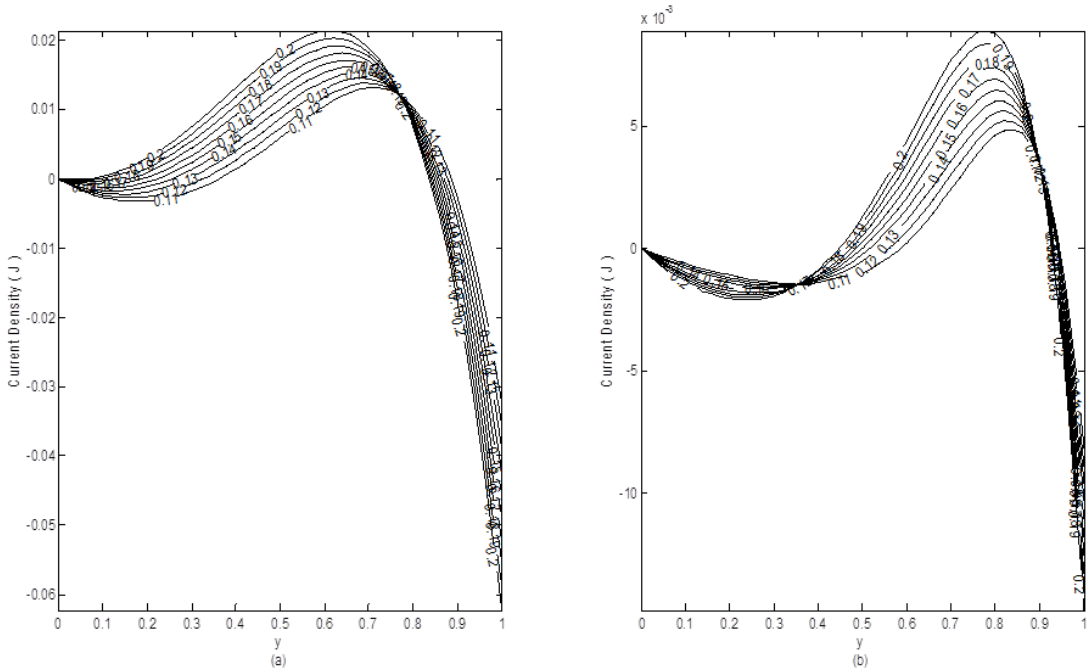


Figure 3.3.9: Current density distribution for $M = 2.0, Pr = 0.71(a)$ and $Pr = 7.0(b)$ at different values of t

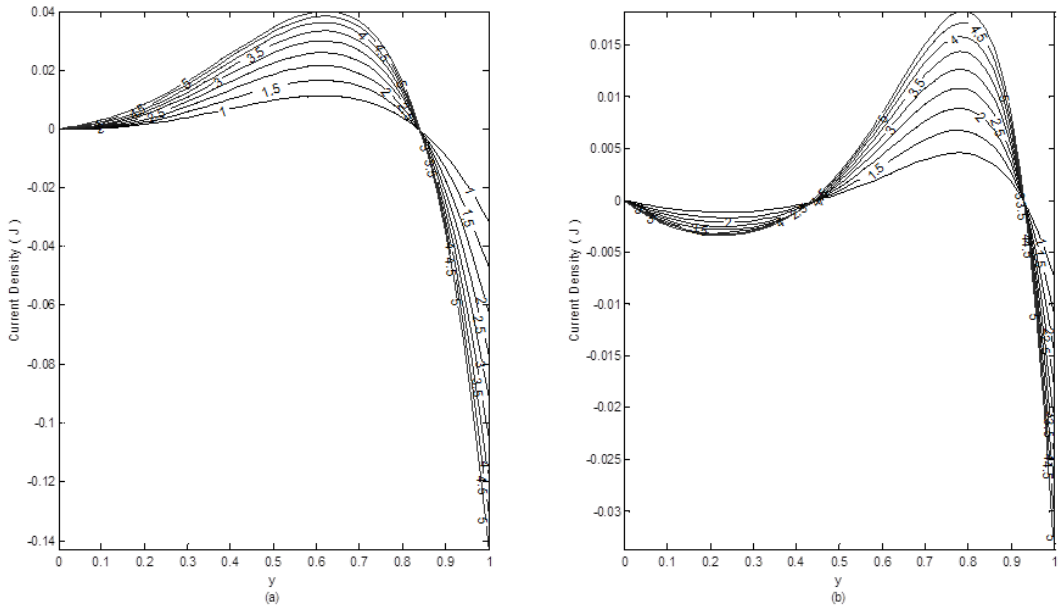


Figure 3.3.10: Current density distribution for $t = 0.2$, $Pr = 0.71(a)$ and $Pr = 7.0(b)$ at different values of M

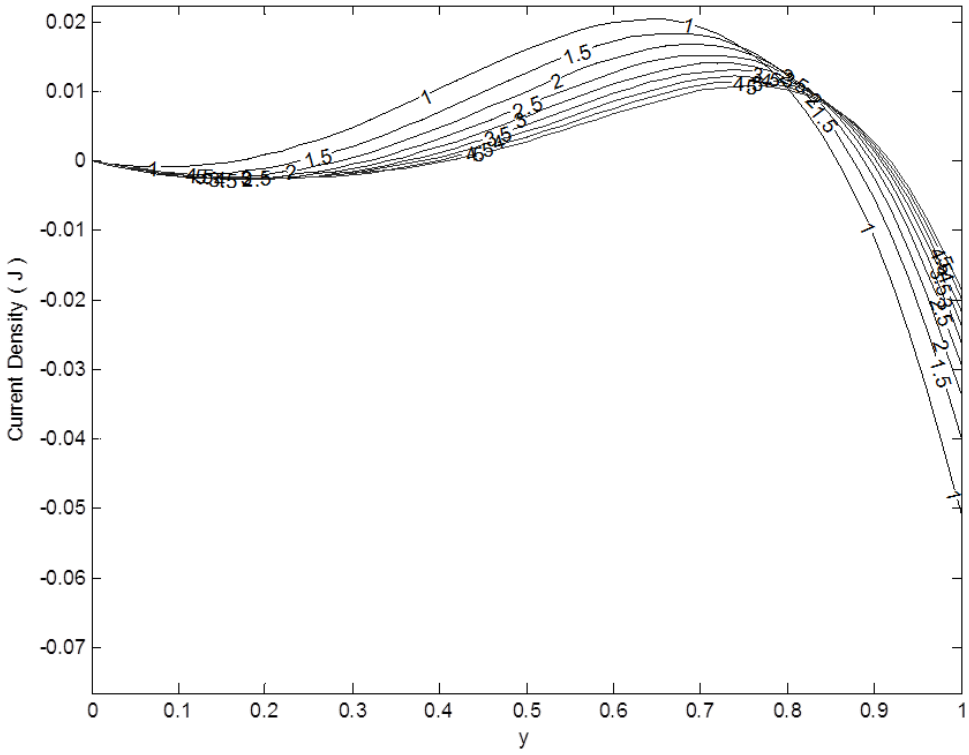


Figure 3.3.11: Current density distribution for $M = 2.0$ and $t = 0.2$, at different values of Pr

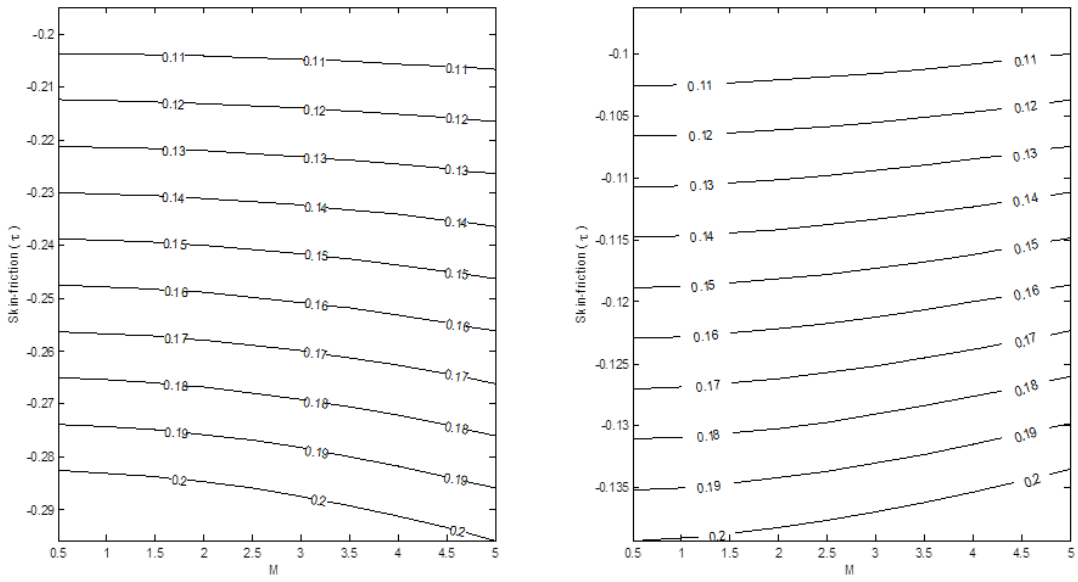


Figure 3.3.12: Skin-friction profile at $y = 1$ for $Pr = 0.71(a)$ and $Pr = 7.0(b)$ at different values of M and t.

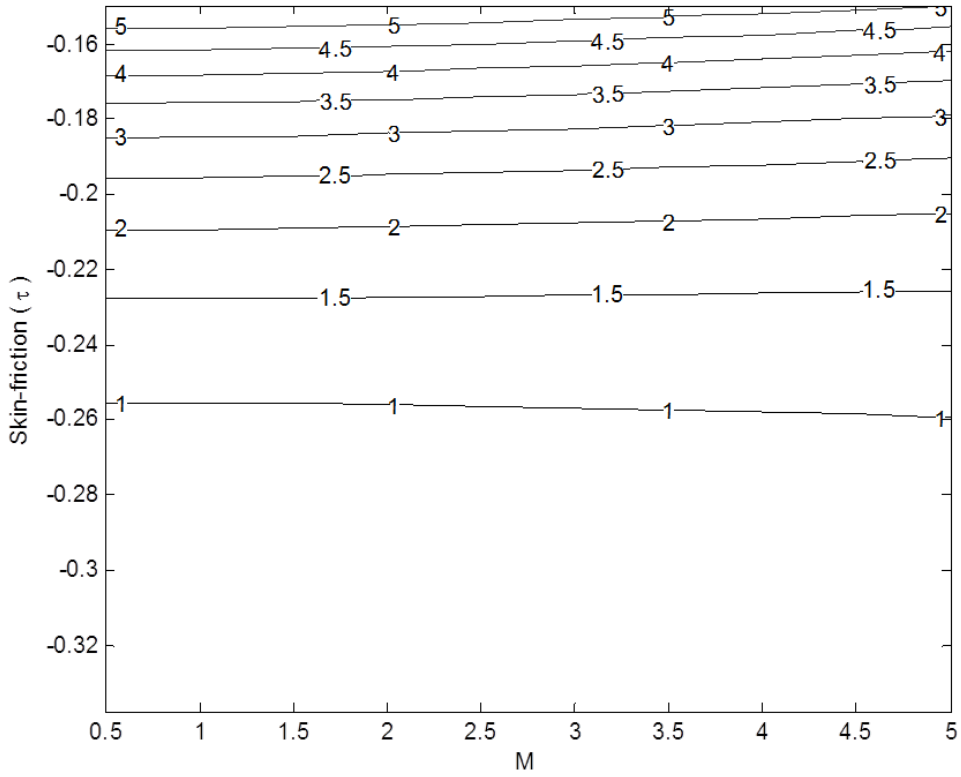


Figure 3.3.13: Skin-friction profile at $y = 1$ for $t = 0.2$ at different values of M and Pr.

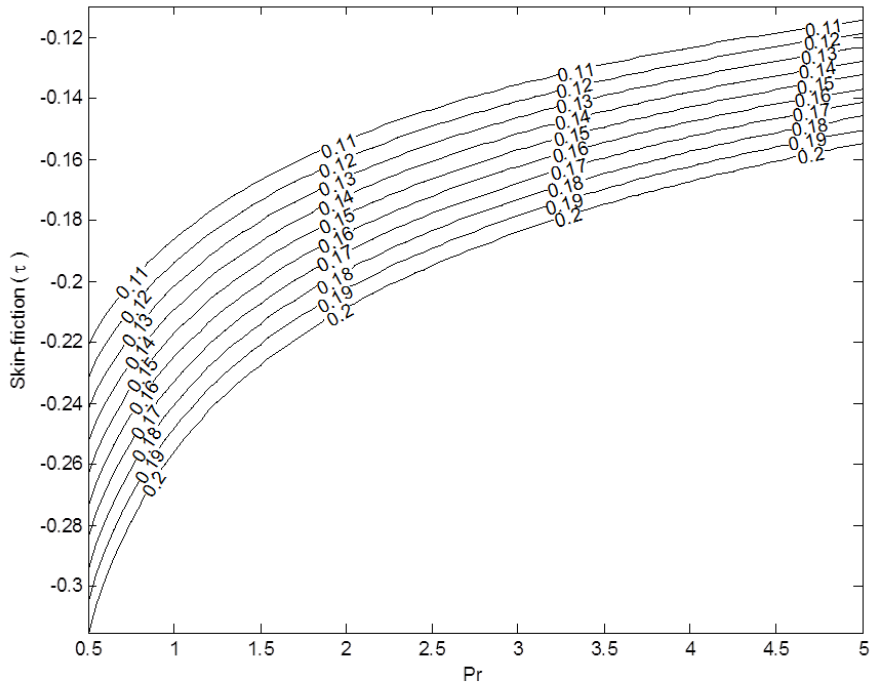


Figure 3.3.14: Skin-friction profile at $y = 1$ for $M = 2.0$ at different values of Pr and t.

CHAPTER FOUR

TIME DEPENDENT MHD FREE CONVECTIVE FLOW IN VERTICAL CHANNEL

In this chapter, a semi-analytical solution to the problems of suction/injection combination on MHD transient free convective flow of an incompressible viscous electrically conducting fluid in a vertical channel formed by two vertical porous and non porous parallel plates in the presence of induced magnetic field have been obtained. In the case of non porous vertical parallel plates, the applied magnetic field is fixed to the moving plate.

4.1 Effects of suction-injection combination (SIC) on MHD transient free-convective flow in a vertical channel in presence of induced magnetic field

In this section, a semi-analytical solution to the problem of suction/injection combination on MHD transient free convective flow of an incompressible viscous electrically conducting fluid in a vertical channel formed by two vertical porous parallel plates in the presence of induced magnetic field have been obtained using Laplace transform technique. However, the inversion from the Laplace domain to the time domain is carried out using the Riemann-sum approximation method of Laplace inversion. The effects of time (t), the suction/injection parameter (S), and Prandtl number (Pr) on the velocity (u), induced magnetic field (h), Temperature (θ), skin friction (τ) and the current density (J) are presented graphically and discussed. We have also obtained the closed form analytical solution for the steady state, further by implicit finite difference method which are used to validate Riemann-sum approximation

approach.

4.1.1 Mathematical Analysis

We consider transient natural convection flow of an incompressible viscous fluid in vertical channel formed by two infinite vertical parallel porous plates. At time $t' \leq 0$, both the fluid and the channel walls are assumed to be at the same temperature T_0. At time $t' > 0$, the temperature of the wall at $y' = 0$ is raised to T_1 while that of the wall $y' = d$ is maintained at T_0. The x'-axis is taken along the vertical porous plates in the direction of the flow and y'-axis taken normal to it. A uniform magnetic field of strength H_0 is applied parallel to y'-axis. The induced magnetic field produced by conducting fluid motion are not negligible in comparison to applied one. Since the porous plates are of infinite extent in the x'-direction, all physical quantities, depend on y' and t' only. Using the Boussinesq's approximation, the mathematical model representing the present physical situation are;

$$\frac{\partial u'}{\partial y'} = 0, \tag{4.1.1}$$

$$\frac{\partial T'}{\partial t'} - v_0' \frac{\partial T'}{\partial y'} = \alpha \frac{\partial^2 T'}{\partial y'^2}, \tag{4.1.2}$$

$$\frac{\partial u'}{\partial t'} - v_0' \frac{\partial u'}{\partial y'} = \nu \frac{\partial^2 u'}{\partial y'^2} + \frac{\mu_e H_0}{\rho} \frac{\partial h'}{\partial y'} + g\beta(T' - T_0), \tag{4.1.3}$$

$$\frac{\partial h'}{\partial t'} - v_0' \frac{\partial h'}{\partial y'} = \frac{1}{\sigma \mu_e} \frac{\partial^2 h'}{\partial y'^2} + H_0 \frac{\partial u'}{\partial y'}, \tag{4.1.4}$$

Since the plates are non-conducting, the initial and boundary conditions of the flow are

$$\begin{gathered} u' = 0, \quad T' = T_0, \quad h' = 0, \quad for\ 0 \leq y' \leq d \ \ at \ \ t' \leq 0, \\ u' = 0, \ \ T' = T_1, \ \ h' = 0 \quad at \quad y' = 0 \ \ for\ t' > 0, \\ u' = 0, \quad T' = T_0, \quad h' = 0, \quad at \quad y' = d \ \ for\ t' > 0. \end{gathered} \tag{4.1.5}$$

The fluid suction/injection takes place through the porous plates of the channel. If $\mathbf{V} = (u', v', w')$ denotes the velocity components. Then the equation of continuity Eq.(4.1.1), on integration gives

$$v' = constant = -v_0', \tag{4.1.6}$$

where v_0' is the normal velocity of suction or injection at the plate according as $v_0' > 0$ for suction or $v_0' < 0$ for injection and $v_0' = 0$ represents the case of non-permeable plate. u' is the velocity of the fluid, h' is the induced magnetic field, T' is the temperature of the fluid, ν is the kinematic viscosity, g is the acceleration due to gravity, β is the coefficient of thermal expansion, μ_e is the magnetic permeability, ρ is the density, μ is the dynamic viscosity, and α is the thermal diffusivity of the fluid.

Now introducing the following dimensionless quantities

$$u = \frac{u'\nu}{g\beta(T_1 - T_0)d^2}, \quad h = \frac{h'(\frac{\mu_e}{\rho})^{\frac{1}{2}}\nu}{g\beta d^2(T_1 - T_0)}, \quad S = \frac{v_0' d}{\nu}, \quad \theta = \frac{(T' - T_0)}{(T_1 - T_0)},$$
$$y = \frac{y'}{d}, \quad t = \frac{t'\nu}{d^2}, \quad Pr = \frac{\nu}{\alpha}, \quad M = \frac{dH_0}{\nu}(\frac{\mu_e}{\rho})^{\frac{1}{2}}, \quad Pm = \sigma\mu_e\nu, \tag{4.1.7}$$

where u is the dimensionless velocity, h is the dimensionless induced magnetic field, t the dimensionless time, y is the dimensionless coordinate normal to the porous plates, θ is the dimensionless temperature, M magnetic parameter, Pm is magnetic Prandtl number, S is suction/injection parameter and Pr is Prandtl number, Therefore, eqs.(4.1.2) - (4.1.4) reduce to

$$\frac{\partial\theta}{\partial t} - S\frac{\partial\theta}{\partial y} = \frac{1}{Pr}\frac{\partial^2\theta}{\partial y^2}, \tag{4.1.8}$$

$$\frac{\partial u}{\partial t} - S\frac{\partial u}{\partial y} = \frac{\partial^2 u}{\partial y^2} + M\frac{\partial h}{\partial y} + \theta, \tag{4.1.9}$$

$$\frac{\partial h}{\partial t} - S\frac{\partial h}{\partial y} = \frac{1}{Pm}\frac{\partial^2 h}{\partial y^2} + M\frac{\partial u}{\partial y}, \tag{4.1.10}$$

and the corresponding initial and boundary conditions are

$$\begin{aligned} u = 0, \quad \theta = 0, \quad h = 0, \quad for\ 0 \leq y \leq 1 \quad at\ t \leq 0, \\ u = 0, \quad \theta = 1, \quad h = 0, \quad at \quad y = 0 \quad for\ t > 0, \\ u = 0 \quad \theta = 0, \quad h = 0 \quad at \quad y = 1 \quad for \quad t > 0. \end{aligned} \tag{4.1.11}$$

The solutions of eqs.(4.1.8) - (4.1.10) under the initial boundary conditions (eq. (4.1.11)) for $Pm = 1$, can be obtained using the Laplace transform technique defined in section 1.6.1. The temperature, the velocity and the induced magnetic field expressions in Laplace domain are:

$$\bar{\theta}(y,s) = \frac{1}{s}\frac{\sinh(\lambda_3(1-y))}{\sinh(\lambda_3)}\exp(-\frac{SPr}{2}y), \tag{4.1.12}$$

$$\begin{aligned} \bar{u}(y,s) = \frac{1}{2}\{&[c_1\cosh(\lambda_1 y) + c_2\sinh(\lambda_1 y)]\exp\frac{-(S+M)}{2}y \\ &+ [c_3\cosh(\lambda_2 y) + c_4\sinh(\lambda_2 y)]\exp\frac{-(S-M)}{2}y\} \\ &- \frac{1}{4}\frac{1}{s\sinh(\lambda_3)}\{\frac{\exp(\lambda_3)\exp(-y(\lambda_3+\frac{SPr}{2})}{d_1} - \frac{\exp(-\lambda_3)\exp(-y(\frac{SPr}{2}-\lambda_3))}{d_2}\} \\ &- \frac{1}{4}\frac{1}{s\sinh(\lambda_3)}\{\frac{\exp(\lambda_3)\exp(-y(\lambda_3+\frac{SPr}{2})}{d_3} - \frac{\exp(-\lambda_3)\exp(-y(\frac{SPr}{2}-\lambda_3))}{d_4}\}, \end{aligned} \tag{4.1.13}$$

$$\begin{aligned} \bar{h}(y,s) = \frac{1}{2}\{&[c_1\cosh(\lambda_1 y) + c_2\sinh(\lambda_1 y)]\exp\frac{-(S+M)}{2}y \\ &- [c_3\cosh(\lambda_2 y) + c_4\sinh(\lambda_2 y)]\exp\frac{-(S-M)}{2}y\} \\ &- \frac{1}{4}\frac{1}{s\sinh(\lambda_3)}\{\frac{\exp(\lambda_3)\exp(-y(\lambda_3+\frac{SPr}{2}} - \frac{\exp(-\lambda_3)\exp(-y(\frac{SPr}{2}-\lambda_3))}{d_2}\} \\ &+ \frac{1}{4}\frac{1}{s\sinh(\lambda_3)}\{\frac{\exp(\lambda_3)\exp(-y(\lambda_3+\frac{SPr}{2})}{d_3} + \frac{\exp(-\lambda_3)\exp(-y(\frac{SPr}{2}-\lambda_3))}{d_4}\}, \end{aligned} \tag{4.1.14}$$

Eqs.(4.1.12) - (4.1.14) are inverted in terms of Riemann-sum approximation method defined in section 1.6.2;

4.1.2 Skin-friction and Current density

The skin-friction is obtain by differentiating eqn.(1.6.6) with respect to y, and evaluated at both porous plates (i.e $y = 0$ and $y = 1$) similar to that obtained in equation (3.1.17).

where

$$\begin{aligned}
\bar{u}_1 = {} & \frac{1}{2}\{\lambda_1(c_1\sinh(\lambda_1 y) + c_2\cosh(\lambda_1 y)) + (-\frac{S}{2} - \frac{M}{2})(c_1\cosh(\lambda_1 y) \\
& + c_2\sinh(\lambda_1 y))\}\exp(-\frac{(S+M)}{2}y) + \frac{1}{2}\{\lambda_2(c_3\sinh(\lambda_2 y) + c_4\cosh(\lambda_2)y) \\
& + \frac{M-S}{2}(c_3\cosh(\lambda_2 y) + c_4\sinh(\lambda_2 y))\}\exp(-\frac{(S-M)}{2}y) \\
& - \frac{1}{4}\frac{1}{p\sinh(\lambda_3)}\{(\frac{(-\lambda_3 - \frac{SPr}{2})\exp(\lambda_3)\exp(-y(\lambda_3 + \frac{SPr}{2}))}{d_1}) \\
& - (\frac{(\lambda_3 - \frac{SPr}{2})\exp(-\lambda_3)\exp(-y(-\lambda_3 + \frac{SPr}{2}))}{d_2})\} \\
& - \frac{1}{4}\frac{1}{p\sinh(\lambda_3)}\{(\frac{(-\lambda_3 - \frac{SPr}{2})\exp(\lambda_3)\exp(-y(\lambda_3 + \frac{SPr}{2}))}{d_3}) \\
& - (\frac{(\lambda_3 - \frac{SPr}{2})\exp(-\lambda_3)\exp(-y(-\lambda_3 + \frac{SPr}{2}))}{d_4})\}
\end{aligned} \tag{4.1.15}$$

In a similar way, the current density is obtained as in equation.(3.1.21);

where

$$\begin{aligned}
\bar{J}_1 = {} & \frac{1}{2}\{\lambda_1(c_1\sinh(\lambda_1 y) + c_2\cosh(\lambda_1 y)) + (-\frac{S}{2} - \frac{M}{2})(c_1\cosh(\lambda_1 y) \\
& + c_2\sinh(\lambda_1 y))\}\exp(-\frac{(S+M)}{2}y) + \frac{1}{2}\{\lambda_2(c_3\sinh(\lambda_2 y) + c_4\cosh(\lambda_2)y) \\
& + \frac{M-S}{2}(c_3\cosh(\lambda_2 y) + c_4\sinh(\lambda_2 y))\}\exp(-\frac{(S-M)}{2}y) \\
& - \frac{1}{4}\frac{1}{p\sinh(\lambda_3)}\{(\frac{(-\lambda_3 - \frac{SPr}{2})\exp(\lambda_3)\exp(-y(\lambda_3 + \frac{SPr}{2}))}{d_1}) \\
& - (\frac{(\lambda_3 - \frac{SPr}{2})\exp(-\lambda_3)\exp(-y(-\lambda_3 + \frac{SPr}{2}))}{d_2})\} \\
& + \frac{1}{4}\frac{1}{p\sinh(\lambda_3)}\{(\frac{(-\lambda_3 - \frac{SPr}{2})\exp(\lambda_3)\exp(-y(\lambda_3 + \frac{SPr}{2}))}{d_3}) \\
& - (\frac{(\lambda_3 - \frac{SPr}{2})\exp(-\lambda_3)\exp(-y(-\lambda_3 + \frac{SPr}{2}))}{d_4})\}
\end{aligned} \tag{4.1.16}$$

4.1.3 Validation

4.1.4 Steady State Solution

The steady state solution of the governing equations are obtain by setting $\frac{\partial}{\partial t}() = 0$ in equations (4.1.8) - (4.1.10). Therefore, the steady state temperature, velocity and induced magnetic field are as follows;

$$\theta_s = c_5 \exp(-SPry) + c_6 \tag{4.1.17}$$

$$\begin{aligned} u_s = \tfrac{1}{2}\{&(\tfrac{c_5 \exp(-SPr)}{SPr(M+S-SPr)} + \tfrac{c_5 \exp(-SPr)}{SPr(S-M-SPr)}) + (\tfrac{c_7}{M+S} + \tfrac{c_{10}}{S-M}) \\ &-c_6[(\tfrac{y}{M+S} - \tfrac{1}{(M+S)^2}) + (\tfrac{y}{S-M} - \tfrac{1}{(S-M)^2})] \\ &+c_8 \exp(-(M+S)y) + c_9 \exp(-(S-M)y)\} \end{aligned} \tag{4.1.18}$$

$$\begin{aligned} h_s = \tfrac{1}{2}\{&(\tfrac{c_5 \exp(-SPr)}{(M+S-SPr)} - \tfrac{c_5 \exp(-SPr)}{SPr(S-M-SPr)}) + (\tfrac{c_7}{M+S} - \tfrac{c_{10}}{S-M}) \\ &-c_6[(\tfrac{y}{M+S} - \tfrac{1}{(M+S)^2}) - (\tfrac{y}{S-M} - \tfrac{1}{(S-M)^2})] \\ &+c_8 \exp(-(M+S)y) - c_9 \exp(-(S-M)y)\} \end{aligned} \tag{4.1.19}$$

where all constants are defined in Appendix B

4.1.5 Implicit Finite Difference Method (IFDM)

The same procedure used in section 3.3.4 is employed here. Therefore, equations.(4.1.8) - (4.1.10) become

$$\begin{aligned} &\frac{\theta(i,j) - \theta(i,j-1)}{\Delta t} - \frac{S}{2\Delta y}[\theta(i+1,j) - \theta(i-1,j)] \\ &= \frac{1}{Pr}\frac{1}{(\Delta y)^2}[\theta(i+1,j) - 2\theta(i,j) + \theta(i-1,j)] \end{aligned} \tag{4.1.20}$$

$$\frac{u(i,j)-u(i,j-1)}{\Delta t}-\frac{S}{2\Delta y}[u(i+1,j)-u(i-1,j)]$$
$$=\frac{1}{(\Delta y)^2}[u(i+1,j)-2u(i,j)+u(i-1,j)]$$
$$+\frac{M}{2\Delta y}[h(i+1,j)-h(i-1,j)]+\theta(i,j) \tag{4.1.21}$$

$$\frac{h(i,j)-h(i,j-1)}{\Delta t}-\frac{S}{2\Delta y}[h(i+1,j)-h(i-1,j)]$$
$$=\frac{1}{Pm}\frac{1}{(\Delta y)^2}[h(i+1,j)-2h(i,j)+h(i-1,j)]$$
$$+\frac{M}{2\Delta y}[u(i+1,j)-u(i-1,j)] \tag{4.1.22}$$

4.1.6 Results and Discussion

In order to get a physical insight into the problem, temperature, velocity, induced magnetic field, current density, and skin-friction are presented graphically for different values of dimensionless time t, magnetic parameter (M) suction/injection parameter S and Prandtl number (Pr).It is worth noting that $S > 0$ corresponds to suction at $y = 0$ and simultaneous injection at $y = 1$. Also $S < 0$ corresponds to injection at $y = 0$ and simultaneous suction at $y = 1$ and $S = 0$ represents the flow formation inside the channel formed by two infinite vertical non-porous parallel plates. During the course of numerical computation, values of S are taken between -5 and $+5$. The effects of the physical parameters on the temperature distribution are displayed in Figures 4.1.1 - 4.1.2. From Figures 4.1.1(a) and 4.1.1(b), it is observed that the temperature increases as time increases in both case of air and water (i.e $Pr = 0.71$ and $Pr = 7.0$), However, the thermal boundary layer for water is less than that of air. This shows that the thermal boundary layer decreases with growing Prandtl number. From Figures 4.1.2(a) and 4.1.2(b), it is observed that fluid temperature increases as injection is increased on the heated porous plate. This is expected since injection through the heated porous plate is bound to act as a boost to heat transfer from the heated porous plate into

the fluid. Suction through the heated porous plate, on the other hand, is in the direction which opposes the heat transfer from the heated porous plate. The resultant effect therefore, is a decrease in fluid temperature as suction increases through the heated porous plate. From Figures 4.1.3(a) and 4.1.3(b), it is observed that the velocity of both air ($Pr = 0.71$) and water ($Pr = 7.0$) increases with time. It attain its maximum near the heated porous plate ($y = 0$) and then gradually descend toward the cold porous plate ($y = 1$). This is because fluid temperature increases with increasing time thereby strengthening convection current which results to enhanced buoyancy effect and growing velocity. Effect of magnetic parameter on the velocity is displayed in Figures 4.1.4(a) and 4.1.4(b). From these Figures, it is observed that the effect of the magnetic parameter is negligible near the heated porous plate ($y = 0$). However, fluid velocity is found to decrease near the central region of the channel as M increases. This is attributed to the deceleration of the fluid motion due to the magnetic field that generate the Lorentz force that retards fluid motion. An interesting observation in Figure 4.1.4 is the spatially dependent response of velocity to the magnetic parameter M. It is observed that fluid velocity decreases with growing M at section close to the heated porous plate ($y = 0$), while it increases near the right porous plate ($y = 1$). This response of velocity due to the change in magnetic parameter is attributed to the presence of induced magnetic field and this has been observed to act in opposition to the fluid flow near the heated porous plate. It is further observed that the effect of magnetic parameter (M) diminish to a negligible level at a fluid section ($y \approx 0.7$). Figures 4.1.5(a) and 4.1.5(b) show the effect of suction/injection parameter S on the velocity corresponding to air and water respectively. It is seen from these Figures that velocity increases as injection increases on the heated porous plate $S < 0$, while it decreases as suction increases on the same porous plate ($S > 0$). This is the same trend as observed in case of temperature (Figure 4.1.2), where temperature grows with increasing S ($S < 0$). It is ob-

served in Figure 4.1.6 that the velocity decreases with Pr as suction/injection (S) increases at a particular fluid layer ($y = 0.5$). This is true because fluids with high Prandtl number (Pr) have small thermal conductivity and high viscosity, which normally result into low heat penetration and a reduced thermal boundary layer thickness.

Figures 4.1.7 - 4.1.10 exhibit the effects of dimensionless time t, suction/injection parameter S, magnetic parameter M and Parndtl number Pr respectively, on the induced magnetic field. It is observed from Figures 4.1.7(a) and 4.1.7(b) that the induced magnetic field assumes positive values near the heated porous plate ($y = 0$) and negative values near the right porous plate. It is clear that the induced magnetic field grows absolutely as time increases, with negligible effect at a location ($y \approx 0.5$) in both air and water. Similar behaviour is noticed in Figures 4.1.8(a) and 4.1.8(b). The spatial extents of these parts seem to depend on the value of the Prandtl number. Figures 4.1.9(a) and 4.1.9(b) show the effects of suction/injection parameter (S) on the induced magnetic field. From these Figures, it is evident that the induced magnetic field increases as injection increases at the heated porous plate ($y = 0$) while a reverse trend is observed with suction in both air and water. Figure 10 shows the combined effect of Pr and S on the induced magnetic field in a particular fluid layer ($y = 0.5$). It is observed that in the presence of injection on the heated porous plate ($S < 0$), the induced magnetic field decreases as Pr increased. However, when suction takes place through the heated porous plate ($S > 0$), the induced magnetic field increases with growing Pr. For the present set of data, there exist a value of suction/injection for which the type of working fluid is immaterial. In that case, the response of the induced magnetic field to Pr is negligible. Figures 4.1.11 - 4.1.13 depicts the Current density (J) distribution at varying values of various parameters as mentioned earlier. It is noticed from Figures 4.1.11(a) and 4.1.11(b) that the current density increases as time increases around the central region of the channel, while it decreases near the

porous plates. This indicates an existence of some cross-section within the flow domain where the current density is independent of t. From Figures 4.1.12(a) and 4.1.12(b), a similar trend is observed as magnetic parameter M increases. The effects of suction/injection parameter (S) on the current density is shown in Figures 4.1.13(a) and 4.1.13(b). From these Figures it is observed that the current density is higher in the presence of suction near the porous plates, while it is higher with injection towards the central region of the channel. It is further observed that the role of suction through the heated porous plate diminishes on the current density when the working fluid is water ($Pr = 7.0$). Figures 4.1.14 - 4.1.17 depicts the effects of varying values of dimensionless time t, magnetic parameter M and Prandtl number Pr, on the skin-friction at both heated and cooled porous plates. Figures 4.1.14 and 4.1.15 show the skin-friction (τ_0) and (τ_1) variation with S for different value of t at $y = 0$ and $y = 1$ respectively. It is observed from these Figures that the skin friction at both porous plates increase with time (t), while it decreases on both porous plates when suction is increased on the heated porous plate. However, for growing injection ($S < 0$) on the heated porous plate, the skin-friction decreases on the heated porous plate while it increases on the cold porous plate. It is further observed in Figure 14(a), that skin-friction τ_0 increases as injection ($S < 0$) decreases and attain its maxima at $S \approx 0$.Furthermore, insignificant effect of time within the range $2 \leq S \leq 5.0$ is noticed in the case of water (Figure 4.1.14(b)). The influence of magnetic parameter and Prandtl number on the skin-friction at $y = 0$ and $y = 1$ are shown in Figures 4.1.16 and 4.1.17. These Figures show an increase in the skin-friction with growing magnetic parameter while it decreases as Pr increases.

Tables 4.1.1 and 4.1.2 show a comparison between transient state and steady state numerical values of velocity and the induced magnetic field obtained by using Riemann-sum approximation method (RSM), finite difference method (FDM) and exact solution for steady state (SS) at varying values of dimen-

sionless time t for $Pr = 0.71$, $S = -0.5$, $Pm = 1.0$ and $M = 2.0$. This reveals an excellent agreement between the three methods at large value of time. Table 4.1.3 depicts the numerical solution of velocity and the induced magnetic field obtained by finite difference method for varying values of magnetic Prandtl number Pm for fixed values of $Pr = 0.71$, $S = -0.5$, $M = 2.0$ and $t = 0.2$. It is observed that as Pm increases the velocity slightly decreases, while the strength of the induced magnetic field increases. This is physically true since an increase in the magnetic permeability (Pm) encourages the penetration of the applied magnetic force to increase the strength of the induced magnetic field within the channel. Consequent upon increase in the strength of the induced magnetic field, there is an increase in the Lorentz force which retards fluid motion, hence the decrease in fluid velocity.

Table 4.1.1: Numerical values of the velocity (u) obtained using the Riemann-Sum approximation method (RSM) compared to those obtained by the finite difference method (FDM) and the steady state (SS) for $Pr = 0.71$, $Pm = 1.0$, $S = -0.5$ and $M = 2.0$ at varying values of t.

	t = 0.2		t = 0.4		t = 0.6		
y	FDM	RSM	FDM	RSM	FDM	RSM	SS
0.0	0.0000	0.0000	0.0000	0.0000	0.0000	0.0000	0.0000
0.1	0.0217	0.0218	0.0267	0.0267	0.0275	0.0276	0.0276
0.2	0.0355	0.0355	0.0449	0.0449	0.0463	0.0463	0.0465
0.3	0.0428	0.0429	0.0557	0.0558	0.0578	0.0578	0.0581
0.4	0.0451	0.0452	0.0604	0.0605	0.0628	0.0628	0.0632
0.5	0.0435	0.0436	0.0599	0.0599	0.0624	0.0624	0.0628
0.6	0.0388	0.0389	0.0548	0.0548	0.0572	0.0573	0.0576
0.7	0.0318	0.0318	0.0458	0.0458	0.0480	0.0480	0.0483
0.8	0.0228	0.0229	0.0335	0.0335	0.0351	0.0351	0.0353
0.9	0.0122	0.0122	0.0181	0.0181	0.0190	0.0190	0.0191
1.0	0.0000	0.0000	0.0000	0.0000	0.0000	0.0000	0.0000

Table 4.1.2: Numerical values of the induced magnetic field (h) obtained using the Riemann-Sum approximation method (RSM) compared to those obtained by the finite difference method (FDM) and the steady state (SS) for $Pr = 0.71$, $Pm = 1.0$,$S = -0.5$ and $M = 2.0$ at varying values of t.

	t = 0.2		t = 0.4		t = 0.6		
y	FDM	RSM	FDM	RSM	FDM	RSM	SS
0.0	0.0000	0.0000	0.0000	0.0000	0.0000	0.0000	0.0000
0.1	0.0035	0.0035	0.0053	0.0053	0.0057	0.0057	0.0058
0.2	0.0037	0.0037	0.0064	0.0064	0.0070	0.0070	0.0071
0.3	0.0020	0.0020	0.0046	0.0046	0.0052	0.0052	0.0053
0.4	-0.0006	-0.0006	0.0012	0.0012	0.0017	0.0017	0.0018
0.5	-0.0032	-0.0032	-0.0027	-0.0027	-0.0024	-0.0024	-0.0024
0.6	-0.0053	-0.0053	-0.0062	-0.0062	-0.0062	-0.0062	-0.0062
0.7	-0.0064	-0.0064	-0.0085	-0.0085	-0.0087	-0.0087	-0.0087
0.8	-0.0062	-0.0062	-0.0087	-0.0087	-0.0090	-0.0090	-0.0090
0.9	-0.0042	-0.0042	-0.0061	-0.0061	-0.0064	-0.0064	-0.0064
1.0	0.0000	-0.0000	0.0000	-0.0000	0.0000	-0.0000	0.0000

Table 4.1.3: Numerical values for velocity (u) and that of the Induced Magnetic field h obtained by the finite difference (FDM) for $Pr = 0.71$, $M = 2.0$, $t = 0.2$, $S = -0.5$ for various values of Pm

	Pm = 0.5		Pm = 1.0		Pm = 1.5	
y	u	h	u	h	u	h
0.0	0.0000	0.0000	0.0000	0.0000	0.0000	0.0000
0.1	0.0218	0.0018	0.0217	0.0035	0.0217	0.0050
0.2	0.0359	0.0019	0.0355	0.0037	0.0352	0.0054
0.3	0.0435	0.0009	0.0429	0.0020	0.0424	0.0031
0.4	0.0459	-0.0005	0.0451	-0.0006	0.0446	-0.0004
0.5	0.0443	-0.0019	0.0435	-0.0032	0.0429	-0.0039
0.6	0.0394	-0.0031	0.0388	-0.0053	0.0384	-0.0067
0.7	0.0321	-0.0037	0.0317	-0.0064	0.0315	-0.0083
0.8	0.0229	-0.0035	0.0228	-0.0062	0.0227	-0.0082
0.9	0.0121	-0.0023	0.0122	-0.0042	0.0123	-0.0057
1.0	0.0000	0.0000	0.0000	0.0000	0.0000	0.0000

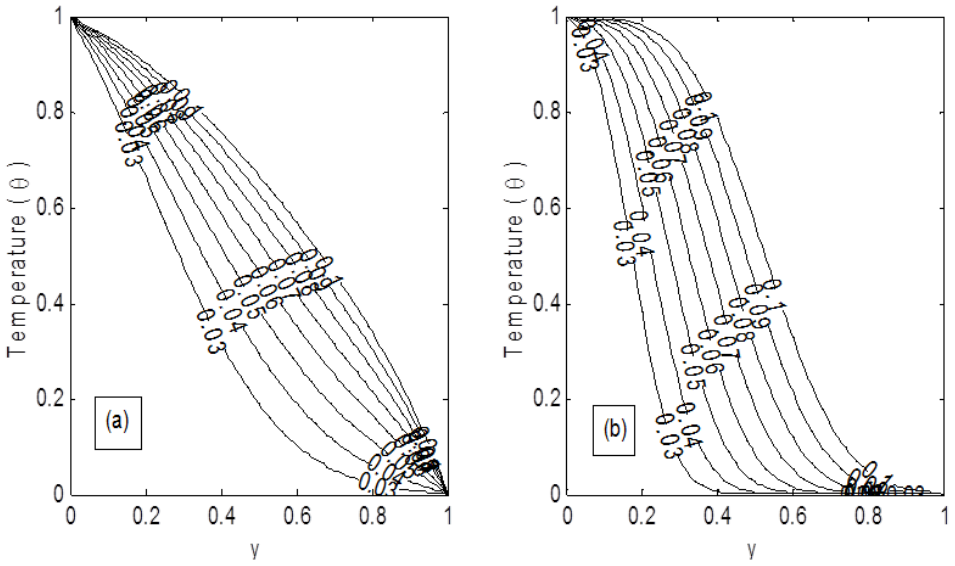


Figure 4.1.1: Temperature (θ) against y for different values of dimensionless time (t) at $S = -0.5$, $Pr = 0.71(a), Pr = 7.0(b)$.

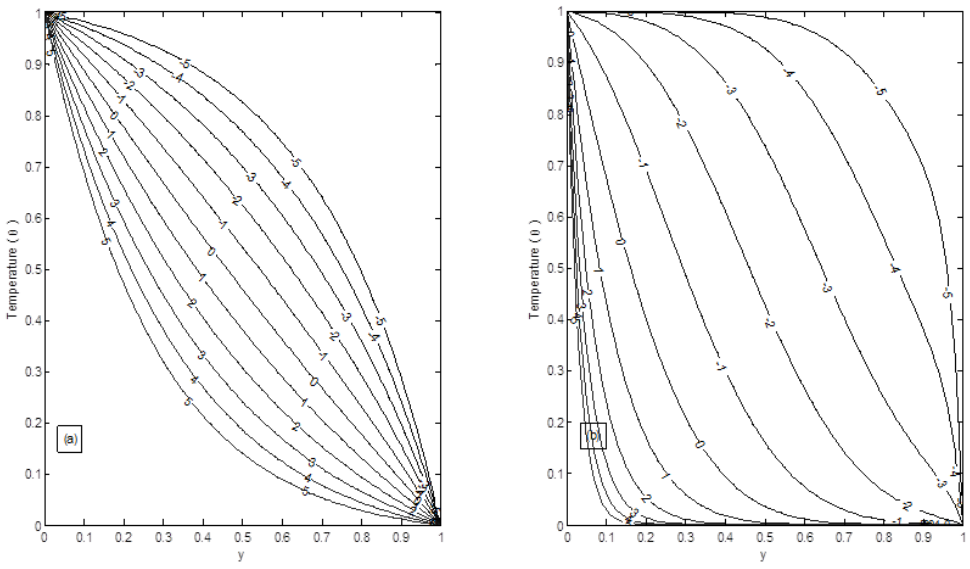


Figure 4.1.2: Temperature (θ) against y for different values of suction/injection (S), at $t = 0.2$, $Pr = 0.71(a), Pr = 7.0(b)$.

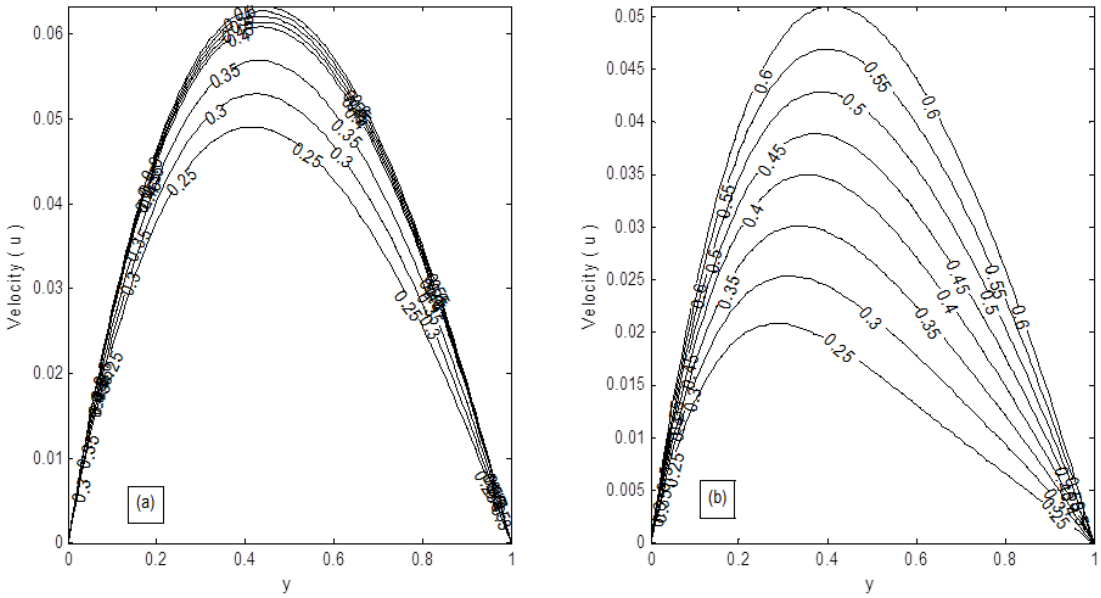


Figure 4.1.3: Velocity (u) profiles against y for different values of dimensionless time (t) at $M = 2.0$, $S = -0.5$, $Pr = 0.71(a), Pr = 7.0(b)$.

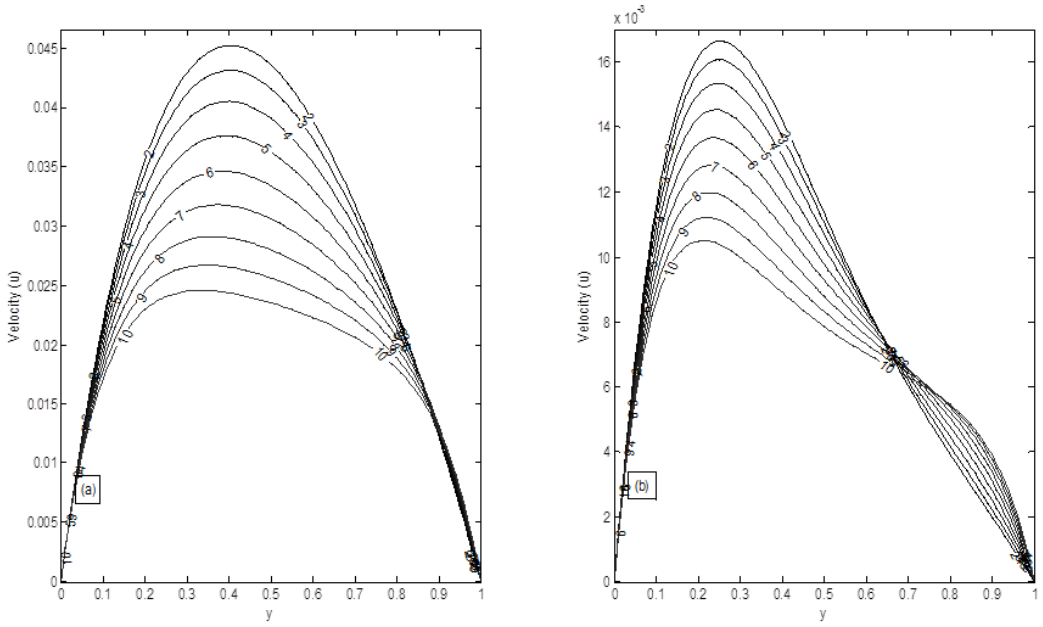


Figure 4.1.4: Velocity (u) profiles against y for different values of magnetic parameter (M) at $t = 0.2$, $S = -0.5$, $Pr = 0.71(a), Pr = 7.0(b)$.

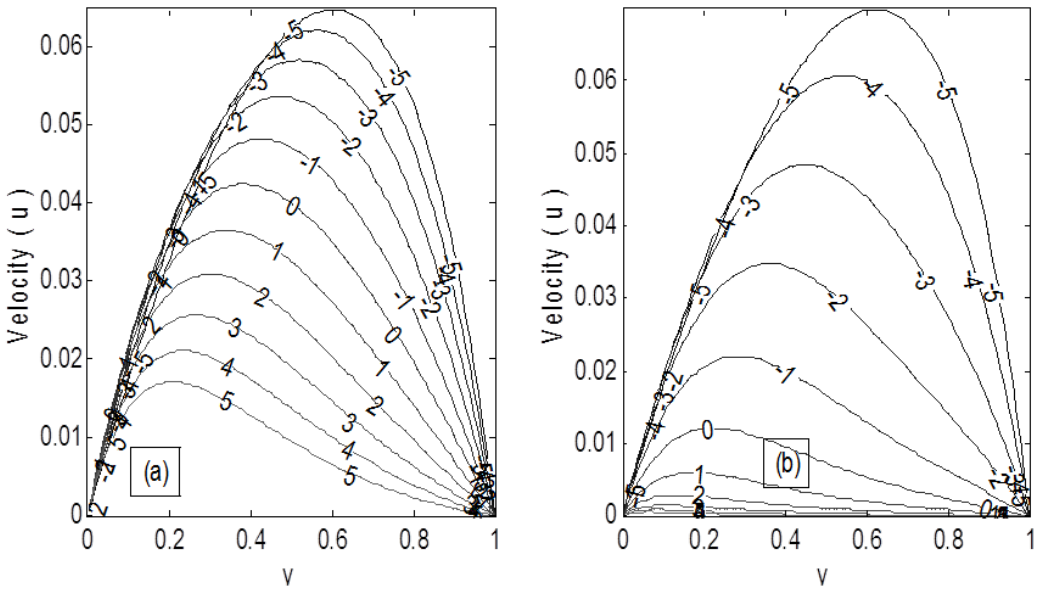


Figure 4.1.5: Velocity (u) profiles against y for different values of suction/injection (S) at $M = 2.0$, $t = 0.2$, $Pr = 0.71(a), Pr = 7.0(b)$.

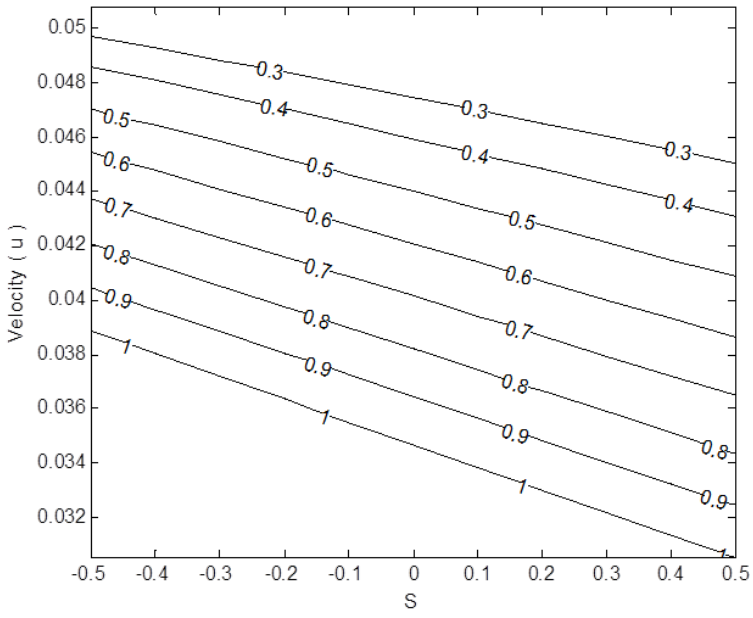


Figure 4.1.6: Velocity (u) profiles versus S for different values of Pr at $M = 2.0$, $t = 0.2$ and $y = 0.5$.

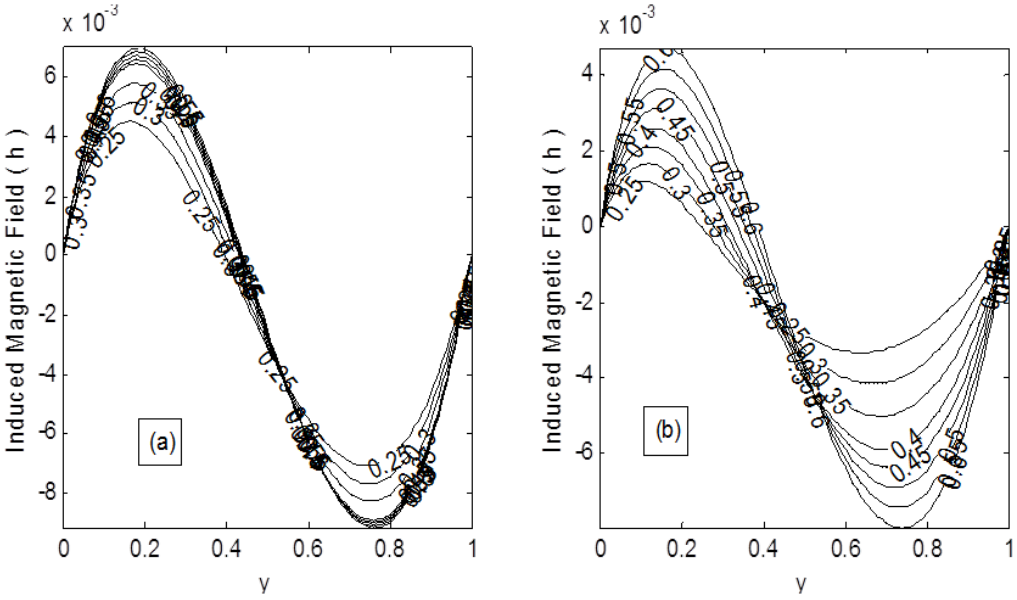


Figure 4.1.7: Induced magnetic field (h) against y for different values of dimensionless time (t) at $S = -0.5$, $M = 2.0$, $Pr = 0.71(a), Pr = 7.0(b)$.

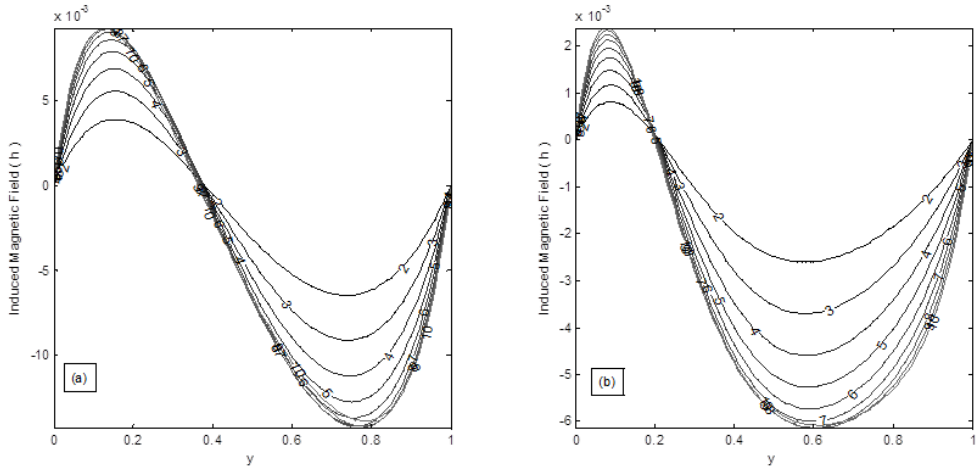


Figure 4.1.8: Induced magnetic field (h) against y for different values of magnetic parameter (M) at $S = -0.5$, $t = 0.2$, $Pr = 0.71(a), Pr = 7.0(b)$.

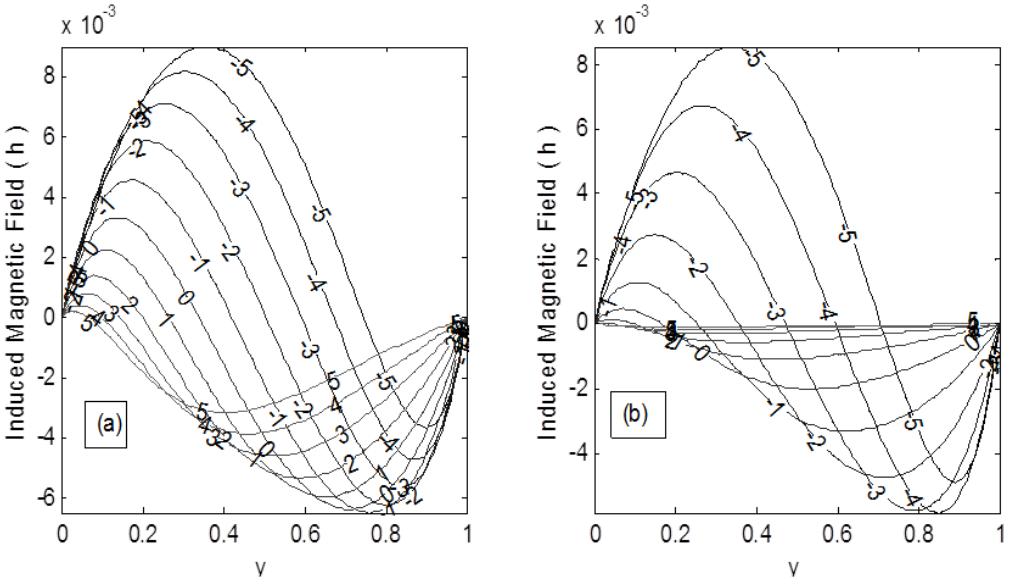


Figure 4.1.9: Induced magnetic field (h) against y for different values suction/injection (S) at $M = 2.0$, $t = 0.2$, $Pr = 0.71(a), Pr = 7.0(b)$.

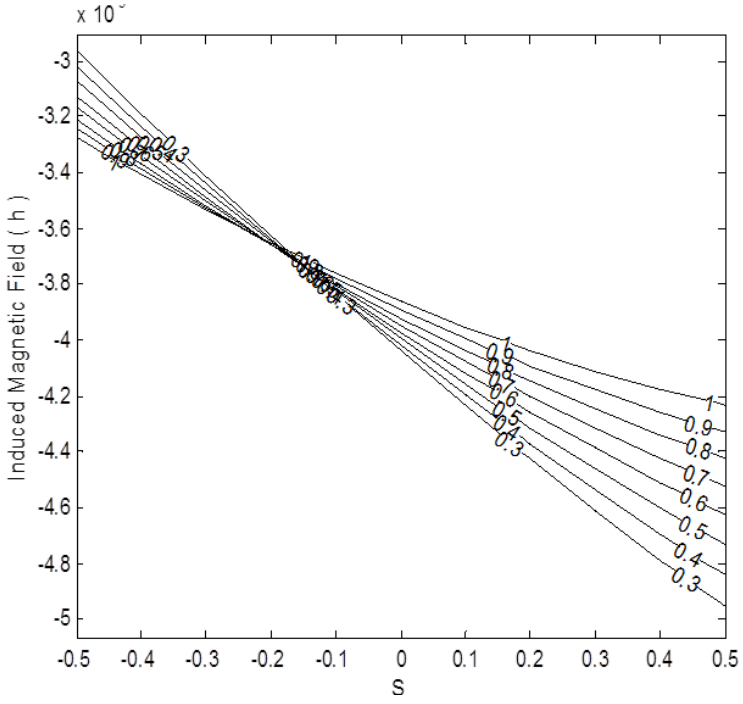


Figure 4.1.10: Induced magnetic field (h) versus S for different values of Pr at $M = 2.0$, $t = 0.2$ and $y = 0.5$.

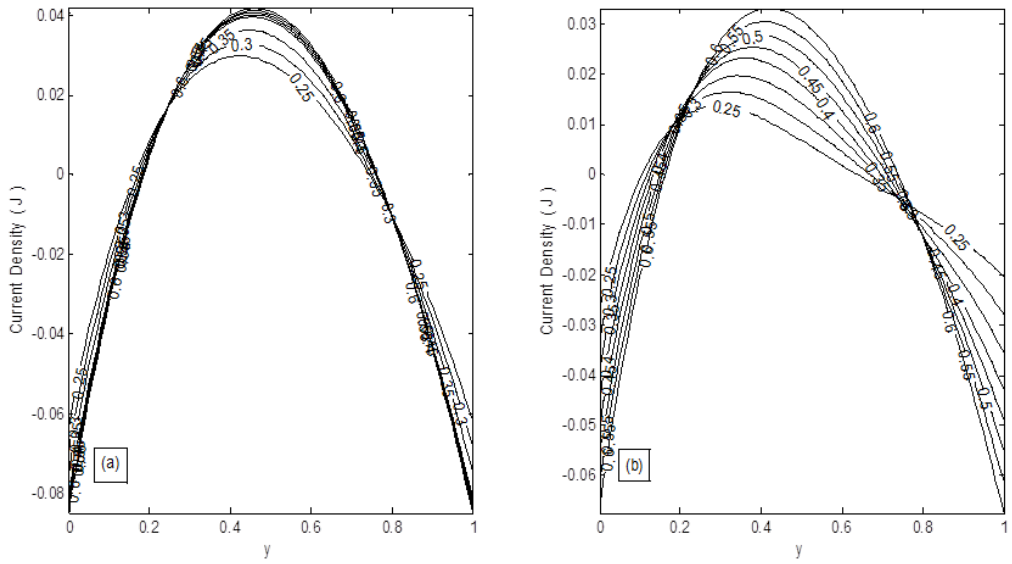


Figure 4.1.11: Current density (J) against y for different values of dimensionless time (t), at $S = -0.5$, $M = 2.0$, $Pr = 0.71(a), Pr = 7.0(b)$.

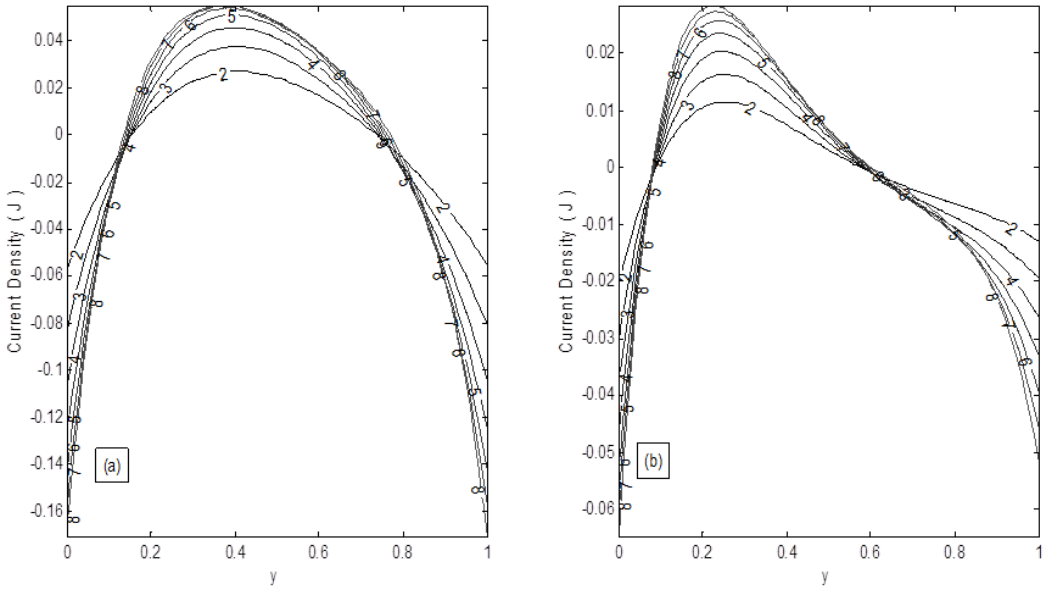


Figure 4.1.12: Current density (J) against y for different values of magnetic parameter (M), at $S = -0.5$, $t = 0.2$, $Pr = 0.71(a), Pr = 7.0(b)$.

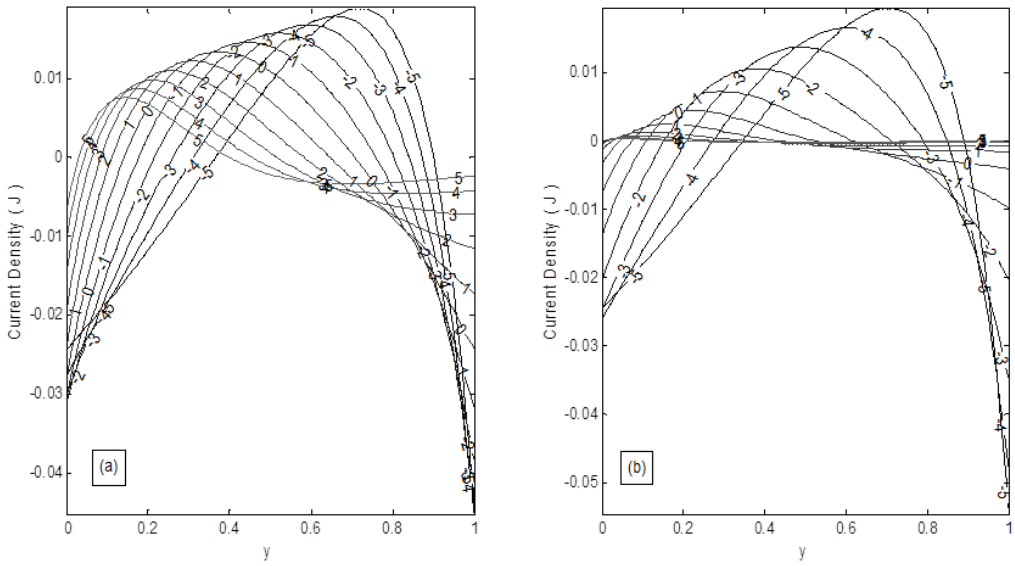


Figure 4.1.13: Current density (J) against y for different values of suction/injection S, at $t = 0.2$, $M = 2.0$, $Pr = 0.71(a), Pr = 7.0(b)$.

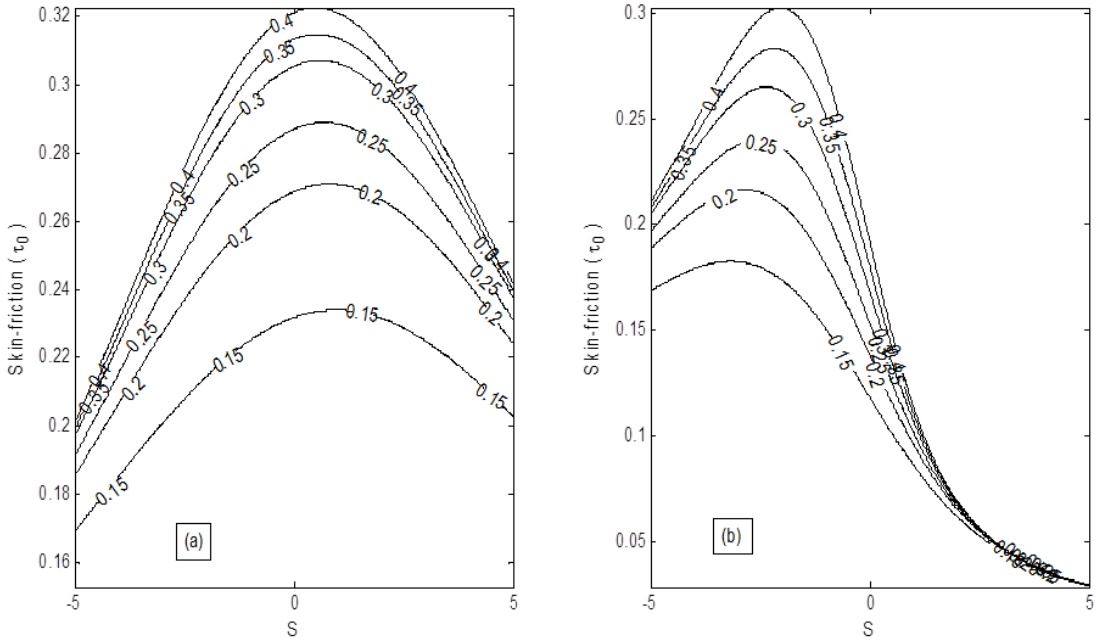


Figure 4.1.14: Skin-friction (τ_0) versus S for different values of dimensionless time (t) for $M = 2.0$, $Pr = 0.71(a), Pr = 7.0(b)$.

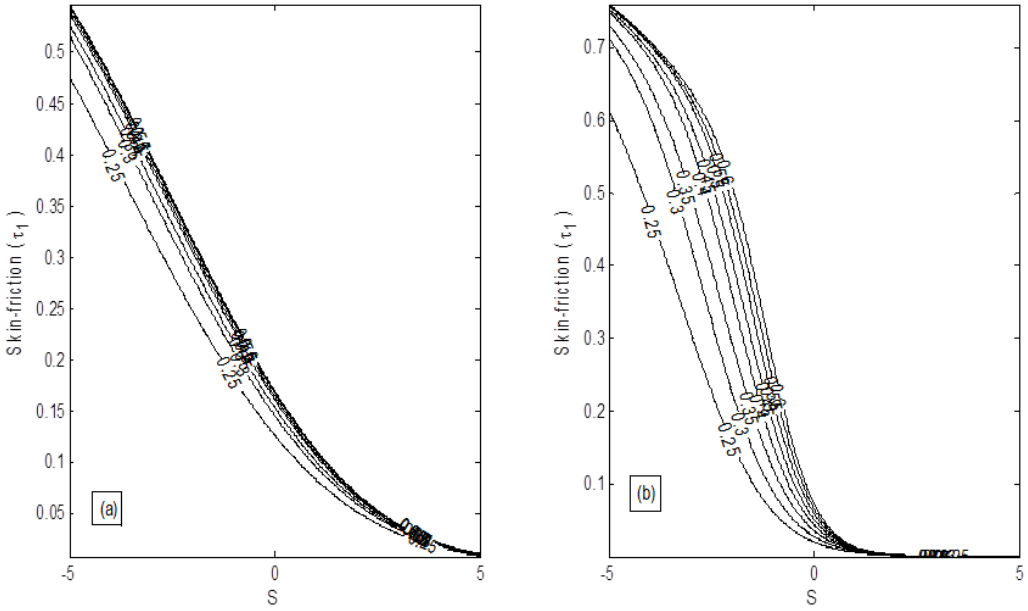


Figure 4.1.15: Skin-friction (τ_1) versus S for different values of dimensionless time (t) at $M = 2.0$, $Pr = 0.71(a), Pr = 7.0(b)$.

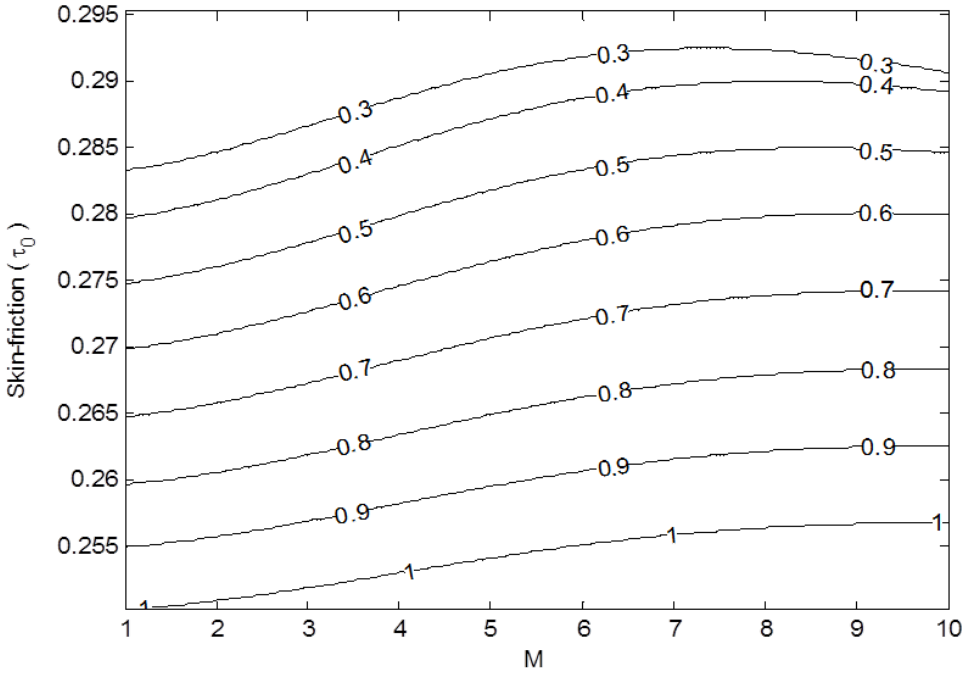


Figure 4.1.16: Skin-friction (τ_0) versus M for different values of Pr at $S = -0.5$, $t = 0.2$.

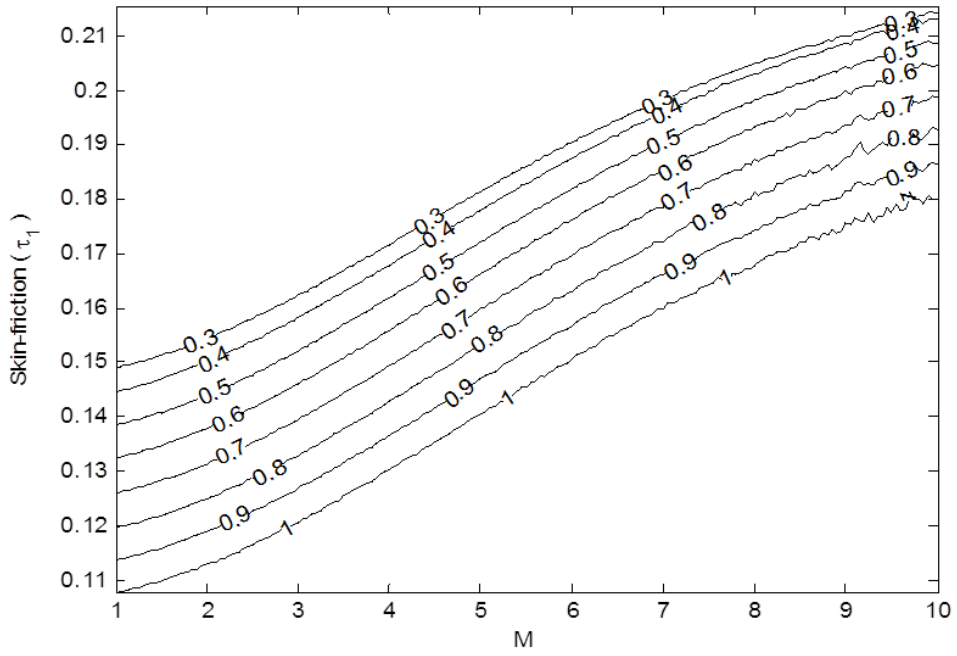


Figure 4.1.17: Skin-friction (τ_1) versus M for different values of Pr at $S = -0.5$, $t = 0.2$.

4.2 Unsteady MHD free-convective Couette flow in presence of Induced Magnetic Field: Impulsive motion

In this section, a semi-analytical solution for the time-dependent MHD flow of an electrically conducting fluid between two parallel plates in the presence of an induced magnetic field is presented. The motion of the fluid is produced by a time-dependent impulsive motion of one of the vertical plate while the other plate is set at rest when the magnetic lines of forces are fixed with the moving plate. The solution of the problem is obtained in the Laplace transform domain, while the inversion of the Laplace transform is carried out by the Riemann-sum approximation. The numerical results obtained are presented graphically for the velocity, induced magnetic field, current density and skin friction for various working parameters at both moving and stationary plate. Moreover, an excellent agreement was found between steady state solution obtained exactly and transient solution obtained by implicit finite difference method or Riemann sum approximation method at large values of time.

4.2.1 Mathematical Analysis

Consider unsteady flow of an electrically conducting, viscous and incompressible fluid between two infinite parallel vertical plates separated by a distance d. Initially, at time $t' \leq 0$, both the fluid and plates are assumed to be at rest and at same temperature T'_0. At time $t' > 0$, one of the plates is assumed to be moving in its own plane parallel to the stationary plate with a uniform velocity U_0. The temperature of the moving plate is instantaneously raised or lowered to T'_w, which is maintained at all time, while the stationary plate ($y' = d$) at distance d apart, is kept fixed and the temperature is assumed to be

of constant value T_0'. The flow is assumed to be in x'- axis which is taken along the fixed plate, and y'-axis taken normal to the direction of flow. A uniform magnetic field of strength H_0 is applied parallel to y'-axis. Taking into account the induced magnetic field. Under the usual *Boussinesq's* approximation the governing equations for this problem are given by

$$\frac{\partial u'}{\partial t'} = \nu \frac{\partial^2 u'}{\partial y'^2} + \frac{\mu_e H_0}{\rho} \frac{\partial h'}{\partial y'} + g\beta(T' - T_0), \tag{4.2.1}$$

$$\frac{\partial h'}{\partial t'} = \frac{1}{\sigma \mu_e} \frac{\partial^2 h'}{\partial y'^2} + H_0 \frac{\partial u'}{\partial y'}, \tag{4.2.2}$$

$$\frac{\partial T'}{\partial t'} = \alpha \frac{\partial^2 T'}{\partial y'^2}. \tag{4.2.3}$$

The initial and boundary conditions for the present problem are

$$\begin{aligned} t' \leq 0; \quad u' &= 0, \quad T' = T_0, \quad h' = 0 \ for \ \ all \ \ y; \\ t' > 0; \quad u' &= U_0, \quad T' = T_w, \quad h = 0 \ \ at \ \ y' = 0, \\ u' &= U_0, \quad T' = T_0, \quad h' = 0 \ \ at \ \ y' = 1, \end{aligned} \tag{4.2.4}$$

where u' is the velocity of the fluid, h' is the induced magnetic field, T' is the temperature of the fluid, ν is the kinematic viscosity, g is the acceleration due to gravity, β is the coefficient of thermal expansion, μ_e is the magnetic permeability, ρ the density, σ the electrical conductivity and α is thermal diffusivity of fluid. Introducing the following non-dimensional quantities

$$\begin{aligned} y &= \frac{y'}{d}, \quad t = \frac{t'\nu}{d^2}, \quad \theta = \frac{(T' - T_0')}{(T_w' - T_0')}, \quad h = \frac{h'(\frac{\mu_e}{\rho})^{\frac{1}{2}}\nu}{g\beta d^2(T_w' - T_0')}, \\ M &= \frac{\sigma \mu_e^2 H_0^2 d^2}{\rho \nu}, \quad U_0 = \frac{g\beta d^2(T_1 - T_0)}{\nu}, \quad Gr = \frac{\beta g(T_w' - T_0')d^3}{\nu U_0}, \\ u &= \frac{u'}{U_0}, \quad Pr = \frac{\nu}{\alpha}, \quad Pm = \sigma \mu_e \nu, \end{aligned} \tag{4.2.5}$$

in Eqs.(4.2.1) - (4.2.3), we have

$$\frac{\partial u}{\partial t} = \frac{\partial^2 u}{\partial y^2} + M \frac{\partial h}{\partial y} + Gr\theta, \tag{4.2.6}$$

$$\frac{\partial h}{\partial t} = \frac{1}{Pm} \frac{\partial^2 h}{\partial y^2} + M \frac{\partial u}{\partial y}, \tag{4.2.7}$$

$$\frac{\partial \theta}{\partial t} = \frac{1}{Pr}\frac{\partial^2 \theta}{\partial y^2}, \tag{4.2.8}$$

with the initial and boundary conditions

$$\begin{aligned} t \leq 0; \quad u &= 0, \quad \theta = 0, \quad h = 0 \ for \ \ all \ \ y; \\ t > 0; \quad u &= A, \quad \theta = 1, \quad h = 0 \ \ at \ \ y = 0, \\ u &= B, \quad \theta = 0, \quad h = 0 \ \ at \ \ y = 1, \end{aligned} \tag{4.2.9}$$

where y is the dimensionless coordinate normal to plates, t the dimensionless time, the dimensionless temperature θ, u is the dimensionless velocity, M is the magnetic parameter which is the square of Hartmann number, h is the dimensionless induced magnetic fields, Gr is the Grashof number and Pm is the magnetic Prandtl number.

Taking the Laplace transform of Eqs.(4.2.6) - (4.2.8) with the help of equation 1.6.2 under initial and boundary conditions (4.2.9) for $Pm = 1$, the following ordinary differential equations result;

$$\frac{d^2\bar{u}}{dy^2} + M\frac{d\bar{h}}{dy} - s\bar{u} = -Gr\bar{\theta}, \tag{4.2.10}$$

$$\frac{d^2\bar{h}}{dy^2} + M\frac{d\bar{u}}{dy} - s\bar{h} = 0, \tag{4.2.11}$$

$$\frac{d^2\bar{\theta}}{dy} - sPr\theta = 0, \tag{4.2.12}$$

where $s > 0$ is the Laplace parameter.

The corresponding boundary conditions are;

$$\begin{aligned} \bar{u} &= \bar{A}s^{-1} \quad \bar{\theta} = s^{-1} \ \bar{h} = 0 \ \ at \ \ y = 0 \\ \bar{u} &= \bar{B}s^{-1} \quad \bar{\theta} = 0 \quad \bar{h} = 0 \ \ at \ \ y = 1 \end{aligned} \tag{4.2.13}$$

The solution of Eq.(4.2.12) considering (4.2.13) is given as;

$$\bar{\theta}(y, s) = \frac{\sinh(b(1-y))}{s\sinh(b)} \tag{4.2.14}$$

Therefore, the solutions of Eqs.(4.2.10) and (4.2.11) together with (4.2.13) gives the velocity and induced magnetic field expressions in Laplace domain. Note that two cases are are involved.

Case I: A = 1, B = 0

$$\bar{u}(y,s) = \frac{1}{2}\{A_1\cosh(\lambda y) + A_2\sinh(\lambda y)\}e^{-\frac{1}{2}My} - \frac{1}{4}\frac{Gr[\frac{e^{b(1-y)}}{d_1} - \frac{e^{-b(1-y)}}{d_2}]}{s\sinh(b)} + \frac{1}{2}\{A_3\cosh(\lambda y) + A_4\sinh(\lambda y)\}e^{\frac{1}{2}My} - \frac{1}{4}\frac{Gr[\frac{e^{b(1-y)}}{d_2} - \frac{e^{-b(1-y)}}{d_1}]}{s\sinh(b)} \tag{4.2.15}$$

$$\bar{h}(y,s) = \frac{1}{2}\{A_1\cosh(\lambda y) + A_2\sinh(\lambda y)\}e^{-\frac{1}{2}My} - \frac{1}{4}\frac{Gr[\frac{e^{b(1-y)}}{d_1} - \frac{e^{-b(1-y)}}{d_2}]}{s\sinh(b)} - \frac{1}{2}\{A_3\cosh(\lambda y) + A_4\sinh(\lambda y)\}e^{\frac{1}{2}My} + \frac{1}{4}\frac{Gr[\frac{e^{b(1-y)}}{d_2} - \frac{e^{-b(1-y)}}{d_1}]}{s\sinh(b)} \tag{4.2.16}$$

where all constants are defined in Appendix C

Case II: A = 0, B = 1

$$\bar{u}(y,s) = \frac{1}{2}\{A_5\cosh(\lambda y) + A_6\sinh(\lambda y)\}e^{-\frac{1}{2}My} - \frac{1}{4}\frac{Gr[\frac{e^{b(1-y)}}{d_1} - \frac{e^{-b(1-y)}}{d_2}]}{s\sinh(b)} + \frac{1}{2}\{A_7\cosh(\lambda y) + A_8\sinh(\lambda y)\}e^{\frac{1}{2}My} - \frac{1}{4}\frac{Gr[\frac{e^{b(1-y)}}{d_2} - \frac{e^{-b(1-y)}}{d_1}]}{s\sinh(b)} \tag{4.2.17}$$

$$\bar{h}(y,s) = \frac{1}{2}\{A_5\cosh(\lambda y) + A_6\sinh(\lambda y)\}e^{-\frac{1}{2}My} - \frac{1}{4}\frac{Gr[\frac{e^{b(1-y)}}{d_1} - \frac{e^{-b(1-y)}}{d_2}]}{s\sinh(b)} - \frac{1}{2}\{A_7\cosh(\lambda y) + A_8\sinh(\lambda y)\}e^{\frac{1}{2}My} + \frac{1}{4}\frac{Gr[\frac{e^{b(1-y)}}{d_2} - \frac{e^{-b(1-y)}}{d_1}]}{s\sinh(b)} \tag{4.2.18}$$

Eqs.(4.2.14) - (4.2.16) are inverted in terms of the usual Riemann-sum approximation (Jha and Apere, 2010) as defined in equation 1.6.6;

4.2.2 Skin-friction

$$\tau = \frac{du}{dy} = \frac{e^{\epsilon t}}{t}[\frac{1}{2}\bar{u_1}(y,\epsilon) + \Re e \sum_{k=1}^{N} \bar{u_1}(y, \epsilon + \frac{ik\pi}{t})(-1)^k] \tag{4.2.19}$$

The skin-friction and and the current density are obtained by differentiating equation.(1.6.6) with respect to y, as obtained in equations (3.1.17 and 3.1.21). Two cases are treated here; For case I

$$\begin{aligned}
\bar{u_1} = \frac{\lambda}{2}[&(A_1\sinh(\lambda y) + A_2\cosh(\lambda y))\exp(-\frac{M}{2}y) \\
&+ (A_3\sinh(\lambda y) + A_4\cosh(\lambda y))\exp(\frac{M}{2}y)] \\
&+ \frac{M}{2}[(A_3\cosh(\lambda y) + A_4\sinh(\lambda y))\exp(\frac{M}{2}y) \\
&- (A_1\cosh(\lambda y) + A_2\sinh(\lambda y))\exp(-\frac{M}{2}y)] \\
&+ \frac{Grb\cosh(b)}{2\sinh(b)}(\frac{1}{d_1} + \frac{1}{d_2})
\end{aligned}$$

and that of case II as;

$$\begin{aligned}
\bar{u_1} = \frac{\lambda}{2}[&(A_5\sinh(\lambda y) + A_6\cosh(\lambda y))\exp(-\frac{M}{2}y) \\
&+ (A_7\sinh(\lambda y) + A_8\cosh(\lambda y))\exp(\frac{M}{2}y)] \\
&+ \frac{M}{2}[(A_7\cosh(\lambda y) + A_8\sinh(\lambda y))\exp(\frac{M}{2}y) \\
&- (A_5\cosh(\lambda y) + A_6\sinh(\lambda y))\exp(-\frac{M}{2}y)] \\
&+ \frac{Grb\cosh(b)}{2\sinh(b)}(\frac{1}{d_1} + \frac{1}{d_2})
\end{aligned}$$

where $\bar{h_1}$ for case I in the case of current density is;

$$\begin{aligned}
\bar{h_1} = \frac{\lambda}{2}[&(A_1\sinh(\lambda y) + A_2\cosh(\lambda y))\exp(-\frac{M}{2}y) \\
&- (A_3\sinh(\lambda y) + A_4\cosh(\lambda y))\exp(\frac{M}{2}y)] \\
&- \frac{M}{2}[(A_3\cosh(\lambda y) + A_4\sinh(\lambda y))\exp(\frac{M}{2}y) \\
&+ (c_1\cosh(\lambda y) + A_2\sinh(\lambda y))\exp(-\frac{M}{2}y)] \\
&+ \frac{Grb\cosh(b)}{2\sinh(b)}(\frac{1}{d_1} + \frac{1}{d_2})
\end{aligned}$$

and that of case II as;

$$\begin{aligned}\bar{h_1} = \frac{\lambda}{2}[&(A_5\sinh(\lambda y) + A_6\cosh(\lambda y))\exp(-\frac{M}{2}y)\\ &- (A_7\sinh(\lambda y) + A_8\cosh(\lambda y))\exp(\frac{M}{2}y)]\\ &- \frac{M}{2}[(A_7\cosh(\lambda y) + A_8\sinh(\lambda y))\exp(\frac{M}{2}y)\\ &+ (A_5\cosh(\lambda y) + A_6\sinh(\lambda y))\exp(-\frac{M}{2}y)]\\ &+ \frac{Grb\cosh(b)}{2\sinh(b)}(\frac{1}{d_1} + \frac{1}{d_2})\end{aligned}$$

4.2.3 Validation

Steady State

To validate the accuracy of the Riemann-sun approximation method, we now calculate the steady state solution for velocity and induced magnetic field, which should coincide with the transient solution at large time. This is achieve by setting $\frac{\partial()}{\partial t}$ in eqs. (4.2.6) - (4.2.8) to zero. Therefore, the solution of the resulting ordinary differential equations yield the required steady state expressions for velocity and the induced magnetic field as

$$u_s = \frac{Gr}{M^2} - \frac{Gr}{M^2}y + \frac{Gr(A_9 - A_{11})}{2M} + \frac{Gr(A_{12}\exp(My) + A_{10}\exp(-My))}{2} \tag{4.2.20}$$

$$h_s = \frac{Gr}{2M}y^2 - \frac{Gr}{M}y + \frac{Gr(A_9 + A_{11})}{2M} + \frac{Gr(A_{10}\exp(-My) - A_{12}\exp(My))}{2} + \frac{Gr}{M^3} \tag{4.2.21}$$

where all constants are defined in Appendix C

Implicit Finite Difference Method (IFDM)

The procedure adopted involves approximation of differential equations by the finite difference equations and then solving the difference equations subject to the prescribed initial and boundary conditions (refer to section 1.6.3). Thus

eqs.(4.2.6) - (4.2.8) under the boundary conditions (4.2.9) become

$$\frac{u(i,j)-u(i,j-1)}{\Delta t}=\frac{1}{(\Delta y)^2}[u(i+1,j)-2u(i,j)+u(i-1,j)]$$
$$+\frac{M}{2\Delta y}[h(i+1,j)-h(i-1,j)]+Gr\theta(i,j) \tag{4.2.22}$$

$$\frac{h(i,j)-h(i,j-1)}{\Delta t}=\frac{1}{Pm}\frac{1}{(\Delta y)^2}[h(i+1,j)-2h(i,j)+h(i-1,j)]$$
$$+\frac{M}{2\Delta y}[u(i+1,j)-u(i-1,j)] \tag{4.2.23}$$

$$\frac{\theta(i,j)-\theta(i,j-1)}{\Delta t}=\frac{1}{Pr}\frac{1}{(\Delta y)^2}[\theta(i+1,j)-2\theta(i,j)+\theta(i-1,j)] \tag{4.2.24}$$

4.2.4 Results and Discussion

In order to get the physical insight into the problem, numerical values of the temperature field, velocity field, induced magnetic field, current density distribution, and the skin-friction are computed for different values of the physical parameters. These physical parameters include the dimensionless time (t), Grashof number (Gr), magnetic parameter (M) and Prandtl number (Pr) which are discussed and graphically presented in Figs. 4.2.1 to 4.2.18. In each of these figures, there are two components (a) for air ($Pr = 0.71$) and (b) for water ($Pr = 7.0$). Note that the state of the plates dictates the value of Gr, hence it can either be positive, zero or negative depending on the temperature of the plates. If $T'_w - T'_0 < 0$, then the moving plate's temperature is less than the temperature of the other plate. In this situation, convection currents flow towards the moving plate, therefore, the moving plate experiences an external heating produced by the heat energy of the fluid. $Gr > 0$ corresponds to external cooling of the moving plate, $Gr < 0$ corresponds to external heating of the moving plate while $Gr = 0$ corresponds to the absence of convection current.

Figs. 4.2.1 - 4.2.4 show the effects of the various dimensionless parameters on the velocity profiles. It is seen from these Figs. that effects of t and Gr is to increase the velocity of both air and water, while effects of M is to decrease the velocity towards the moving plate with a reverse behaviour towards the other plate as earlier mentioned. Furthermore, the velocity of air is greater than the velocity of water, which is expected since convection current is weak for water compared to air. Fig. 4.2.5 depicts the influence of varying Pr on the velocity. This suggest that in presence of induced magnetic field, magnetic parameter play a role in accelerating the fluid motion. It is remarkable to point out that for all magnetic parameters considered here, there exists a location inside the flow domain where the velocity field is independent of magnetic parameter. It is observed that increase in Pr decreases the velocity. Physically this is possible because fluids with high Prandtl number have greater viscosity which makes the fluid thick and hence reduced thermal conductivity.

Figs. 4.2.6 - 4.2.9 show the effects of the various dimensionless parameters on the induced magnetic field distribution. It is observed from these Figs. that the induced magnetic field increases and attain its maximum towards the moving plate and decreases gradually towards the other plate as t and Gr increases with a variation of location of the inflexion point, while the effects of varying M is to increase the induced magnetic field (Figs.4.2.6 - 4.2.8). This indicates an existence of a location inside the flow domain where the induced magnetic field is independent of the considered parameter. This behaviour is more conspicuous in air compared to water. Increase in Pr decreases the induced magnetic field towards the moving plate while it increases towards the other plate (Fig.4.2.9).

Distribution of current density showing the effects of the dimensionless parameters are shown in Figs. 4.2.10 - 4.2.13. It is seen from Figs.4.2.10 and 4.2.11 that an increase in t as well as Gr leads to an increase in the current density

around the central region of the channel, while a decrease is observed towards the plates. While in Fig.4.2.12, it is observed that an increase in M leads to an increase in current density towards the moving plate with a reverse flow towards the other plate. Effects of varying Pr is depicted in Figure 4.2.13. From this Figure it is observed that the current density is higher near the moving plate and decreasing towards the stationary plate. It is also observed that the current density increases with growing Pr near the channel boundaries while it decreases with increase in Pr around the central region of the channel.

Figs. 4.2.14 - 4.2.16 illustrate the variation of skin-friction τ_0 with M at different values of t, Gr and Pr. It is observed from Figs.4.2.14 and 4.2.15, that the skin-friction τ_0 increases with increasing t and M. Furthermore, the skin-friction in case of air is greater than that of the water. It is observed from Fig. 4.2.16 that the skin-friction τ_0 decreases with increasing Pr. This is physically true since large Prandtl number fluids promotes high viscous effects thereby causing an enhanced frictional force. A reverse trend is observed in Figs. 4.2.17 - 4.2.18 which illustrate the variation of skin-friction τ_1 with M under same physical parameters.

Tables 4.2.1,4.2.2, 4.2.4 and 4.2.5 show a comparison between transient state and steady state numerical values of velocity and the induced magnetic field obtained by the Riemann-sum approximation method (RSM), finite difference method (FDM) and exact solution for steady state (SS) at varying values of dimensionless time t for $Pr = 0.71$, $Gr = -10.0$, $Pm = 1.0$ and $M = 0.5$. This reveals an excellent agreement between the three methods at large value of time ($t \geq 1.0$). Tables 4.2.3 and 4.2.6 depicts the numerical solution of velocity and the induced magnetic field obtained by finite difference method for varying values of magnetic Prandtl number Pm for fixed values of $Pr = 0.71$, $Gr = -10.0$, $M = 0.5$ and $t = 0.2$. It is observed that as Pm increases the velocity slightly decreases, while the strength of the induced magnetic field

increases. This is physically true since an increase in the magnetic permeability (Pm) encourages the penetration of the applied magnetic force to increase the strength of the induced magnetic field within the channel. Consequent upon increase in the strength of the induced magnetic field, there is an increase in the Lorentz force which retards fluid motion, hence the decrease in fluid velocity.

4.2.5 Concluding Remarks

In this chapter, the problem of unsteady MHD free-convective Couette flow in presence of induced magnetic field of an incompressible, viscous and electrically conducting fluid between parallel insulated walls with an applied transverse magnetic field has been studied. The coupled non linear governing equations, which accounted for the effects of time, magnetic parameter (M), Grashof number (Gr), and Prandtl number (Pr) were obtained, non-dimensionalized and solved semi-analytically by the combination of Laplace transform technique and the Riemann-sum approximation. The following conclusions are drawn;

1. increase in t and Gr increases the velocity, increases the induced magnetic field and attain its maximum towards the moving plate and decreases gradually towards the other plate

2. increase in Pm increases the velocity slightly resulting in increase in the strength of induced magnetic field within the channel

3. in presence of induced magnetic field, the magnetic field parameter accelerate the fluid flow

4. with growing physical parameters, the current density increases

5. there exists a location within the flow domain which is a function of the

Case I

Table 4.2.1: Numerical values of the velocity u obtained using the Riemann-Sum approximation method (RSM) compared to those obtained by the finite difference method (FDM) and the steady state (SS) for $Gr = -10.0$ $Pr = 0.71, Pm = 1.0$ and $M = 0.5$ with varying values of t.

	t=0.2		t=0.4		t=1.0		
y	RSM	FDM	RSM	FDM	RSM	FDM	SS
0.0	0.9974	1.0000	0.9974	1.0000	0.9974	1.0000	1.0000
0.1	0.6561	0.6524	0.6438	0.6219	0.6597	0.6143	0.6142
0.2	0.3912	0.3921	0.3320	0.3343	0.3286	0.3199	0.3198
0.3	0.2046	0.2052	0.1254	0.1259	0.1044	0.1060	0.1060
0.4	0.0778	0.0786	-0.0147	-0.0145	-0.0386	-0.0377	-0.0377
0.5	-0.0005	0.0004	-0.0977	-0.0973	-0.1217	-0.1217	-0.1218
0.6	-0.0411	-0.0403	-0.1334	-0.0133	-0.1562	-0.1562	-0.1563
0.7	-0.0536	-0.0529	-0.1320	-0.1317	-0.1514	-0.1514	-0.1515
0.8	-0.0461	-0.0456	-0.1030	-0.1028	-0.1171	-0.1171	-0.1172
0.9	-0.0260	-0.0258	-0.0560	-0.0559	-0.0634	-0.0634	-0.0634
1.0	0.0000	0.0000	0.0000	0.0000	-0.0000	-0.0000	0.0000

considered physical parameters

6. the skin-friction τ_0 decreases as Pr increases while the effect of M reverse this trend in the case of τ_1

7. there is an excellent agreement between the three methods at large value of time.

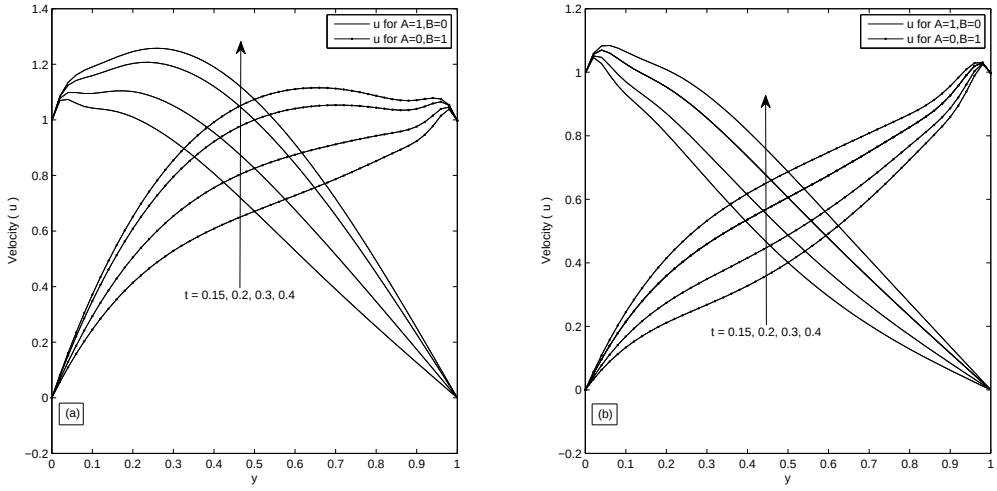


Figure 4.2.1: Velocity (u) distribution at different values of time t for $Gr = 10$, $M = 0.5$, $Pr = 0.71(a)$ and $7.0(b)$.

Table 4.2.2: Numerical values of the induced magnetic field h obtained using the Riemann-Sum approximation method (RSM) compared to those obtained by the finite difference method (FDM) and the steady state (SS) for $Gr = -10.0$ $Pr = 0.71$, $Pm = 1.0$ and $M = 0.5$ with varying values of t.

	t=0.2		t=0.4		t=1.0		
y	RSM	FDM	RSM	FDM	RSM	FDM	SS
0.0	0.0000	0.0000	0.0000	0.0000	0.0000	0.0000	0.0000
0.1	-0.0299	-0.0297	-0.0352	-0.0346	-0.0369	-0.0357	-0.0357
0.2	-0.0448	-0.0448	-0.0526	-0.0527	-0.0549	-0.0544	-0.0544
0.3	-0.0495	-0.0495	-0.0586	-0.0586	-0.0604	-0.0605	-0.0605
0.4	-0.0473	-0.0472	-0.0561	-0.0561	-0.0576	-0.0577	-0.0577
0.5	-0.0409	-0.0409	-0.0481	-0.0481	-0.0492	-0.0492	-0.0492
0.6	-0.0324	-0.0324	-0.0373	-0.0373	-0.0379	-0.0378	-0.0378
0.7	-0.0233	-0.0233	-0.0258	-0.0258	-0.0258	-0.0258	-0.0258
0.8	-0.0145	-0.0145	-0.0150	-0.0150	-0.0147	-0.0147	-0.0147
0.9	-0.0066	-0.0066	-0.0062	-0.0062	-0.0059	-0.0059	-0.0059
1.0	0.0000	0.0000	0.0000	0.0000	-0.0000	-0.0000	-0.0000

Table 4.2.3: Numerical values for velocity u and that of the induced magnetic field h obtained by the finite difference method (FDM) for $Gr = -10.0$, $Pr = 0.71$, $Pm = 1.0$, $t = 0.2$ at varying values of M.

	M = 0.5		M = 1.0		M = 1.5	
y	u	h	u	h	u	h
0.0	1.0000	0.0000	1.0000	0.0000	1.0000	0.0000
0.1	0.6524	-0.0297	0.6502	-0.0592	0.6466	-0.8809
0.2	0.3921	-0.0448	0.3909	-0.0889	0.3889	-0.1319
0.3	0.2052	-0.0494	0.2064	-0.0981	0.2083	-0.1451
0.4	0.0786	-0.0472	0.0823	-0.0937	0.0883	-0.1385
0.5	0.0004	-0.0409	0.0060	-0.0811	0.0152	-0.1201
0.6	-0.0403	-0.0324	-0.0336	-0.0645	-0.0228	-0.0958
0.7	-0.0529	-0.0232	-0.0462	-0.0465	-0.0355	-0.0697
0.8	-0.0456	-0.0144	-0.0401	-0.0292	-0.0312	-0.0442
0.9	-0.0258	-0.0066	-0.0225	-0.0135	-0.0172	-0.0208
1.0	0.0000	0.0000	0.0000	0.0000	0.0000	0.0000

Case II

Table 4.2.4: Numerical values of the velocity u obtained using the Riemann-Sum approximation method (RSM) compared to those obtained by the finite difference method (FDM) and the steady state (SS) for $Gr = -10.0$ $Pr = 0.71, Pm = 1.0$ and $M = 0.5$ with varying values of t.

	t=0.2		t=0.4		t=1.0		
y	RSM	FDM	RSM	FDM	RSM	FDM	SS
0.0	0.0000	0.0000	0.0000	0.0000	0.0000	0.0000	0.0000
0.1	-0.1454	-0.1452	-0.1757	-0.1752	-0.1844	-0.1828	-0.1828
0.2	-0.2051	-0.2046	-0.2619	-0.2619	-0.2763	-0.2762	-0.2762
0.3	-0.1927	-0.1919	-0.2711	-0.2707	-0.2900	-0.2904	-0.2905
0.4	-0.1206	-0.1197	-0.2129	-0.2125	-0.2354	-0.2357	-0.2357
0.5	-0.0005	0.0004	-0.0977	-0.0973	-0.1217	-0.1217	-0.1218
0.6	0.1573	0.1581	0.0648	0.0649	0.0406	0.4178	0.0417
0.7	0.3437	0.3443	0.2645	0.2649	0.2430	0.2451	0.2451
0.8	0.5503	0.5512	0.4909	0.4933	0.4878	0.4789	0.4788
0.9	0.7755	0.7718	0.7635	0.7412	0.7807	0.7336	0.7336
1.0	0.9974	1.0000	0.9974	1.0000	0.9974	1.0000	1.0000

Table 4.2.5: Numerical values of the induced magnetic field h obtained using the Riemann-Sum approximation method (RSM) compared to those obtained by the finite difference method (FDM) and the steady state (SS) for $Gr = -10.0$ $Pr = 0.71$, $Pm = 1.0$ and $M = 0.5$ with varying values of t.

	t=0.2		t=0.4		t=1.0		
y	RSM	FDM	RSM	FDM	RSM	FDM	SS
0.0	0.0000	0.0000	0.0000	0.0000	0.0000	0.0000	0.0000
0.1	0.0084	0.0084	0.0094	0.0094	0.0092	0.0092	0.0092
0.2	0.0221	0.0221	0.0252	0.0252	0.0253	0.0253	0.0253
0.3	0.0375	0.0374	0.0435	0.0435	0.0440	0.0440	0.0440
0.4	0.0515	0.0514	0.0605	0.0605	0.0617	0.0617	0.0617
0.5	0.0617	0.0616	0.0733	0.0732	0.0751	0.0751	0.0751
0.6	0.0663	0.0662	0.0793	0.0792	0.0814	0.0815	0.0816
0.7	0.0637	0.0636	0.0764	0.0763	0.0786	0.0788	0.0788
0.8	0.0525	0.0524	0.0628	0.0629	0.0655	0.0650	0.0650
0.9	0.0317	0.315	0.0383	0.0378	0.0402	0.0390	0.0391
1.0	-0.0000	0.0000	0.0000	0.0000	-0.0000	-0.0000	-0.0000

Table 4.2.6: Numerical values for velocity u and that of the induced magnetic field h obtained by the finite difference method (FDM) for $Gr = -10.0$, $Pr = 0.71$, $M = 0.5$, $t = 0.2$ at varying values of Pm.

	Pm = 0.5		Pm = 1.0		Pm = 1.5	
y	u	h	u	h	u	h
0.0	0.0000	0.0000	0.0000	0.0000	0.0000	0.0000
0.1	-0.1458	0.0058	-0.1452	0.0084	-0.1448	0.0082
0.2	-0.2057	0.0141	-0.2046	0.0221	-0.2039	0.0246
0.3	-0.1932	0.0229	-0.1919	0.0374	-0.1910	0.0442
0.4	-0.1209	0.0308	-0.1197	0.0514	-0.1188	0.0627
0.5	-0.0006	0.0363	0.0004	0.0616	0.0012	0.0770
0.6	0.1576	0.0384	0.1581	0.0662	0.1586	0.0843
0.7	0.3443	0.0364	0.3443	0.0636	0.3445	0.8240
0.8	0.5515	0.0296	0.5511	0.0524	0.5511	0.0690
0.9	0.7723	0.0176	0.7718	0.0315	0.7715	0.0422
1.0	1.0000	0.0000	1.0000	0.0000	1.0000	0.0000

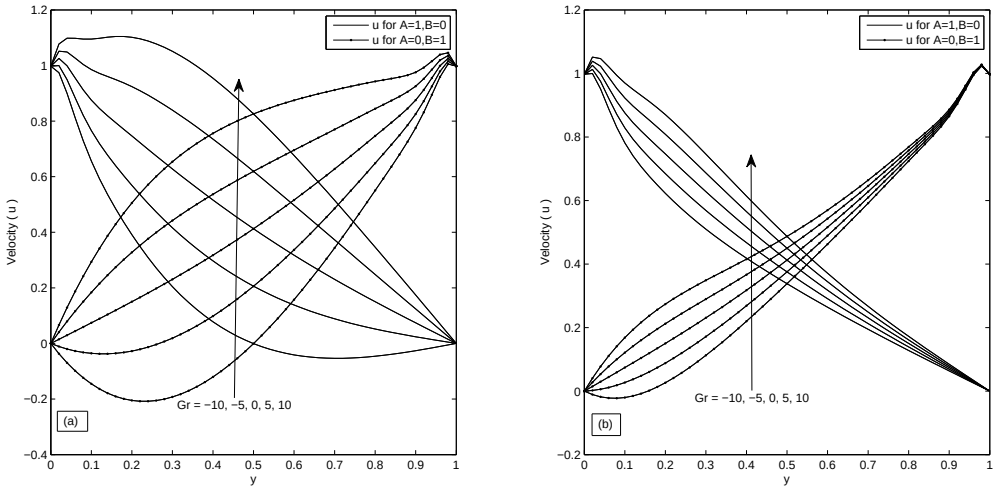


Figure 4.2.2: Velocity (u) distribution at different values of Gr for $t = 0.2$, $M = 0.5$, $Pr = 0.71(a)$ and $7.0(b)$.

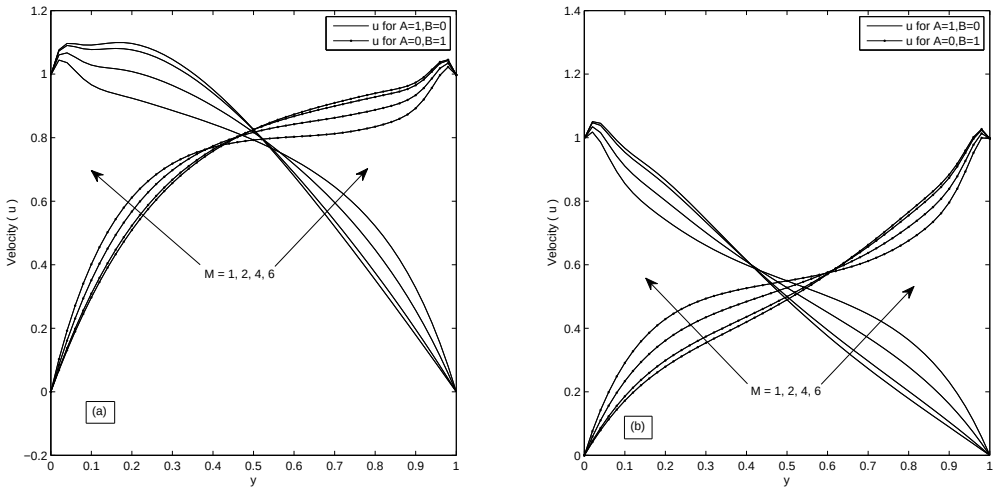


Figure 4.2.3: Velocity (u) distribution at different values of M for $Gr = 10$, $t = 0.2$, $Pr = 0.71(a)$ and $7.0(b)$.

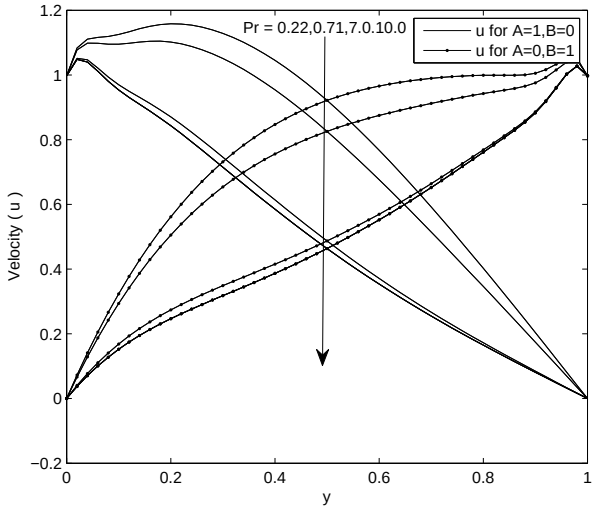


Figure 4.2.4: Velocity (u) distribution at different values of Pr for $Gr = 10$, $M = 0.5$, $t = 0.2$.

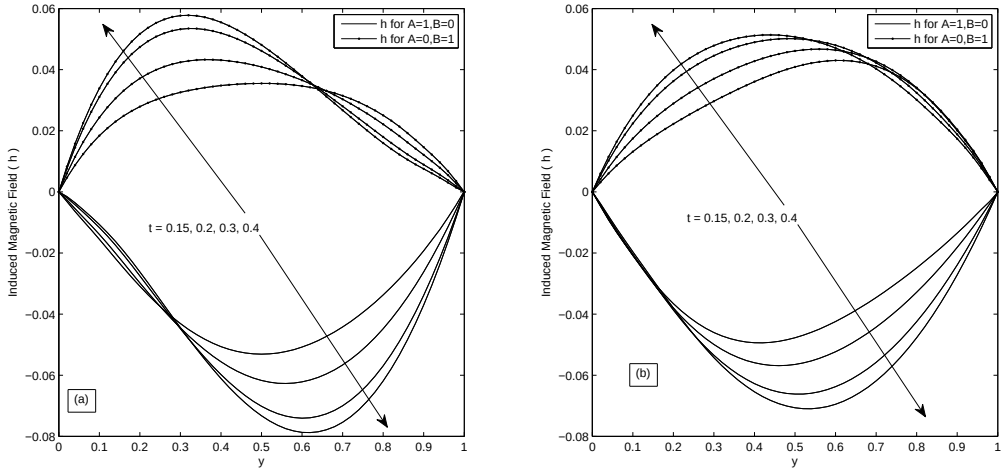


Figure 4.2.5: Induced Magnetic Field (h) at different values of time t for $Gr = 10$, $M = 0.5$, $Pr = 0.71(a)$ and $7.0(b)$.

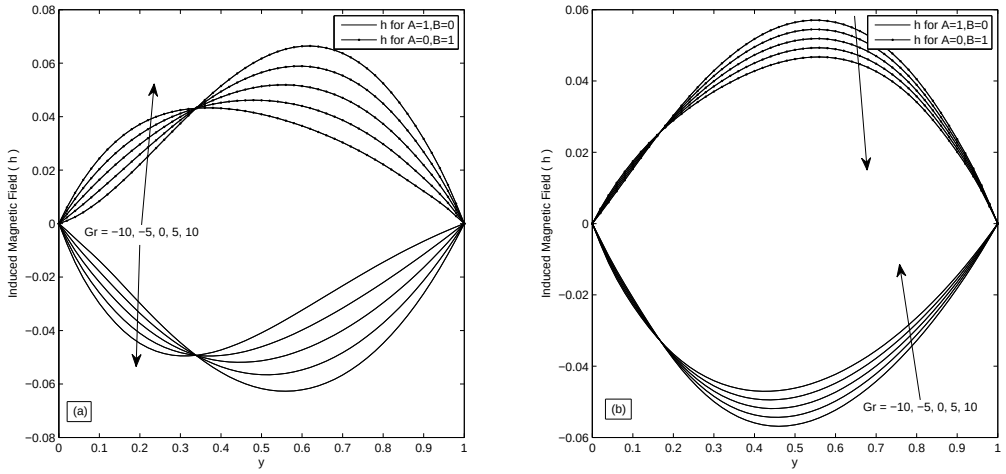


Figure 4.2.6: Induced Magnetic Field (h) at different values of Gr for $t = 0.2$, $M = 0.5$, $Pr = 0.71(a)$ and $7.0(b)$.

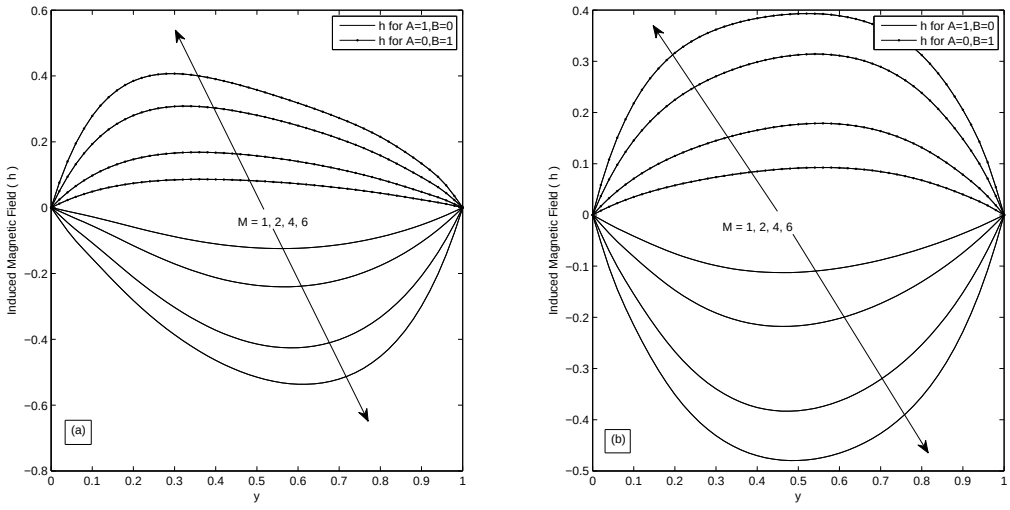


Figure 4.2.7: Induced Magnetic Field (h) at different values of M for $Gr = 10$, $t = 0.2$, $Pr = 0.71(a)$ and $7.0(b)$.

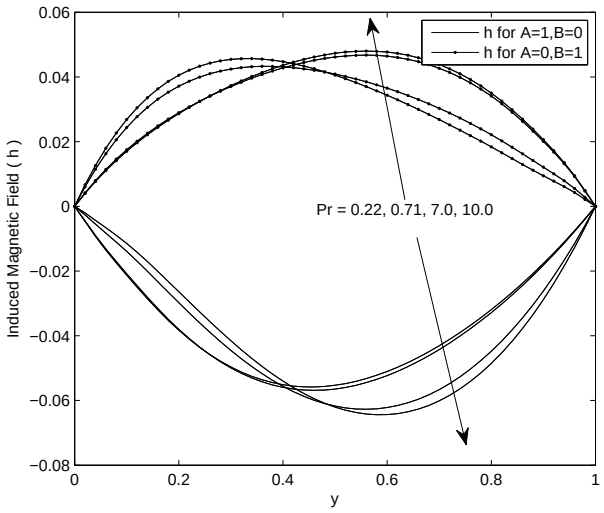


Figure 4.2.8: Induced Magnetic Field (h) at different values of Pr for $Gr = 10$, $M = 0.5$, $t = 0.2$.

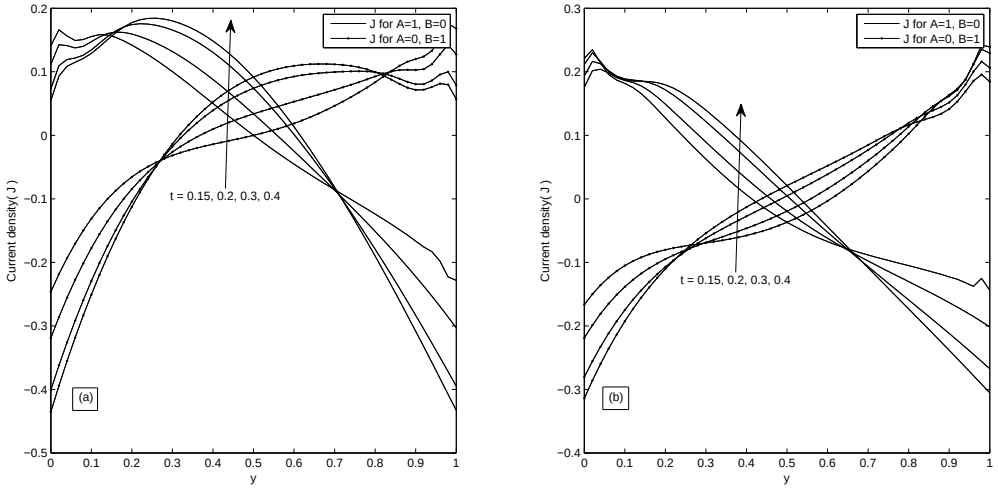


Figure 4.2.9: Current density (J) at different values of time t for $Gr = 10$, $M = 0.5$, $Pr = 0.71(a)$ and $7.0(b)$.

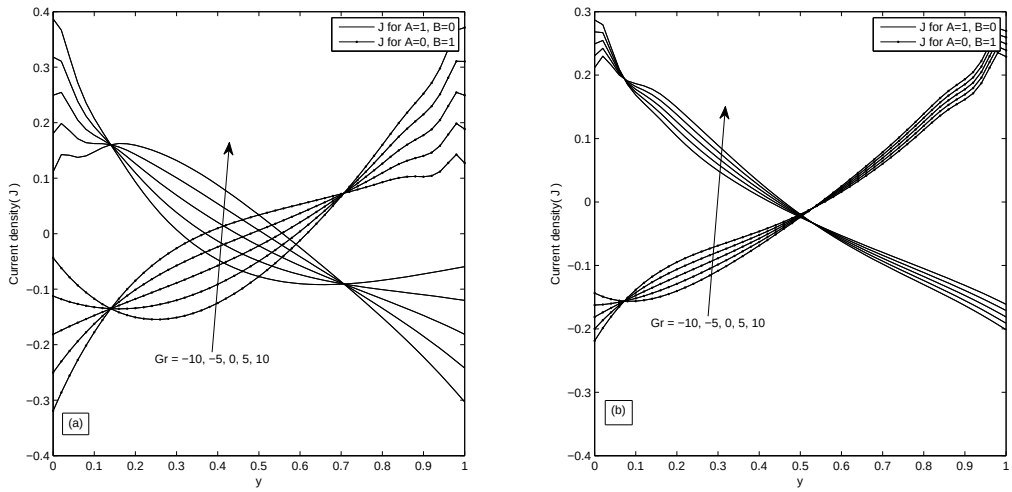


Figure 4.2.10: Current density (J) at different values of Gr for $t = 0.2$, $M = 0.5$, $Pr = 0.71(a)$ and $7.0(b)$.

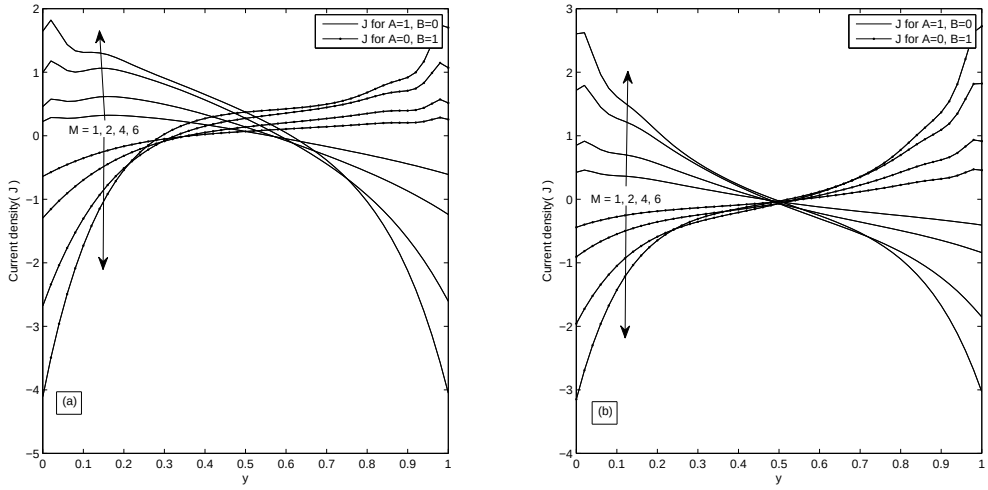


Figure 4.2.11: Current density (J) at different values of M for $Gr = 10$, $t = 0.2$, $Pr = 0.71(a)$ and $7.0(b)$.

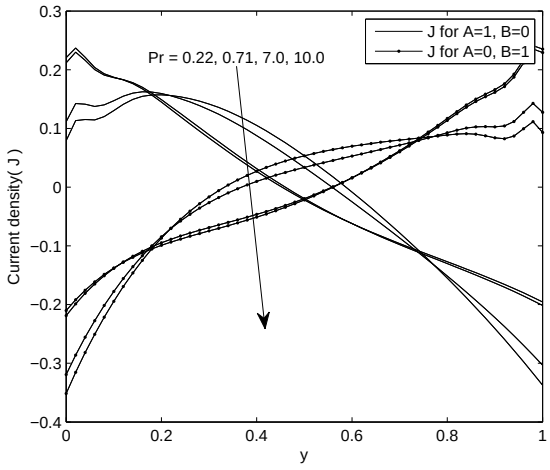


Figure 4.2.12: Current density (J) at different values of Pr for $Gr = 10$, $M = 0.5$, $t = 0.2$.

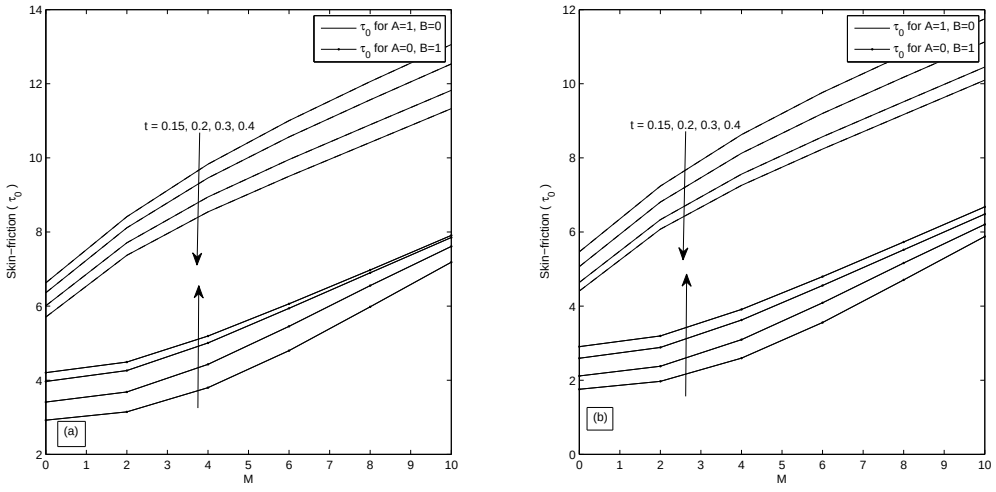


Figure 4.2.13: Skin-friction (τ_0) against M at different values of time t for $Gr = 10$, $M = 0.5$, $Pr = 0.71(a)$ and $7.0(b)$.

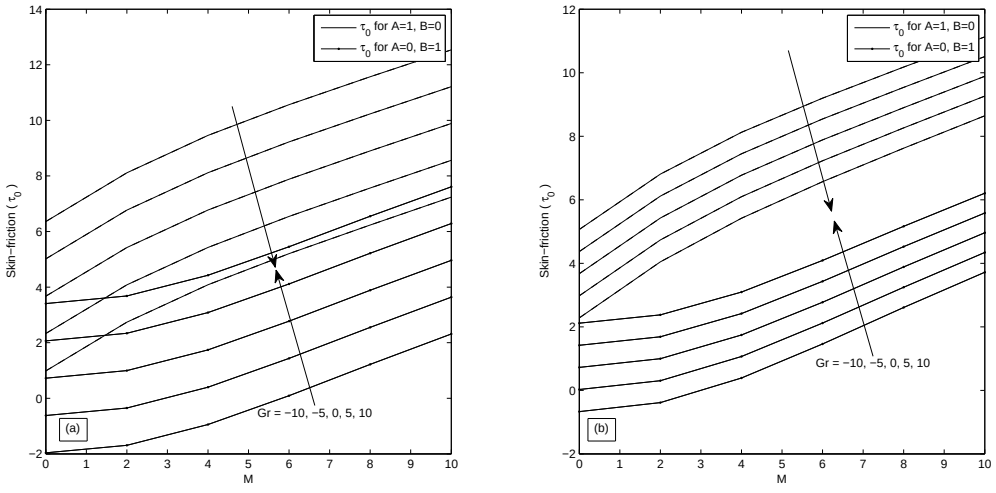


Figure 4.2.14: Skin-friction (τ_0) against M at different values of Gr for $t = 0.2$, $M = 0.5$, $Pr = 0.71(a)$ and $7.0(b)$.

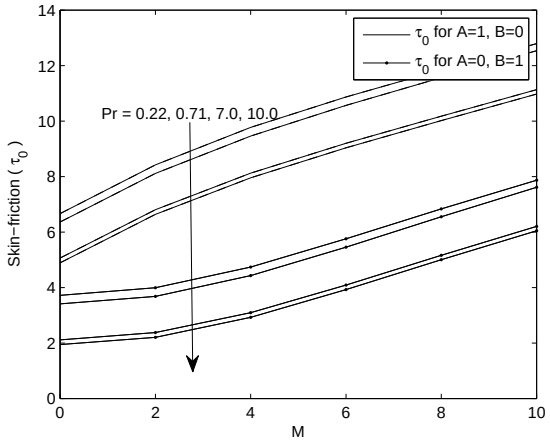


Figure 4.2.15: Skin-friction (τ_0) against M at different values of Pr for $Gr = 10$, $t = 0.2$.

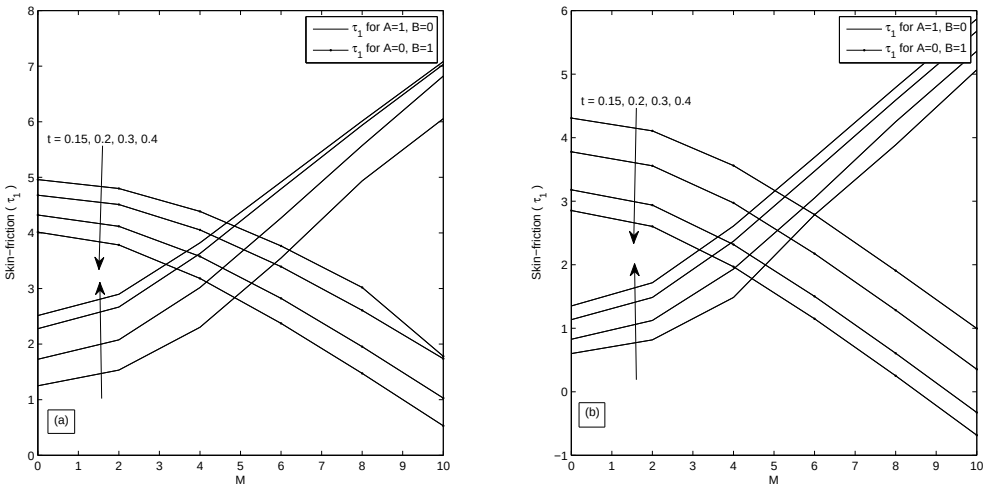


Figure 4.2.16: Skin-friction (τ_1) against M at different values of time t for $Gr = 10$, $M = 0.5$, $Pr = 0.71(a)$ and $7.0(b)$.

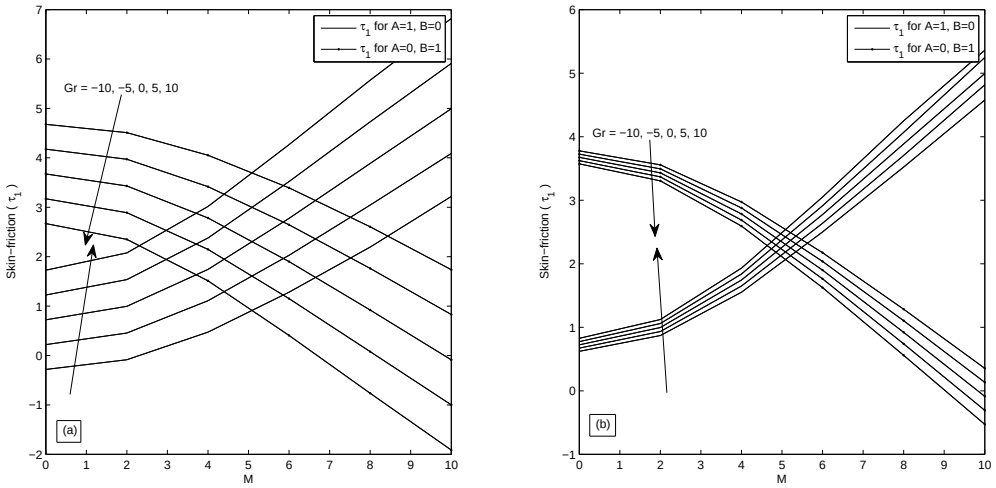


Figure 4.2.17: Skin-friction (τ_1) against M at different values of Gr for $t = 0.2$, $M = 0.5$, $Pr = 0.71(a)$ and $7.0(b)$.

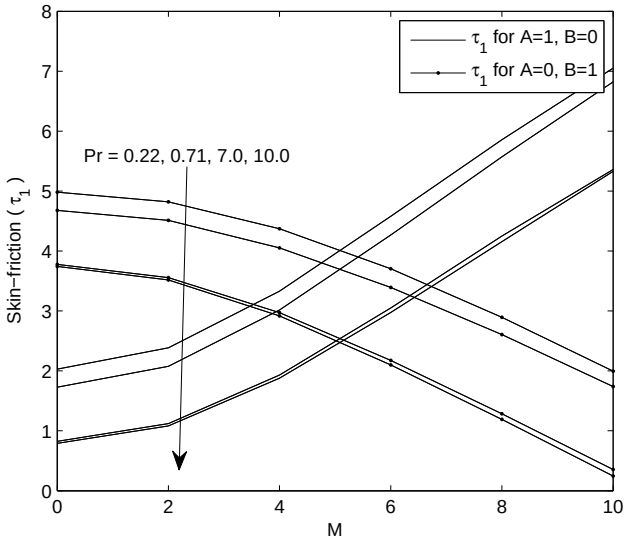


Figure 4.2.18: Skin-friction (τ_1) against M at different values of Pr for $Gr = 10$, $t = 0.2$.

CHAPTER FIVE

MHD FREE CONVECTION FLOW IN VERTICAL MICRO-CHANNEL

This chapter presents an exact solution of steady fully developed natural convection flow of viscous, incompressible, electrically conducting fluid in a vertical annular micro-channel in presence of radial magnetic field in first part while in the second part, the effect of transverse magnetic field in presence of velocity slip and temperature jump at the annular micro – channel surfaces.

5.1 MHD NATURAL CONVECTION FLOW IN VERTICAL MICRO-CONCENTRIC ANNULI IN PRESENCE OF RADIAL MAGNETIC FIELD: AN EXACT SOLUTION

The objective of this section is to investigate the influence of wall surface curvature on steady fully developed MHD natural convection flow of viscous, incompressible, electrically conducting fluid in micro-concentric annuli under a radial magnetic field. In fact, this is an extension of Weng and Chen (2008) for conducting fluid in presence of radial magnetic field. The area of micro and nanofluidics is fundamentally important due to the necessity of understanding the nature of fluid flow at this scale Gad-el Hak (1999). Free-convective gas microflow, encountered in many engineering fields, i.e., microelectrochemical cell transport, microheat exchanging, and microchip cooling, is an attractive branch of microfluidics due to its reliability, simplicity, and cost effectiveness in flow and heat transfer mechanism (Weng and Chen, 2008). Therefore, this result will no doubt increase the pool of the existing literature.

5.1.1 Mathematical Analysis

The flow considered is a fully developed steady (time independent) natural convection flow of viscous, incompressible, electrically conducting fluid in micro-concentric annuli under the effect of radial magnetic field. The x-axis is parallel to the gravitational acceleration g but in the opposite direction while the the radius of the inner and outer cylinder walls are k_1 and k_2 respectively as presented in Figure 5.1.1. Also a magnetic field is directed radial outward and is of the form $\frac{H_{0k_2}}{r}$, where H_0 is constant strength of the applied magnetic field and r is the radial distance from the axis of the micro-annulus. Such form of magnetic field was first discussed by Globe (1959). It is assumed that the magnetic Reynolds number is very small, which corresponds to negligibly induced magnetic field compared to the externally applied one. The outer surface of the inner cylinder is heated to a temperature (T_1) greater than that of the surrounding fluid having temperature (T_0) and the inner surface of the outer cylinder is maintained at temperature (T_0). Due to this temperature difference, natural convection occurs in the vertical annular micro-channel. Since the flow is fully developed and cylinders are of infinite length, the flow depends only on radial coordinate (r). Using the following dimensionless quantities

$$r = \frac{r-k_1}{w},\ w = k_2 - k_1,\ U = \frac{u}{u_c},\ \theta = \frac{T-T_0}{T_1-T_0},\ u_c = \frac{u\nu}{g\beta(T_w-T_0)w^2},$$
$$Pr = \frac{C_p\mu}{k},\ Kn = \frac{\lambda}{w},\ F = \frac{\beta_t}{\beta_\nu},\ \beta_\nu = \frac{2-\sigma_\nu}{\sigma_\nu},\ \beta_t = \frac{2-\sigma_t}{\sigma_t}\frac{2\gamma}{\gamma+1}\frac{1}{Pr},\ \eta = \frac{k_1}{k_2},$$
$$\lambda = \frac{\sqrt{\frac{\pi\widehat{R}T_0}{2\mu_0}}}{\rho},\ M^2 = \frac{\sigma\mu_e^2H_0^2w^2}{\rho_0\nu}. \tag{5.1.1}$$

The mathematical model representing present physical situation in dimensionless form in presence of velocity slip and temperature jump on annular micro-channel surfaces are:

$$\frac{1}{[\eta+(1-\eta)R]}\frac{d}{dR}\left[[\eta+(1-\eta)R]\frac{dU}{dR}\right] - \frac{M^2U}{[\eta+(1-\eta)R]^2} + \theta = 0, \tag{5.1.2}$$

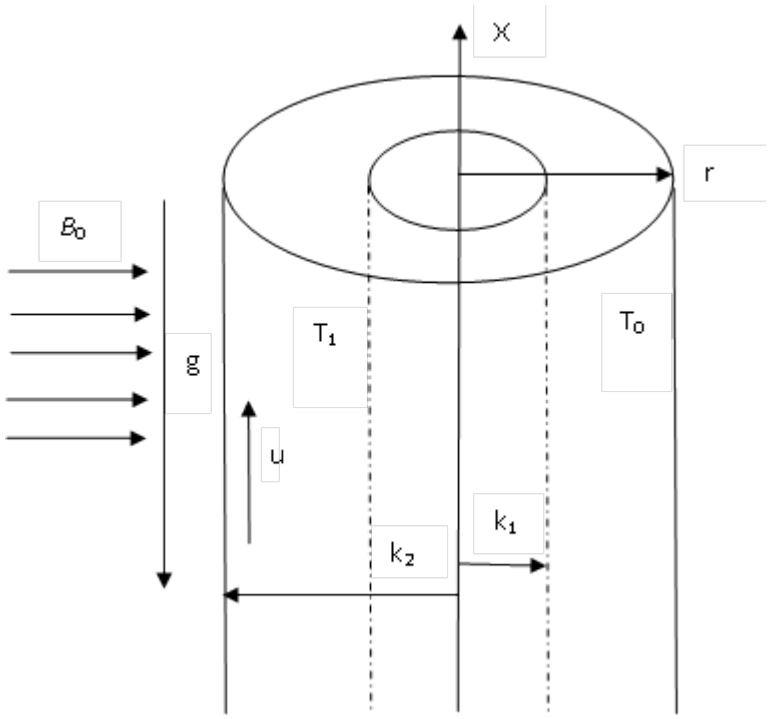


Figure 5.1.1: Flow configuration and coordinate system.

$$\frac{1}{[\eta+(1-\eta)R]}\frac{d}{dR}\left[[\eta+(1-\eta)R]\frac{d\theta}{dR}\right]=0. \tag{5.1.3}$$

The boundary conditions which describe velocity slip and temperature jump conditions at the fluid – wall interface, are (Weng and Chen, 2009)

$$\begin{cases} U(0)=\beta_\nu Kn\frac{dU}{dR}|_{R=0}, \quad \theta(0)=1+\beta_\nu KnF\frac{d\theta}{dR}|_{R=0}, \\ U(1)=-\beta_\nu Kn\frac{dU}{dR}|_{R=1}, \quad \theta(1)=-\beta_\nu KnF\frac{d\theta}{dR}|_{R=1} \end{cases} \tag{5.1.4}$$

By using the transformation $Z=\eta+(1-\eta)R$, the equations (5.1.2) to (5.1.4) can be transformed and written as:

$$\frac{1}{Z}\frac{d}{dZ}[Z\frac{dU}{dZ}]-\frac{M^2U}{(1-\eta)^2Z^2}+\frac{\theta}{(1-\eta)^2}=0, \tag{5.1.5}$$

$$\frac{1}{Z}\frac{d}{dZ}[Z\frac{d\theta}{dZ}]=0, \tag{5.1.6}$$

subject to the boundary conditions

$$\begin{cases} U(\eta)=\beta_\nu Kn(1-\eta)\frac{dU}{dZ}|_{Z=\eta}, \quad U(1)=-\beta_\nu Kn(1-\eta)\frac{dU}{dZ}|_{Z=1}, \\ \theta(\eta)=1+\beta_\nu KnF(1-\eta)\frac{d\theta}{dZ}|_{Z=\eta}, \quad \theta(1)=-\beta_\nu KnF(1-\eta)\frac{d\theta}{dZ}|_{Z=1}. \end{cases} \tag{5.1.7}$$

Integrating equation (5.1.6) and applying the boundary conditions (5.1.7) gives;

$$\theta(Z) = A_0 + A_1 In(Z), \tag{5.1.8}$$

where

$$A_0 = -\beta_\mu KnF(1-\eta)A_1$$

and

$$A_1 = \frac{1}{In(\eta) - \beta_\mu KnF(1-\eta)(1+\frac{1}{\eta})}$$

. The expression for the temperature in equation (5.1.8) is exactly the same as those given by Weng and Chen (2009). Substituting eq.(5.1.8) into the momentum eq.(5.1.5) and solving it using the boundary condition (5.1.7) gives

$$U(Z) = C_1(Z)^{\frac{M}{1-\eta}} + C_2(Z)^{\frac{M}{1-\eta}} - \frac{Z^2(A_0 + A_1 In(Z))}{4(1-\eta)^2 - M^2} + \frac{4A_1(1-\eta)^2 Z^2}{(4(1-\eta)^2 - M^2)^2}. \tag{5.1.9}$$

Using the expression for velocity field, the expression for volume flow rate, and skin – frictions are obtained. The dimensionless volume flow rate is:

$$Q = \frac{q}{2\pi w^2 u_c} = \frac{1}{(1-\eta)^2}\int_\eta^1 ZU(Z)dZ. \tag{5.1.10}$$

Substituting eq.(5.1.9) into eq.(5.1.10), one obtain

$$Q = \frac{1}{(1-\eta)^2}\left[\frac{C_1(1-\eta)^{(\frac{M}{1-\eta}+2)}}{(\frac{M}{1-\eta}+2)} + \frac{C_2(1-\eta)^{(2-\frac{M}{1-\eta})}}{(2-\frac{M}{1-\eta})} + \frac{A_1(1-\eta)^2(1-\eta^4)}{(4(1-\eta)^2 - M^2)^2}\right] - \frac{1}{16(1-\eta)^2}\left(\frac{(4A_0 - A_1)(1-\eta^4) - 4\eta^4 ln(\eta)A_1}{4(1-\eta)^2 - M^2}\right). \tag{5.1.11}$$

The skin - frictions (τ) at the cylinder walls are obtained by differentiating the velocity as follows;

$$\tau_0 = \frac{dU}{dR}|_{R=0} = (1-\eta)\frac{dU}{dZ}|_{Z=0}, \tag{5.1.12}$$

$$\tau_0 = \left[C_1(\eta)^{(\frac{M}{1-\eta}-1)} - C_2(\eta)^{(\frac{M}{1-\eta}-1)}\right]M + \frac{4A_1(1-\eta)^3 2\eta}{[4(1-\eta)^2 - M^2]^2} - \frac{(1-\eta)\left[2\eta A_0 + A_1\{2\eta ln(\eta) + \eta\}\right]}{4(1-\eta)^2 - M^2}, \tag{5.1.13}$$

$$\tau_1 = \frac{dU}{dR}|_{R=1} = (1-\eta)\frac{dU}{dZ}|_{Z=1}, \tag{5.1.14}$$

$$\tau_1 = [C_1 - C_2]\, M + \frac{8A_1(1-\eta)^3}{\left[4(1-\eta)^2 - M^2\right]^2} - \frac{(1-\eta)\,[2A_0 + A_1]}{4(1-\eta)^2 - M^2}. \tag{5.1.15}$$

5.1.2 Results and Discussion

In this study, the interactive effects of the radius ratio (η), Hartmann number (M), rarefaction parameter $\beta_\nu Kn$, and fluid-wall interaction parameter (F) on heat and fluid flow are investigated. To examine the influence of these controlling parameters, the variations of velocity, volume flow rate and skin-friction are presented in Figures 5.1.2 – 5.1.10. The present parametric study has been performed in the continuum and slip flow regimes ($Kn = 0.1$) . Also, for air and various surfaces, the values of β_ν and β_t range from near 1 to 1.667 and from near 1.64 to more than 10, respectively. So, this study has been performed over the reasonable ranges of $0 \leq \beta_\nu Kn \leq 0.1$ and $0 \leq F \leq 10$. The selected reference values of $\beta_\nu Kn$, and F for the present analysis are 0.05 and 1.64 respectively as given in Weng and Chen (2009). In addition, the values of Hartmann number (M) are taken over the range of $1 \leq M \leq 2$ with a reference value of $M = 2$ while the selected reference values of η are $0.2, 0.5, 0.8$. The effects of the rarefaction parameter ($\beta_\nu Kn$), and fluid-wall interaction parameter (F) on the temperature profile and rate of heat transfer which is expressed as the Nusselt number are exactly the same as those given by Weng and Chen (2009). Figure 5.1.2 shows the velocity distribution for different values of rarefaction parameter ($\beta_\nu Kn$) with fixed values of $M = 2.0$ and $F = 1.64$. It is observed that, as rarefaction parameter increases, the velocity slip at the cylindrical surfaces increase which reduces the retarding effect of the boundaries. This yields an observable increase in the fluid velocity near both boundaries. This is due to the fact that, as $\beta_\nu Kn$ increases, the temperature jump increases and this reduces the amount of heat transfer from

the cylindrical surfaces to the fluid (Weng and Chen, 2009). This reduction in heat transfer reduces the buoyancy effect, which drives the flow and hence reduces the fluid velocity far from the outer surface of inner cylinder (near the inner surface of outer cylinder). The reduction in velocity due to the reduction in heat transfer is offset by the increase in velocity due to the reduction in the frictional retarding forces near the cylindrical surfaces. Furthermore, the slip induced by rarefaction effect increases as radius ratio (η) increases. Figure 5.1.3 shows the velocity distribution for different values of fluid-wall interaction parameter (F) with fixed values of $\beta_\nu Kn = 0.05$ and $M = 2.0$. It is evident from Figure 5.1.3 that, the increase in fluid-wall interaction parameter (F) leads to the decrease in fluid velocity and increase in velocity slip near the outer surface of the inner cylinder while reverse trend is observed at inner surface of the outer cylinder. Also, it is clear from Figure 5.1.3 that there exist points of inflection inside the micro-channel where velocity field is independent of fluid wall interaction parameter and these strongly depend on radius ratio parameter (η). In addition, the slip induced by fluid-wall interaction parameter (F) increases as radius ratio parameter (η) decreases. Although, the impact of fluid-wall interaction parameter (F) on the slip is more visible for smaller radius ratio parameter (η). Figure 5.1.4 depicts the velocity distribution for different values of Hartmann number (M) with fixed values of $\beta_\nu Kn = 0.05$ and $F = 1.64$. It is observed that as Hartmann number (M) increases, there is decrease in the fluid velocity. It is also observed that there is higher slip at outer surface of inner cylinder compare to inner surface of outer cylinder. In addition, for fixed Hartmann number (M) , as radius ratio parameter (η) increases there is an increase in the velocity slip. Further, it is seen that particular case of equation (12) corresponding $M \to 0$ reduces to the one in Weng and Chen (2009).

Figure 5.1.5 shows the variation of volume flow rate (Q) against the rarefaction parameter ($\beta_\nu Kn$) for different values of fluid-wall interaction parameter (F).

It is interesting to note that the volume flow rate (Q) is a decreasing function of fluid-wall interaction parameter . Furthermore, it is found that increase in radius ratio (η) and rarefaction parameter ($\beta_\nu Kn$) leads to increase in the volume flow rate. Figure 5.1.6 reveals the volume flow rate (Q) plotted against the rarefaction parameter $\beta_\nu Kn$ for different values of Hartmann number (M). It is observed from Figure 5.1.6 that, the volume flow rate (Q) decreases as Hartmann number (M) and rarefaction parameter $\beta_\nu Kn$ increases. Figure 5.1.7 depicts the variation of skin-friction at outer surface of inner cylinder ($R = 0$). It is clear from Figure 5.1.7 that, the skin - friction decreases with the increase of fluid - wall interaction parameter (F) and rarefaction parameter ($\beta_\nu Kn$).

Figure 5.1.8 shows variation of skin-friction at inner surface of outer cylinder ($R = 0$). It is obvious from Figure 5.1.8 that increase in radius ratio η, rarefaction parameter $\beta_\nu Kn$ and fluid – wall interaction parameter (F) leads to the increase in the skin-friction at inner surface of outer cylinder. It is interesting to note that the impact of fluid – wall interaction parameter (F) is significant for higher value of radius ratio (η). Figure 5.1.9 and 5.1.10 presents variation of skin-friction at outer surface of inner cylinder and inner surface of outer cylinder ($R = 1$), respectively for different values of Hartmann number (M). It is observed from these Figures that, skin friction decreases as Hartmann number (M) increases.

Table 5.1.1 gives a comparison of the numerical values of the velocity obtained in the present work when $M \to 0$ with those obtained by Weng and Chen (2009) for $F = 1.64$. As can be seen from the table, the solutions of the present work perfectly agree with those of Weng and Chen (2009)

Table 5.1.1: Comparison of the values of velocity obtained in the present work with those obtained by Weng and Chen (2009)

η	R	Velocity ($F = 1.64$)	
		(Weng and Chen, 2009)	Present work ($M \to 0$)
0.2	0.2	0.0527	0.0527
	0.4	0.0538	0.0538
	0.6	0.0431	0.0431
	0.8	0.0270	0.0270
0.5	0.2	0.0651	0.0651
	0.4	0.0730	0.0730
	0.6	0.0624	0.0624
	0.8	0.0409	0.0409
0.8	0.2	0.0713	0.0713
	0.4	0.0838	0.0838
	0.6	0.0746	0.0746
	0.8	0.0505	0.0505

5.1.3 Concluding Remark

Exact solution is obtained for the steady fully developed MHD natural convection flow of a viscous, incompressible, electrically conducting fluid in vertical annular micro-channel in presence of radial magnetic field. The influence of the radius ratio (η), Hartmann number (M), rarefaction parameter ($\beta_\nu Kn$), and fluid – wall interaction (F) on the fluid velocity, volume flow rate and skin-friction is analysed. It is worthy to note that the results for $M \to 0$ perfectly agree with the results of Weng and Chen (2009) The main conclusions are as follows:

1. It is found that as the Hartmann number (M) increases, there is a decrease in the fluid velocity.

2. The slip induced by fluid – wall interaction parameter (F) increases as the radius ratio (η) decreases.

3. The increase in radius ratio (η) and rarefaction parameter ($\beta_\nu Kn$) leads to an increase in the volume flow rate.

4. The increase in the Hartmann number (M) leads to a decrease in the volume flow rate.

5. Finally, the skin friction decreases as the Hartmann number (M) increases.

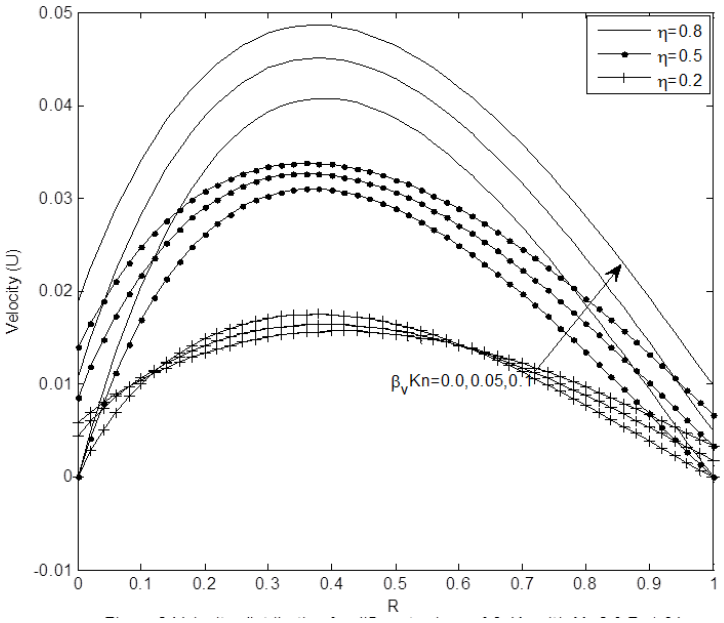


Figure 5.1.2: Velocity distribution for different values of $\beta_\nu Kn$ with $F = 1.64$ and $M = 2.0$

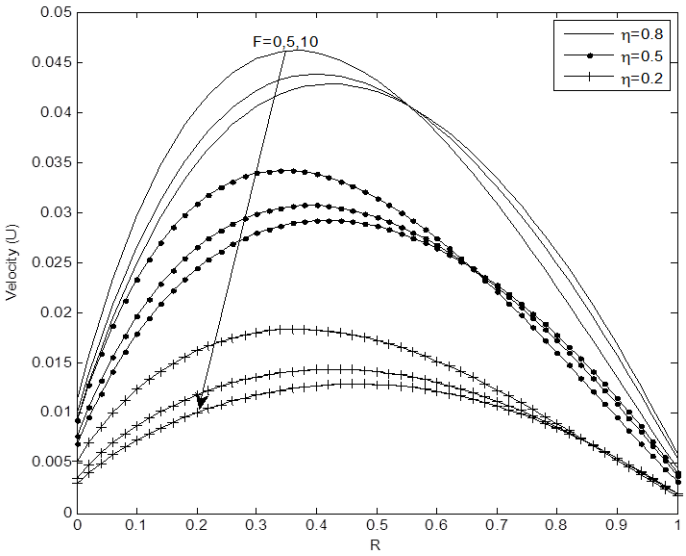


Figure 5.1.3: Velocity distribution for different values of F with $\beta_\nu Kn = 0.05$ and $M = 2.0$

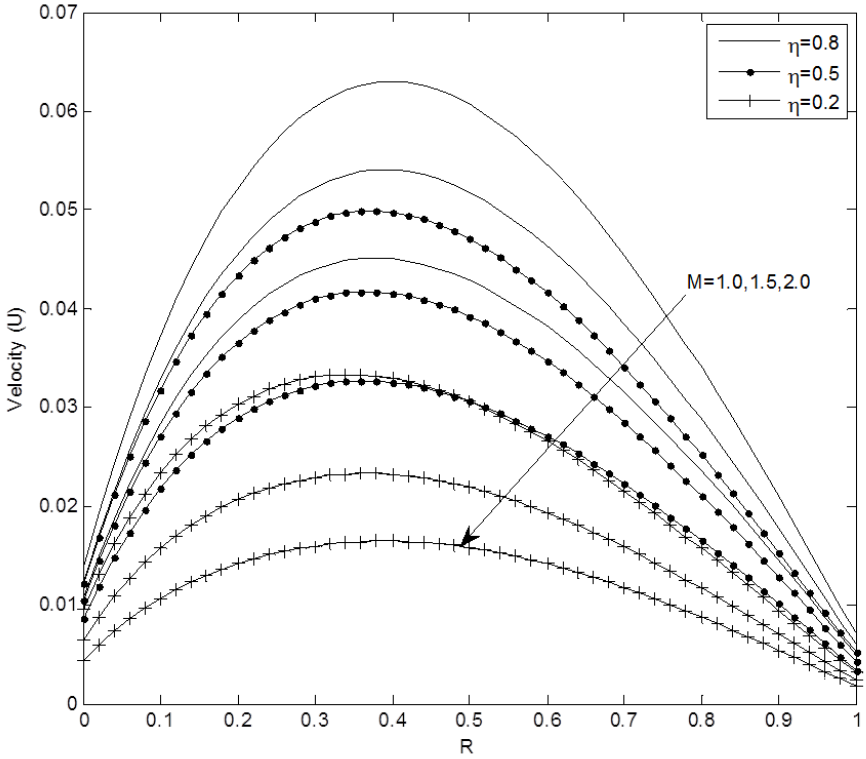


Figure 5.1.4: Velocity distribution for different values of M with $\beta_\nu Kn = 0.05$ and $F = 1.64$

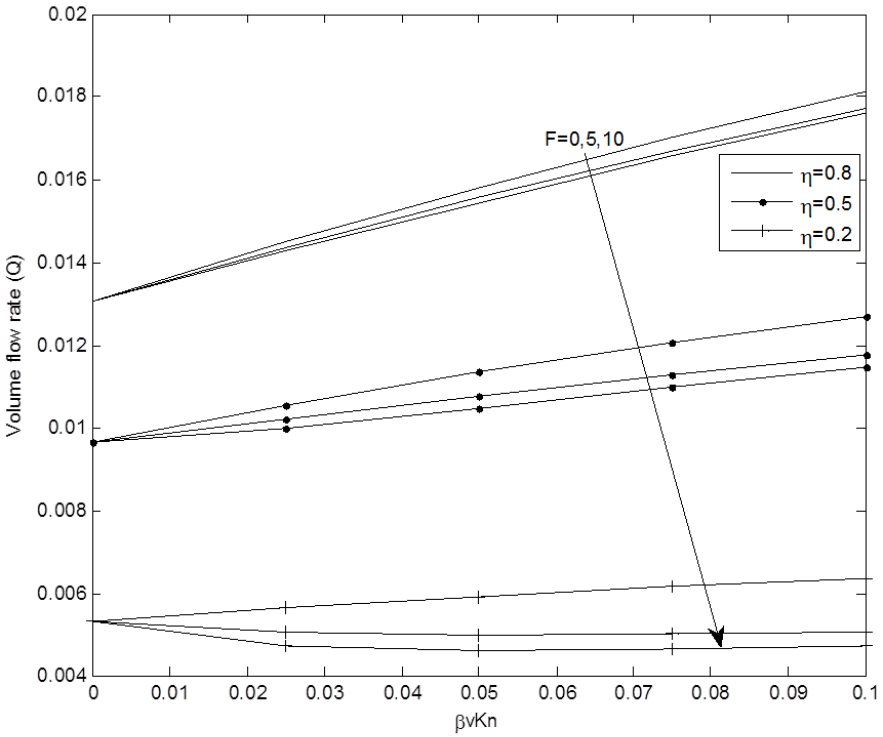


Figure 5.1.5: Volume flow rate versus $\beta_\nu Kn$ for different values of F with $M = 2.0$

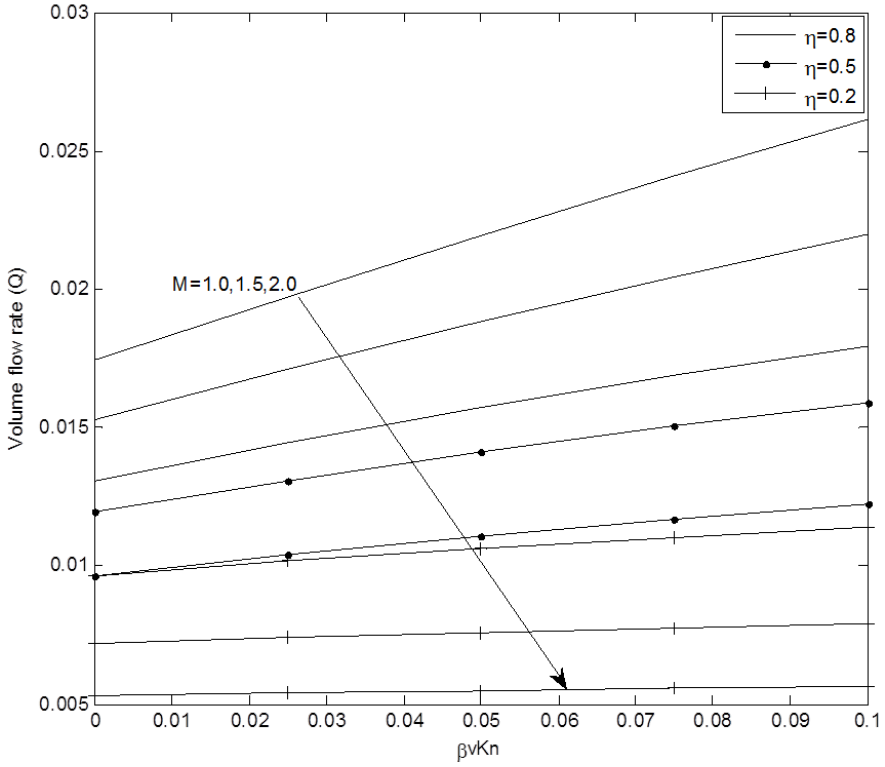


Figure 5.1.6: Volume flow rate versus $\beta_\nu Kn$ for different values of M with $F = 1.64$

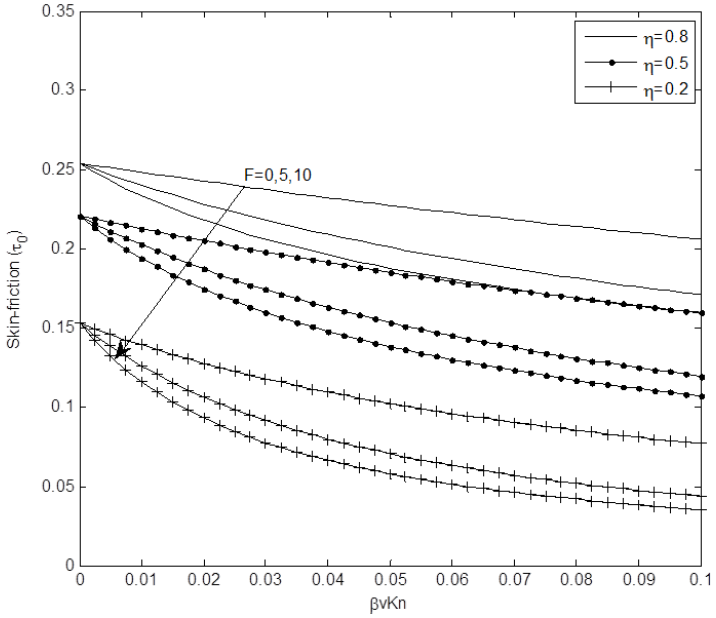


Figure 5.1.7: Variation of skin friction for different values of F at $R = 0$

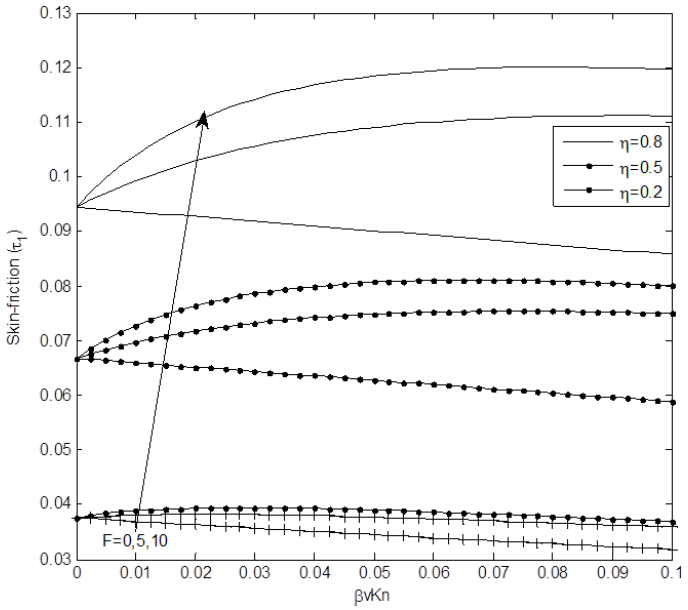


Figure 5.1.8: Variation of skin friction for different values of F at $R = 1$

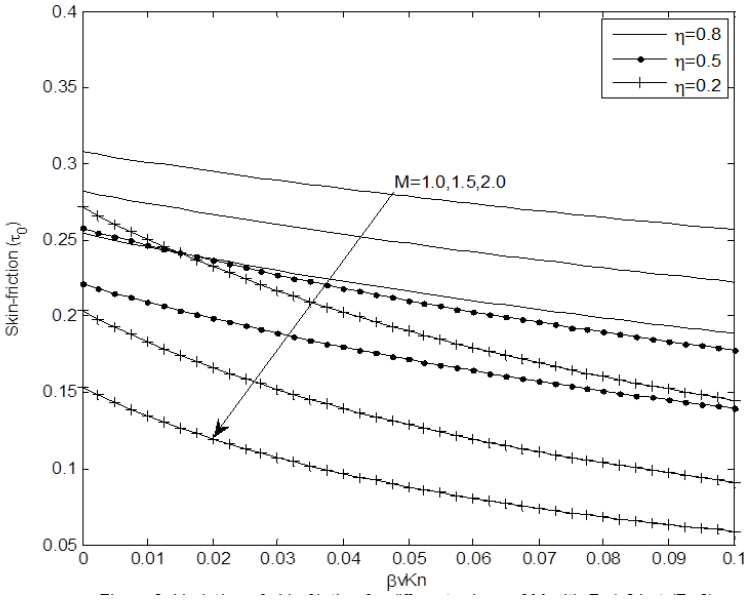


Figure 5.1.9: Variation of skin friction for different values of M at $R = 0$

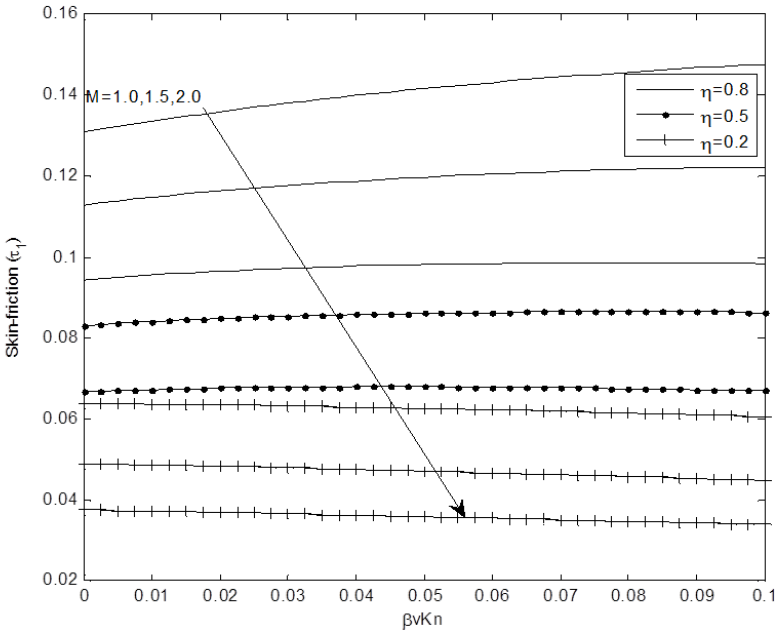


Figure 5.1.10: Variation of skin friction for different values of M at $R = 1$

5.2 FULLY DEVELOPED MHD NATURAL CONVECTION FLOW IN A VERTICAL ANNULAR MICRO-CHANNEL: AN EXACT SOLUTION

An exact solution of steady fully developed natural convection flow of viscous, incompressible, electrically conducting fluid in a vertical annular micro-channel with the effect of transverse magnetic field in presence of velocity slip and temperature jump at the annular micro – channel surfaces is presented in this section which is a further extension of Weng and Chen (2009). Exact solution is expressed in terms of modified Bessel function of first kind and second kind. The solution obtained is graphically represented and the effects of radius ratio (η), Hartmann number (M), rarefaction parameter ($\beta_\nu Kn$), and fluid-wall interaction parameter (F) on the flow is investigated. During the course of numerical computations, it is found that increase in Hartmann number leads to decrease in the fluid velocity, volume flow rate and skin friction. Furthermore, it is found that increase in curvature radius ratio leads to increase in the volume flow rate.

5.2.1 Mathematical Analysis

The flow considered is a fully developed steady natural convection flow of viscous, incompressible, electrically conducting fluid in vertical annular micro-channel under the effect of transverse magnetic field as presented in 5.2.1. The X - axis is parallel to the gravitational acceleration g but in the opposite direction while the r - axis is in the radial direction. The radius of the inner and outer cylinder walls are k_1 and k_2 respectively. A magnetic field of uniform strength B_0 is assumed to be applied in the direction perpendicular to the

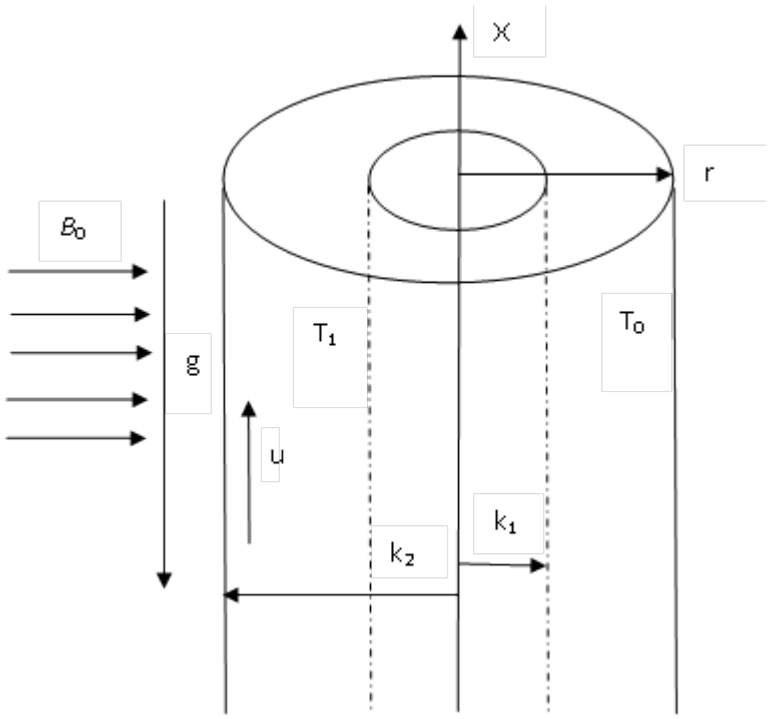


Figure 5.2.1: Flow configuration and coordinate system.

direction of flow. It is assumed that the magnetic Reynolds number is very small, which corresponds to negligibly induced magnetic field compared to the externally applied one ((Sarris et al., 2006); (Jha and Apere, 2013); (Cramer and Pai, 1973); (Pai, 1962)). The outer surface of the inner cylinder is heated to a temperature (T_1) greater than that of the surrounding fluid having temperature (T_0) and the inner surface of the outer cylinder is maintained at temperature (T_0). Due to this temperature difference, natural convection occurs in the vertical annular micro-channel. Since the flow is fully developed and cylinders are of infinite length, the flow depends only on radial coordinate (r). In the recent past, Weng and Chen (2009) analysed the drag reduction and heat transfer enhancement of viscous incompressible fluid in vertical micro-annulus. Following Weng and Chen (2009) and considering the viscous incompressible electrically conducting fluid in the presence of a transverse magnetic field to the flow direction, the mathematical model for the present physical situation under Boussinesq's approximation in dimensional form is

$$\frac{\nu}{r}\frac{d}{dr}(r\frac{du}{dr}) + g\beta_0(T - T_0) - \frac{\sigma B_0^2 u}{\rho} = 0, \tag{5.2.1}$$

$$\frac{1}{r}\frac{d}{dr}(r\frac{dT}{dr}) = 0, \tag{5.2.2}$$

The boundary conditions for the velocity and temperature field in the presence of velocity slip and temperature jump are ((Weng and Chen, 2009); (Avci and Aydin, 2009)):

$$u(r = k_1) = \frac{2-\sigma_\nu}{\sigma_\nu}\lambda\frac{du}{dr}|_{r=k_1}, \tag{5.2.3}$$

$$u(r = k_2) = -\frac{2-\sigma_\nu}{\sigma_\nu}\lambda\frac{du}{dr}|_{r=k_2}, \tag{5.2.4}$$

$$T(r = k_1) = T_1 + \frac{2-\sigma_t}{\sigma_\nu}\frac{2y}{\gamma+1}\frac{\lambda}{Pr}\frac{dT}{dr}|_{r=k_1}, \tag{5.2.5}$$

$$T(r = k_2) = T_0 - \frac{2-\sigma_t}{\sigma_\nu}\frac{2y}{\gamma+1}\frac{\lambda}{Pr}\frac{dT}{dr}|_{r=k_2}, \tag{5.2.6}$$

By introducing the following non-dimensional quantities

$$R = \frac{r-k_1}{w},\ w = k_2 - k_1, U = \frac{u}{u_c},\ \theta = \frac{T-T_0}{T_1-T_0},\ u_c = \frac{\rho_0 g\beta_0(T_1-T_0)w^2}{\mu_0},\ Pr = \frac{C_{p0}\mu_0}{k},$$
$$Pr = \frac{C_p\mu}{k},\ Kn = \frac{\lambda}{w},\ F = \frac{\beta_t}{\beta_\nu},\ \beta_\nu = \frac{2-\sigma_\nu}{\sigma_\nu},\ \beta_t = \frac{2-\sigma_t}{\sigma_t}\frac{2\gamma}{\gamma+1}\frac{1}{Pr},\ \eta = \frac{k_1}{k_2},$$
$$\lambda = \frac{\sqrt{\frac{\pi\widehat{R}T_0}{2\mu}}}{\rho},\ M^2 = \frac{\sigma\mu_e^2 H_0^2 w^2}{\rho_0\nu}, \tag{5.2.7}$$

Using Eq. (5.2.7) in Eqs. (5.2.1) – (5.2.6), the mathematical model representing the present physical situation in dimensionless form in the presence of velocity slip and temperature jump on annular micro-channel surfaces is:

$$\frac{1}{[\eta+(1-\eta)R]}\frac{d}{dR}\left[[\eta+(1-\eta)R]\frac{dU}{dR}\right] - M^2U + \theta = 0, \tag{5.2.8}$$

$$\frac{1}{[\eta+(1-\eta)R]}\frac{d}{dR}\left[[\eta+(1-\eta)R]\frac{d\theta}{dR}\right] = 0, \tag{5.2.9}$$

The boundary conditions which describe velocity slip and temperature jump conditions at the fluid – wall interface in dimensionless form are ((Weng and Chen, 2009))

$$U(0) = \beta_\nu KnF\frac{dU}{dR}|_{R=0},\quad U(1) = -\beta_\nu KnF\frac{dU}{dR}|_{R=1}, \tag{5.2.10}$$

$$\theta(0) = 1 + \beta_\nu KnF\frac{d\theta}{dR}|_{R=0},\quad \theta(1) = -\beta_\nu KnF\frac{d\theta}{dR}|_{R=1}. \tag{5.2.11}$$

The physical quantities used in the above equations are defined in the nomenclature. By using the transformation $Z = \eta + (1-\eta)R$, the eqns. (5.2.8) to (5.2.11) can be written as:

$$\frac{1}{Z}\frac{d}{dZ}[Z\frac{dU}{dZ}] - \frac{M^2U}{(1-\eta)^2} + \frac{\theta}{(1-\eta)^2} = 0, \tag{5.2.12}$$

$$\frac{1}{Z}\frac{d}{dZ}[Z\frac{d\theta}{dZ}] = 0, \tag{5.2.13}$$

subject to the boundary conditions

$$U(\eta) = \beta_\nu KnF(1-\eta)\frac{dU}{dZ}|_{Z=0}, \quad U(1) = -\beta_\nu KnF(1-\eta)\frac{dU}{dZ}|_{Z=1}, \tag{5.2.14}$$

$$\theta(\eta) = 1 + \beta_\nu KnF(1-\eta)\frac{d\theta}{dZ}|_{Z=0}, \quad \theta(1) = -\beta_\nu KnF(1-\eta)\frac{d\theta}{dZ}|_{Z=1}. \tag{5.2.15}$$

Integrating eq.(5.2.13) and applying the boundary conditions (5.2.15) gives

$$\theta(Z) = A_0 + A_1 In(Z) \tag{5.2.16}$$

The general solution of Eq. (5.2.12) after substitution of equation (5.2.16) in Eq. (5.2.12) is obtained by rearranging the homogeneous part to take the general form of the Bessel equation (Arpaci, 1966). The particular solution of Eq. (5.2.12) is sought by assuming an appropriate form (according to the forcing function i.e., the right hand side of Eq. (5.2.12)). The exact solution of Eq. (5.2.12) under the appropriate velocity slip condition defined in Eq.(5.2.14) is:

$$U(Z) = C_1 I_0(ZE) + C_2 K_0(ZE) + \frac{\theta(Z)}{M^2}. \tag{5.2.17}$$

Two important parameters for convective micro-flow are the volume flow rate, and skin-friction. The dimensionless volume flow rate is:

$$Q = \frac{q}{2\pi w^2 u_c} = \frac{1}{(1-\eta)^2}\int_\eta^1 ZU(Z)dZ. \tag{5.2.18}$$

Substituting equation (5.2.17) into Eq. (5.2.18), one obtains

$$Q = \frac{1}{(1-\eta)^2}[\frac{C_1 I_0(E) + C_2 K_0(E)}{E} + \frac{\eta(C_1 I_0(E) + C_2 K_0(E))}{E} + (1-\eta)^2\{\frac{A_0}{2M^2} - \frac{A_1}{4M^2}\} - \frac{A_1}{2M^2}\eta^2 In(\eta)]. \quad (5.2.19)$$

The skin-frictions (τ) at the cylinder walls are obtained by differentiating the velocity as follows:

$$\tau_0 = \frac{dU}{dR}|_{R=0} = (1-\eta)\frac{dU}{dZ}|_{Z=0}, \quad (5.2.20)$$

$$\tau_0 = [\{C_1 I_1(\eta E) + C_2 K_1(\eta E)\}E + \frac{A_1}{M^2\eta}](1-\eta), \quad (5.2.21)$$

$$\tau_1 = \frac{dU}{dR}|_{R=1} = (1-\eta)\frac{dU}{dZ}|_{Z=1}, \quad (5.2.22)$$

$$\tau_1 = [\{C_1 I_1(E) + C_2 K_1(E)\}E + \frac{A_1}{M^2\eta}](1-\eta). \quad (5.2.23)$$

All constants are defined in appendix E

5.2.2 Results and Discussion

Numerical values of the velocity, volume flow rate, and skin friction are computed and the graphs are presented in Figs. 5.2.2 - 5.2.10 so that the influences of radius ratio (η), Hartmann number (M), rarefaction parameter ($\beta_\nu Kn$), and fluid – wall interaction parameter (F) can be easily seen at a glance. The present parametric study has been performed in the continuum and slip flow regimes $Kn \leq 0.1$. Also, for air and various surfaces, the values of β_ν and β_{nu} range from near 1 to 1.667 and from near 1.64 to more than 10, respectively. So, this study has been performed over the reasonable ranges of $0 \leq \beta_\nu Kn \leq 0.1$ and $0 \leq F \leq 10$. The selected reference values of $\beta_\nu Kn$, and F for the present analysis are 0.05 and 1.64 respectively as given in Weng and Chen (2009). The present work extends the work of Weng and Chen (2009) by considering the influence of externally applied transverse magnetic field on a steady fully developed natural convection flow of viscous, incompressible,

electrically conducting fluid in a vertical annular micro-channel. The values of Hartmann number (M) are taken over the range of $1 \leq M \leq 2$ with a reference value of $M = 2$. The expression for the temperature in Eq.(5.2.10), the effect of the rarefaction parameter $\beta_\nu Kn$, and fluid – wall interaction parameter (F) on the temperature profile and rate of heat transfer which is expressed as the Nusselt number are exactly the same as those given by Weng and Chen (2009).

Fig.5.2.2 shows the velocity distribution for different values of rarefaction parameter ($\beta_\nu Kn$) with fixed values of $M = 2.0$ and $F = 1.64$. It is observed that, as rarefaction parameter $\beta_\nu Kn$ increases, the velocity slip at the cylindrical surfaces increases which reduces the retarding effect of boundaries. This yields an observable increase in the fluid velocity near both boundaries. This is due to the fact that, as $\beta_\nu Kn$ increases, the temperature jump increases and this reduces the amount of heat transfer from the cylindrical surfaces to the fluid (Weng and Chen, 2009). This reduction in heat transfer reduces the buoyancy effect, which derives the flow and hence reduces the fluid velocity far from the outer surface of inner cylinder (near the inner surface of outer cylinder). The reduction in velocity due to the reduction in heat transfer is offset by the increase in velocity due to the reduction in the frictional retarding forces near the cylindrical surfaces. Furthermore, the slip induced by rarefaction effect increases as radius ratio (η) increases.

Fig. 5.2.3 shows the velocity distribution for different values of fluid–wall interaction parameter (F) with fixed values of β_ν, $Kn = 0.05$ and $M = 2.0$. It is evident from Fig.5.2.3 that, the increase in fluid – wall interaction parameter (F) leads to the decrease in fluid velocity and increase in slip velocity near the outer surface of the inner cylinder while the reverse trend is observed at the inner surface of the outer cylinder. In addition, the slip induced by fluid – wall interaction parameter (F) increases as the radius ratio (η) decreases while, the impact of fluid – wall interaction parameter (F) on the slip is more visible for

smaller radius ratio (η). Fig.5.2.4 depicts the velocity distribution for different values of the Hartmann number (M) with fixed values of $\beta_\nu Kn = 0.05$ and $F = 1.64$. It is observed that as the Hartmann number (M) increases, there is a decrease in the fluid velocity and an increase in slip velocity. It is also observed that there is higher slip at the inner surface of outer cylinder compared to the outer surface of the inner cylinder. In addition, for the fixed Hartmann number (M), as radius ratio (η) increases there is an increase in the slip. Further, it is seen that the particular case of Eq. (5.2.17) corresponding $M \longrightarrow 0$ reduces to the one in Weng and Chen (2009). Fig. 5.2.5 shows the variation of volume flow rate (Q) against the rarefaction parameter ($\beta_\nu Kn$) for different values of fluid – wall interaction (F). It is interesting to note that the volume flow rate (Q) is a decreasing function of fluid – wall interaction (F). Furthermore, it is found that an increase in radius ratio (η) and rarefaction parameter ($\beta_\nu Kn$) leads to an increase in the volume flow rate. Fig. 5.2.6 reveals the volume flow rate (Q) plotted against the rarefaction parameter ($\beta_\nu Kn$) for different values of Hartmann number (M). It is observed from Fig. 5.2.6 that, the volume flow rate (Q) decreases as Hartmann number (M) increases. Also, it is interesting to note that an increase in the rarefaction parameter ($\beta_\nu Kn$) leads to an increase in the volume flow rate. Fig. 5.2.7 depicts the variation of skin-friction at the outer surface of the inner cylinder ($R = 0$). It is clear from Fig. 5.2.7 that, the skin - friction decreases with the increase of fluid – wall interaction parameter (F) and rarefaction parameter ($\beta_\nu Kn$). It is interesting to note that the impact of these parameters is significant for a small value of radius ratio (η).

Fig.5.2.8 shows a variation of skin-friction at the inner surface of the outer cylinder (R= 1). It is obvious from Fig. 5.2.8 that increases in radius ratio (η) and rarefaction parameter ($\beta_\nu Kn$) lead to the increase in the skin-friction at the inner surface of the outer cylinder. Figs.5.2.9 and 5.2.10 presents a variation of skin-friction at the outer surface of the inner cylinder ($R = 0$) and

the inner surface of outer cylinder ($R = 1$), respectively for different values of the Hartmann number (M). It is observed from these figures that, skin friction decreases as the Hartmann number (M) increases.

5.2.3 Concluding Remark

This study considered the fully developed steady natural convection flow of a viscous, incompressible, electrically conducting fluid in vertical annular microchannel under the effect of a transverse magnetic field. The influence of the radius ratio (η), Hartmann number (M), rarefaction parameter ($\beta_\nu Kn$), and fluid - wall interaction (F) on the fluid velocity, volume flow rate and skin-friction is analysed. This study exactly agrees with the finding of Weng and Chen (2009) in the absence of a magnetic field and further concludes as follows;

1. It is found that as the Hartmann number (M) increases, there is a decrease in the fluid velocity and an increase in slip velocity.

2. The slip induced by rarefaction effect and the Hartmann number increases as the radius ratio (η) increases while the slip induced by fluid–wall interaction parameter (F). increases as the radius ratio (η) decreases.

3. The increase in radius ratio (η) and rarefaction parameter ($\beta_\nu Kn$) leads to an increase in the volume flow rate.

4. The increase in the Hartmann number (M) leads to a decrease in the volume flow rate.

5. Finally, the skin friction decreases as the Hartmann number (M) increases.

Constants used in this section are defined in Appendix D;

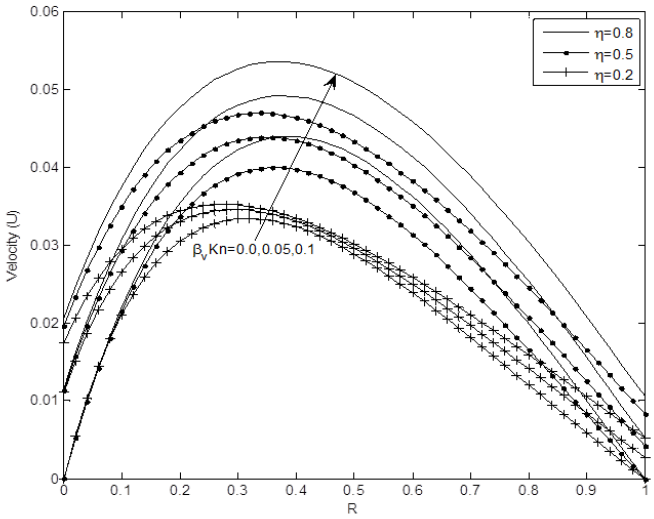


Figure 5.2.2: Velocity distribution for different values of $\beta_\nu Kn$ with $F = 1.64$ and $M = 2.0$

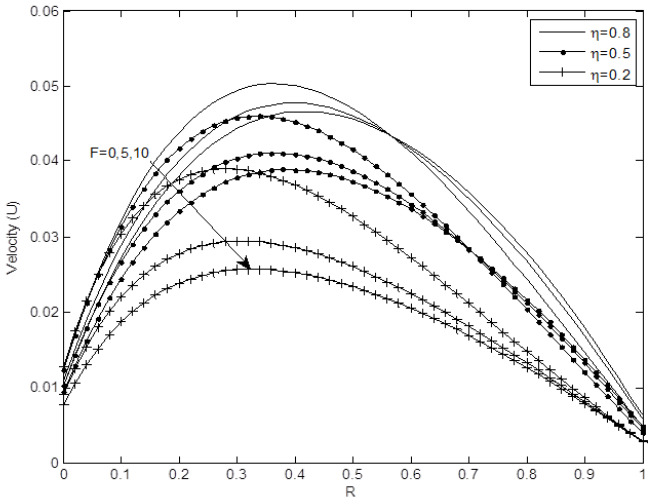


Figure 5.2.3: Velocity distribution for different values of F with $\beta_\nu Kn = 0.05$ and $M = 2.0$

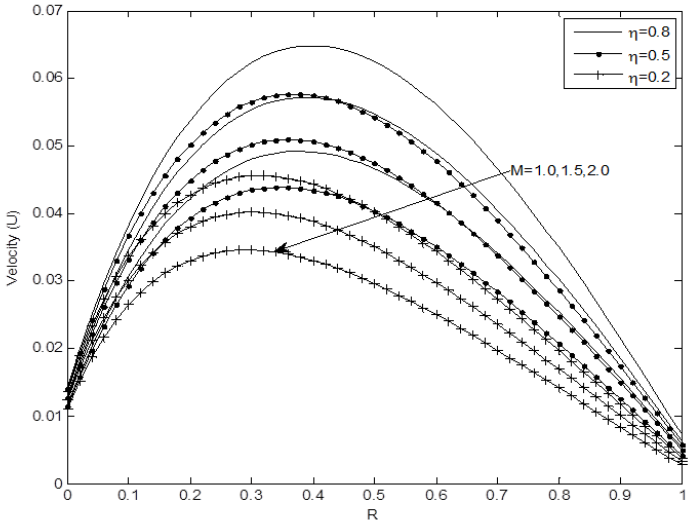


Figure 5.2.4: Velocity distribution for different values of M with $\beta_\nu Kn = 0.05$ and $F = 1.64$

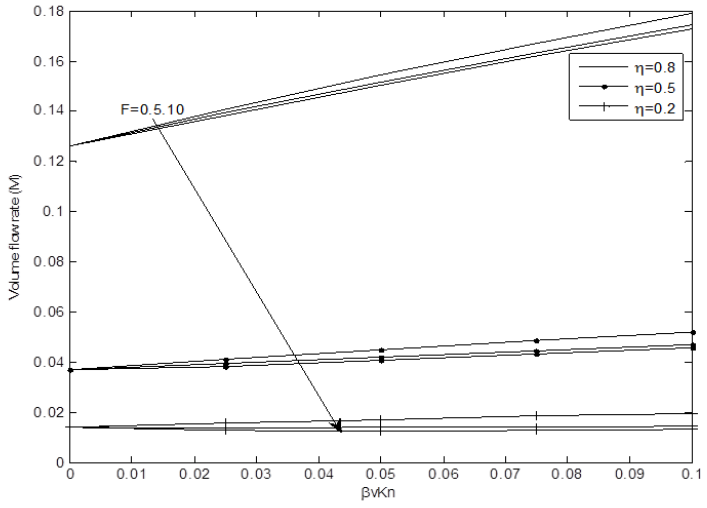


Figure 5.2.5: Volume flow rate versus $\beta_\nu Kn$ for different values of F with $M = 2.0$

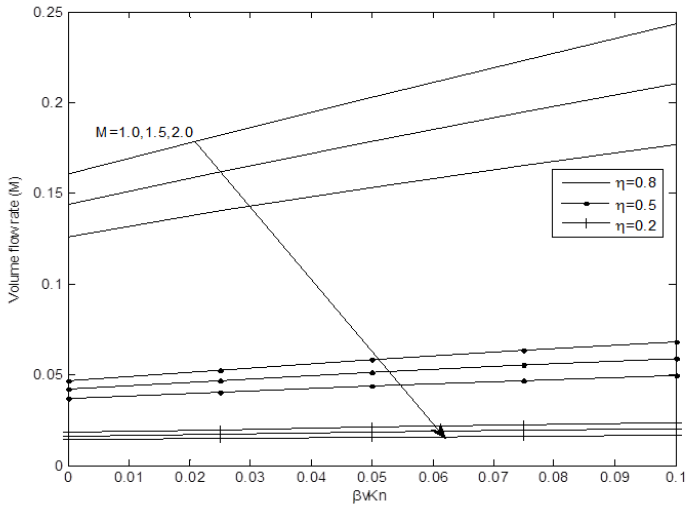


Figure 5.2.6: Volume flow rate versus $\beta_\nu Kn$ for different values of M with $F = 1.64$

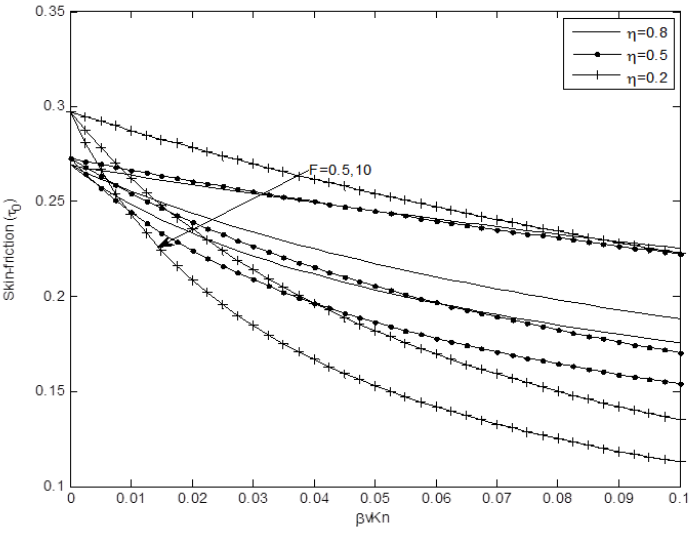


Figure 5.2.7: Variation of skin friction for different values of F at $R = 0$

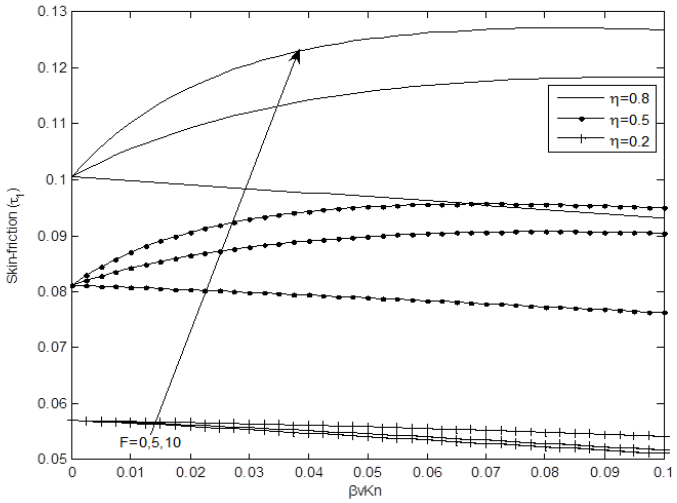


Figure 5.2.8: Variation of skin friction for different values of F at $R = 1$

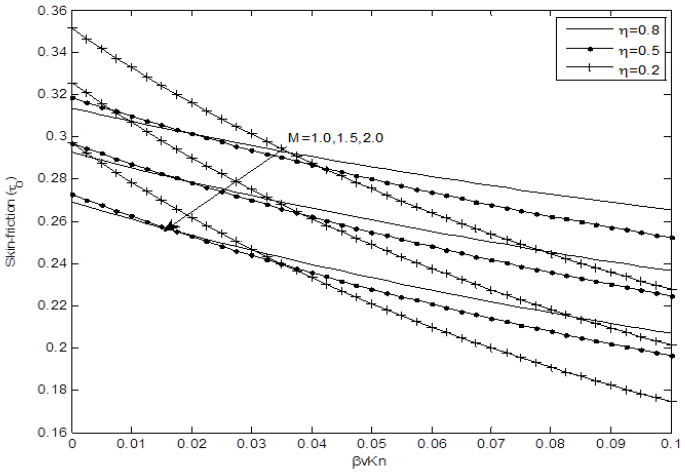


Figure 5.2.9: Variation of skin friction for different values of M at $R = 0$

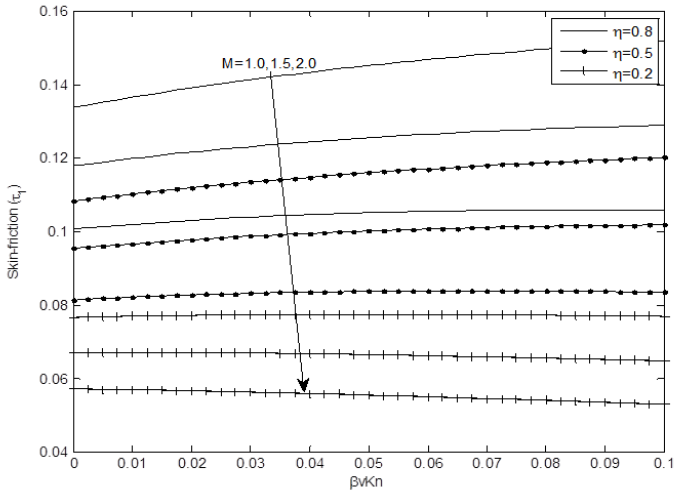


Figure 5.2.10: Variation of skin friction for different values of M at $R = 1$

CHAPTER SIX

MHD FREE CONVECTIVE FLOW IN ANNULAR MICRO-CHANNEL

This chapter presents an analysis of the influence of wall surface curvature on transient MHD free convective flow in vertical micro-concentric annuli in presence of velocity slip and temperature jump at the outer surface of the inner cylinder. Survey of literature suggests that this has not been given attention in the past. A wide range of applications of micro-electro-mechanical systems and nano-technology have given a fillip to research area where a non-continuum behaviour is present. In the present work, we are interested in studying surface-fluid interaction where slip flow regime occurs. In this regard, Knudsen number is a deciding factor, which is a measure of molecular mean free path to characteristic length. When the Knudsen number Kn is very small, no slip is observed between the surface and the fluid and is in tune with the essence of continuum mechanics. Furthermore, when Knudsen number Kn lies in the range 0.001 to 0.1, slip occurs at the surface - fluid interaction and is generally studied under the light of model Maxwell-Smoluchowskn first-order slip boundary conditions. Extensive investigations have been conducted recently in the field of micro geometry flow, but the literature lacks studies that take into account the role of wall surface curvature on transient MHD free convective flow in vertical micro-concentric annuli. However, to cite a few works in this direction, Khadrawi et al. (2005) investigated analytically the transient thermal behaviour of a stagnant gas confined in a horizontal micro-channel under the effect of the dual-phase-lag heat conduction model. Khadrawi (2011) studied the transient hydrodynamic and thermal behaviours of fluid flow in a vertical porous micro-channel under the effect of hyperbolic heat conduction model. The unsteady hydrodynamics and thermal behaviour of fluid flow in an open – ended vertical parallel-plate micro-channel are investigated semi-analytically under the effect of the dual-phase-lag heat conduction model by

Khadrawi and Al-Nimr (2007).

6.1 TRANSIENT MHD FREE CONVECTIVE FLOW IN VERTICAL MICRO-CONCENTRIC ANNULI

This section analyses the transient magnetohydrodynamic free convective flow in vertical micro-concentric annuli in the presence of velocity slip and temperature jump at the outer surface of the inner cylinder and the inner surface of the outer cylinder. The Laplace transform technique has been used to find the solutions for the velocity and temperature fields by solving the governing partial differential equations in Laplace domain. However, the Riemann-sum approximation method is used to invert the Laplace domain to the time domain. The solution derived is validated by assenting comparison with exact solutions derived for the steady state which has been derived separately. An excellent agreement was found for transient and steady state at large value of time. The solution obtained for the velocity has been used to compute the skin friction, while the temperature has been used to compute the Nusselt number. The effect of various flow parameters entering into the problem such as time, Prandtl number, curvature radius ratio, Hartmann number, rarefaction parameter, and fluid–wall interaction parameter are discussed with the aid of line graphs

6.1.1 Mathematical Analysis

This study considers viscous, incompressible, electrically conducting fluid in vertical micro-concentric annuli under the effect of transverse magnetic field.

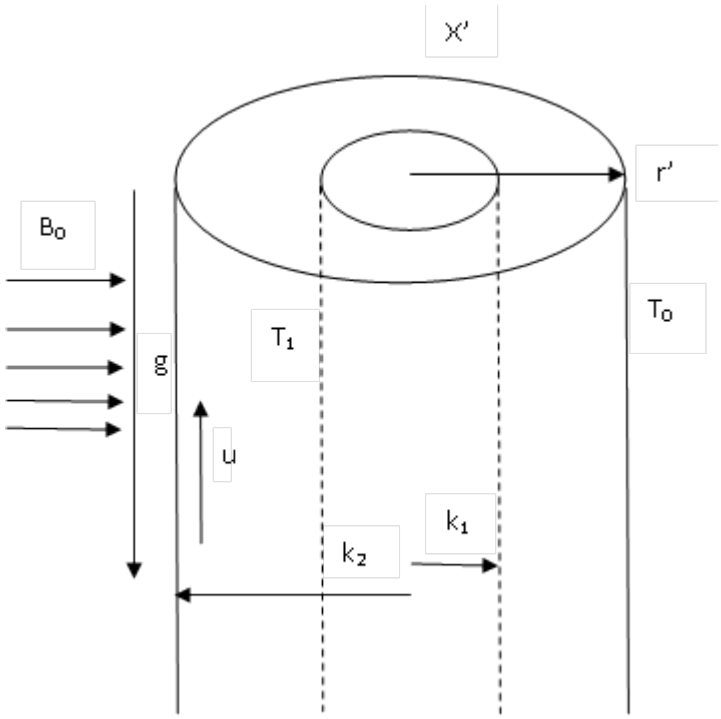


Figure 6.1.1: Flow configuration and coordinate system.

The X'- axis is taking along the axis of the cylinders in the vertical upward direction and r'- axis is in the radial direction. The radius of the inner and outer cylinder are k_1 and k_2 respectively, as shown in Fig 6.1.1. A magnetic field of uniform strength B_0 is assumed to be applied in the direction perpendicular to the direction of flow. It is assumed that the magnetic Reynolds number is very small, which corresponds to negligibly induced magnetic field compared to the externally applied one. At time $t' < 0$ both fluid and cylinders are assumed to be at temperature T_0 . At time $t' \geq 0$ the temperature of the outer surface of inner cylinder at $r = k_1$ is raised to $T_1(T_1 > T_0)$ causing the flow of transient free convection currents. Since the flow is fully developed and cylinders are of infinite length, the flow depends only on radial coordinate (r') and time (t'). Under the usual Boussinesq's approximation, the governing equations in dimensional form are:

$$\frac{\partial u}{\partial t'} = \frac{1}{r}\frac{\partial}{\partial r}(r\frac{\partial u}{\partial r}) - \frac{\sigma B_0^2 u}{\rho} + g\beta(T - T_0), \tag{6.1.1}$$

$$\frac{\partial T}{\partial t'} = \alpha\frac{1}{r}\frac{\partial}{\partial r}(r\frac{\partial T}{\partial r}). \tag{6.1.2}$$

The initial and boundary conditions for the problem are:

$$t \leq 0 : u = 0 \;\; T = T_0 \;\; for \;\; k_1 \leq r \leq k_2,$$

$$t' > 0 : \begin{cases} u = \beta_\nu Kn \frac{\partial u}{\partial r}, \;\; T = T_1 + \beta_\nu KnF \frac{\partial T}{\partial r}; \; r = k_1 \\ u = -\beta_\nu Kn \frac{\partial u}{\partial r}, \;\; T' = T_0 - \beta_\nu KnF \frac{\partial T}{\partial r}; \; r = k_2. \end{cases} \tag{6.1.3}$$

Introducing the following dimensionless quantities in equations (6.1.1) - (6.1.3)

$$t = \frac{t'\nu}{w^2}, \; R = \frac{r - k_1}{w}, \; w = k_2 - k_1, \; U = \frac{u}{u_c}, \; \theta = \frac{T - T_0}{T_1 - T_0}, \; u_c = \frac{\nu u}{g\beta(T_1 - T_0)w^2},$$
$$Pr = \frac{C_p \mu}{k}, \; Kn = \frac{\lambda}{w}, \; F = \frac{\beta_t}{\beta_\nu} \; \beta_\nu = \frac{2 - \sigma_\nu}{\sigma_\nu}, \; \beta_t = \frac{2 - \sigma_t}{\sigma_t} \frac{2\gamma}{\gamma + 1} \frac{1}{Pr}, \; \eta = \frac{k_1}{k_2},$$
$$\lambda = \frac{\sqrt{\frac{\pi \widehat{R} T_0}{2\mu_0}}}{\rho}, \;\; M^2 = \frac{\sigma \mu_e^2 H_0^2 w^2}{\rho_0 \nu}, \tag{6.1.4}$$

we now have

$$\frac{\partial U}{\partial t} = \frac{1}{[\eta + (1 - \eta)R]} \frac{\partial}{\partial R} [[\eta + (1 - \eta)R] \frac{\partial U}{\partial R}] - M^2 U + \theta, \tag{6.1.5}$$

$$\frac{\partial \theta}{\partial t} = \frac{1}{Pr} \frac{1}{[\eta + (1 - \eta)R]} \frac{\partial}{\partial R} [[\eta + (1 - \eta)R] \frac{\partial \theta}{\partial R}], \tag{6.1.6}$$

and also the following dimensionless initial and boundary conditions, which describe first-order velocity slip and temperature jump conditions at the fluid wall interface are:

$$t \leq 0 : U = 0, \;\; \theta = 0 \;\; for \;\; 0 \leq R \leq 1$$

$$t > 0 : \begin{cases} U = \beta_\nu Kn \frac{\partial U}{\partial R}, \;\; \theta = 1 + \beta_\nu KnF \frac{\partial \theta}{\partial R}; \; R = 0, \\ U = -\beta_\nu Kn \frac{\partial U}{\partial R}, \;\; \theta = -\beta_\nu KnF \frac{\partial \theta}{\partial R}; \; R = 1. \end{cases} \tag{6.1.7}$$

The physical quantities used in the above equations are defined in the nomenclature. By using the transformation $Z = \eta + (1 - \eta)R$, the equations (6.1.5) to (6.1.7) can be written as:

$$\frac{\partial U}{\partial t} = \frac{1}{Z} \frac{\partial}{\partial Z} [Z \frac{\partial U}{\partial Z}](1 - \eta)^2 - M^2 U + \theta, \tag{6.1.8}$$

$$\frac{\partial \theta}{\partial t} = \frac{1}{Pr} \frac{1}{Z} \frac{\partial}{\partial Z} [Z \frac{\partial \theta}{\partial Z}](1 - \eta)^2, \tag{6.1.9}$$

subject to the initial and boundary conditions

$$t \leq 0 : U = 0, \quad \theta = 0, \quad for \quad \eta \leq Z \leq 1$$

$$t > 0 : \begin{cases} U = \beta_\nu Kn(1-\eta)\frac{\partial U}{\partial Z}, \quad \theta = 1 + \beta_\nu KnF(1-\eta)\frac{\partial \theta}{\partial Z}; \quad Z = \eta \\ U = -\beta_\nu Kn(1-\eta)\frac{\partial U}{\partial Z}, \quad \theta = -\beta_\nu KnF(1-\eta)\frac{\partial \theta}{\partial Z}; Z = 1. \end{cases} \tag{6.1.10}$$

The solutions of equations (6.1.8) and (6.1.9) can be obtained by using the Laplace transform technique. Defining the following transform variables:

$$\bar{U}(Z,s) = \int_0^\infty U(Z,t)e^{-st}dt \tag{6.1.11}$$

$$\bar{\theta}(Z,s) = \int_0^\infty \theta(Z,t)e^{-st}dt \tag{6.1.12}$$

where s is the Laplace parameter and $s > 0$. Taking the Laplace transform of equations (6.1.8) and (6.1.9) with the corresponding initial and boundary condition (6.1.10). Equations (6.1.8) and (6.1.9) then become, respectively,

$$\frac{d^2\bar{U}}{dZ^2} + \frac{1}{Z}\frac{d\bar{U}}{dZ} - \left[\frac{s}{(1-\eta)^2} + \frac{M^2}{(1-\eta)^2}\right]\bar{U} = -\frac{\bar{\theta}}{(1-\eta)^2} \tag{6.1.13}$$

$$\frac{d^2\bar{\theta}}{dZ^2} + \frac{1}{Z}\frac{d\bar{\theta}}{dZ} - \frac{sPr}{(1-\eta)^2}\bar{\theta} = 0 \tag{6.1.14}$$

Therefore, the solution of equation (6.1.13) and (6.1.14) are, respectively,

$$\bar{U}(Z,s) = C_3 I_0(\delta_2 Z) + C_4 K_0(\delta_2 Z) - \frac{[C_1 I_0(\delta_1 Z) + C_2 K_0(\delta_1 Z)]}{(1-\eta)^2[\delta_1^2 - \delta_2^2]} \tag{6.1.15}$$

$$\bar{\theta}(Z,s) = C_1 I_0(\delta_1 Z) + C_2 K_0(\delta_1 Z) \tag{6.1.16}$$

All constants used in this chapter are defined in appendix F

Equations (6.1.15) and (6.1.16) are to be inverted in order to determine the velocity and temperature in the time domain. Since these equations are difficult to invert in closed form, we use a numerical procedure used in Jha and Apere (2010) and Khadrawi and Al-Nimr (2007) which is based on the Riemann-sum approximation. In this method, functions in the Laplace domain s can be

inverted to the time domain as follows:

$$U(Z,t) = \frac{e^{\epsilon t}}{t}[\frac{1}{2}\bar{U}(Z,\epsilon) + \Re e \sum_{k=1}^{N} \bar{U}(Z, \epsilon + \frac{ik\pi}{t})(-1)^k] \tag{6.1.17}$$

$$\theta(Z,t) = \frac{e^{\epsilon t}}{t}[\frac{1}{2}\bar{\theta}(Z,\epsilon) + \Re e \sum_{k=1}^{N} \bar{\theta}(Z, \epsilon + \frac{ik\pi}{t})(-1)^k] \tag{6.1.18}$$

Where $\Re e$ refers to the 'real part', $i = \sqrt{(-1)}$ is imaginary number, N is the number of terms used in the Riemann-sum approximation and ϵ is the real part of the Bromwich contour that is used in inverting Laplace transforms. The Riemann-sum approximation for the Laplace inversion involves a single summation for the numerical process. Its accuracy depends on the value of ϵ and the truncation error dictated by N. According to Tzou (1997), the value of ϵ must be selected so that the Bromwich contour encloses all the branch point. For faster convergence the quantity $\epsilon t = 4.7$ gives the most satisfactory results.

6.1.2 Transient Volume Flow Rate

$$\begin{aligned} Q &= \frac{1}{(1-\eta)^2}\int_{\eta}^{1} ZU(Z)dZ \\ &= \frac{1}{(1-\eta)^2}\left[\frac{\{C_3 I_1(\delta_2 Z) - C_4 K_1(\delta_2 Z)\}_{\eta}^{1}}{\delta_2} - \frac{\{C_1 I_1(\delta_1 Z) - C_2 K_1(\delta_1 Z)\}_{\eta}^{1}}{\delta_1(1-\eta)^2[\delta_1^2 - \delta_2^2]}\right] \end{aligned} \tag{6.1.19}$$

6.1.3 Skin-Friction and Rate of Heat Transfer

The skin friction τ and the rate of heat transfer, which is represented by the Nusselt number Nu are similarly obtained by differentiating the velocity and temperature, respectively, with respect to Z as follows:

$$\tau = \frac{dU}{dZ} = \frac{e^{\epsilon t}}{t}\left[\frac{1}{2}\bar{U}_1(Z,\epsilon) + Re\sum_{k=1}^{N}\bar{U}_1(Z, \epsilon + \frac{ik\pi}{t})(-1)^k\right] \tag{6.1.20}$$

$$Nu = \frac{d\theta}{dZ} = \frac{e^{\epsilon t}}{t}\left[\frac{1}{2}\bar{\theta_1}(Z,\epsilon) + Re\sum_{k=1}^{N}\bar{\theta_1}(Z,\epsilon+\frac{ik\pi}{t})(-1)^k\right] \tag{6.1.21}$$

where

$$\bar{U_1} = (1-\eta)\left[\delta_2(C_3I_1(\delta_2 Z) - C_4K_1(\delta_2 Z))\right] - \frac{[\delta_1(C_1I_1(\delta_1 Z) - C_2K_1(\delta_1 Z))]}{(1-\eta)[\delta_1^2 - \delta_2^2]} \tag{6.1.22}$$

$$\bar{\theta_1} = \delta_1(1-\eta)\left[(C_1I_1(\delta_1 Z) - C_2K_1(\delta_1 Z))\right] \tag{6.1.23}$$

Equations (6.1.20) and (6.1.21) represent the general expressions for the skin friction and rate of heat transfer, respectively, between fluid layers amidst the vertical micro-concentric annuli. The skin friction and rate of heat transfer on the surface of vertical micro-concentric annuli can then be calculated by setting $Z = \eta$ and $Z = 1$ in equations (6.1.22) and (6.1.23).

6.1.4 Validation of the Method

In order to validate the accuracy of the Riemann-sum approximation method, we set out to find the solution of the steady state, which should coincide with the transient solution at large time. The expressions for the steady state velocity and temperature are obtained by setting $\frac{\partial()}{\partial t}$ in equations (6.1.5) and (6.1.6) to zero. We now obtain the following ordinary differential equations

$$\frac{1}{Z}\frac{d}{dZ}(Z\frac{dU}{dZ}) - \frac{M^2U}{(1-\eta)^2} + \frac{\theta}{(1-\eta)^2} = 0 \tag{6.1.24}$$

$$\frac{1}{Z}\frac{d}{dZ}(Z\frac{d\theta}{dZ}) = 0 \tag{6.1.25}$$

The solutions of equations (6.1.24) and (6.1.25) using the boundary conditions (6.1.7) gives:

$$U_s(Z) = C_1I_0(ZE) + C_2K_0(ZE) + \frac{1}{M^2}(A_0 + A_1In(Z)) \tag{6.1.26}$$

$$\theta_s(Z) = A_0 + A_1In(Z) \tag{6.1.27}$$

6.1.5 Results and Discussion

The basic parameters that governed this flow are time (t), Prandtl number (Pr) which is inversely proportional to the thermal diffusivity of the working fluid, radius ratio (η), Hartmann number (M), rarefaction parameter ($\beta_\nu Kn$), and fluid-wall interaction parameter (F). To examine the influence of these controlling parameters, the variations of temperature, velocity, volume flow rate, rate of heat transfer, and skin-friction are presented in Figures 6.1.2 - 6.1.25. The present parametric study has been performed in the continuum and slip flow regimes ($Kn \leq 0.1$). Also, for air and various surfaces, the values of β_ν and β_t range from near 1 to 1.667 and from near 1.64 to more than 10, respectively. So, this study has been performed over the reasonable ranges of $0 \leq \beta_\nu Kn \leq 0.1$ and $0 \leq F \leq 10$. The selected reference values of $\beta_\nu Kn$, and F for the present analysis are 0.05 and 1.64 respectively as given in Weng and Chen [4]. In addition, the values of Hartmann number (M) are taken over the range of $1 \leq M \leq 2$ with a reference value of $M = 2$. The variation of the temperature with respect to time (t) is shown in Figure 6.1.2. It is observed that an increase in time (t) causes an increase in the temperature distribution and finally attains its steady state value. The variation of the temperature for different values of Prandtl number (Pr) is illustrated in Figure 6.1.3. It is clear from Figure 6.1.3 that as Prandtl number increases, the temperature decreases. This is because fluids with high Prandtl number (Pr) have a small thermal conductivity and high viscosity, which causes low heat penetration and reduce thermal boundary layer.

Figure 6.1.4 show the temperature distribution for different values of rarefaction parameter ($\beta_\nu Kn$). It is found from Figure 6.1.4 that, the increase in rarefaction parameter ($\beta_\nu Kn$) leads to an increase in the temperature jump on the surfaces of cylinder. This is due to the weak interaction between the fluid molecules and the heated outer surface of inner cylinder. In addition,

increase in rarefaction parameter ($\beta_\nu Kn$) leads to decrease in temperature. Figure 6.1.5 depicts the variation of temperature distribution for different values of fluid-wall interaction parameter (F). It is observed that, the increase in fluid-wall interaction causes an increase in the temperature jump on the surfaces of cylinder. Also, increase in fluid-wall interaction leads to decrease in temperature. Figure 6.1.6 reveals the velocity distribution for different values of time (t). It is revealed from Figure 6.1.6 that increase in time (t) leads to increase in velocity and finally reached its steady value. Furthermore, it is found that there is increase in velocity slip as radius ratio increases. The effects of Prandtl number (Pr) on velocity distribution is shown in Figure 6.1.7. It is clear that as Prandtl number (Pr) increases, there is decrease in the fluid velocity. Physically speaking, as the Prandtl number (Pr) increases, the temperature inside the flow decreases, this causes weak convection current inside the flow domain. Also, it is interesting to note from Figure 6.1.7, that the impact of Prandtl number (Pr) on fluid velocity is more pronounced for higher values of radius ratio (η). Figure 6.1.8 shows the variation of velocity for different values of rarefaction parameter ($\beta_\nu Kn$). It is observed that, as rarefaction parameter ($\beta_\nu Kn$) increases, the velocity slip at the wall increases which reduces the retarding effect of the surfaces of cylinder. This yields an observable increase in the fluid velocity near the surfaces of cylinder. However, as increases, the temperature jump increases and this reduces the amount of heat transfer from the outer surface of inner cylinder to the fluid. This reduction in heat transfer reduces the buoyancy effect, which derives the flow and hence reduces the fluid velocity far from the heated outer surface of the inner cylinder. The reduction in velocity due to the reduction in heat transfer is offset by the increase in velocity due to the reduction in the frictional retarding forces near the inner surface of outer cylinder. Furthermore, the slip induced by rarefaction effect increases as radius ratio increases. Figure 6.1.9 depicts the variation of velocity for different values of fluid-wall interaction parameter

(F). It is found from Figure 6.1.9 that, the increase in fluid-wall interaction parameter (F) leads to decrease in the fluid velocity while the increase in fluid-wall interaction parameter (F) cause increase in velocity slip. In addition, it is clear from figure 6.1.9 that the impact of fluid-wall interaction parameter (F) is more significant for small value of radius ratio. The velocity variations for different values of Hartmann number (M) is shown in figure 6.1.10. It is clear from Figure 6.1.10 that as Hartmann number (M) increases, the fluid velocity decrease while velocity slip at surfaces of cylinder increases, but the velocity slip is more pronounced at the outer surface of inner cylinder compare to inner surface of outer cylinder.

Figure 6.1.11 show the volume flow rate (Q) plotted against the rarefaction parameter ($\beta_\nu Kn$) for different values of time (t). It is observed from figure 6.1.11 that the volume flow rate (Q) is a increasing function of time (t). In addition, it is clear that there is significant impact of time (t) on the volume flow rate for higher values of radius ratio (η). Also, it is clear that time required to reach steady state is higher for higher value of radius ratio (η). Figure 6.1.12 depicts the volume flow rate (Q) plotted against the rarefaction parameter ($\beta_\nu Kn$) for different values of fluid-wall interaction parameter (F). It is evident that the volume flow rate (Q) is a decreasing function of fluid-wall interaction parameter (F). Furthermore, it is observed that the significant impact of fluid-wall interaction parameter (F) on the volume flow rate (Q) can be seen for higher values of radius ratio (η). Figure 6.1.13 shows the variation of volume flow rate versus rarefaction parameter ($\beta_\nu Kn$) for different values of Hartmann number (M). It is interesting to note that the volume flow rate (Q) is decreasing function of Hartmann number (M). Also, Figure 6.1.13 suggest that the impact of Hartmann number (M) on the volume flow rate (Q) is more visible for higher radius ratio (η).

The rate of heat transfer on the outer surface of inner cylinder and inner surface

of outer cylinder, which is represented by the Nusselt number Nu are presented in Figure 6.1.14 and 6.1.15, respectively. It is observed from figure 6.1.14 that the rate of heat transfer decrease with increase in time (t) and radius ratio (η). Contrarily, it is clear from Figure 6.1.15 that the increase in time (t) leads to increase in the rate of heat transfer. In addition, it is interesting to note that as rarefaction parameter increase there is a decrease in the rate of the heat transfer. The variation of the rate of heat transfer versus rarefaction parameter ($\beta_\nu Kn$) for different values of Prandtl number (Pr) at $r = 0$ and $r = 1$, is presented in Figure 6.1.16 and 6.1.17, respectively. From Figure 6.1.16, it is observed that as rarefaction parameter ($\beta_\nu Kn$) and Prandtl number (Pr) increases, the rate of heat transfer increase while in Figure 6.1.17, it is found that the increase in rarefaction parameter ($\beta_\nu Kn$) and Prandtl number (Pr) leads to decrease in the rate of heat transfer, in addition, it is interesting to note that the impact of Prandtl number on the rate of heat transfer is not significant for higher value of Prandtl number (Pr). Figure 6.1.18 and 6.1.19 depicts the variation of rate of heat transfer versus rarefaction parameter ($\beta_\nu Kn$) for different values of fluid-wall interaction parameter (F). It is observes in figure 6.1.18 that increase in fluid-wall interaction parameter (F) leads to increase in the rate of heat transfer at $r = 0$, while, in Figure 6.1.19, it is found that increase in fluid-wall interaction parameter (F) leads to decrease in the rate of heat transfer at $r = 1$.

The variation of skin-friction versus rarefaction parameter ($\beta_\nu Kn$) for different value of time (t) at $R = 0$ and $R = 1$, is depicted respectively in Figure 6.1.20 and 6.1.21. It is evident from the figure that as the time is increases, the skin-friction increases. In addition as rarefaction parameter ($\beta_\nu Kn$) increases, the skin-friction decreases. The skin-friction versus rarefaction parameter ($\beta_\nu Kn$) for different values of fluid-wall interaction parameter (F) at $r = 0$ and $r = 1$, is presented in Figures 6.1.22 and 6.1.23. It is interesting to note that as fluid-wall interaction parameter (F) and rarefaction parameter ($\beta_\nu Kn$) increases,

the skin-friction decreases on the cylindrical surfaces. Figures 6.1.24 and 6.1.25 shown the skin-friction versus rarefaction parameter ($\beta_\nu Kn$) for different values of Hartmann number (M) at $r = 0$ and $r = 1$. It is clear from the figures that as Hartmann number increase, the skin friction decrease. Also, increase in rarefaction parameter ($\beta_\nu Kn$) leads to decrease in skin friction on both cylindrical surfaces.

Table 6.1.1: Comparison of the numerical value of the transient state velocity obtained using Riemann-sum approximation method and the steady state obtained analytically when $M = 2.0$, $F = 1.64$, $Pr = 0.71$, $\beta_\nu Kn = 0.05$ and $\eta = 0.5$.

t	r	Velocity	
		Transient state	Steady State
	0.2	0.0025	0.0393
0.02	0.4	0.0005	0.0434
	0.6	0.0000	0.0351
	0.8	0.0000	0.0207
	0.2	0.0066	0.0393
	0.4	0.0030	0.0434
0.04	0.6	0.0008	0.0351
	0.8	0.0001	0.0207
	0.2	0.0283	0.0393
	0.4	0.0286	0.0434
0.2	0.6	0.0212	0.0351
	0.8	0.0118	0.0207
	0.2	0.0372	0.0393
	0.4	0.0406	0.0434
0.4	0.6	0.0325	0.0351
	0.8	0.0190	0.0207
	0.2	0.0393	0.0393
	0.4	0.0434	0.0434
1.0	0.6	0.0351	0.0351
	0.8	0.0207	0.0207

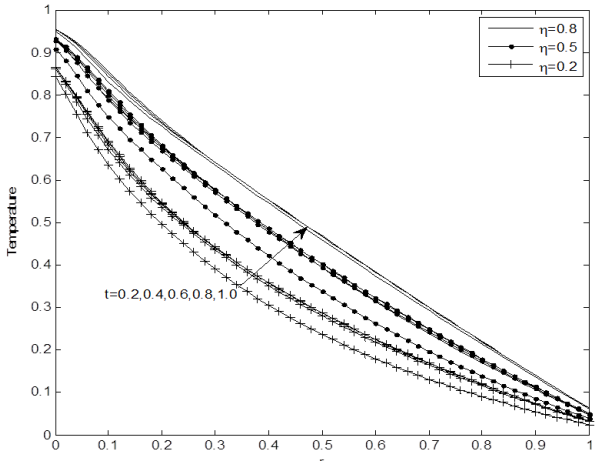


Figure 6.1.2: Temperature distribution for different values of time (t) with $F = 1.64$, $Pr = 0.71$, $\beta_\nu Kn = 0.05$.

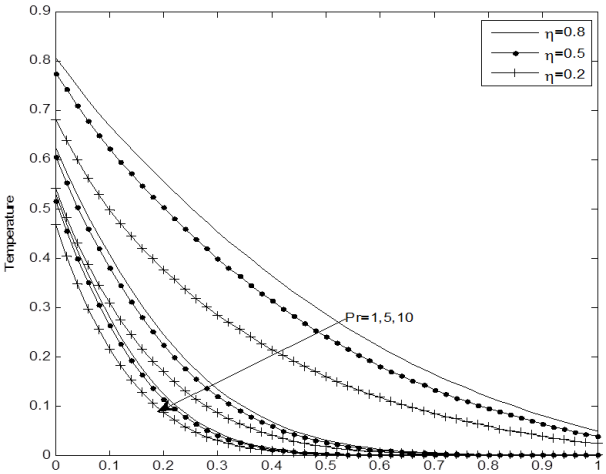


Figure 6.1.3: Temperature distribution for different values of Pr with $t = 0.2$,$\beta_\nu Kn = 0.05$, $F = 1.64$.

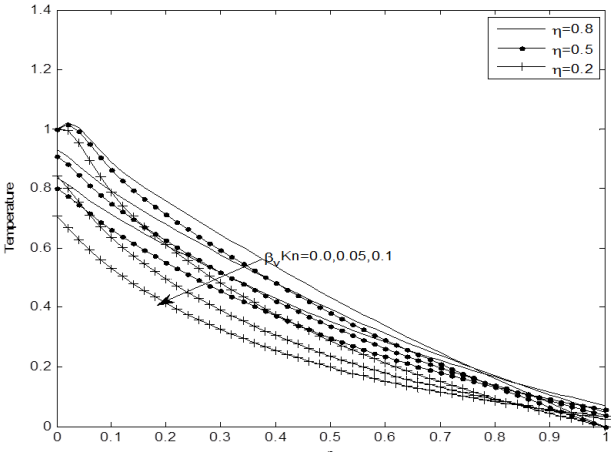


Figure 6.1.4: Temperature distribution for different values of $\beta_\nu Kn$ with $t = 0.2$, Pr, $F = 1.64$.

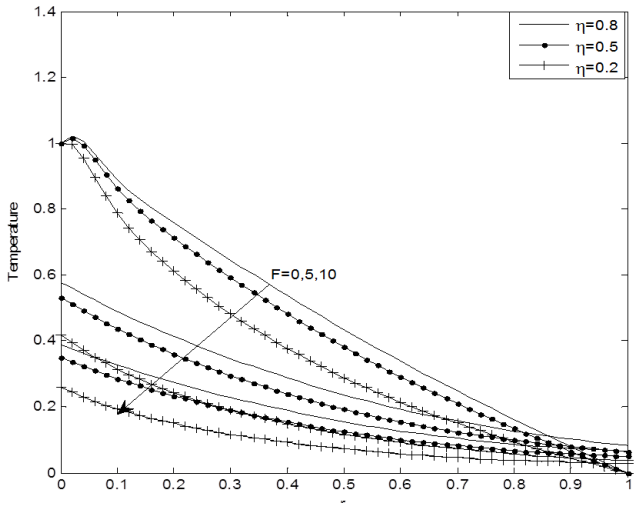


Figure 6.1.5: Temperature distribution for different values of F with $t = 0.2$, $Pr = 0.71$, $\beta_\nu Kn = 0.05$.

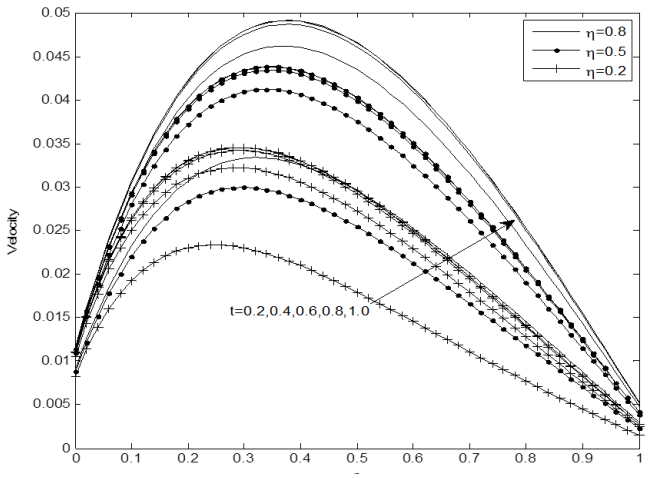


Figure 6.1.6: Velocity distribution for different values of time (t) with $M = 2$, $F = 1.64$, $Pr = 0.71$, $\beta_\nu Kn = 0.05$.

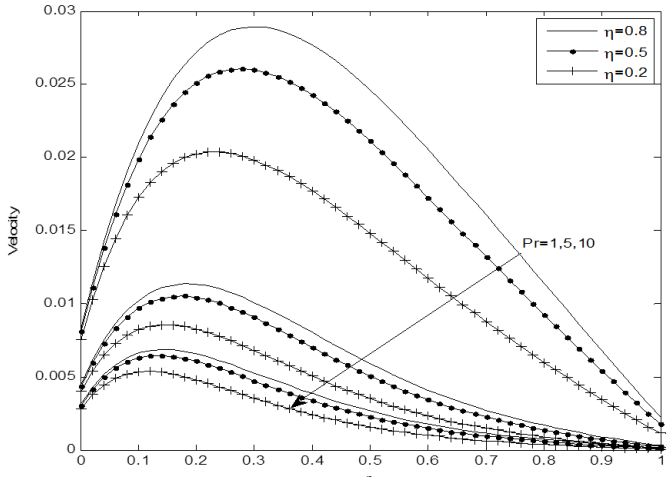


Figure 6.1.7: Velocity distribution for different values of Pr with $M = 2.0$, $t = 0.2$, $\beta_\nu Kn = 0.05$, $F = 1.64$.

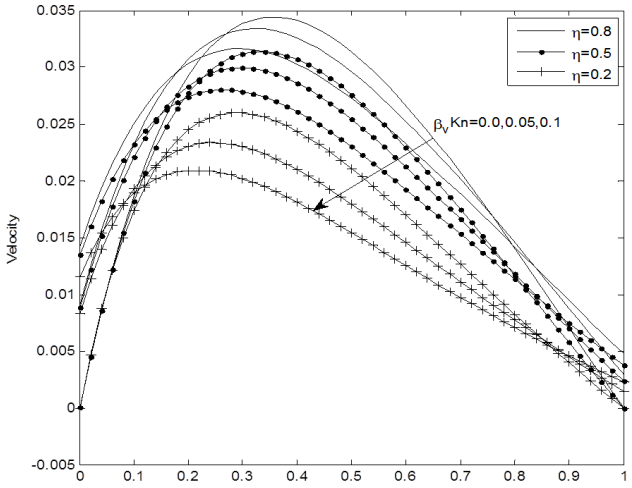


Figure 6.1.8: Velocity distribution for different values of $\beta_\nu Kn$ with $t = 0.2$, $Pr = 0.71$, $F = 1.64$.

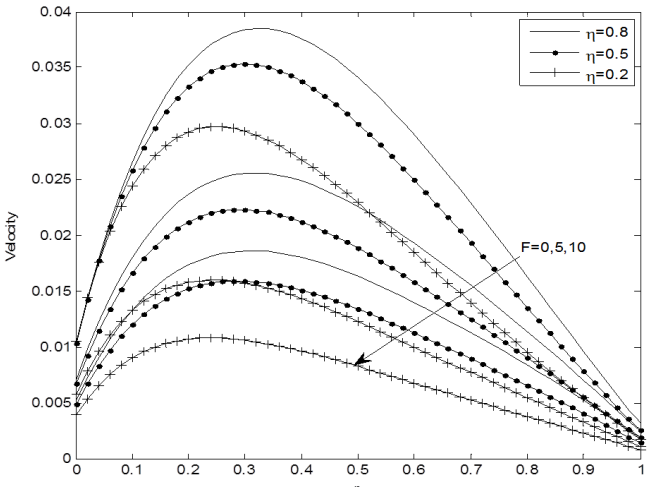


Figure 6.1.9: Velocity distribution for different values of F with $M = 2, t = 0.2$, $Pr = 0.71$, $\beta_\nu Kn = 0.05$.

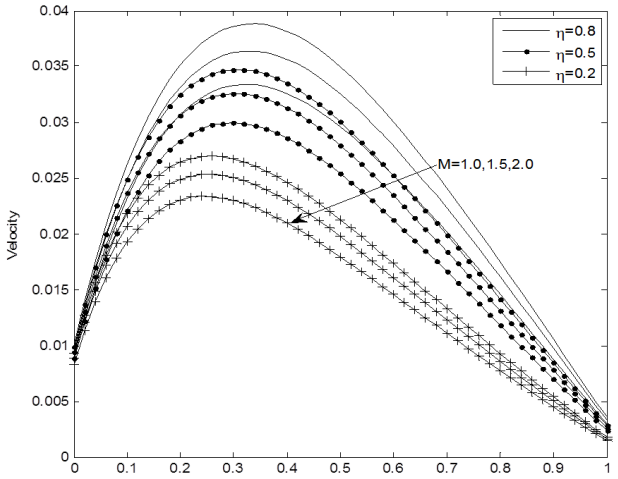


Figure 6.1.10: Velocity distribution for different values of M, with $t = 0.2$, Pr, $F = 1.64$, $\beta_\nu Kn$.

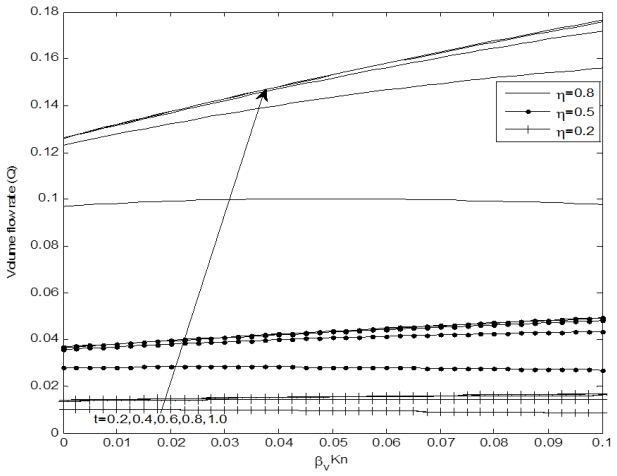


Figure 6.1.11: Volume flow rate versus $\beta_\nu Kn$ for different values of time (t) with $F = 1.64$, $M = 2.0$, $Pr = 0.71$.

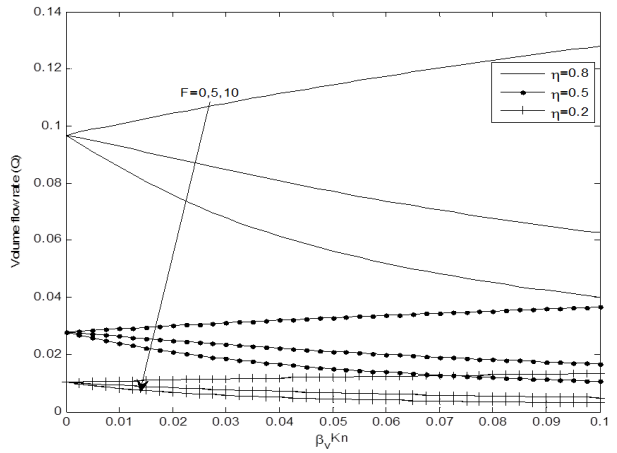


Figure 6.1.12: Volume flow rate versus $\beta_\nu Kn$ for different values of F with $M = 2$, $t = 0.2$, $Pr = 0.71$.

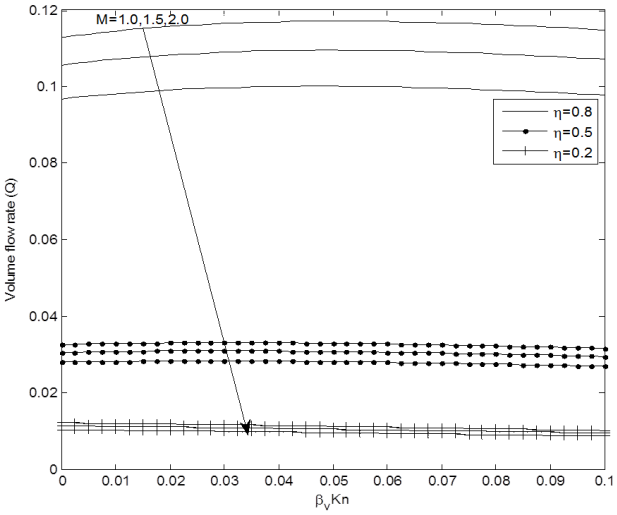


Figure 6.1.13: Volume flow rate versus $\beta_\nu Kn$ for different values of M with $t = 0.2$, $Pr = 0.71$, $F = 1.64$.

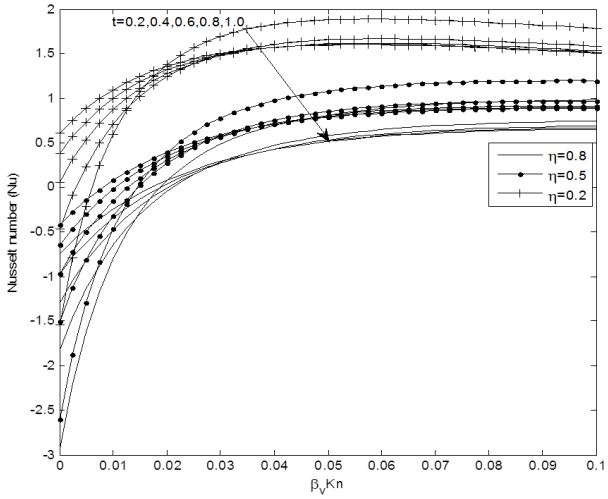


Figure 6.1.14: Rate of heat transfer versus $\beta_\nu Kn$ for different values of time (t) with $F = 1.64$, $Pr = 0.71$ at $r = 0$.

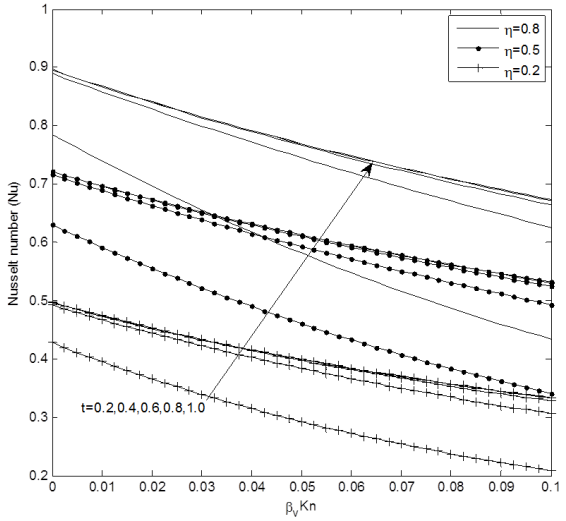


Figure 6.1.15: Rate of heat transfer versus $\beta_\nu Kn$ for different values of time (t) with $F = 1.64$, $Pr = 0.71$ at $r = 1$.

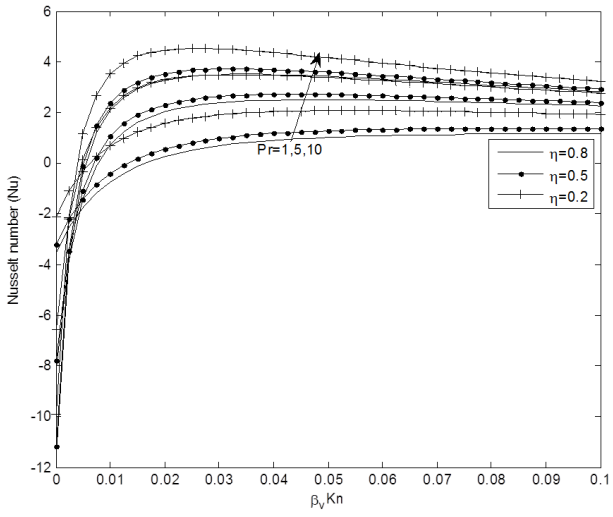


Figure 6.1.16: Rate of heat transfer versus $\beta_\nu Kn$ for different values of Pr with $t = 0.2$, $F = 1.64$ at $r = 0$.

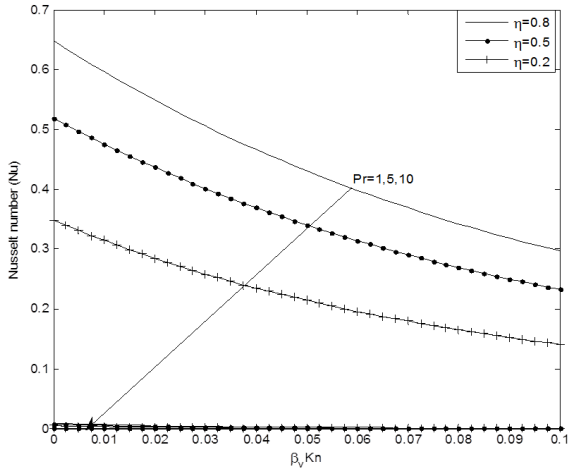


Figure 6.1.17: Rate of heat transfer versus $\beta_\nu Kn$ for different values of Pr with $t = 0.2$, $F = 1.64$ at $r = 1$.

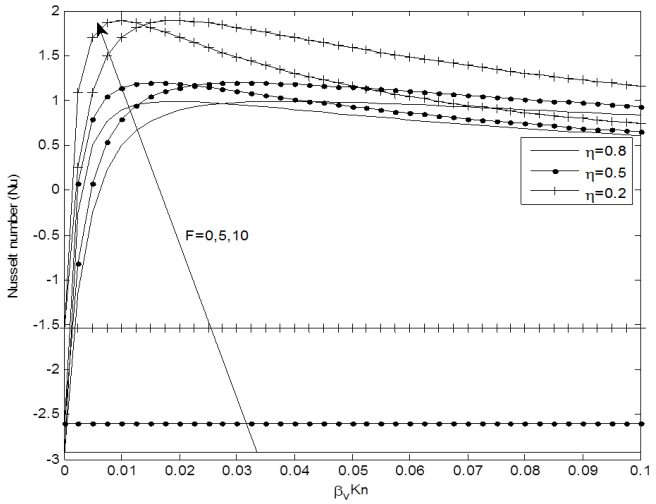


Figure 6.1.18: Rate of heat transfer versus $\beta_\nu Kn$ for different values of F with $t = 0.2$, $Pr = 0.71$ at $r = 0$.

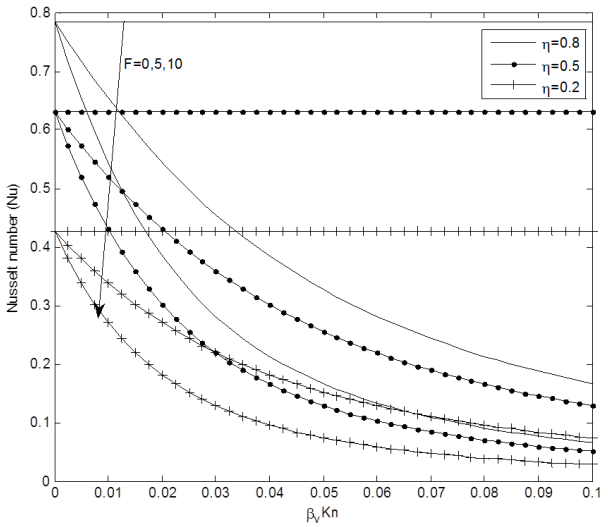


Figure 6.1.19: Rate of heat transfer versus $\beta_\nu Kn$ for different values of F with $t = 0.2$, $Pr = 0.71$ at $r = 1$.

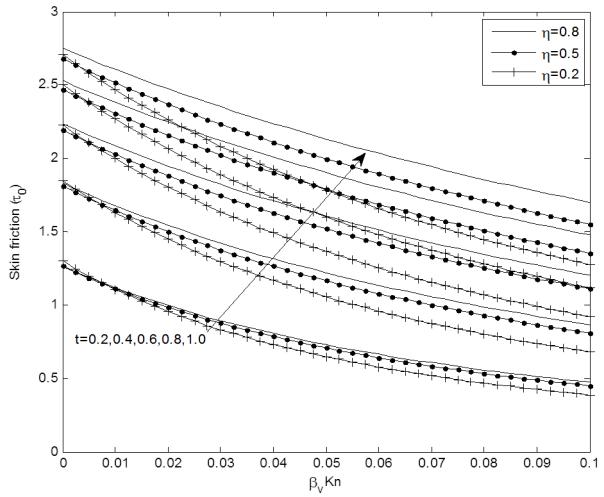


Figure 6.1.20: Skin friction versus $\beta_\nu Kn$ for different values of time (t) with $F = 1.64$, $M = 2.0$, $Pr = 0.71$ at $r = 0$.

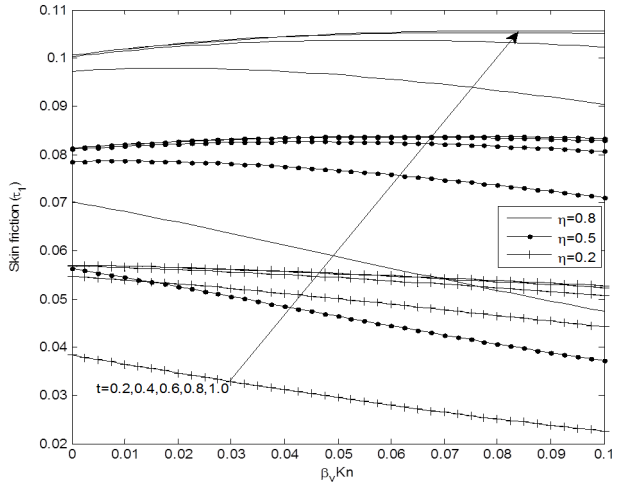


Figure 6.1.21: Skin friction versus $\beta_\nu Kn$ for different values of time (t) with $F = 1.64$, $M = 2.0$, $Pr = 0.71$ at $r = 1$.

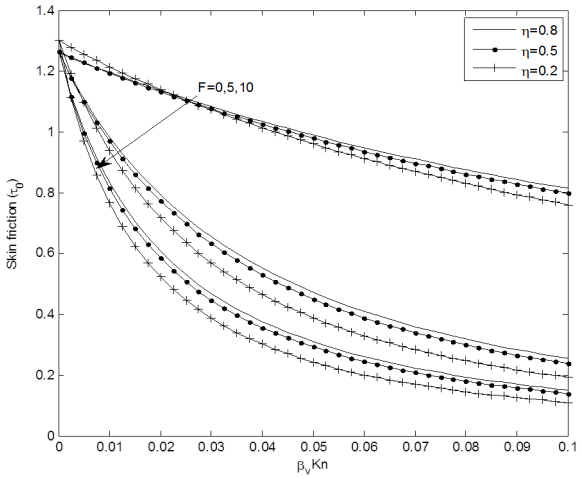


Figure 6.1.22: Skin friction versus $\beta_\nu Kn$ for different values of F with $M = 2.0$, $t = 0.2$, $Pr = 0.71$ at $r = 0$.

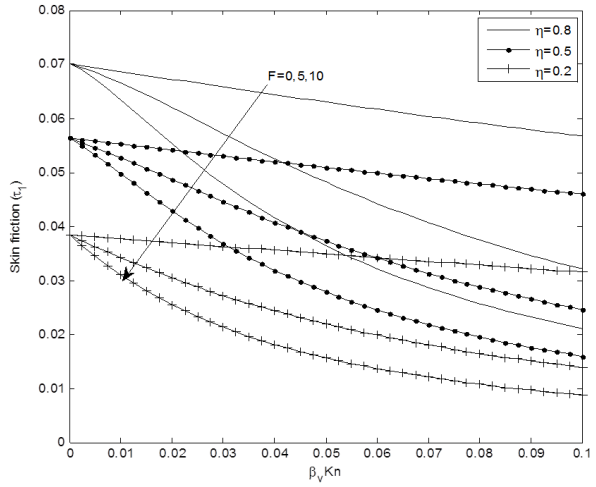


Figure 6.1.23: Skin friction versus $\beta_\nu Kn$ for different values of F with $M = 2.0$, $t = 0.2$, $Pr = 0.71$ at $r = 1$.

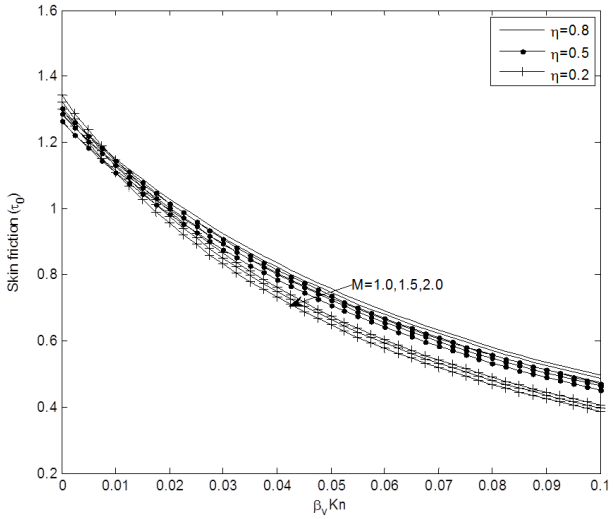


Figure 6.1.24: Skin friction versus $\beta_\nu Kn$ for different values of M with $F = 1.64$, $t = 0.2$, $Pr = 0.71$ at $r = 0$.

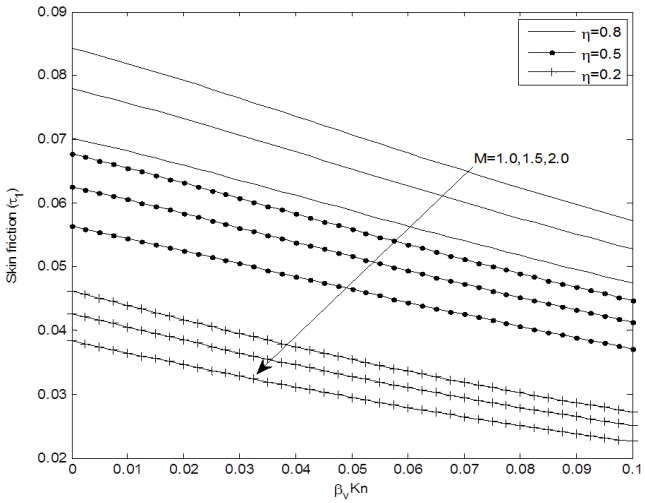


Figure 6.1.25: Skin friction versus $\beta_\nu Kn$ for different values of M with $F = 1.64$, $t = 0.2$, $Pr = 0.71$ at $r = 1$.

CHAPTER SEVEN

CONCLUSIONS AND RECOMMENDATIONS

7.1 Summary

In this thesis we have studied the flow of viscous incompressible fluid in a channel formed by two two vertical parallel plates or an annulus formed by two vertical concentric cylinders under different physical situations. The different physical situations considered includes: Role of induced magnetic field on transient natural convection flow in a vertical channel: The Riemann sum approximation approach, Computational treatment of MHD transient natural convection flow in a vertical channel due to symmetric heating in presence of induced magnetic field which are treated in chapter three. While in chapter four the Effects of suction/injection combination (SIC) on MHD transient free-convective flow in a vertical channel in presence of induced magnetic field and unsteady MHD free-convective Couette flow in presence of induced magnetic field:The impulsive motion are solved. The problems of MHD natural convection flow in a vertical micro-concentric annuli in presence of radial magnetic field: An exact solution, Fully Developed MHD Natural Convection flow in a Vertical annular Micro-channel: An exact solution and Transient MHD Free Convective Flow in Vertical Micro-concentric Annuli are respectively presented in chapters five and six. The system of partial differential equations describing the different flow problems have been formulated and both analytical and numerical solutions are obtained in either case. The Laplace transform techniques are used to reduce the system of partial differential equations to ordinary differential equations; the resulting boundary value problems are then solved analytically where possible or the Riemann-sum approximation method where direct inversion is difficult. The implicit finite difference method is used to verify the Riemann-sum approximation method. MATLAB programmes

are written to compute and generate the graphs for the velocities and the skin frictions. The result obtained demonstrates the reliability of the Riemann-sum approximation method.

7.2 Conclusion

Mathematical analysis and solutions of MHD flow of an incompressible fluids in macro-channels and micro-channels have been carried out. The effects of different dimensionless parameters on the flow regime are given in chapters one through chapter seven and the following general conclusions are drawn:

1. The velocity of the fluid increases with increase in time (t) while decreases with increase in the value of the Prandtl number (Pr),

2. An Increase in the Hartmann Number (M) decreases the velocity of the fluid.

3. The impact of magnetic Prandtl number on induced magnetic field is more pronounced while on velocity field is not significant for considered values of Pm.

4. An increase in (η) and $\beta_\nu Kn$ leads to an increase in volume flow rate

5. The Nusselt number (Nu) depends on the fluid, as indicated by Pr

6. The skin-friction decreases as Pr increases as well as M increases

7.3 Recommendations

The increasing interest in the study of macro-channels and micro-channels in vast areas of applications as outlined earlier in this thesis calls for much in-

vestigation. Moreover, this work can be extended by taking into consideration the effect of porous media, porous walls of channels. Future work can also be undertaken by considering compressible fluid, the effect of rarefaction and viscous heating for thermally developing range. It is therefore recommended that, interdisciplinary and collaborative work be undertaken to allow clear and maximum utilization of findings.

REFERENCES

Ahmed, S. (2012). Mathematical model of induced magnetic field with viscous/magnetic dissipation bounded by a porous vertical plate in presence of radiation. *International Journal Applied Math. Mech.*, 8:86 – 104.

Ahmed, S., Bég, O., Vedad, S., Zeinalkhani, M., and Heidari, A. (2012). Mathematical modeling of magnetohydrodynamic transient free and forced convective flow with induced magnetic field effects. *International Journal of Pure and Applied Science Technology*, 11:109 – 125.

Ajibade, A. O. (2009). A study on some problems in the presence of heat and mass transfer. Ph.D Dissertation.

Al-Nimr, M. (1993). Analytical solution for transient laminar fully developed free convection in vertical concentric annuli. *Int. J.Heat Mass Transfer*, 36:2385 – 2395.

Al-Nimr, M. (1995). Mhd free-convection flow in open-ended vertical concentric porous annuli. *Applied Energy*, 50:293 – 311.

Al-Nimr, M. and Darabseh, T. (1995). Analytical solution for transient laminar fully developed free convection in open-ended vertical con-centric porous annuli. *J. Heat Transfer (ASME)*, 117:762 – 765.

Al-Nimr, M. and Khadrawi, A. (2004). Thermal behavior of a stagnant gas confined in a horizontal microchannel as described by the dual-phase-lag heat conduction model. *Int. J. Thermophys*, 25:1953 – 1964.

Alfvén, H. (1942). Existence of electromagnetic-hydrodynamic waves. *Nature*, 150:405.

Alom, M. M., Rafiqul, I. M., and Rahman, F. (2008). Steady heat and mass transfer by mixed convection flow from a vertical porous plate with induced magnetic field, constant heat and mass fluxes. *International Journal of Science Technology*, 13:1 – 13.

Andreozzi, A., Buonomo, B., and Manca, O. (2009). Transient natural convection in vertical channels symmetrically heated at uniform heat flux. *Numerical Heat Transfer, Part A, Applications*, 55:409 – 431.

Antimirov, M. Y. and Kolyshkin, A. A. (1984). Nonstationary mhd flow in an annular channel in a radial magnetic field. *Magnetohydrodynamics*, 20:285 – 288.

Anwar, B. O., Bakier, A. Y., Prasad, V., Zueco, J., and Ghosh, S. K. (2009). Magnetohydrodynamic shear flow along a flat plate with uniform suction or blowing. *International Journal of Thermal Sciences*, 48:1596 – 1606.

Arpaci, V. S. (1966). *Conduction Heat Transfer*. AddisonWesley, Reading.

Ashorynejad, H. R., Sheikholeslami, Pop, I., and Ganji, D. D. (2013). Nanofluid flow and heat transfer due to a stretching cylinder in the presence of magnetic field. *Heat Mass Transfer*, 49:427 – 436.

Attia, H. A. (1998). Hall current effects on the velocity and temperature fields of an unsteady hartmann flow. *Canadian Journal of Physics*, 76:739–746.

Attia, H. A. (2004). Unsteady hartmann flow of a viscoelastic fluid considering the hall effect. *Canadian Journal of Physics*, 82:127–136.

Aung, W. (1972). Fully developed laminar free convection between vertical plates heated asymmetrically. *International J. Heat and Mass Transfer*, 15:1577–1580.

Avci, M. and Aydin, O. (2006). Laminar forced convection with viscous dissipation in a concentric annular duct. *Comptes Rendus Mecanique*, 334:164 – 169.

Avci, M. and Aydin, O. (2008). Laminar forced convection slipflow in a microannulus between two concentric cylinders. *Int. J. Heat and Mass Transfer*, 51:3460 – 3467.

Avci, M. and Aydin, O. (2009). Mixed convection in a vertical microannulus between two concentric microtubes. *ASME, J. Heat Transfer*, 131:014502–4.

Barletta, A., Lazzari, S., and Magyari, E. (2008). Buoyant poiseuille-couette flow with viscous dissipation in vertical channel. *ZAMP*, 59:1039 – 1056.

Berman, A. S. (1953). Laminar flow in channels with porous walls. *J. Applied Physics (9)*, 24:1232 – 1235.

Bianco, N., Langellotto, L., Manca, O., and Naso, V. (2006). Numerical analysis of radiative effects on natural convection in vertical convergent and symmetrically heated channels. *Numerical Heat Transfer, Part A, Applications*, 49:369 – 391.

Cengel, Y. A. (2003). *Heat and Mass Transfer: A Practical Approach,3rd Edition.* McGraw Hill, JBoston.

Chauhan, D. S. and Agrawal, R. (2012). Effects of hall current on mhd couette flowin a channel partiallyfilled with porous medium in a rotating system. *Meccanica*, 47:405 – 421.

Chen, C. and Weng, H. (2005). Natural convection in a vertical microchannel. *Journal of Heat Transfer*, 127:1053–1056.

Cramer, R. and Pai, S. I. (1973). *Magnetofluid dynamics for Engineers and applied physicists.* McGraw Hill Book Company, New York.

Dalton, D. S. (2009). *Lectures in Magnetohydrodynamics.* Springer-Verlag Berlin Heidelberg 2009. Springer.

Davidson, P. A. (2001). *An Introduction to Magnetohydrodynamics.* Cambridge University Press.

Deka, R. K. and Bhattacharya, A. (2011). Unsteady free convective couette flow of heat generation/absorbing fluid in porous medium. *Int. J. Math. Archive*, 2:853 – 863.

Dubner, H. and Abate, J. (1968). Numerical inversion of laplace transforms by relating them to the finite fourier cosine transform. *Journal of the Association for Computing Machinery*, 75:115 – 23.

El-Shaarawi, M. A. and Al-Nimr, M. A. (1990). Fully developed natural convection in open-ended vertical concentric annuli. *Int. J. Heat and Mass Transfer*, 33:1873 – 1884.

Faraday, M. (1832). Experimental researches in electricity. *Philosophical Transactions of the Royal Society*, 1:125 – 162.

Farhad, A., Khan, I., Samiulhaq, Mustapha, M., and S, S. (2012a). Unsteady magnetohydrodynamic oscillatory flow of viscoelastic fluids in a porous channel with heat and mass transfer. *Journal of the Physical Society of Japan*, 81:064402.

Farhad, A., Khan, I., Samiulhaq, and Sharidan, S. (2013a). Conjugate effects of heat and mass transfer on mhd free convection flow over an inclined plate embedded in a porous medium. *PLoS ONE*, 8:e65223.

Farhad, A., Khan, I., and Sharidan, S.and Norzieha, M. (2013b). Heat and mass transfer with free convection mhd flow past a vertical plate embedded in a porous medium. *Mathematical Problems in Engineering, Special Issue Mathematical Modeling of Heat and Mass Transfer in Energy Science and Engineering*, 2013:346281.

Farhad, A., Khan, I., and Sharidan, S. (2014). Closed form solutions for unsteady free convection flow of a second grade fluid over an oscillating vertical plate. *PLoS ONE*, 9:e85099.

Farhad, A., Norzieha, M., Sharidan, S., Khan, I., and Samiuthaq (2012b). On hydromagnetic rotating flow in a porous medium with slip condition and hall current. *International Journal of the Physical Sciences*, 7:1540 – 1548.

Fleisch, D. A. (2008). *A Student's Guide to Maxwell's Equations*. Cambridge University Press.

Gad-el Hak, M. (1999). The fluid mechanics of microdevices-the freeman scholar lecture. *J. Fluids Engng*, 121:5 – 33.

Garandet, J. P., Alboussiere, T., and Moreau, R. (1992). Buoyancy driven convection in a rectangular enclosure with a transverse magnetic field. *International J. Heat Mass Transfer*, 35:741 – 748.

Ghosh, S. K., Bég, O. A., and Zueco, J. (2010). Hydromagnetic free convection flow with induced magnetic field effects. *Meccanica*, 45:175 – 185.

Ghosh, S. K. and Bhattacharjee, P. K. (2000). Hall effects on steady hydromagnetic flow in a rotating channel in the presence of an inclined magnetic field. *Czech. Journal of Physics*, 50.

Globe, S. (1959). Laminar steady-state magnethydrodynamic flow in an annular channel. *Physics of Fluids*, 2.

Gupta, A. S., Misra, J., and Reza, M. (1974). Radiation effect on hydromagnetic convection in a vertical channel. *J. Heat and Mass Transfer*, 17:1437 – 1442.

Gupta, A. S., Misra, J., and Reza, M. (2005). Magnetohydrodynamic shear flow along a flat plate with uniform suction or blowing. *ZAMP*, 56:1030 – 1047.

Hartmann, J. (1937). Theory of laminar flow of an electrically conducting liquid in a homogeneous magnetic field. *Kgl.Danske Videnskabernes Selskab,Mathematisk-Fysiske Meddelelser*, 15:00–00.

Hartmann, J. and Lazarus, F. (1937). Experimental investigations on the flow of mercury in a homogeneous magnetic field. *Kgl.Danske Videnskabernes Selskab,Mathematisk-Fysiske Meddelelser*, 15:00–00.

Jain, R. K. and Mehta, K. N. (1962). Fully developed laminar mhd flow in annular porous walls. *Phys. Fluids*, 5:1207 – 1211.

Jana, R. N. and Datta, N. (1977). Hall effects on unsteady couette flow. *Int. J. Engng. Sci.*, 15:35 – 43.

Jana, R. N., Datta, N., and Mazumder, B. S. (1977). Magnetohydrodynamic couette flow and heat transfer in a rotating system. *Journal of Physical Society of Japan.*, 42:1034 – 1039.

Jha, B., Aina, B., and Joseph, S. (2014a). Natural convection flow in a vertical micro-channel with suction/injection. *J. Process Mech. Eng.*, 228:171 – 180.

Jha, B. K. (1998). Effects of applied magnetic field on transient free convective flow in a vertical channel. *Indian J. pure appl. math.*, 29:441 – 445.

Jha, B. K. (2001). Transient free convective flow in a vertical channel with heat sinks. *International Journal of Applied Mechanics and Engineering*, 6:279–286.

Jha, B. K., Aina, B., and Shehu, A. (2014b). Combined effects of suction/injection and wall surface curvature on natural convection flow in a vertical micro-porous-annulus. *Journal of Thermophysics and Aerodynamics.*, 00:in press.

Jha, B. K. and Ajibade, A. O. (2010). Transient natural convection flow between vertical parallel plates: one plate isothermally heated and the other thermally insulated. *Journal of Process Mechanical Engineering*, 224:247 – 252.

Jha, B. K. and Apere, C. A. (2010). Unsteady mhd couette flow in an annuli: the riemann-sum approximation approach. *J. Phys. Soc. Jpn*, 79:124403.

Jha, B. K. and Apere, C. A. (2011). Magnetohydrodynamics free convective couette flow with suction and injection. *Journal of Heat Transfer*, 133:1 –12.

Jha, B. K. and Apere, C. A. (2012). Magnetohydrodynamic transient free convective flow in a vertical annulus with thermal boundary condition of the second kind. *Journal of Heat Transfer*, 134:15 – 22.

Jha, B. K. and Apere, C. A. (2013). Time-dependent mhd couette flow in a porous annulus. *Commun Nonlinear Sci Numer Simulat*, 18:1959 – 1969.

Jha, B. K., Samaila, A. K., and Ajibade, A. O. (2011). Transient free-convective flow of reactive viscous fluid in a vertical channel. *International Communication Heat Mass Transfer*, 38:633 – 637.

Jha, B. K., Samaila, A. K., and Ajibade, A. O. (2012). Unsteady/steady free convective couette flow of reactive viscous fluid in a vertical channel formed by two vertical porous plates. *International Scholarly Research Network*, 38:doi:10.5402/2012/794741.

Jha, B. K., Singh, A. K., and Takhar, H. S. (2003). Transient free convective flow in a vertical channel due to symmetric heating. *Int. J. Appl. Mech. Eng*, 8:497–502.

Jibril, H. M. (2012). A study on some flow behaviour of conducting fluids. preprint.

Joshi, H. M. (1988). Transient effects in natural convection cooling of vertical parallel plates. *International Communications in Heat and Mass Transfer*, 15:227–238.

Katagiri, M. (1962). Flow formation in couette motion in magnetohydrodynamics. *J. Physical Society of Japan*, 17:393 – 396.

Khadrawi, A. F. (2011). Transient hydrodynamic and thermal behaviours of fluid flow in a vertical porous microchannel under the effect of hyperbolic heat conduction model. *World Academy of Science, Engineering and Technology*, 60:60.

Khadrawi, A. F. and Al-Nimr, M. A. (2007). Unsteady natural convection fluid flow in a vertical microchannel under the effect of the dual-phase-lag heat-conduction model. *International Journal of Thermophysics*, 28:1387–1400.

Khadrawi, A. F., Othman, A., and Al-Nimr, M. A. (2005). Transient free convection fluid flow in a vertical microchannel as described by the hyperbolic heat conduction model. *International Journal of Thermophysics*, 26:905–918.

Khan, I. and Ellahi, R. (2008). Some unsteady mhd flows of a second grade fluid through porous medium. *Journal Porous Media*, 11:389 – 400.

Koshiba, Y., Matsushita, T., and Ishikawa, M. (2002). Influence of induced magnetic field on large-scale pulsed mhd generator. In *AIAA 33rd Plasma dynamics and Lasers Conference*.

Krishna, G. S. (2009). Analytical solution to the problem of mhd free convective flow of an electrically conducting fluid between two heated parallel plates in the presence of an induced magnetic field. *International Journal of Applied Mathematics and Computation*, 1:183 – 193.

Kumar, A. and Singh, A. K. (2013). Effect of induced magnetic field on natural convection in vertical concentric annuli heated/cooled asymmetrically. *Journal of Applied Fluid Mechanics*, 6:15 – 26.

Langellotto, L., Manca, O., and Nardini, S. (2007). Numerical investigation of transient natural convection in air in a convergent vertical channel symmetrically heated at uniform heat flux. *Numerical Heat Transfer, Part A, Applications*, 51:1065 – 1086.

Mahmud, S. and Andrew, F. R. (2005). Flow, thermal, and entropy generation characteristics inside a porous channel with viscous dissipation. *International Journal of Thermal Sciences*, 44:21 – 32.

McDonough, J. M. (2009). Lectures in elementary fluid dynamics: Physics, mathematics and applications. University of Kentucky, Lexington.

Megakhed, A. A. (1974). Effect of induced magnetic field and heat transfer on nonstationary magnetohydrodynamic flow around a porous plate. *Magnetohydrodynamics*, 10:48 – 52.

Mishra, S. P. and Mohapatra, P. (1975). Unsteady free convection flow from a vertical plate in the presence of a uniform magnetic field. *ZAMM*, 55:759 – 762.

Mishra, S. P. and Muduli, J. C. (1980). Unsteady flow through two porous flat walls in presence of a magnetic field. *Rev. Roum des Sci. Tech. Serie de Mech. Appl.*, 25:21 – 27.

Molokov, S., Moreau, R., and Moffat, H. K. (2007). *Magnetohydrodynamics. Historical Evolution and Trends.* Springer.

Muhuri, P. K. (1963). Flow formation in couette motion in magnetohydrodynamics with suction. *J. Physical Society of Japan*, 18:1671 – 1675.

Muzychka, Y. and Yovanovich, M. M. (2006). Unsteady viscous flows and stoke's first problem. In *Proceedings of the Internaional Mechanical Engineering Congress and Exposition,*, number 2.

Nadeem, S. and Akbar, N. S. (2010). Effects of induced magnetic field on peristaltic flow of johnson-segalman fluid in a vertical symmetric channel. *Applied Mathematics Mechanics English Edition*, 31:969 – 978.

Nandi, S. (1973). Steady hydromagnetic viscous flow in an annulus with porous walls. *PAGEOPH*, 105:825 – 835.

Nanousis, N., Georgantopouos, G., and Papaioannou, A. I. (1980). Hydromagnetic free convection flow in the stokes problem for a porous vertical limiting surface with constant suction. *Astrophysics Space Science*, 70:377 – 383.

Narahari, M. (2008). Transient free convection flow between two long vertical parallel plates with constant temperature and mass diffusion. In *Proceedings of the World Congress on Engineering*.

Narahari, M., Sreenadh, S., and Soundalgekar, V. M. (2002). Transient free convection flow between long vertical parallel plates with constant heat flux at one boundary. *Journal of Thermophysics and Aeromechanics*, 254:82–93.

Oreper, G. M. and Szekely, J. (1983). The effect of an externally imposed magnetic field on buoyancy driven flow in rectangular cavity. *Journal of Crystal Growth*, 64:505 – 515.

Osterle, J. F. and Young, F. J. (1961). Natural convection between heated vertical plates in horizontal magnetic field. *Journal of Fluid Mechanics*, 11:512–518.

Ostrach, S. (1952). Laminar natural-convection flow and heat transfer of fluids with or without heat sources in channels with constant wall temperatures. *NASA, Report No. NACA-TN*, 2863.

Pai, S. I. (1962). *Magnetohydrodynamics and Plasma dynamics*. Springer - Verlag Berlin.

Paul, T., Jha, B. K., and Singh, A. K. (1996). Transient free convection flow in vertical channel with constant heat flux on walls. *Heat Mass Transfer*, 32:61 – 63.

Poots, G. (1961). Laminar natural convection flow in magnetohydrodynamics. *International Journal of Heat and Mass Transfer*, 3:1–25.

Quanrong, W. and Hongbin, Z. (2015). On different numerical inverse laplace methods for solute transport problems. *Advances in Water Resources*, 75:80 – 92.

Ram, P., Bhandari, A., and Sharma, K. (2010). Effect of magnetic field-dependent viscosity on ferrofluid flow due to rotating disc. *Journal of Magnetism and Magnetic Materials*, 322:3476 – 3480.

Raptis, A. A., Perdikis, C., and Leontitsis, A. (2003). Effects of radiation in an optically thin gray gas flowing past a vertical infinite plate in the presence of a magnetic field. *Heat and mass Transfer*, 39:771–773.

Romig, M. F. (1964). The influence of electric and magnetic fields on heat transfer to electrically conducting fluids. *Advances in Heat Transfer*, 1:267 – 354.

Sarris, I., Zikos, G., Grecos, A., and Vlachos, N. (2006). On the limits of validity of the low magnetic reynolds number approximation in mhd natural convection heat transfer. *Numer. Heat Transfer: Part B – Fundam.*, 50:157 – 180.

Sarveshanand and Singh, A. K. (2014). Free convection between vertical concentric annuli with induced magnetic field when inner cylinder is electrically conducting. *International J. Computers and Technology*, 13:5062 – 5074.

Schlichting, H. (1960). *Boundary Layer Theory.* McGraw.Hill Book Co.Inc., New York.

Seth, G. S., Ansari, M. S., and Nandkeolyar (2011). Unsteady hydromagnetic couette flow within a porous channel. *Tamkang. J.Sci.Eng.*, 14:7 – 14.

Seth, G. S. and Maiti, M. K. (1982). Mhd couette flow and heat transfer in a rotating system. *Ind. J. Pure and Appl. Math.*, 13:931 – 945.

Sheikholeslami, M., Gorji-Bandpay, M., and D., G. D. (2014). Magnetic field effects on natural convection around a horizontal circular cylinder inside a square enclosure filled with nanofluid. *International Communications in Heat and Mass Transfer*, 39:978 – 986.

Sheikholeslami, M., Gorji-Bandpy, M., Ganji, D. D., Soheil, S., and Seyyedi, S. (2012). Natural convection of nanofluids in an enclosure between a circular and a sinusoidal cylinder in the presence of magnetic field. *International Communications in Heat and Mass Transfer*, 39:1435 – 1443.

Sheikholeslamia, M., Gorji-Bandpay, M., Ellahi, R., Mohsan, H., and Soheil, S. (2014a). Effects of mhd on cu–water nanofluidflow and heat transfer by means of cvfem. *Journal of Magnetism and Magnetic Materials*, 349:188 – 200.

Sheikholeslamia, M., Gorji-Bandpy, M., Ganji, D. D., Rana, P., and Soleimani, S. (2014b). Magnetohydrodynamic free convection of al2o3–water nanofluid considering thermophoresis and brownian motion effects. *Computers and Fluid*, 94:147–160.

Sheikholeslamia, M., Gorji-Bandpy, M., Ganji, D. D., and Soheil, S. (2013). Effect of a magnetic field on natural convection in an inclined half-annulus enclosure filled with cu-water nanofluid using cvfem. *Advanced Powder Technology*, 24:980 – 991.

Simon, R. M., Strout, M. T., and Weiss, G. H. (1972). Numerical inversion of laplace transforms with application to percentage labelled experiments. *Comput. Biomed. Res.*, 6:596–607.

Singh, A. K. (1988). Natural convection in unsteady couette motion. *Defence Science Journal*, 31:35–41.

Singh, A. K., Gbolami, H. R., and Soundalgekar, V. M. (1996). Transient free convection flow between two vertical parallel plates. *Heat and Mass Transfer*, 31:329 – 331.

Singh, A. K. and Kumar, N. (1983). Unsteady hydromagnetic couette flow. *Wear*, 89:125 – 129.

Singh, A. K. and Paul, T. (2006). Transient natural convection between two vertical walls heated/cooled asymmetrically,. *International Journal of Applied Mechanics and Engineering*, 11.

Singh, R. K. and Singh, A. K. (2012). Effect of induced magnetic field on natural convection in vertical concentric annuli. *ACTA Mech.Sin*, 28:315 – 323.

Singh, R. K., Singh, A. K., Sacheti, N. C., and Chandran, P. (2010). On hydromagnetic free convection in the presence of induced magnetic field. *Heat Mass Transfer*, 46:523 – 529.

Singh, R. K., Singh, T. R., and Kataria, H. R. (2014). Induced magnetic field effects on mixed convection. *IOSR Journal of Mathematics*, 10:76 – 85.

Singh, S. K., Jha, B. K., and Singh, A. K. (1997). Natural convection in vertical concentric annuli under a radial magnetic field. *Heat Mass Transfer*, 32:399 – 401.

Singha, K. G. (2009). Analytical solution to the problem of mhd free convective flow of an electrically conducting fluid between two heated parallel plates in the presence of an induced magnetic field. *International Journal of Applied Mathematics and Computation*, 1:183 – 193.

Singha, K. G. and Deka, P. N. (2006). Skin-friction for unsteady free convection mhd flow between two heated vertical parallel plates. *Theoretical Applied Mechanics*, 33:259 – 280.

Soundalgekar, V. M. (1965). Hydromagnetic flow near an accelerated plate in the presence of a magnetic field. *Applied Scientific Research*, 12:151 – 156.

Soundalgekar, V. M. (1967). On the flow of an electrically conducting incompressible fluid near an accelerated plate in the presence of a parallel plate under transverse magnetic field. *Proc. Ind. Acad. Sci.,*, 65:179 – 187.

Stokes, G. (1851). On the effect of the internal friction of fluids on the motion of pendulums. *Transactions of the Cambridge Philosophical Society*, 9:8 —-106.

Sutton, G. W. and Sherman, A. (1965). *Engineering Magnetohydrodynamics.* McGraw.Hill Book Co.Inc.

Takhar, H. S., Chamkha, A. J., and Nath, G. (1999). Unsteady flow and heat transfer on a semi-infinite flat plate with an aligned magnetic field. *International Journal of Engineering Science*, 37:1723 – 1736.

Takhar, H. S., M.A., A., and M., S. V. (1989). Stability of mhd couette flow in a narrow gap annulus. *Appl. Sci. Res.*, 46:1.

Terrill, R. M. (1982). An exact solution for flow in a porous pipe. *J. Applied Mathematical Physics (ZAMP)*, 33:547 – 52.

Terrill, R. M. (1983). Laminar flow in a porous tube. *J. Fluids Engineering*, 105:303 – 306.

Terrill, R. M. and Shrestha, G. M. (1966). Laminar flow in a uniformly porous channel with an applied transverse magnetic field. *Applied Science Research*, 105:203 – 211.

Tsangaris, S., Kondaxakis, D., and Vlachakis, N. W. (2007). Exact solution for flow in a porous pipe with unsteady wall suction and/or injection. *Communications in Nonlinear Science and Numerical Simulation*, 12:1181 – 1189.

Tzou, D. (1997). *Macro to Microscale Heat Transfer: The Lagging Behaviour.* Taylor and Francis.

Veldman, A. E. P. (2011). Boudary layers in fluid dynamics. In *Lecture Notes in Applied Mathematics.*

Weng, H. and Chen, C. (2008). Fully developed thermocreep-diven gas microflow. *Appl. Phys. Lett*, 92:094105.

Weng, H. and Chen, C. (2009). Drag reduction and heat transfer enhancement over a heated wall of a vertical annular microchannel. *International Journal of Heat and Mass Transfer*, 52:1075–1079.

Weng, H. and Chen, C. (2013). Magnetogasdynamic flow and heat transfer in a microchannel with isothermally heated walls. *International Journal of Heat and Mass Transfer*, 57:16–21.

Živojin, M. S., Dragiśa, D. N., Miloś, M. K., and Jelena, D. N. (2012a). Mhd flow and heat transfer of two immiscible fluids with induced magneticc field effects. *Therm. Scie*, 16:S373 – S387.

Živojin, M. S., Dragiśa, D. N., Miloś, M. K., and Nikodijević, J. D. (2012b). Mhd flow and heat transfer of two immiscible fluids with induced magnetic field effects. *Thermal Sciences*, 16:S373 – S387.

APPENDIX A

Role of induced magnetic field on transient natural convection flow in a vertical channel: The Riemann-sum Approximation Approach

$\lambda = (\frac{M}{4} + s)^{\frac{1}{2}}$,

$a_1 = \frac{1}{2s\sinh(b)}[\frac{e^b}{d_1} - \frac{e^{-b}}{d_2}]$,

$a_3 = \frac{1}{2s\sinh(b)}[\frac{e^b}{d_2} - \frac{e^{-b}}{d_1}]$

$a_2 = \frac{Mbe^{\frac{M}{2}}}{s\sinh(\lambda)\sinh(b)[(sPr-s)^2-M^2sPr]} - [\frac{\cosh(\lambda)}{\sinh(\lambda)}]a_1$,

$a_4 = \frac{-Mbe^{\frac{-M}{2}}}{s\sinh(\lambda)\sinh(b)[(sPr-s)^2-M^2sPr]} - [\frac{\cosh(\lambda)}{\sinh(\lambda)}]a_3$,

$a_5 = \frac{[d_4e^{-M}-d_3]M}{e^{-M}-1}$,

$a_6 = \frac{d_3-d_4}{e^{-M}-1}$,

$a_7 = \frac{M[d_5e^{M}-d_6]}{e^{M}-1}$,

$a_8 = \frac{d_5-d_6}{e^{M}-1}$

$a_9 = \frac{[f_2\lambda-f_1\sinh(\lambda)]}{[\lambda\cosh(\lambda)+\frac{M}{2}\sinh(\lambda)]}$,

$a_{10} = \frac{[\frac{f_2M}{2}-\lambda\cosh(\lambda)]}{[\lambda\cosh(\lambda)+\frac{M}{2}\sinh(\lambda)]}$,

$a_{11} = \frac{-[f_1\sinh(\lambda)+\frac{M}{2}\lambda f_2]}{[\frac{M}{2}\sinh(\lambda)-\lambda\cosh(\lambda)]}$,

$a_{12} = \frac{[f_1\sinh(\lambda)+\frac{M}{2}\lambda f_2]}{[\frac{M}{2}\sinh(\lambda)-\lambda\cosh(\lambda)]}$,

$b = \sqrt{sPr}$,

$d_1 = sPr - Mb - s$,

$d_2 = sPr + Mb - s$,

$d_3 = \frac{a_5}{M} + a_6e^{-M}$,

$d_4 = \frac{a_5}{M} + a_6$,

$d_5 = \frac{a_7}{M} + a_8$,

$d_6 = \frac{a_7}{M} + a_8e^{M}$

$d_7 = sPr + Mb - s$,

$d_8 = sPr - Mb - s$,

$f_1 = \frac{-2MPr}{s\cosh(b)[(sPr-s)^2-M^2sPr]}$,

$f_2 = \frac{e^{\frac{M}{2}}}{2s\cosh(b)}[\frac{e^b}{d_7} + \frac{e^{-b}}{d_8}]$,

$f_3 = \frac{e^{\frac{-M}{2}}}{2s\cosh(b)}[\frac{e^b}{d_8} + \frac{e^{-b}}{d_7}]$,

APPENDIX B

Computational treatment of MHD transient natural convection flow in a vertical channel due to symmetric heating in presence of induced magnetic field

$\lambda_1 = \sqrt{(\frac{S+M}{2})^2 + p} \quad \lambda_2 = \sqrt{(\frac{S-M}{2})^2 + p} \quad \lambda_3 = \sqrt{(\frac{SPr}{2})^2 + pPr}$

$d_1 = (\lambda_3 + \frac{SPr}{2})^2 - (S+M)(\lambda_3 + \frac{SPr}{2}) - p$

$d_2 = (\lambda_3 - \frac{SPr}{2})^2 + (S+M)(\lambda_3 - \frac{SPr}{2}) - p$

$d_3 = (\lambda_3 + \frac{SPr}{2})^2 - (S-M)(\lambda_3 + \frac{SPr}{2}) - p$

$d_4 = (\lambda_3 - \frac{SPr}{2})^2 + (S-M)(\lambda_3 - \frac{SPr}{2}) - p$

$c_1 = \frac{1}{2psinh(\lambda_3)[\frac{\exp(\lambda_3)}{d_1} - \frac{\exp(-\lambda_3)}{d_2}]}, \qquad c_2 = \frac{[f_2 - f_1.cosh(\lambda_1)]}{sinh(\lambda_1)}, \quad f_1 = c_1$

$c_3 = \frac{1}{2psinh(\lambda_3)}[\frac{\exp(\lambda_3)}{d_3} - \frac{\exp(-\lambda_3)}{d_4}], \quad c_4 = \frac{[f_4 - f_3.cosh(\lambda_2)]}{sinh(\lambda_2)}, \quad f_3 = c_3$

$f_2 = \frac{\exp(\frac{1}{2}(M+S-SPr))}{2psinh(\lambda_3)}[\frac{1}{d_1} - \frac{1}{d_2}] \qquad f_4 = \frac{\exp(\frac{1}{2}(S-M-SPr))}{2psinh(\lambda_3)}[\frac{1}{d_3} - \frac{1}{d_4}]$

$c_5 = \frac{-1}{\exp(-SPr)-1}, \quad c_6 = \frac{\exp(-SPr)}{\exp(-SPr)-1}, \quad c_7 = \frac{(f_6 - f_5\exp(-(M+S)))(M+S)}{1-\exp(-(M+S))}$

$c_8 = \frac{f_5 - f_6}{1-\exp(-(M+S))}, \quad c_9 = \frac{(f_8 - f_7\exp(-(S-M)))(S-M)}{1-\exp(-(S-M))}, \quad c_{10} = \frac{f_7 - f_8}{1-\exp(-(S-M))}$

$f_5 = -\frac{c_5}{SPr(M+S-SPr)} - \frac{c_6}{(M+S)^2},$

$f_6 = c_6(\frac{1}{(M+S)} - \frac{1}{(M+S)^2}) - \frac{c_5\exp(-SPr)}{SPr(M+S-SPr)},$

$f_7 = -\frac{c_5}{SPr(S-M-SPr)} - \frac{c_6}{(S-M)^2},$

$f_8 = c_6(\frac{1}{(S-M)} - \frac{1}{(S-M)^2}) - \frac{c_5\exp(-SPr)}{SPr(S-M-SPr)},$

APPENDIX C

Effects of suction-injection combination (SIC) on MHD transient free-convective flow in a vertical channel in presence of induced magnetic field

$b = \sqrt{sPr},\ \ d_1 = sPr - Mb - s,\ \ d_2 = sPr + Mb - s,\ \ \lambda = \sqrt{\frac{M}{4} + s},$

$A_1 = \frac{Gr}{2s\sinh(b)}(\frac{e^b}{d_1} - \frac{e^{-b}}{d_2}) + \frac{1}{s}, \quad A_3 = \frac{G}{2s\sinh(b)}(\frac{e^b}{d_2} - \frac{e^{-b}}{d_1}) + \frac{1}{s},$

$A_2 = \frac{GrMbe^{(\frac{M}{2})}}{s\sinh(b)\sinh(\lambda)[(sPr-s)^2 - M^2 sPr]} - \frac{\cosh(\lambda)}{\sinh(\lambda)}c_1,$

$A_4 = \frac{-GrMbe^{-(\frac{M}{2})}}{s\sinh(b)\sinh(\lambda)[(sPr-s)^2 - M^2 sPr]} - \frac{\cosh(\lambda)}{\sinh(\lambda)}c_3,$

$A_5 = \frac{Gr}{2s\sinh(b)}(\frac{e^b}{d_1} - \frac{e^{-b}}{d_2}), \quad A_7 = \frac{Gr}{2s\sinh(b)}(\frac{e^b}{d_2} - \frac{e^{-b}}{d_1}),$

$A_6 = \frac{\exp(\frac{M}{2})}{s} + \frac{GrMbe^{(\frac{M}{2})}}{s\sinh(b)\sinh(\lambda)[(sPr-s)^2 - M^2 sPr]} - \frac{\cosh(\lambda)}{\sinh(\lambda)}a_1,$

$A_8 = \frac{\exp(\frac{-M}{2})}{s\sinh(b)} + \frac{-GrMbe^{-(\frac{-M}{2})}}{s\sinh(b)\sinh(\lambda)[(sPr-s)^2 - M^2 sPr]} - \frac{\cosh(\lambda)}{\sinh(\lambda)}a_3.$

$A_9 = \frac{M[d_4\exp(-M) - d_3]}{\exp(-M)-1},\ A_{10} = \frac{M[d_3 - d_4]}{\exp(-M)-1},\ A_{11} = \frac{M[d_5\exp(M) - d_6]}{\exp(-M)-1},$

$A_{12} = \frac{M[d_5 - d_6]}{\exp(-M)-1} \quad d_3 = d_6 = \frac{1}{2M} - \frac{1}{M^3},\ d_4 = \frac{1}{Gr} - \frac{1}{M^2} - \frac{1}{M^3},$

$d_5 = \frac{1}{M^2} - \frac{1}{M^3} - \frac{1}{Gr}.$

APPENDIX D

MHD natural convection flow in vertical micro-concentric annuli in presence of radial magnetic field: An exact solution

$C_1 = \frac{E_6E_2 - E3E5}{E_2E_4 - E_1E_5}$,

$C_2 = \frac{E_6E_1 - E3E4}{E_1E_5 - E_2E_4}$, $E = \frac{M}{1-\eta}$

$E_1 = [I_0(E\eta) - (\beta_\nu Kn(1-\eta)E)I_1(E\eta)]$

$E_2 = [K_0(E\eta) + (\beta_\nu Kn(1-\eta)E)K_1(E\eta)]$

$E_3 = \frac{A_1}{M^2\eta}\beta_{nu}Kn(1-\eta) - \frac{1}{M^2}(A_0 + A_1In(\eta))$

$E_4 = [I_0(E) - (\beta_\nu Kn(1-\eta)E)I_1(E)]$

$E_5 = [K_0(E) + (\beta_\nu Kn(1-\eta)E)K_1(E)]$

$E_6 = -[\frac{A_0}{M^2} + \frac{|beta_\nu Kn(1-\eta)A_1}{M^2}]$

APPENDIX E

Fully Developed MHD Natural Convection flow in a Vertical annular Microchannel: An exact solution

$$A_0 = -\beta_\nu KnF(1-\eta)A_1,\ A_1 = \frac{1}{In(\eta) - \beta_\nu KnF(1-\eta)(1+\frac{1}{\eta})},$$

$$C_1 = \frac{E_1E_2 - E_3E_5}{E_2E_4 - E_1E_5},\ C_2 = \frac{E_1E_6 - E_3E_4}{E_1E_5 - E_2E_4},\ E = \frac{M}{(1-\eta)},$$

$$E_1 = I_0(E\eta) - (\beta_\nu Kn(1-\eta)E)I_1(E\eta),$$

$$E_2 = K_0(E\eta) + (\beta_\nu Kn(1-\eta)E)K_1(E\eta),$$

$$E_3 = \frac{A_1}{M^2\eta}\beta_\nu Kn(1-\eta) - \frac{1}{M^2}\left[A_0 + A_1In(\eta)\right],$$

$$E_4 = I_0(E) + (\beta_\nu Kn(1-\eta)E)I_1(E),$$

$$E_5 = K_0(E) - (\beta_\nu Kn(1-\eta)E)K_1(E),$$

$$E_6 = -\left[\frac{A_0}{M^2} + \frac{\beta_\nu Kn(1-\eta)A_1}{M^2}\right].$$

APPENDIX F

Transient MHD Free Convective Flow in Vertical Micro-concentric Annuli

$$\delta_1 = \frac{\sqrt{sPr}}{(1-\eta)},\ \delta_2 = \frac{\sqrt{s+M^2}}{(1-\eta)},\ A_0 = -\beta_\nu KnF(1-\eta)A_1,$$

$$A_1 = \frac{1}{In(\eta) - \beta_\nu KnF(1-\eta)(1+\frac{1}{\eta})},\ C_1 = -\frac{d_4}{s[d_2d_3 - d_1d_4]},$$

$$C_2 = -\frac{d_3}{s[d_2d_3 - d_1d_4]},\ C_3 = \frac{d_{10}d_{14} - d_{11}d_{13}}{d_{10}d_{12} - d_9d_{13}},\ C_4 = \frac{d_{11}d_{12} - d_9d_{14}}{d_{10}d_{12} - d_9d_{13}},$$

$$C_5 = \frac{E_6E_2 - E_3E_6}{E_2E_4 - E_1E_5},\ C_6 = \frac{E_1E_6 - E_3E_4}{E_1E_5 - E_2E_4},\ d_1 = I_0(\delta_1\eta) - \beta_\nu KnF\delta_1(1-\eta)I_1(\delta_1\eta),$$

$$d_2 = K_0(\delta_1\eta) + \beta_\nu KnF\delta_1(1-\delta)K_1(\delta_1\eta),\ d_3 = I_0(\delta_1) + \beta_\nu KnF\delta_1(1-\eta)I_1(\delta_1),$$

$$d_4 = K_0(\delta_1) - \beta_\nu KnF\delta_1(1-\delta)K_1(\delta_1),\ d_5 = -\frac{C_1I_0(\delta_1\eta) + C_2K_0(\delta_1\eta)}{(1-\eta)^2\left[\delta_1^2 - \delta_2^2\right]}$$

$$d_6 = -\frac{\delta_1\left[C_1I_1(\delta_1\eta) - C_2K_1(\delta_1\eta)\right]}{(1-\eta)^2\left[\delta_1^2 - \delta_2^2\right]},\ d_7 = -\frac{C_1I_0(\delta_1) + C_2K_0(\delta_1)}{(1-\eta)^2\left[\delta_1^2 - \delta_2^2\right]},$$

$$d_8 = \frac{\delta_1\left[C_1I_1(\delta_1) - C_2K_1(\delta_1)\right]}{(1-\eta)^2\left[\delta_1^2 - \delta_2^2\right]},\ d_9 = I_0(\delta_2\eta) - \beta_\nu Kn\delta_2(1-\eta)I_1(\delta_2\eta),$$

$$d_{10} = K_0(\delta_2\eta) + \beta_\nu Kn\delta_2(1-\eta)K_1(\delta_2\eta),\ d_{11} = \beta_\nu Knd_6 - d_5,$$

$$d_{12} = I_0(\delta_2) + \beta_\nu Kn\delta_2(1-\eta)I_1(\delta_2\eta),\ d_{13} = K_0(\delta_2) - \beta_\nu Kn\delta_2(1-\eta)K_1(\delta_2),$$

$$d_{14} = \beta_\nu Knd_8 - d_7,\ E = \frac{1}{(1-\eta)\sqrt{\frac{1}{M^2}}},$$

$$E_1 = I_0(E\eta) - (\beta_\nu Kn(1-\eta)E)I_1(E\eta),$$

$$E_2 = K_0(E\eta) + (\beta_\nu Kn(1-\eta)E)K_1(E\eta),$$

$$E_3 = \frac{A_1}{M^2\eta}\beta_\nu Kn(1-\eta) - \frac{1}{M^2}[A_0 + A_1In(E\eta)],$$

$$E_4 = I_0(E) - (\beta_\nu Kn(1-\eta)E)I_1(E),$$

$$E_5 = K_0(E) - (\beta_\nu Kn(1-\eta)E)K_1(E),$$

$$E_6 = -\left[\frac{A_0}{M^2} + \frac{\beta_{nu}Kn(1-\eta)A_1}{M^2}\right].$$

APPENDIX G

Transient natural convection in a vertical channel with induced magnetic field (VELOCITY)

$[y,t] = meshgrid(0.0:0.02:1.0, 0.1:0.1:0.4);$

$[y,t] = meshgrid(0.0:0.2:1.0, 0.2:0.4:2.4);$

$[y,p] = meshgrid(0.0:0.02:1.0, 1.0:1.0:10.0);$

$w = (y - y + 1).*(p - p + 1);$

$t = 0.2.*w;$

$m = 0.5.*w;$

$ep = 4.7.*w;$

$eps = ep./t;$

$se = 4.7.*w;$

$clc;$

$zx = 0*w;$

$n = 1;$

$whilen < 100;$

$x1 = (-1).^{n};$

$x2 = eps + (i.*n.*pi./t);$

$b = sqrt(x2.*p);$

$al = sqrt(x2 + (m./2.).^{2});$

$d1 = x2.*p - (m.*b) - x2;$

$d2 = x2.*p + (m.*b) - x2;$

$x3 = (exp(b)./d1) - (exp(-b)./d2);$

$c1 = x3./(2.*x2.*sinh(b));$

$x4 = -(cosh(al)./sinh(al)).*c1;$

$x5 = sinh(al).*x2.*sinh(b).*((((b.*b) - x2).^{2}) - (m.*m.*x2.*p));$

$x6 = exp(0.5.*m).*(m.*b);$

$c2 = (x6./x5) + x4;$

$x7 = (exp(b)./d2) - (exp(-b)./d1);$

$$c3 = x7./(2. * x2. * sinh(b));$$

$$x8 = sinh(al). * x2. * sinh(b). * ((((b. * b) - x2).^2) - (m. * m. * x2. * p));$$

$$x10 = -(cosh(al)./sinh(al)). * c3;$$

$$c4 = (x9./x8) + x10;$$

$$x12 = (exp(b. * (1. - y)))./d1;$$

$$x13 = (exp(-b. * (1. - y)))./d2;$$

$$x14 = -(x12 - x13)./(2. * x2. * sinh(b));$$

$$x15 = (c1. * cosh(al. * y) + c2. * sinh(al. * y)). * exp(-0.5. * m. * y);$$

$$x16 = (exp(b. * (1. - y)))./d2;$$

$$x17 = (exp(-b. * (1. - y)))./d1;$$

$$x18 = -(x16 - x17)./(2. * x2. * sinh(b));$$

$$x19 = (c3. * cosh(al. * y) + c4. * sinh(al. * y)). * exp(0.5. * m. * y);$$

$$w = x15 + x14;$$

$$v = x19 + x18;$$

$$w1 = 0.5. * (w - v);$$

$$zx = zx + w1. * x1;$$

$$n = n + 1;$$

$$end$$

$$re = real(zx);$$

$$z1 = eps;$$

$$zb = sqrt(z1. * p);$$

$$zal = sqrt(z1 + (m./2.).^2);$$

$$zd1 = z1. * p - (m. * zb) - z1;$$

$$zd2 = z1. * p + (m. * zb) - z1;$$

$$zx3 = (exp(zb)./zd1) - (exp(-zb)./zd2);$$

$$zc1 = zx3./(2. * z1. * sinh(zb));$$

$$zx4 = -(cosh(zal)./sinh(zal)). * zc1;$$

$$zx5 = sinh(zal). * z1. * sinh(zb). * ((((zb. * zb) - z1).^2) - (m. * m. * z1. * p));$$

$$zx6 = exp(0.5. * m). * (m. * zb);$$

$$zc2 = (zx6./zx5) + zx4;$$

$$zx7 = (exp(zb)./zd2) - (exp(-zb)./zd1);$$

$$zc3 = zx7./(2. * z1. * sinh(zb));$$

$$zx8 = sinh(zal). * z1. * sinh(zb). * ((((zb. * zb) - z1).^2) - (m. * m. * z1. * p));$$

$$zx9 = -exp(-0.5. * m). * (m. * zb);$$

$$zx10 = -(cosh(zal)./sinh(zal)). * zc3;$$

$$zc4 = (zx9./zx8) + zx10;$$

$$zx12 = (exp(zb. * (1. - y)))./zd1;$$

$$zx13 = (exp(-zb. * (1. - y)))./zd2;$$

$$zx14 = -(zx12 - zx13)./(2. * z1. * sinh(zb));$$

$$zx15 = (zc1. * cosh(zal. * y) + zc2. * sinh(zal. * y)). * exp(-0.5. * m. * y);$$

$$zx16 = (exp(zb. * (1. - y)))./zd2;$$

$$zx17 = (exp(-zb. * (1. - y)))./zd1;$$

$$zx18 = -(zx16 - zx17)./(2. * z1. * sinh(zb));$$

$$zx19 = (zc3. * cosh(zal. * y) + zc4. * sinh(zal. * y)). * exp(0.5. * m. * y);$$

$$zw = zx15 + zx14;$$

$$zv = zx19 + zx18;$$

$$w2 = 0.5. * (zw - zv);$$

$$z2 = exp(se)./t;$$

$$u = z2. * (0.5 * w2 + re)$$

$$d4 = -(1./m.^2) - (1./m.^3);$$

$$d3 = (0.5./m) - (1./m.^3);$$

$$y2 = (d4. * exp(-m) - d3). * m;$$

$$c5 = y2./y1;$$

$$c6 = (d3 - d4)./y1;$$

$$y3 = (c5./m) + (c6. * exp(-m. * y));$$

$$y4 = -(y./m) + (1./m.^2);$$

$$y5 = ((y.^2)./m) - ((2. * y)./m.^2) + (2./m.^3);$$

$$sw = y4 + (0.5. * y5) + y3;$$

$d5 = (1./m.^2) - (1./m.^3);$

$d6 = (0.5./m) - (1./m.^3);$

$c8 = (d5 - d6)./(exp(m) - 1.);$

$c7 = (m. * (d5. * exp(m) - d6))./(exp(m) - 1.);$

$y6 = (y./m) + (1./m.^2);$

$y7 = ((y.^2)./m) + ((2. * y)./m.^2) + (2./m.^3);$

$y8 = -(c7./m) + (c8. * exp(m. * y));$

$sv = y6 - (0.5. * y7) + y8;$

$su = 0.5. * (sw - sv)$

$[C, h] = contour(y, u, p)$

$set(h,'showText','on','textStep', get(h,'levelStep'));$

$colormapgray$

$ylabel('InducedMagneticField(h)')$

$xlabel('y')$

$print - depssani1.eps$